

Characterising Epithelial to Mesenchymal Transition and pro-fibrotic processes in Chronic Obstructive Pulmonary Disease

Helen Victoria Carlin



School of Environment and Life Sciences, College of
Science & Technology,

University of Salford, Salford, UK

Submitted in Fulfilment of the Requirements of the
Degree of Doctor of Philosophy, 2015

TABLE OF CONTENTS

CONTENTS	I
FIGURES AND TABLES	VIII
ACKNOWLEDGEMENTS	XIII
ABBREVIATIONS	XIV
ABSTRACT	XVI
<u>CHAPTER 1: INTRODUCTION</u>	<u>1</u>
1.1 COPD EPIDEMIOLOGY	1
1.2 COPD DIAGNOSIS	2
1.3 CELL PATHOLOGY IN COPD	4
1.4 INFLAMMATORY MECHANISMS IN COPD	7
1.5 ROLE OF LEUKOCYTES AND NEUTROPHILS IN INFLAMMATION AND FIBROSIS.	11
1.6 FIBROSIS FOR NORMAL REPAIR AND PATHOLOGICAL PROCESS.	13
1.7 EPITHELIAL TO MESENCHYMAL TRANSITION.	16
1.8 AIMS AND OBJECTIVES.	25
<u>CHAPTER 2: MATERIALS AND METHODOLOGIES</u>	<u>27</u>
2.1 HUMAN LUNG TISSUE	27
2.1.1 LUNG TISSUE SAMPLE ORIGIN	27
2.1.2 PATIENT DEMOGRAPHICS	28
2.1.3 PROCESSING OF BIOPSIES OF LUNG RESECTION	29
2.1.4 PROCESSING OF FORMALIN FIXED TISSUE	29
2.1.5 TISSUE EMBEDDING	30
2.1.6 TISSUE SECTIONING (MICROTOMY)	30

2.1.7 POSITIVE CONTROL CELLS FOR IHC	31
2.1.8 FFPE CELL SUSPENSION	31
2.1.9 CELL CYTOSPINS	32
2.1.10 IMMUNOHISTOCHEMISTRY	33
2.1.11 HAEMOTOXYLIN & EOSIN AND COLLAGEN STAINING	36
2.1.12 MICROSCOPE IMAGING	37
2.1.13 IMAGE ANALYSIS	38
2.2 IHC STATISTICAL ANALYSIS	39
2.2.1 CELL COUNTS	39
2.2.2 MANUAL COUNTING VS. COLOUR DECONVOLUTION	40
2.2.3 ANALYSIS OF PATIENT SAMPLES	40
2.3 LASER CAPTURE MICRO DISSECTION	40
2.3.1 CRYOSECTIONING	41
2.3.2 RAPID IHC	41
2.3.3 LCMD	42
2.4 QRT-PCR.	43
2.4.1 RNA ISOLATION	43
2.4.2 DENATURING RNA GEL ELECTROPHORESIS	44
2.4.3 TWO-STEP QUANTITATIVE REVERSE TRANSCRIPTASE – POLYMERASE CHAIN REACTION (QRT-PCR)	45
2.5 CELL CULTURE.	50
2.5.1 ISOLATION OF FIBROBLASTS FROM LUNG RESECTION BIOPSIES	50
2.5.2 GROWING CELL LINES	51
2.5.3 TRYPSINISATION	51
2.5.4 COLLAGEN COATING OF PLATES	52
2.5.5 CELL CRYOPRESERVATION	52
2.5.6 IHC TO CHARACTERISE CELL LINES	53

2.6 CELL CULTURE EXPERIMENTS	53
2.6.1 GENERATION OF CIGARETTE SMOKE EXTRACT	53
2.6.2 EXERTING STRETCH FORCES ON CULTURED CELLS	54
2.7 MTT ASSAY FOR CELL VIABILITY	55
2.8 BENDER 11PLEX ASSAY	56
2.9 ENZYME LINKED IMMUNOSORBENT ASSAY	57
<u>CHAPTER 3: INVESTIGATION OF EMT IN HUMAN LUNG TISSUE VIA IMMUNOHISTOCHEMISTRY</u>	<u>60</u>
3.1 BACKGROUND	60
3.1.1 AIMS	63
3.2 METHODS	64
3.2.1 IMMUNOHISTOCHEMISTRY	65
3.2.2 IMAGING	66
3.2.3 IMAGE ANALYSIS	67
3.2.4 ANALYSIS	68
3.2.5 STATISTICAL ANALYSIS	69
3.3 RESULTS	70
3.3.1 ANTIBODY OPTIMISATION	70
3.3.2 LP#624 POSITIVE CONTROL	77
3.3.3 TISSUE STRUCTURES: EXAMPLE OF SAMPLE STAINS	83
3.3.4 POSITIVE CONTROLS: CELL LINES	85
3.3.5 PATIENT GROUP DATA (LUNG SAMPLE IHC)	90
3.3.6 EMT REVERSIBILITY	95
3.3.7 COPD patients versus Control subjects	99

3.3.8 Correlation of demographics to EMT biomarkers	103
3.3.8.1 Lung function	103
3.3.8.2 Pack year history	107
3.4 Discussion	111
3.4.1 Antibody optimisation: Positive controls	111
3.4.2 Epithelial markers: optimisation	111
3.4.3 EMT/Fibrotic marker optimisation	113
3.4.4 Leukocyte markers	114
3.4.5 H&E and Collagen	115
3.4.6 Patient Examples (1 COPD and 1 control subject)	116
3.4.7 Validation of repeatability in the S100A4 positive control	116
3.4.8 Group data findings	
3.4.8.1 Epithelia markers	117
3.4.8.2 Fibrotic Markers	119
3.4.8.3 Leukocytes	123
3.4.9 Conclusion	126

CHAPTER 4: CHARACTERISATION OF SIGNALLING PATHS MEDIATING EMT IN HUMAN LUNG TISSUE:

QUANTITATIVE RT-PCR GENE EXPRESSION ANALYSIS OF LASER CAPTURE MICRO DISSECTED TISSUE **128**

4.1 Background	128
4.1.1 TGF- β is a key mediator of EMT	128

4.1.2	TGF- β signalling	130
4.1.3	Rationale of Lazer Capture Microscopy Dissected Tissue (LCMD) followed by QRT-PCR technologies used in this chapter.	131
4.1.4	Chapter 4 aims	133
4.2	Methods	134
4.2.1	Demographics of lung patients used for immuno-LCMD study	134
4.2.2	Tissue Preparation for Lazer Capture Microscopy Dissection and QRT-PCR	134
4.2.3	Comparative C_t method ($2^{-\Delta\Delta C_t}$)	135
4.2.4	ΔC_t and $2^{-\Delta\Delta C_t}$ calculations	137
4.2.5	Statistical Analysis of PCR CT values	138
4.3	Results	138
4.3.1	Original cohort (n=12) Account and Overview of Study Limitations	138
4.3.2	Validation of RNA yield was comparable between immuno-LCMD and LCMD without prior staining.	140
4.3.3	Group Data: Gene Expression from Whole Lung Tissue	141
4.3.4	Group Data: Gene Expression from immune-LCMD: epithelia versus EMT regions.	143
4.3.5	Group Data: Fold changes of Gene Expression from immune-LCMD: epithelia versus EMT regions in COPD and control subjects.	145
4.4	Discussion	147
<u>CHAPTER 5: INVESTIGATION OF CULTURED PRIMARY LUNG FIBROBLAST CYTOKINE AND VIABILITY RESPONSES TO CIGARETTE SMOKE AND STRETCH FORCES.</u>		152

5.1 Background	152
5.1.1 <i>In vitro</i> models of COPD: What can it tell us?	152
5.1.2 Cigarette Smoke Extract (CSE) <i>in vitro</i> studies	152
5.1.3 Aims	156
5.2 Methods	158
5.2.1 Primary cell expansion, cell culture and cytopins	159
5.2.3 CSE exposure vs. CSE with Stretch Experiments with ELISA readout	159
5.2.5 MTT bromide assay for cell viability	161
5.3 Results	162
5.3.1 Cytopins	162
5.3.2 Bender 11plex	163
5.3.3 ELISA	164
5.3.3.1 Grouped Data: all patients	164
5.3.3.2 IL-6 Responses	166
5.3.3.3 IL8 Responses	171
5.3.3.4 TGF β 1 Responses	176
5.3.3.5 Comparing data between groups: 24 hours	181
5.3.3.6 Cytokine Responses to Stretch Forces	184
5.3.4 Cell Viability MTT assays	185
5.4 Discussion	189
CHAPTER 6: DISSCUSION & CONCLUSIONS	197

6.1	Discussion and Conclusions for future work	197
-----	--	-----

REFERENCES	204
-------------------	------------

APPENDIX A	227
-------------------	------------

APPENDIX B	231
-------------------	------------

Figures and Tables

CHAPTER 1: INTRODUCTION	1
FIGURE 1.1: X-RAY & CT OF SEVERE EMPHYSEMA	2
TABLE 1.1: GOLD CLASSIFICATION	3
FIGURE 1.2: CROSS SECTION OF NORMAL AND EMPHYSEMOUS LUNG	6
FIGURE 1.3: DIAGRAM OF AIRWAY REMODELLING	10
FIGURE 1.4: NORMAL AND COPD LUNG STAINED WITH H&E AND COLLAGEN	13
FIGURE 1.5: EMT PROCESS: VARIOUS FORMS	18
FIGURE 1.6: ONE CELL MULTIPLE ORIGINS	19
CHAPTER 2: MATERIALS AND METHODOLOGIES	27
TABLE 2.1: ALL SUBJECT DEMOGRAPHIES	28
FIGURE 2.1: PROCESSING OF HUMAN LUNG TISSUE BIOPSY	29
TABLE 2.2: DILUTION AND OPTIMAL ANTIBODY CONDITIONS	35
FIGURE 2.2: LCMD TISSUE ISOLATION	43
FIGURE 2.3: OVERVIEW OF SYBERGREEN QPCR	47
FIGURE 2.4: NHLFs 70% CONFLUENT	51
FIGURE 2.5: CSE PRODUCTION	53
FIGURE 2.6: FLEXERCELL TENSION PLUS SYSTEM	55
FIGURE 2.7: ELISA OVERVIEW	57
TABLE 2.3: ELISA SENSITIVITY RANGES AND REAGENT DILUENTS REQUIRED	59
CHAPTER 3: INVESTIGATION OF EMT IN HUMAN LUNG TISSUE VIA IMMUNOHISTOCHEMISTRY	60

TABLE 3.1: IHC DEMOGRAPHICS	64
TABLE 3.2: ANTIBODY OPTIMAL CONDITIONS AND DILUTIONS	66
FIGURE 3.3.1 IHC OPTIMISATION	72
FIGURE 3.3.2 EMT MARKERS	74
FIGURE 3.3.3 LEUKOCYTE MARKERS	76
TABLE 3.3: OPTIMAL DILUTION SUMMARY	77
FIGURE 3.3.4 THRESHOLD IMAGES	78
FIGURE 3.35A THRESHOLD DETERMINATION IMAGES	79
FIGURE 3.35B THRESHOLD DETERMINATION GRAPH	80
FIGURE 3.36A POSITIVE CONTROL COMPARISON	82
FIGURE 3.36B POSITIVE CONTROL MANUAL VS. CAS	82
FIGURE 3.3.7A&B COPD AND CONTROL LUNG STAINING PATTERNS	84
FIGURE 3.38 H&E AND COLLAGEN STAINING OF CELL LINES	86
FIGURE 3.39 EPITHELIAL MARKER STAINING OF CELL LINES	87
FIGURE 3.3.10 FIBROTIC/EMT MARKER STAINING OF CELL LINES	88
FIGURE 3.3.11 LEUKOCYTE MARKER STAINING OF CELL LINES	89
FIGURE 3.3.12A&B EPITHELIAL MARKERS BETWEEN SEPARATE PATIENT GROUPS	92
FIGURE 3.3.12C-F FIBROTIC MARKERS BETWEEN SEPARATE PATIENT GROUPS	93
FIGURE 3.3.12G-I LEUKOCYTE MARKERS BETWEEN SEPARATE PATIENT GROUPS	94
FIGURE 3.3.13A&B EPITHELIAL MARKERS BETWEEN SMOKING STATUS	96
FIGURE 3.3.13C-F FIBROTIC MARKERS BETWEEN SMOKING STATUS	97
FIGURE 3.3.13G-I LEUKOCYTE MARKERS BETWEEN SMOKING STATUS	98
FIGURE 3.3.14A&B EPITHELIAL MARKERS BETWEEN COPD AND CONTROL	100
FIGURE 3.3.14C-F FIBROTIC MARKERS BETWEEN COPD AND CONTROL	101
FIGURE 3.3.14G-I LEUKOCYTE MARKERS BETWEEN COPD AND CONTROL	102
FIGURE 3.3.15A&B LINEAR REGRESSION LF AND EPITHELIAL MARKERS	104

FIGURE 3.3.15C-F LINEAR REGRESSION LF AND FIBROTIC MARKERS	105
FIGURE 3.3.15G-I LINEAR REGRESSION LF AND LEUKOCYTE MARKERS	106
FIGURE 3.3.16A&B LINEAR REGRESSION PYH AND EPITHELIAL MARKERS	108
FIGURE 3.3.16C-F LINEAR REGRESSION PYH AND FIBROTIC MARKERS	109
FIGURE 3.3.16G-I LINEAR REGRESSION PYH AND LEUKOCYTE MARKERS	110

CHAPTER 4: CHARACTERISATION OF SIGNALLING PATHS MEDIATING EMT IN HUMAN LUNG TISSUE: QUANTITATIVE RT-PCR GENE EXPRESSION ANALYSIS OF LASER CAPTURE MICRO DISSECTED TISSUE

Figure 4.1. Proposed mechanisms of TGF- β regulation of EMT	129
Table 4.1 Demographics of lung patients used for immuno-LCMD study	134
Figure 4.2 LCMD: Fibrotic tissue isolation	135
Table 4.2: Shows an example of the validated results for the SNAI1 target	136
Table 4.3: Target efficiencies for all gene targets used	137
Figure 4.3.1 Denaturing RNA gel 1.5% electrophoresis: LCMD RNA isolations	140
Figure 4.3.2 A-D: Gene expression IL-6, TGF β 1, SNAI1 and SMAD3 Δ Ct data of control and COPD groups on whole tissue	142
Figure 4.3.3 A-D: Gene expression between immune-LCMD epithelia and regions of EMT ('fibrotic')	144
Figure 4.3.4 A-D: Fold change in gene expression when comparing EMT regions to epithelial tissue. Control subjects versus COPD patients.	146

CHAPTER 5: INVESTIGATION OF CULTURED PRIMARY LUNG FIBROBLAST CYTOKINE AND VIABILITY RESPONSES TO CIGARETTE SMOKE AND STRETCH FORCES.

Table 5.1 The effects of cigarette smoke (CSE) on human lung cells <i>in vitro</i>	154
---	-----

Table 5.2 Demographics of lung patients used for CSE and CSE with stretch study	158
Table 5.3 Demographics of lung patients used for MTT study	160
Figure 5.2.1: Mitochondrial reduction of MTT into formazan	161
Table 5.4 Depicts staining of primary fibroblast isolations	163
Figure 5.3.1 Graphical representation of TGF β 1, IL-8, and IL-6 released, (pg/mL) from all primary fibroblast assessed	165
Figure 5.3.2 IL6 responses (pg/mL) to CSE over time	167
Figure 5.3.3 IL-6 responses (% change) to CSE over time all ex-smokers all current smokers	168
Figure 5.3.4 IL-6 responses (% change) to CSE over time: all control subjects and all COPD patients	169
Figure 5.3.5 IL-6 responses (% change) to CSE over time: normal ex-smokers versus normal current smokers.	170
Figure 5.3.6 IL-8 responses (pg/mL) to CSE over time EX, CS, CEX & CCS	172
Figure 5.3.7 IL8 responses (%change) to CSE over time: all ex-smokers and all current smokers	173
Figure 5.3.8 IL-8 responses (%change) to CSE over time: all control subjects and all COPD patients	174
Figure 5.3.9 IL-8 responses (% change) to CSE over time normal current smokers versus COPD current smokers.	175
Figure 5.3.10 TGF β 1 responses (pg/mL) to CSE over time: EXS, CS, CEX & CCS	177
Figure 5.3.11 TGF β 1 responses (% change) to CSE over time: all ex-smokers and all current smokers	178

Figure 5.3.12 TGF β responses (% change) to CSE over time: all control subjects and all COPD patients	179
Figure 5.3.13 TGF β 1 responses (% change) to CSE over time in: normal ex-smokers versus normal current smokers.	180
Figure 5.3.14 24 hour data comparison between all controls and all COPD	182
Figure 5.3.15 24 hour data comparison all groups	183
Figure 5.3.16 IL-8 and TGF β 1 responses (pg/mL) to stretch forces and/or 10% CSE over time.	184
Figure 5.3.17 Primary human Fibroblast viability responses to doses of CSE measured by MTT assay: group data	186
Figure 5.3.18 Primary human Fibroblast viability responses to doses of CSE measured by MTT assay: Control groups	187
Figure 5.3.19 Primary human Fibroblast viability responses to doses of CSE measured by MTT assay: COPD	188

CHAPTER 6: DISCUSSION AND CONCLUSIONS FOR FUTURE WORK **197**

Figure 6.1: Overview of where this thesis work sits in current research and how it directs future research	203
--	-----

Acknowledgements

First and foremost I would like to thank the people without which this PhD would not have been possible. I would like to thank especially my first supervisor Dr Lucy J Smyth for without her help, encouragement and support through really difficult times I would not have completed my work. Both Dr Lucy J Smyth and Dr Jeremy Allen have been supportive throughout the course of my studies and have nudged me in the correct direction and reined me in, whenever required, I give my utter most thanks.

I would additionally like to thank all of the technical staff for their help in the laboratory, giving me reagents and keeping me sane during the hard times. Thanks to all of the PhD students and everyone at Salford University for support and encouragement along the way especially my fellow laboratory partner in crime Ross Gordon.

I would also like to thank Dr Dave Singh and his wonderful team Airway Pharmacology Group, Institute of Inflammation and Repair, University of Manchester for providing the Human Lung samples my work was mainly based upon. I would also like to thank Simon Stephan for allowing me to use the Laser Capture microscope North West Lung Research Centre, University Hospital South Manchester NHS Foundation Trust.

Most importantly I would like to thank my husband Peter Joseph Carlin for all the support encouragement and love he has given me throughout my PhD; without him I would of given up a long time ago and I wouldn't be where I am today. I would also like to thank my family especially my parents Colin and Margaret Ann Smith and brother Jordan Lee Smith for mental, emotional, financial and emergency dog minding support; and finally my friends for supporting me and giving me a nudge or two to complete my thesis, as well as laughs every step of the way.

Abbreviations

Alpha-1 antitrypsin (AAT)

Alveolar epithelial cell (AEC)

Alpha smooth muscle actin (α SMA/ASMA)

Alveolar macrophages (AMØ)

Analysis of variance (ANOVA)

CD45 lymphocyte common antigen

CD68 monocyte lineage common antigen

Chronic obstructive pulmonary disease (COPD)

Cigarette smoke extract (CSE)

Colour deconvolution (CD)

COPD current smoker (CCS)

COPD ex-smoker (CEX)

Current smoker (CS)

Extra cellular matrix (ECM)

Endothelial -mesenchymal transition (EndMT)

Epithelial - mesenchymal transition (EMT)

Ex-smoker (EXS)

Forced exhaled in one second (FEV₁)

Forced vital capacity (FVC)

Global Initiative for Chronic Obstructive Pulmonary Disease (GOLD)

Human bronchial epithelial cells (16HBE140)

Human lung adenocarcinoma epithelia cell line (A549)

Interleukin-6 (IL-6)

Interleukin-8 (IL-8)

Laser capture microscope (LCM)

Laser Capture Micro dissection (LCMD)

Lung patient (LP#)

Matrix metalloproteinases, (MMPs)

Neutrophil elastase (NE)

Non-smoker (NS)

Normal human lung fibroblasts (NHLFs)

Pack year history (PYH)

Platelet derived growth factor (PDGF)

Reagent dilution buffer (RDB)

Red blood cells (RBC)

Red, green and blue (RGB)

Research cigarette (1R3F)

Transcription factor promoter gene for EMT (SNAI1)

Small calcium binding protein/ EMT marker (S100A4)

Smooth muscle (SM)

Type 1 cytokines (TH1)

Type 2 cytokines (TH2)

Transforming growth factor – Beta 1 (TGF- β 1)

Abstract

Background Rationale

Chronic Obstructive Pulmonary Disease (COPD) is an irreversible disease reducing lung function via processes of inflammation, emphysema and fibrosis. Patient treatment options are limited including bronchodilators and inhaled corticosteroids that are poorly effective. Linked with a significant history of cigarette smoking, pathology is characterised by recruitment of inflammatory cells to the lung (alveolar macrophages, neutrophils and lymphocytes: TH1 and CD8); dysregulated neutrophils and macrophages release tissue lysing proteases causing enlargement of airspaces (emphysema). Most severe pathology includes dysregulated epithelial repair and overgrowth of lung fibroblasts (fibrosis). The source of fibroblasts is not clear. Fibrosis in renal, liver and heart disease is partly mediated by epithelial-mesenchymal transition (EMT) differentiation whereby epithelia acquire fibrotic biomarkers such as desmin, S100A4 and α -smooth muscle actin. In COPD this has not been characterised, further the molecular mechanisms in the lung are poorly understood. Identifying these processes is key to developing improved future therapeutic interventions.

Aims

To characterise human COPD lungs for expression of EMT biomarkers compared to control subjects to determine the processes of lung fibrosis in COPD. Further, to identify the signalling mechanisms within the EMT tissue to identify the regulatory processes that may be intervened in future therapies. Finally, to assess primary human fibroblast responses to cigarette smoke extract (CSE) and stretch forces to establish a new model of emphysema and lung fibrosis for future research.

Methods

Patients were recruited from the North West Lung Centre at the University Hospital of South Manchester who were undergoing lobectomy surgery as part of their normal clinical care. Lung resections were prepared for histochemical analysis by formalin fixing and wax embedding. 5µm microtome slices were immunohistochemically stained for typical mesenchymal (EMT) and epithelia biomarkers. Statistical comparisons were made between control groups: non-smokers (NS), current smokers (CS) ex-smokers (EXS), and COPD patients: COPD current smokers (CCS) and COPD ex-smokers (CEX). Identified regions of EMT tissue were laser capture microscopy dissected, RNA isolated, and target genes assessed by Q-RTPCR. Tissue culture experiments were performed by expanding fibroblasts from 1mm lung sections in RPMI culture media that were seeded in wells and exposed to stretch forces and doses of cigarette smoke extract (1 cigarette bubbled into 25ml RPMI media =100%) over time. IL-6, IL-8 and TGFβ1 responses were measured by ELISA and statistical comparisons made.

Results

EMT marker S100A4 was significantly ($P<0.05$) raised in COPD patients. The other EMT biomarkers (desmin, αSM actin and collagen) also showed numerical increases over NS but were not significant. S100A4, desmin and collagen expression were all significantly raised in current smokers and ex-smokers compared to never smokers regardless of airway obstruction. S100A4+ve regions were selected for EMT identification for immune-laser capture microscopy. SMAD3, SNAI1, TGFβ1 and IL6 were all numerically raised in EMT/S100A4+ve regions however the small subset sample numbers did not offer enough statistical power for the study. Primary fibroblast cultures released cytokines IL-6 and IL-8 dose dependently to CSE: % (1, 5, 10, 20, 50), particularly at later time points (24 and 48hours) assessed by % change to 0%CSE. Absolute levels (pg/mL) were much higher at 24 and 48 hours compared to 4 and 6 hours, which was particularly notable in COPD patients for all 3 cytokines. MTT assay showed viability was good 100-80% when cells were cultured and a small (~5% decrease) dose response to CSE

for all cytokines. Approximately 5% viability is lost over the time course 0-48 hours; which is more notable (an extra 5%) in COPD patients.

Discussion

This study showed EMT processes are possibly associated with S100A4 expression and particularly with smoking pack year history rather than airway obstruction. We therefore demonstrated that there are possible EMT processes are involved in smoking related pulmonary fibrosis. Further, S100A4 fibrotic regions are linked with TGF β 1 signalling components SMAD3 and SNAI1 and downstream outputs TGF β 1 and IL-6; this study needs expanding with more patients, to determine if this molecular mechanism is EMT related in COPD. CSE directly induced pro-inflammatory mediator release and raised fibroblast responses seen in COPD patients and current smokers imply a pre-activated state contributing to their lung pathology. Stretch forces did not increase cytokine release beyond responses to CSE alone. Good starting cell viability indicates this is a suitable model for studying possible EMT driven lung fibrosis in COPD. CSE doses induced raised cell death responses in COPD patients over time; implicating their enhanced susceptibility to apoptosis and supporting contemporary literature. This *in vitro* primary fibroblast model will be useful for testing effectiveness of novel anti-inflammatory and anti-fibrotic drugs in future.

Chapter 1

Introduction

1.1 COPD epidemiology

Chronic obstructive pulmonary disease (COPD) is a long-term respiratory disorder, which is characterised by frequent and persistent limitation to the airways with an increase in irreversible airway resistance. (Nowark *et al* 2004; Currie 2009; Tortora *et al* 2009). Within the UK, COPD is one of the most common respiratory diseases affecting people over the age of 35; there is approximately 835,000 people within the UK diagnosed with COPD and in the region of 2 million people who either haven't been diagnosed (Currie 2009; NHS 2010), or have been miss diagnosed with another condition such as asthma (Scullion 2008). It is hard to be certain precisely how many people have COPD but it is thought that the number of people diagnosed constitutes only the tip of the iceberg, (Currie 2009). COPD causes around 25,000 deaths within the UK every year and is a major cause of morbidity and mortality worldwide, (Agusti *et al* 2003; Bousquet and Khaltaev 2007) causing 3 million deaths in 2005 worldwide (Green and Turner 2013). In 2007, the world health organisation (WHO) suggested that globally COPD affected in the region of 210 million people, (Bousquet and Khaltaev 2007).

It is projected that by 2020, COPD is to be the third most prevalent disease globally (Sarir *et al* 2008; Cosio *et al* 2009; Rangasamy *et al* 2009). COPD's global prevalence is approximately 10% among individuals over the age of 40, (Barnes 2008; Green and Turner 2013).

With this it is clear that the economic burden of COPD is considerable, not only in the UK but worldwide and it will continue to grow considerably, as the number of people surviving longer continues to increase, (Bousquet and Khaltaev 2007).

1.2 COPD Diagnosis

Before the official diagnosis is made, it has to be considered that the symptoms such as breathlessness on exertion and reduced ability to exercise, could be a condition that presents features similar to COPD, such as of a number of other lung (e.g. asthma, cancer) or heart (e.g. valve/heart muscle problems or failure) conditions or even anaemia, (Currie 2009). This is conducted by first considering the patient's medical and family history as well as social background. Following this the patient undergoes physical examinations and specific specialised tests such as imaging the lungs by means of x-ray and/or computerised tomography (CT) scanning (see figure 1.1). Blood tests are also conducted, measuring blood cell counts and oxygen levels; but the most definitive diagnostic tool is airflow tests to assess the patient's lung function such as spirometry conducted on a spirometer, (Midgley *et al* 2008; Currie 2009).

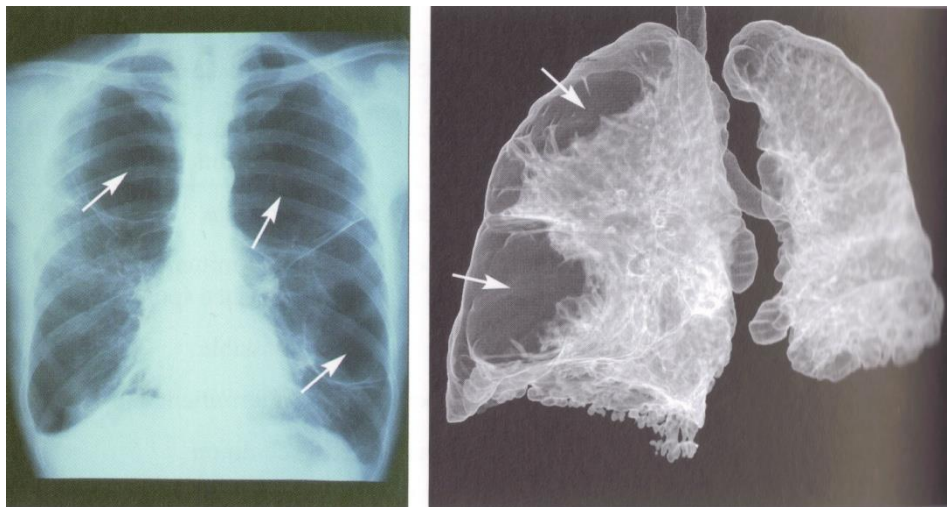


Figure 1.1: Show images of lungs from patients whom have severe emphysema. The first image (left) is an X-ray. The arrows point to large areas in the lung that have trapped air, called bullae. The second image (right) shows a detailed image of emphysemous lungs taken by a CT scan; this shows the bullae as large transparent areas. It is images such as these which can help determine if removal of damaged lung tissue may help the patient. Midgley *et al* 2008.

COPD is a disease that is clinically characterised by a reduced maximal expiratory flow and slow forced emptying of the lungs, (Sarir *et al* 2008). The severity of the disease is categorised into one of 5 stages (0-4) introduced by the Global Initiative for Chronic Obstructive Pulmonary Disease (GOLD); it is based on the measurement of airflow limitation during forced expiration, (Hogg *et al* 2004). Each stage is determined by the volume of air that can be forced exhaled in one second (FEV₁) and the ratio of FEV₁ to the forced vital capacity (FVC) the volume of air that can be forcibly exhaled after full inspiration. The lower the FEV₁/FVC ratio indicates the more severe and therefore higher the stage of COPD, (Hogg *et al* 2004; MacNee 2008) for example $<70\%/0.70$ = GOLD stage 1, (MacNee 2008).

Stage	Severity of COPD	Possible symptoms	Airflow limitation
0	At risk	Chronic cough and sputum production	At predicted normal level
1	Mild	Mild airflow limitation with associated chronic cough and sputum production; but not in all cases. Patients can often be unaware that they have an abnormal lung function.	At least 80% of predicted normal level
2	Moderate	Worsening airflow limitation and usually progression of symptoms such as shortness of breath on exertion.	Less than 80% of predicted, but more than 50%
3	Severe	Further worsening of airflow limitation, increased shortness of breath and repeated exacerbations which have an impact on quality of life	Less than 50% of predicted, but more than 30%
4	Very Severe	Severe airflow limitation. Quality of life is appreciably impaired and exacerbations may be life threatening	Less than 30% predicted. Also includes individuals with a higher FEV ₁ but signs of respiratory failure or right side heart failure.

Table 1.1:. This table shows the GOLD classification used to determine the diagnosis and the severity of COPD. The results used from the spirometry test are ones taken after the patient has been treated with a bronchodilator, this helps to ensure that the airway limitation is not the result of a reversible condition such as asthma. Adapted from Midgley *et al* 2008

In addition to the local effect on the lungs, COPD can also have systemic effects; these can either be structural such as weight loss, skeletal muscle wasting or osteoporosis or functional such as inflammation or cardiovascular. These processes are often interdependent in a vicious closely linked cycle; known as co-morbidities (Bousquet and Khaltaev 2007; Chilos *et al* 2012).

1.3 Cell pathology in COPD

Physiological changes within the lung periphery are generally thought to be the major contributor to airflow limitation in patients whom develop COPD, (Barnes 2000; Battaglia *et al* 2007) these are caused by different pathological changes of the two principle types of COPD which are chronic bronchitis and emphysema (Sutherland *et al* 2003; Nowark *et al* 2004).

Chronic Bronchitis is an airway disease that involves the hyper-secretion of bronchial mucus, which is closely associated by a productive cough, that is caused by a constant chronic irritation of the bronchial linings and is an attempt to clear the excess mucus, (Nowark *et al* 2004) that lasts for at least three consecutive months of a year for two consecutive years (Tortora *et al*, 2009). The increase in resistance and obstruction to the airflow of the smaller conducting airways is one of the causes of a low value produced from the FEV₁/FVC ratio, (Hogg *et al* 2004; Curtis *et al* 2007).

Emphysema disease involves the destruction of alveoli walls which produces unusually large air spaces (see Figure 1.3) that retain air during exhalation, (Tortora and Derrickson 2009) this loss of lung capacity and trapping of air causes abnormal lung enlargement. Due to this there is further bursting of alveoli, resulting in the patient having hyperinflation of the lungs. This gives an increase in total lung capacity yet a decrease in vital capacity due to the reduction in elastic recoil, (Puente-Maestu and Stringer, 2006). Other contributors to emphysematous lung destruction include age -related alterations such as epigenetic changes, cellular senescence and a low grade chronic inflammation, (Cosio *et al* 2009). A decrease

in lung compliance is another cause of the reduced FEV₁/FVC ratio, (Hogg *et al* 2004; Curtis *et al* 2007).

Reduced elastic recoil of the lungs is due to fibrosis (scarring) of the lung tissue. The reduction and fibrogenesis of alveoli and alveolar walls results in a loss of surface area therefore reducing gas exchange (Nowark *et al* 2004). Aggressive fibrogenesis found within patients that have COPD often have a very poor prognosis with a life expectancy ~3 years, (Ishikawa *et al* 2010).

Depending on the cellular pathology, COPD symptoms are wide and varying; as the disease progresses most patients start to show symptoms of progressively more of the effects. These effects include wheezing caused by air trying to squeeze through mucus narrowed passageways (chronic bronchitis) and breathlessness which is caused by barrel chest (emphysema), this is formed by years of added exertion during inhalation caused by the increasing amount of air being trapped within the enlarged air spaces- damaging more alveolar walls and further reducing lung elastic recoil- resulting in increased size of the patient's chest cage, (Tortora *et al* 2009).

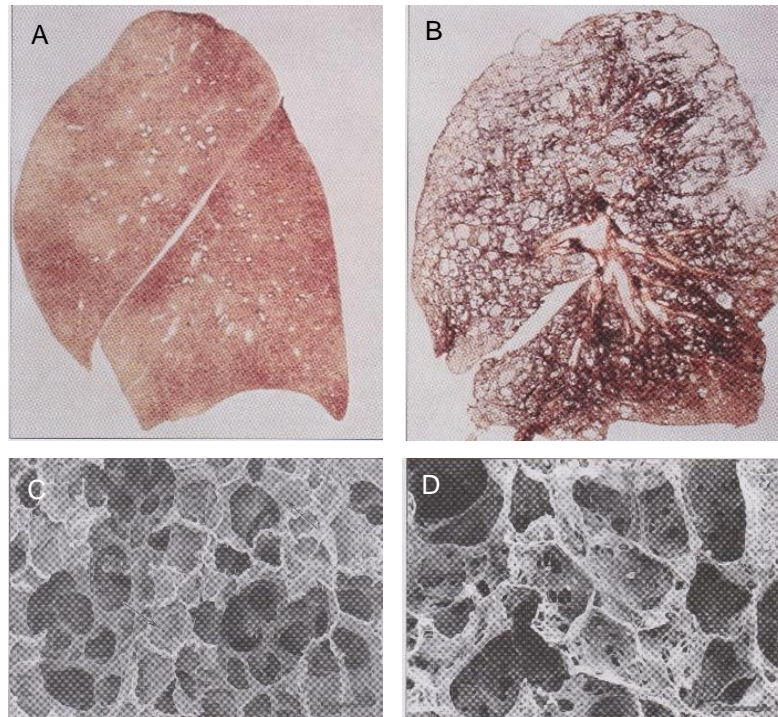


Figure 1.2. Images of cross-section of a Normal lung (A) and lung with advanced emphysema (B). Scanning electron microscopy images (x50 magnification) of normal alveoli (C) and patient with emphysema. Image edited from Midgley et al 2008.

Curtis *et al* 2007 states that the persistent injury to lung tissue is produced by the chronic inhalation of toxic particles and gases. There are many environmental and self-inflicted causes of COPD which includes smoking cigarettes, tobacco and cigars, which is widely recognised as the major source of the disease (Togo *et al* 2008) as well as air pollution, occupational exposure to industrial and agricultural dusts. There are sometimes genetic causes for example alveolar wall destruction can be caused by an enzyme imbalance, such as an α_1 -antitrypsin deficiency (Stolk *et al* 2006), within the specific patient (Curtis *et al* 2007; Tortora *et al* 2009). It is generally agreed today that 95% of COPD cases are reportedly linked to cigarette smoking (Sutherland *et al* 2003; Bagole *et al* 2006; Casio *et al* 2006 and Van der Strate *et al* 2006). But it also interesting to see that only 15-20% of all smokers will eventually develop the disease (Sutherland *et al* 2003; Casio *et al* 2006 and Van der Strate *et al* 2006) which suggests there is a high degree of elemental patient variability in the pathologic changes induced by cigarette smoke. It has come to light that telomere length can be a susceptibility factor for emphysema, (Alder *et*

al 2011). Even with this in mind only a minority of smokers reach the more advanced levels (GOLD 3 & 4) of COPD, (Curtis *et al* 2007), indicating that a possible genetic variation that could be caused by one or multiple changes in a polymorphic site, two or more genes that have the same effect independently or a variation of two or more genes that operate jointly, with neither being sufficient to cause problems on their own in addition to which environmental agent is present; pure chance could also play a role with lung fibrosis operating independently of an etiologic agent, (Pass *et al* 1996).

It is estimated that there is only <0.1% (variable base equivalent of about 0.5-1% and 1% allele frequency) of DNA variation between all individuals. Variation on a larger scale occurs very rarely at a heterozygosity of <1% in the whole world. Most of these variations are neutral but a small selection can affect phenotype and can be/have been/may become subject to selection, any of these variants could contribute to a disease, (Stearns and Koella 2008). With this in mind it can be seen why a genetic variation related to COPD allowing the identification of susceptible individuals, has not yet been discovered.

1.4 Inflammatory mechanisms in COPD

Current understanding of COPD pathology is that there are a range of leukocytes found in the lungs of a COPD patient; each having a role in pathogenesis of the disease. They are however non-specific in the sense that they protect against a wide range of foreign material that includes parasites, microbes, toxins and particles. Paradoxically it is the over active functioning of these cells that cause the disease, (Midgley *et al* 2008). The leukocytes can be activated by inhaled cigarette smoke, amongst other inhaled irritants, which contains a complex mixture of over 4500 chemical species that includes bioactive lipopolysaccharide (LPS) a bacterial cell wall component, (Hasday *et al* 1999), free radicals and oxidants, (Carnevali *et al* 2003; Bagloli *et al* 2006; Domagala-Kulawik *et al* 2008; Kang *et al* 2008; Sarir *et al* 2008) able to induce oxidative stress and are known to be antigenic, cytotoxic, mutagenic and carcinogenic (Domagala-Kulawik *et al* 2008; Green and Turner 2013). Each “puff” of a cigarette yields an approximate 1×10^7 oxidant molecules,

(Baglolle *et al* 2006). In literature by Domagala-Kulawik *et al* 2008 it is stated that cigarette smoke particles are capable of reaching the small airways as the mean size of the cigarette particles is 0.1-0.5µm, and therefore avoiding mucociliary clearance that only have the capability to clear particles that are greater than 2µm, (Midgley *et al* 2008).

The most common leukocytes that are found within a COPD patient's lung are Neutrophils, Macrophages, two families of CD45+ T lymphocytes, (mainly CD8 + with some CD4+ T lymphocyte involvements), dendritic cells and Eosinophils. Each have their specific functionality which play a critical role in defence for the lungs (as well as the rest of the body) but when exposed to repeated and extended periods of for example: smoke particles, the persistent inflammatory responses become irreversible and each type of cell become destructive to their environment - in this case the lungs. This is known as chronic inflammation.

Chronic inflammation permanently damages the lungs. Smoke particles and other toxins that reach the small airways and alveoli (that have no mucus or cilia to protect them) become deposited and stick to the tissue surfaces. This causes irritation and damage to the cells which release stress signals (in the form of cytokines/chemokines) causing the start of the inflammatory response (Kisseleva and Brenner 2008). This causes a mass recruitment of phagocytic leukocytes (macrophages, neutrophils and eosinophils) to the area. These release proteases (protein digesting enzymes) such as elastase, which are normally used by these cells to digest microbes they have internalised; when they come in contact with the surrounding lung tissue they break down proteins found in the cell wall and extra cellular matrix (ECM). Under normal circumstances the lung periphery is protected by a natural elastase inhibitor, alpha-1 antitrypsin (AAT); however in chronic inflammation the mass recruitment and stimulation of phagocytes overwhelms the amount of AAT and damage to the lung tissue occurs, (Midgley *et al* 2008). A small number of people have a defective gene that causes an AAT deficiency; these patients tend to develop COPD at a young age, even if they have not smoked, (Needham and Stockley 2004).

In addition to leukocytes, airway Epithelial cells are an important source of inflammatory mediators (Barnes, 2003) and Fibroblasts which are the most abundant, (Barnes 2002) key structural cells found within the lungs whose primary function is to maintain and repair damaged tissue via the production of extra cellular matrix (ECM), (Bagloli *et al* 2006 and Carnevali *et al* 2003). ECM is an intricate network of macromolecules (proteins and polysaccharide chains) which is locally secreted between cells that forms tissues; under normal circumstances it is assembled into an organised structure, in close association with the surface of its surrounding cells (Alberts *et al* 2002; De Franco *et al* 2007; Tortora and Derrickson 2009) providing support, forming architecture of tissues, aids in tissue segregation, has influence in organisation of cell cytoskeletons and the regulation in intracellular communication, (Alberts *et al* 2002). Some of the cells and cytokines involved are depicted in Figure 1.3

.

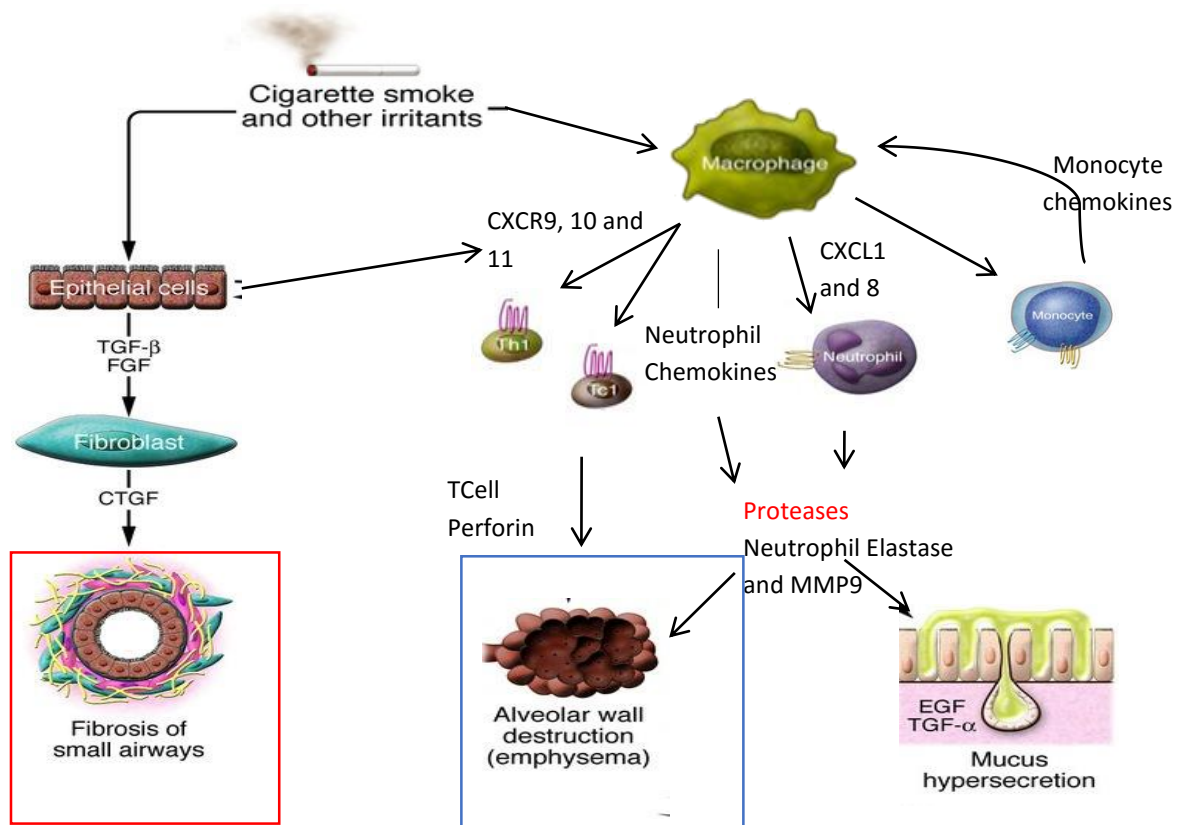


Figure 1.4 There are three distinct processes involved in the pathogenesis of COPD. The first is **Airway Remodelling – Thickening** (working left to right) High concentrations of TGF-B1, produced from activated epithelial cells, can induce epithelial cells to differentiate into Fibroblasts (via epithelial mesenchymal transition) which are key cells in degradation of existing and fresh over synthesis of extracellular matrix. This process is the focus of much of this thesis. The second process is **Alveolar Wall destruction** by T cells and over production of proteolytic enzymes by neutrophils and macrophages. Large airspaces cause ‘stale’ air to become trapped in large defective airspaces and the lung to stretch (emphysema). The third process is **Mucus hyper-secretion**; excess mucus is produced from goblet cells which collects forming a thick layer that narrows the airways. Resulting in the reduction in gas exchange and ciliary function; the reduction in ciliary function allows collections of mucus secretions where inhaled pathogens can multiply causing chronic infections. The net result of all these three processes is airway blockage. Diagram adapted from Barnes 2008.

These 3 key pathology processes produce a cocktail of cytokines, chemokines and growth factors and as found in other inflammatory diseases they play a role in orchestrating chronic inflammation, (Barnes 2009). Over 50 cytokines have been identified in COPD including interleukin-6 (IL-6) a pro-inflammatory cytokine that provides a link between innate and adaptive immunity (Barnes 2009) as well as inducing fibroblast collagen transcription (Satio *et al* 2008) Interleukin-8 (IL-8) a neutrophil chemotractant (Kent *et al* 2008) as well as also linked with fibrotic cell proliferation (Palena *et al* 2012) and growth factor called TGF- β 1 (transforming growth factor - β 1) that is a fibroblast chemotractant, induces fibroblast proliferation via an autocrine platelet derived growth factor (PDGF)-dependant pathway, (Allen and Spiteri 2002) smooth muscle cell proliferation, deposition of ECM and epithelial repair. Both of the mentioned cytokines are found to be increased within COPD patients' lungs, (Barnes 2009).

Results chapters 3+4 of this thesis are focussed on the fibrotic processes and understanding the cellular changes that are key to this process (highlighted in red in figure 1.3). Results chapter 5 addresses aspects of emphysema and how the enlargement and stretch of the lung may be regulating inflammatory processes; highlighted in blue in figure 1.3.

1.5 Role of leukocytes (CD45 & CD68) and Neutrophils (NE) in Inflammation and fibrosis.

Numerous studies have characterised pathological hallmarks of leukocytes in COPD. It is widely published that there are marked increases in macrophages, neutrophils and lymphocytes within the airway mucosa and lung parenchyma when compared to patients without the disease, (Caramori and Adcock 2003; Hogg 2007, Todd *et al* 2012).

Leukocyte markers CD45 the lymphocyte common antigen, CD68 a macrophage marker and neutrophil elastase are widely used to identify these cells residing in different tissues.

Neutrophils are the first cells recruited to the lung in response to cell injury they phagocytose apoptotic bodies and any residing cell debris. This then in turn activates the neutrophils causing cell degranulation, release inflammatory and pro-fibrotic cytokines. Macrophages are then recruited and they infiltrate the damaged tissues, these cells also phagocytose and secrete fibrogenic cytokines. Macrophages are a major source of TGF- β 1 in fibrosing organs. T and B lymphocytes are also recruited to the site of injury and further facilitate secretion of fibrogenic cytokines. (Barnes 2003; Barnes 2008; Kisseleva and Brenner 2008).

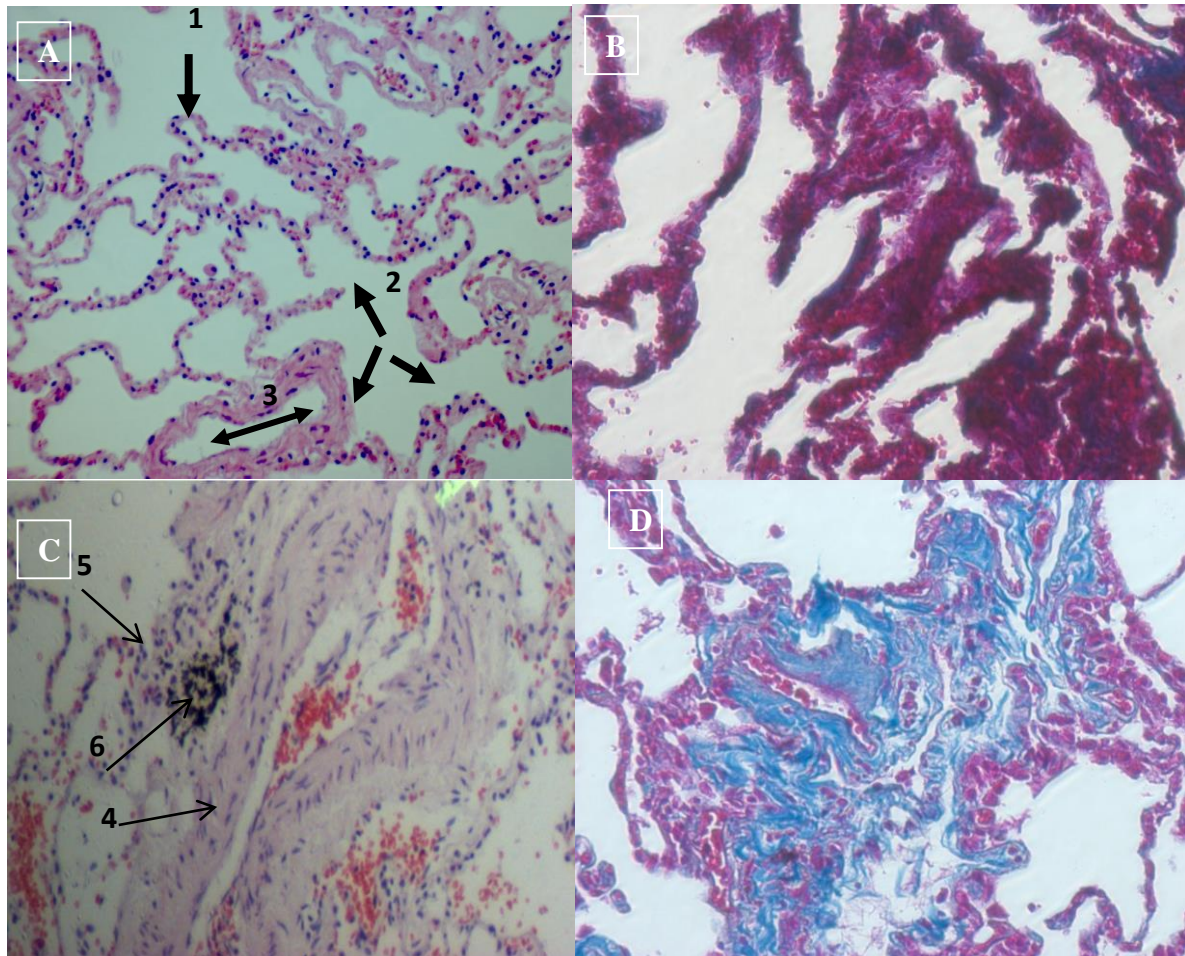


Figure 1.4. Shows a typical 'healthy' lung (A + B) and sections of a lung from a patient who has COPD (C + D). In images A + C these lung sections have been stained with H&E and the lung sections in images B + D have been stained with masons trichrome (collagen stain). It can be seen in image A that 1. The healthy lung tissues have thin alveolar walls which allow rapid gas diffusion, 2. These form the typical lung architecture (alveolar sacs) 3. There are larger airway lumens present which would lead to a vast network of airways. Image B represents that when stained for collagen healthy lungs are pink – indicating mostly normal lung epithelia are present. Image C shows 4 that in the lungs of a COPD patient many of the airways are thicker therefore reducing efficiency of gas diffusion, 5 there is a high presence of leukocytes (indicating inflammation) and 6 there are fewer air sacs as the lung cells are being destroyed. In their place are deposits of black tar. Image D shows that in COPD lungs there is a large amount of abnormal remodelling where excess collagen (ECM) is deposited (stained in blue). Images taken at x200 magnification

1.6 Fibrosis for normal repair and pathological process

Fibrosis is the replacement of normal tissue by the formation of excess fibrous connective tissue (ECM proteins e.g. collagen) in an organ or tissue in a reparative or reactive process. It can also be a complex pathological response, common to many tissues in response to injury (Kisseleva and Brenner 2008). The onset of

normal lung repair is the response to acute injury by a variety of etiological factors, (Strieter 2008). Acute injury and normal repair in the lungs, depends on the rapid replacement of damaged alveolar epithelium, this is initiated by the activation of the intrinsic and extrinsic coagulation pathways leading to the deposition of fibrin and early ECM deposits. The chemokine/cytokines released by the damaged epithelium also initiate alveolar epithelial cell (AEC) migration, specifically of the type II pneumocytes, progenitors for alveolar repair (Willis and Borok 2007; Kisseleva and Brenner 2008) and subsequent proliferation to cover the wound; associated with the migration of fibroblasts into the wound space. These differentiate into myofibroblasts that contract the wound and construct the new ECM, (Willis and Borok 2007; Strieter 2008). Myofibroblasts are cells that arise from populations of tissue specific fibroblasts that proliferate and undergo activation in response to injury, (Hinz *et al* 2007; Kisseleva and Brenner 2008) a change in their stress-shielded mechanical environment, injury due to excessive stretch or tissue tearing, is also an activation factor (Hinz *et al* 2007). They are mainly present in the wound and express high levels of α SMA which enhance their ability to contract the ECM, (Leask and Abraham 2004).

Subsequently, when the architecture is complete the myofibroblasts disappear and migrated epithelial cells differentiate into type I pneumocytes, resulting in the normal lung structure pre-injury, (Hinz *et al* 2007). This is a normal response to injury, inflammation or stress.

In contrast, pathology arises when wound healing responses become dysregulated and fails to stop. This excessive fibrotic process can be prolonged over months to years and it can lead to the compromised function of the specific tissue/organ. Lung fibrosis has a bleak prognosis and causes a major clinical burden as it leads to organ dysfunction and death within 2-5 years of diagnosis. There are no antifibrotic therapies; only anti-inflammatory medications that are poorly effective. Often the only way of significant life improvement is organ transplantation, but with the demand high and supply very low, patients will often die whilst waiting to receive a suitable organ (Leask and Abraham 2004). This is primarily caused as the aetiology of the fibrotic disease is unknown.

One of the largest groups of disorders for which there is no effective therapy is fibrotic diseases and thus represents a major unmet medical need, (Leask and Abraham 2004).

There are many different fibrotic conditions both genetic and injury induced such as: **Myocardial fibrosis**, fibrosis of the myocardium (heart tissue) due to either disease induced ischemia, acute inflammation (infection) or severe anaemia. It also could be endomyocardial fibrosis a condition mainly associated with Africans where there is gross thickening of the endocardium (Alstead *et al* 1989; Falase and Ogah 2012). **Liver fibrosis**, in the form of cirrhosis where there is an overgrowth of the supporting connective tissue due to injury such as alcohol abuse or in the form of hydatid cysts due to parasitic infections *Schistosoma mansoni* and *S. japonicum* (Anthony *et al* 2010). **Cystic fibrosis** is caused by a genetic mutation of the CF transmembrane conductance regulator. This causes an imbalance in Na⁺ Cl⁻ and fluid transport causing chronic inflammation and ultimately lung damage and remodelling, (Maillé *et al* 2011).

Condensation fibrosis, the development of fibrous tissue in an organ through the disappearance of the normal parenchyma with the resulting false impression of proliferative fibrosis, formation of fibrous tissue due to the proliferation of connective-tissue cells, as a normal part of an organ or tissue or during effective repair process. When this occurs in the lung, these changes disrupt the specific tissue architecture and gas exchange function causing great morbidity and mortality, (Perez *et al* 2011 and Rock *et al* 2011).

1.7 Epithelial to Mesenchymal Transition (EMT)

Chronic inflammation, repetitive and/or persistent injury due to the repeated exposure to a stimulant such as cigarette smoke, is essential in the pathological development of dysregulated fibrosis in COPD, (Strieter, 2008; Tod *et al* 2012). The process of lung fibrosis involves a complex interaction between immune cells and cellular constituents of the lung parenchyma. It is associated with the loss of resident epithelial cells, loss of basal membrane integrity leading to alveolar collapse, unregulated proliferation of epithelia and the recruitment and proliferation of activated fibroblastic cells with randomised ECM deposition (Strieter, 2008).

Rock *et al* 2011 states that in the lung the characteristic features of fibrosis, include the focal accumulation of cells with fibroblast like morphology (myofibroblasts) and excessive production of ECM.

There are four possible intrapulmonary precursors of myofibroblasts that all can contribute to fibrotic tissue formation in the lungs. They can be put into two categories, ones that induce excessive fibrogenesis such as resident interstitial fibroblast unchecked activation (proliferation and differentiation) causing an increased number of wound fibroblasts and enhanced trans-differentiation into the myofibroblast phenotype such as endothelial -mesenchymal transition (EndMT) and epithelial - mesenchymal transition (EMT). The second category is the increase in number of fibroblasts at fibrotic foci derived from circulating bone marrow-derived progenitors expressing CD45, CD34, collagen I and chemokine receptor 4, CXCR4 (Hinz *et al* 2007) and fibrocytes attracted to regions of lung injury, as well as cells derived through EMT (Perez *et al* 2011; Rock *et al* 2011; Lomas *et al* 2012; Tod *et al* 2012). It has been suggested that 30-50% of the fibrotic cells arise from EMT of type II lung epithelial cells, (Perez *et al* 2011 and Rock *et al* 2011).

EMT is a multistage biological process where polarized epithelial cells undergo phenotypic changes and convert into mesenchymal cells, (Kallui and Weinberg 2009; Marmai *et al* 2011; Perez *et al* 2011, Sohal *et al* 2011 and Lomas *et al* 2012) in response to both intracellular and extracellular signalling events, (Wang *et al* 2012) The completion of EMT is signalled by the degradation of the underlying basal

membrane and the formation of a mesenchymal-like cell which can then migrate away from the epithelial layer where it originated, (Kalluri and Weinberg 2009)

EMT is a key mechanism that is well described in embryogenesis (Blanco *et al* 2004), in embryonic development epithelia are highly plastic and can switch during between epithelia and mesenchyme, (Kalluri 2009) it is also recapitulated metastatic malignant disease (Blanco *et al* 2004) especially associated with S100A4 expression in non-small cell lung cancer, and as part of the repair process in renal disease following tissue injury, (Kalluri 2009; Kisseleva and Brenner 2008 Sohal *et al* 2011). In adult tissues EMT represents a rare event during wound healing (Kisseleva and Brenner 2008).

Kalluri (2009) reported that EMT during embryogenesis occurs in an immunologically privileged setting driven by internal molecular programmes and proposed that immune privilege might be necessary for the EMT associated with embryo development, whereas inflammation and epigenetics are likely inducers of EMT in the pathological settings of organ fibrosis and cancer progression; a likely scenario during chronic inflammatory conditions such as COPD.

There are three classifications of EMT based on biological functions and expressed biomarkers:

1. Embryonic development- neither causes fibrosis nor induces an invasive phenotype.
2. Wound healing, tissue regeneration following injury and ceases once inflammation is attenuated but if it becomes unregulated it leads to fibrosis and eventually disruption to the organ. EMT of cells associated with chronic inflammation have been noted to continue to exhibit epithelial-specific morphology and molecular markers such as cytokeratin but also express α SMA and S100A4. These cells are more likely to represent the intermediate stages of EMT but will ultimately lose all their epithelial characteristics and become fully mesenchymal.

3. Cancer progression; genetic and epigenetic changes affect oncogenes and tumour suppressor genes that can generate invading and metastasizing cells resulting in life-threatening cancer manifestations. These cells will pass through EMT to different extents with some cells retaining epithelial traits and others becoming fully mesenchymal. The full spectrum of signalling events remains unclear.

Each type of EMT represent a distinct biological process that possess a common set of underlying genetic elements and biochemical processes.

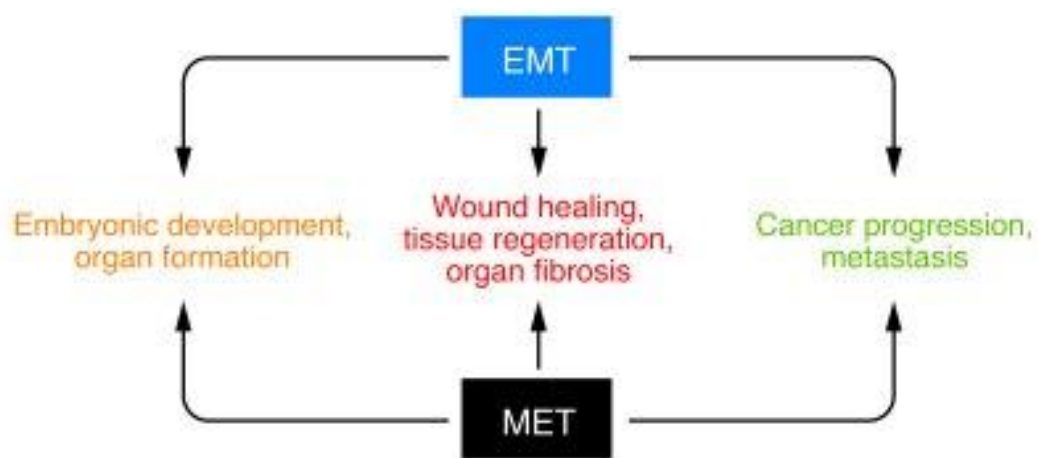


Fig. 1.5 Outline of the various forms of EMT processes that are currently widely accepted.

In lung fibrosis, alveolar damage is an important initial event in the development of pulmonary fibrosis. When the degree of lung injury is mild, damaged tissues will normally be repaired. More severe damage causing large amounts of cell death may not be repairable and lead to irreversible lung damage and pulmonary fibrosis (Ohbayashi *et al* 2014).

MYOFIBROBLAST PROGENITORS

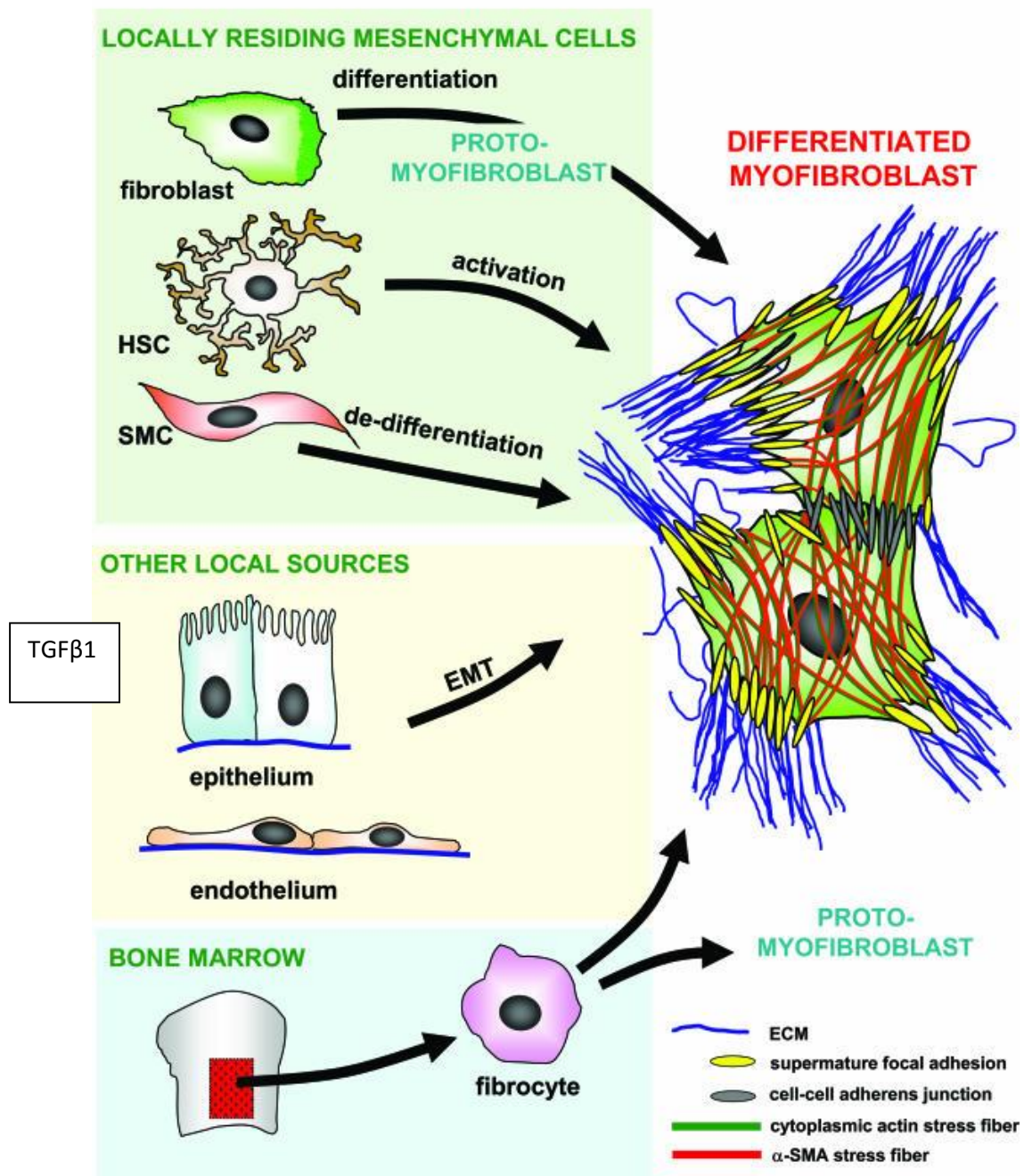


Figure 1.6 One cell, multiple origins: Diagram depicting myofibroblast progenitors, in liver – hepatic stellate cells (HSCs) Smooth muscle cells (SMC). (Hinz *et al* 2007)

Tissue fibrosis can occur in response to steroid treatment, radiation and chemotherapeutic agents (e.g. bleomycin, methotrexate). This is also true for the lung parenchyma, in particular type II pneumocytes which are radiosensitive, (Pass et al 1996).

In fibrotic lung diseases it is thought that fibrotic thickening and remodelling of airways is due to defective and uncontrolled repair to the damaged epithelia the EMT process; which is linked with the over production of ECM. The process of EMT is characterised by the decrease in expression of epithelial associated genes such as E-cadherin and cytokeratin (Perez *et al* 2011 and Pirozzi *et al* 2011). E-cadherin is a transmembrane protein expressed by epithelial cells (Didon *et al* 2010); it is an adherent junction protein that plays a critical role in mediating homo-typic calcium dependant cell-cell adhesion (Blanco *et al* 2004), by the formation of homodimers with E-cadherin proteins on adjacent cells. It has a crucial role in cell adhesion, polarity and epithelial tightness forming the paracellular barrier and subsequent maintenance in tissue architecture, (Kisseleva and Brenner 2008; Naydenov *et al* 2012). Thus the hallmark of EMT is associated with the downregulation of E-cadherin, (Nightingale *et al* 2004).

Cytokeratin is found in the cell cytoplasm where it forms filaments that add to the complex intra-cytoplasmic cytoskeleton, connecting nuclear and plasma membranes implicating an aid in cellular signalling and organisation, (Kim and Coulombe 2007 and Windoffer *et al* 2011). Cytokeratin is widely accepted as a useful epithelial marker and has been used to distinguish between fibrotic and non-fibrotic cells (Sohal *et al* 2011). It has been characterised in epithelial cell lines that when undergoing EMT there is a loss of cytokeratin and E-cadherin due to reduced transcription and it is replaced with fibrotic markers such as alpha smooth muscle actin (α SMA); and that it is not present in fibrotic cells (Kalluri and Neilson 2003).

In contrast with a decrease in expression of epithelial associated genes there is a transcriptional induction of mesenchymal cell associated genes such as vimentin,

fibronectin, collagen, N-cadherin and α SMA. Vimentin is an intermediate filament protein, which is a cytoskeletal component responsible for maintaining cell integrity that plays a significant role in support and organise the position of organelles in the cytosol (Krimpenfort *et al* 1988 and Rogel *et al* 2011). Rogel *et al* 2011 shows that it is required for cell motility, as they observed that expression of vimentin intermediate filaments are required during periods of increased cellular migration; this is linked to cell activation by TGF- β 1. In addition to this, vimentin also promotes collagen synthesis by stabilising collagen mRNA, (Challa and Stefanovic 2011). Fibronectin is the main adhesion protein that links collagen fibres and ground substance (an amorphous gel-like substance present in ECM) and promotes cell migration required for wound healing, (Alberts *et al* 2002; Tortora and Derrickson 2009).

When secreted into the extracellular space, collagen forms into high-order polymers called collagen fibrils often aggregating into larger cable-like bundles linking to each other and to other components in the ECM. It also allows for fibroblast mobility and as the cells crawl over it, they pull the fibres causing it to contract, (Alberts *et al* 2002) a typical process that occurs in wound closure and tissue remodelling, (Chen *et al* 2007).

It has been suggested that cigarette smoke inhibits the growth and functionality of lung fibroblasts grown from patients with emphysema, (Nobukuni *et al* 2002) however more recently it has been found that CSE did not affect fibroblast activity to deposit collagen, (Larsson-Callerfelt *et al* 2013). This shows that an increased amount of tissue injury occurs through smoking, induces the recruitment of inflammatory leukocytes, that in turn facilitates the process of EMT and excessive production and deposition of collagen, (Kisseleva and Brenner 2008; Tanjore *et al* 2009).

N-cadherin is a transmembrane glycoprotein that mediates homophilic interactions between neighbouring cells and is considered a path finding molecule involved in invasion and migration. The homophilic binding at the trailing edge of fibroblasts have been suggested to provide clues in defining the direction of migration, it also has been suggested that it may stimulate invasion by forming adheren junctions

linked to the cytoskeleton, (De wever *et al* 2004). ASMA is the actin isoform typically associated with vascular smooth muscle cells which plays an important role in the contraction of fibrous connective tissue, (Hinz *et al* 2001). In fibrosis α SMA is the underlying molecule that constitutes stress fibres and enhances cell traction forces. It was shown that an increase in its expression enhances fibroblast contractility; the cells use these traction forces to organise ECM, maintain cellular shape, probe the surrounding physical environments and generate mechanical signals, (Chen *et al* 2007).

Desmin is a cytoplasmic protein associated with muscle cells. it has been shown that desmin knockout mice can go through myogenesis unaffected which suggests that once the fibrotic cells has used the desmin i.e. for cell contractility it may down regulate this marker and replace it with the other contractile protein α SMA, (Costa *et al* 2004). It has also been shown in mouse carcinoma cell studies that they acquire the mesenchymal phenotype and express desmin amongst other mesenchymal markers (Kalluri and Weinberg 2009)

In fibrosis, desmin can be expressed in α SMA-positive fibroblastic spindle shaped cells and it is also present in the smooth muscle of bronchial walls (Lofdahl *et al* 2011). Pilling *et al* 2009 did not detect any expression of desmin in fibrocytes derived from human peripheral blood or normal human dermal fibroblasts; interestingly these cells only had variable expression of α SMA. Taking into account data found by Lofdahl *et al* (2011) these findings seem to support evidence of desmin and α SMA being co-expressed in a range of cell types.

Rock *et al* (2011) proposed that expression of α SMA in myofibroblasts is dynamic over the course of fibrosis, with higher levels early in progression. Lofdahl *et al* 2011 found that COPD patients had significantly higher α SMA expression than smokers and non-smokers which was associated with the overall obstruction of the airways. Obstruction has also been linked with large fibrotic areas of the lung including thickened blood vessels (Santos *et al* 2002 and Karvonen *et al* 2013). Pilling *et al*

(2009) describe variable expression of α SMA in both fibroblasts and fibrocytes which may be due to deviation in fibroblast origins; either EMT derived or which have been recruited to sites of lung injury.

From studies in a range of conditions including liver fibrosis, phenotypically EMT is characterised by a loss of epithelia architecture and functional polarity, the loss of their defined cell-cell contacts (cell adhesion) both of which are involved in the change of morphology. They become spindle shaped, show a front-rear polarity, weak cell-cell contacts and resistance to apoptosis, which is similar to activated fibroblasts. They also possess an increase in cell mobility and invasiveness which aids the movement to the lamina propria, (Marmai *et al* 2011; Pirozzi *et al* 2011; Sohal *et al* 2011; Lomas *et al* 2012 and Wang *et al* 2012).

The process of EMT in the lung requires further characterisation, however it may be a similar process of a shift from epithelial (E-cadherin) expression to mesenchymal (N-cadherin) calcium ion-dependant adhesion accompanied by the gain of other mesenchymal markers such as α SMA, (Lomas *et al* 2012).

Furthering understanding of how EMT contributes to COPD pathology will guide future research and therapies. For example, active airway EMT in COPD could potentially relate to subsequent fibrotic activity in the sub-epithelial tissue, however, it may simply reflect the severity of COPD pathology, (Sohal *et al* 2011).

The pathological conversion of small airway epithelia into fibroblasts has been proposed as one of the mechanisms for increased fibroblast numbers and has been demonstrated to occur in lung alveolar epithelial cells, in COPD and pulmonary fibrosis (Câmara and Jarai 2010).

Understanding what regulates EMT processes will also be useful in developing anti-fibrotic therapies. TGF- β 1 is an abundant cytokine present in a number of organs undergoing fibrosis; this cytokine is the central mediator of the fibrotic response (Leask and Abraham 2004) and has been implemented in fibrotic diseases such as hepatic fibrosis and COPD, (Pass *et al* 1996). It promotes wound healing and repair via promotion of fibroblast ECM deposition and subsequent contraction (Leask and

Abraham 2004) and under pathological conditions it orchestrates cross talk between parenchymal, inflammatory and collagen expressing cells.

TGF- β 1 is not expressed constitutively but is strongly upregulated during injury and inflammation (Kisseleva and Brenner 2008). Several reports describe TGF- β 1 having a crucial role in EMT, (Wang *et al* 2012) and is shown to be the single most potent inducer of EMT in lung epithelial cells, (Perez *et al* 2011; Wang *et al* 2012). TGF- β 1 is also required for fibroblast activation which is linked with fibrosis progression, (Allen *et al* 2002); however this is dependent on TGF- β being in its active form (Gauldie *et al* 2002). TGF- β signalling will be introduced in detail in chapter 4.

It has been proposed that IL-6 may be responsible for initiating EMT processes in various human cancer cell lines, but the role of TGF β -1 may come secondarily when fibroblasts produce both TGF- β 1 and IL-6, (Ohbayashi *et al* 2014).

Of note there is a dramatic rise in plasma TGF β levels in cancer patients treated with radiotherapy, implicating this treatment may actually promote EMT and induce or worsen any underlying lung fibrosis. Cancer treatment with methotrexate (a mild immunosuppressant) may also induce fibrosis via EMT; *in vitro* studies of A549 cells exhibited raised IL-6 and TGF β responses to this treatment (Ohbayashi *et al* 2014).

Host immune responses to aetiological factors affecting the lung appear to lead to uncontrolled remodelling damaged tissue by either restoring or replacing epithelium in the addition of the synthesis of new ECM in an attempt to return the tissue to its original state, (Hogg *et al* 2004). It is proposed that the constant exposure to toxic gases and particles, in cigarette smoke, initiates chronic inflammatory responses which in turn leads to the over synthesis of ECM and epithelial trans-differentiation into fibroblasts. Collective pathologies may lead to airway scarring, airway thickening and loss of elasticity and emphysema, (Wynn 2008). COPD exacerbations linked with recurrent bacterial infections that fail to clear, may have a role in EMT processes: bacterial products may interact with epithelial cells and induce intracellular signalling via Toll-like Receptors (TLRs) to secrete fibrogenic cytokines (Kisseleva and Brenner 2008).

1.8 Aims and Objectives

Clearly there is growing evidence that EMT processes are responsible for lung fibrosis pathology however the extent of this is not yet clear in relation to COPD. Characterising the EMT phenotype in COPD lungs will further enhance understanding of the pathological processes in fibrosis, and direct future research in this area. Current information available on lung fibrotic events has come from studies conducted on limited number of samples/patients; this study aims to develop this information using a larger patient cohort which will enable both airway obstruction linked with COPD, and smoking history to be considered separately.

Hypothesis

We propose that with a decrease in epithelial markers found within the lung there will be an increase in fibrotic marker, working within an inverse relationship. Suggesting EMT driven fibrosis within the lung parenchyma.

Aims

Specifically:

Chapter 3 is an immunohistochemical characterisation study of human lung tissue for biomarkers linked with EMT and epithelia. Fresh tissue is used from a cohort of subjects that have never smoked (non-smokers, NS) current smoker (CS), ex-smokers (EXS) and COPD patients that currently smoke (CCS) and COPD ex-smokers (CEX).

Chapter 4 develops the findings of the IHC characterisation study using laser capture to observe genes expressed in EMT tissue in comparison to epithelia tissue.

Chapter 5 is an *in vitro* tissue culture study of human lung fibroblast cytokine responses when exposed to pro-fibrotic conditions. Our culture system advances many other tissue culture systems in two ways 1) using human lung fibroblasts; 2) by using stretch forces to simulate movement linked with breathing and pathology

of emphysema in combination with cigarette smoking (cigarette smoke extract generated from research grade cigarettes).

Chapter 2

Materials and Methodologies

2.1 Human Lung Tissue

2.1.1 Lung tissue sample origin

Lung tissue used was from patients already undergoing lung resection for removal of cancerous tissue. Samples used were taken far distant from the cancerous tissue in the resected lung, by trained pathologists qualified to make the decision. Each patient gave informed written consent and was recruited at Wythenshawe Hospital, Northwest Lung Centre, Manchester. The study received ethical approval from South Manchester committee. RGEC reference REP10/077

2.1.2 Patient Demographics

All research was conducted as a blind study. Demographics were received once results were obtained. Each chapter of work has its own specific demographic table and will be included in that work.

Table 2.1 All subject demographics

Variable	COPD										Controls						
	Total					Current Smoker					Ex-Smoker			Total	Current Smoker	Ex-Smoker	Non Smoker
Gold Stage	ALL	3	2	1	unknown	ALL	3	2	1	unknown	ALL	2	1	0	0	0	0
Subject Number	25	2	17	3	3	16	2	2	9	3	9	8	1	46	16	18	12
Sex	M=14 F= 11	M= 2 F= 0	M= 8 F= 9	M= 2 F= 1	M= 2 F= 1	M= 8 F= 8	M= 2 F= 0	M= 1 F= 1	M= 3 F= 6	M= 2 F= 1	M= 6 F= 3	M= 5 F= 3	M= 1 F= 0	M= 20 F= 26	M= 7 F= 9	M= 9 F= 9	M= 4 F= 8
Age	67.16 ±6.76	68 ±9.9	68.1 8 ±7	60.33 ±3.1	67.67 ±4.61	67.94 ±5.57	68 ±9.9	60 ±4.24	69.7 8 ±4.3 2	67.67 ±4.61	65.78 ±8.7	66.38 ±9.1	61	67.53 ±11.2 7	61.06 ±10.06	70.61 ±10.93	69.58 ±12.42
Pack year History	47.73 ±19.8 7	49 ± 12.7 3	45.5 3 ±17. 6	56.17 ±44.5 7	50.93 ±5.25	53.8 ±15.3 2	49 ± 12.7 3	76.55 ±37.8 3	50.7 2 ±9.1 1	50.93 ±5.25	39.94 ±23.2 2	39.69 ±23.2 1	15	26.51 ±25.9 6	39.69 ±21.58	32.28 ±25.29	0
FEV₁ % Predicted	64.95 ±8.97	76.5 ±3.5 4	63.8 7 ±8.6 3	69.27 ±11.5	59.03 ±2.63	67.18 ±8.06	76.5 ±3.5 4	75.4 ±6.22	65.9 9 ±6.9 7	59.03 ±2.63	60.99 ±9.58	61.49 ±10.1 2	57	96.40 ±17.2 5	89.63 ±20.36	98.48 ±16.13	104.71 ±12.18
FEV₁/FVC Ratio, %	55.64 ±8.07	50.2 8 ±6.6 6	55.6 1 ±8.4 3	62.83 ±7.16	52.19 ±3.9	55.7 ±6.57	50.2 8 ±6.6 6	60.66 ±8.61	56.9 8 ±6.5 1	52.19 ±3.9	55.52 ±10.6 9	54.02 10.44	67.1 7	73.58 ±10.3 2	69.74 ±11.26	76.14 ±7.9	74.41 ±11.25

2.1.3 Processing of biopsies of lung resection

Working in aseptic conditions (Cellbind class II safety cabinet); the lung tissue was washed in sterile Phosphate Buffered Saline (PBS) to remove any excess blood. This was then drained (excess PBS via gently squeezing each piece on the side of the bijou) and transferred to a petri dish, where the tissue was then sliced into four sections; one piece was inflated with neutral buffered formalin and then immersed in 3mL of formalin for tissue fixation ready for further processing, two pieces were snap frozen in liquid nitrogen and then stored at -80°C and the final piece was used for the isolation of primary fibroblasts.

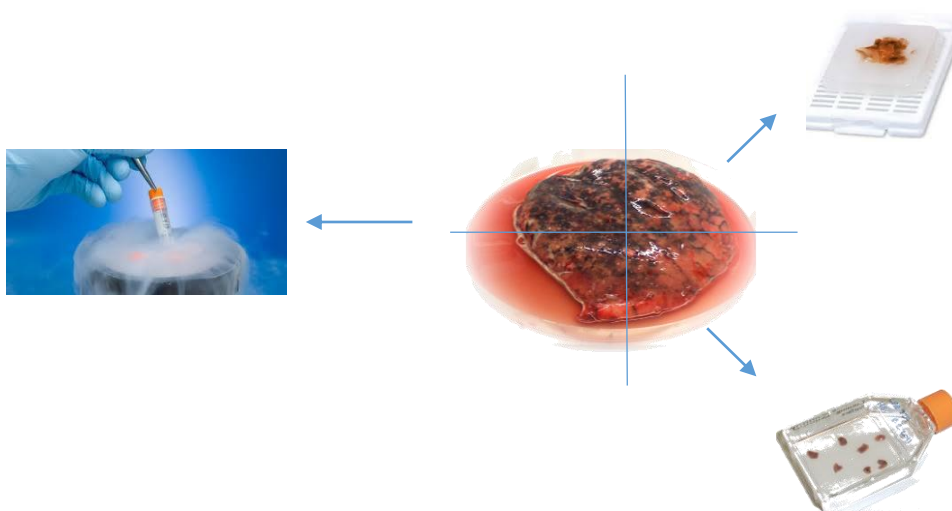


Figure 2.1 Processing of human lung tissue biopsy

2.1.4 Processing of formalin fixed tissue

The following methodology enables the indefinite storage of normally degradable tissue at room temperature. Married with an identification number linked to demographics, FFPE tissue provides an important resource for many years of research.

Using sterile forceps the fixed tissue was carefully removed from formalin and placed into a tissue cassette; that were labelled with pencil for tissue identification. The cassettes were then placed into a tissue basket and connected to the pre-programmed Leica TP1020 automatic tissue processor. The tissue was placed

through a series of stages (under vacuum) that dehydrate, clear and impregnate the tissue. Dehydration: tissue was put through stages of ethanol 50%, 70% 90% and 100% for 1 hour each, this is to remove the residual fixative and H₂O contained within the tissue. Clearing: the tissue was then submerged into two buckets of histo-clear for 1 hour each replacing the alcohol with a fluid that is miscible with embedding medium. Impregnation: The basket was then transferred to molten paraffin (60°C) for 2 x 1.5 hours; this replaces the clearing fluid with the embedding medium.

2.1.5 Tissue Embedding

Once finished the cassettes (containing processed lung tissue) was removed from the automated tissue processor. When the tissue is impregnated with paraffin it must be constrained within a solid block of paraffin that provides a rigid supporting structure for sectioning of the tissue. Using forceps the paraffin-impregnated tissue was transferred into individual moulds containing a small amount of molten paraffin, quickly the tissue was aligned so that the 'face' to be sectioned lies parallel to the bottom of the mould. Once aligned the assembly was placed on a cold plate, partially solidifying the paraffin to hold the tissue in place. The mould was then filled with more molten paraffin and the plastic cassette was fitted onto the mould. The filled assembly was then placed on a cold plate to cool and harden for ~30 minutes. When set, the paraffin blocks (containing tissue) were stored until required for sectioning.

2.1.6 Tissue Sectioning (Microtomy)

Using a Lecia RM2125 microtome with disposable steel knives, the selected lung patients FFPE tissue was sectioned. The embedded tissue 5µm thick where cut forming a ribbon of serial sections. The ribbon was carefully transferred from the blade edge (using forceps and a fine brush) and floated in a water bath set to 10°C below paraffin melting point, 50°C. This was left for ≥ 30 seconds and then individual sections were gently separated. The individual sections was attached to pre-labelled polysine adhesion slide (Menzel-Gläser, Thermo Scientific, Braunschweig)

- featuring a permanent bio-adhesive material and then transferred to a hotplate (set at paraffin melting point, 60°C) and was left to dry for at least 4 hours for maximum tissue adhesion.

2.1.7 Positive control cells for IHC

Positive controls were made from cell lines with known characteristics to confirm the chosen antibodies were suitable for the immunohistochemical study, as patient tissue collected can be variable depending on disease state, medications and genetics.

2.1.8 Formalin fixed paraffin embedded cell suspension

The following method is adapted from Morgan 2001. The normal human lung fibroblasts ((NHLFs) CC-2512, Clonetics®, Lonza Wakersville Inc.) and human lung adenocarcinoma epithelia cell line (A549 Cells, Sigma Aldrich, Gillingham UK) were grown, harvested and counted according to normal methods, see following cell culture methodology. The cells were washed in pre-warmed sterile PBS and then centrifuged at 400g for 10 minutes to create a cell pellet. The PBS was removed and discarded appropriately; the cell pellet was resuspended in neutral buffered formalin at room temperature at a concentration of 2×10^6 cells/mL. This was left standing for 2 hours to allow the cells to sediment out of solution. Once the cells had collected in 1-1.5mL volume the bulk of the formalin was removed with a pastette and discarded. The remaining 1.5mL cell suspension was then transferred to a microcentrifuge tube for further sedimentation, 20-30 minutes. The remainder of the formalin was removed which left a pellet with ~50µL volume. The microcentrifuge tube containing the cell pellet was placed into a 60°C water bath for 2-3 minutes. Using a warmed plastic pastette and equal amount of pre-made 4% agarose gel was added to the pelleted cells and holding the level of the mixture just below the surface of the water, it was gently mixed by taking it up and extruding it twice. The cell-agarose suspension was then quickly transferred to a mould (1mL syringe (internal diameter 4mm) with bottom removed), extruding carefully to avoid air bubbles. The mix was left to set at room temperature for 5 minutes then was

transferred to 4°C for a further 2-3 minutes. The mixture was then extruded from the mould by slowly pushing the syringe plunger and was cut to the required size, forming cell-agarose plugs.

The plugs were placed in 10% formalin for 2 hours at room temperature with occasional agitation. Using a spatula the plugs were removed from formalin and then dehydrated through a graded series of ethanol 10-100% (in steps of 10%) for 1 hour at each step; the cell-agarose plugs were left in 70% ethanol overnight. The plugs were then cleared through histo-clear II for 2 hours (with several changes) and then impregnated in molten paraffin for a further 2 hours. The impregnated plugs were then mounted into paraffin blocks, stored and sectioned as methods seen above.

2.1.9 Cell Cytospins

A technique used to gently deposit a small circular monolayer of cells onto a glass slide for further downstream experiments such as immunohistochemistry.

Cryopreserved NHLFs and A549s were defrosted by placing the vial (containing NHLFs/A549s in freezing mix (10% Dimethyl Sulfoxide (DMSO) in FBS) in 37°C water bath for 2 minutes; the contents were then added to 20mLs of pre-warmed RPMI, drop by drop, for dispersion to reduce toxicity from DMSO contained in the freezing mix. The cell suspension was centrifuged for 10 minutes at 400g. The supernatant was discarded and cells re-suspended in 1mL of supplemented RPMI; using 1:1 ratio of cell suspension and trypan blue, cells were counted utilising a haemocytometer. Once counted the cell suspension was made up to 0.5×10^6 cells/mL, with supplemented RPMI.

The sample chambers were assembled, cytoclip, filter card (dampened with PBS, to allow for regulated absorption of suspension media), and cytofunnel with a labelled polysine adhesion slide. These were placed within the cytocentrifuge and 100µl of the cell suspension was loaded into the cytofunnels; these were spun at 700rpm for 5 minutes with low acceleration. The slides were carefully removed from the sample chamber assembly and air-dried on the bench for 5 minutes. The deposited layer of cells were fixed to the slides by immersing the slides into a series

of ethanol concentrations, 50% -1 minute, 75% - 2 minutes, 90% - 3 minutes and 100% for 5 minutes.

The slides were then stored until IHC procedure.

2.1.10 Immunohistochemistry (IHC)

IHC is a biochemical assay that enables the detection of antigens (proteins) present within cells of a tissue section; this is achieved by antibodies binding specifically to the antigen of interest. A peroxidase enzyme bound secondary antibody general to all antibodies of the same species as the primary, binds to the untagged primary antibody. A coloured product forms at the antibody binding site when a chemical reaction occurs catalysed by the peroxidase enzyme.

IHC standard single label immunoperoxidase

All antibody optimisation was conducted on one lung patient (LP#624) whose demography is COPD ex-smoker. Once pre-treatment and antibody dilution were determined all positive controls and study lung tissue were stained using the same timings and procedure.

Day 1

The tissue sections were cleared by immersing the slides in two stages of histoclear II 2x 5 minutes and then were rehydrated by immersing them in a range on ethanol concentrations 100% - 5 minutes, 90% - 3 minutes, 75% - 2 minutes and 50% for 1 minute, subsequently placed under running water for 5 minutes. The samples stained for E-cadherin were pre-treated with the appropriate buffer by placing the slides in a coplin jar inside an appropriate heatproof beaker filled with the relevant buffer. The assembly was placed into a pressure cooker for 30 minutes; this was then left to cool on the bench for a further 20 minutes; all other slides required no pre-treatment step. The slides were left under running water for 5

minutes to wash away any residual buffer and each slide was gently dried using tissue paper avoiding the tissue section.

Each tissue section was drawn around using an immunostaining PAP pen to providing a hydrophobic barrier to keep subsequent reagents localised to the tissue section.

The tissue was blocked in Vectastain® Horse normal serum (Elite, PK-6100 Mouse IgG, Vectastain® ABC Kit; Vector, Peterborough, UK) or Vectastain® Goat normal serum (Elite, PK-6102 Rabbit IgG, Vectastain® ABC Kit; Vector, Peterborough, UK) made in PBS, for 30 minutes at room temperature. The block was gently tipped off and the relevant slides were incubated with a range of dilutions (dependant on data sheets and previous concentrations used in literature) of the specific primary antibodies (see Table 2), diluted in normal serum overnight at 4°C in a humid box to avoid evaporation.

Day 2

All of the slides were placed in a coplin jar and washed for three minutes three times in 1x TBS with tween, (3 x 3 minutes). Following this Vectastain® Anti-Mouse/Anit-Rabbit IgG Biotinlayted secondary antibody made in normal blocking serum and PBS was added to the lung tissue and was incubated at room temperature for 30 minutes. TBS washing step, 3 x 3 minutes was repeated followed by endogenous peroxidise blocking, by adding 3% hydrogen peroxide in methanol to the lung tissue and incubated at room temperature for 30 minutes. After this the slides were placed under running water in the coplin jar for 5 minutes followed by washing in TBS for a further 5 minutes. The pre-made (in PBS) Elite Vectastain® ABC A&B reagent was added to the slides and incubated at room temperature for 30 minutes, followed by a TBS washing step (3 x 3minutes) and the subsequent addition of 3,3-Diaminobenzidine (DAB (ImmPACT™ peroxidise substrate kit, SK-4105; Vector, Peterborough, UK)). The positive staining of the cells (brown colouration) were monitored under light microscope, when there were sufficient staining the reaction was stopped by immersing the slides in a coplin jar filled with deionised H₂O, they were then placed under running water for 5 minutes.

The tissue was counterstained with a nucleic stain haematoxylin, achieved by immersing the slides in the haematoxylin solution for 25 seconds; excess was rinsed off and slides were left under running water for 5 minutes. The tissue was then dehydrated by running through a series of ethanol concentrations (same as fixation) and cleared through histoclear for 10 minutes. Finally the slides were left to air dry and then mounted with a cover slip and DPX (Sigma-Aldrich, UK) in preparation of examination using microscopy technique.

The optimal staining dilution and conditions was achieved for all of the antibodies, this can be seen in table 2.2. These conditions were used for subsequent staining of the relevant lung tissue and positive controls, method same as above.

Table 2.2 Table of optimal dilution and staining conditions for each antibody

Primary Antibody	Mono-clonal	Clone / Cat No	Source	Dilution	Pre-treatment	Cell target and Localisation
E-cadherin	Mouse	G10	Insight Biotech-	1:100	Tris-EDTA	Epithelia: Membrane
Cytokeratin	Mouse	AE1/AE 3	Dako	1: 200	-	Epithelia: cytoplasmic
Desmin	Mouse	D33	Dako	1:100	-	Mesenchymal cells: cytoplasmic, may show fibrillar aspect
S100A4	Rabbit	A5114	Dako-cytomation	1:2500	-	Mesenchymal cells: nuclear, cytoplasmic and/or membrane staining
Alpha Smooth Muscle Actin	Mouse	61001	Progen	1:100	-	Mesenchymal Cells: Cytoskeletal
CD68	Mouse	PG-M1	Dako	1:500	-	Macrophages: cytoplasmic
CD45	Mouse	2B11+P D7/26	Dako	1:300	-	Lymphocytes: Membrane but some cytoplasmic may occur
Neutrophil Elastase	Mouse	NP57	Dako-cytomation	1:500	-	Neutrophils: cytoplasmic

2.1.11 Haematoxylin & Eosin and Collagen staining

Haematoxylin & Eosin (H&E) is a basic histological stain that utilises acidic and basic binding principles. Haematoxylin is a blue stain that binds to DNA complexes within the nucleus where eosin counterstain binds to eosinophilic structures such as intracellular and extracellular proteins e.g. cytoplasm, staining them pinky-red.

The collagen stain used is Masson's Trichrome, this a three stage stain also used in histology. It distinguished collagen from surrounding tissues by staining collagen-blue, fibrin-pink, erythrocytes-red and nuclei- dark blue/black,

These two stains were performed using the Lecia CP023 auto slide stainer. Reagents were supplied by Fisher Scientific UK. Both protocols were pre-programmed and are as follows.

H&E tissue staining

The rack containing relevant slides was taken into an oven station for 13 minutes to facilitate de-waxing of tissue samples. The samples were then cleared by being dipped into two steps of histo-clear II for 5 minutes each. The tissue was rehydrated by being submerged in two buckets containing ethanol 100% for a total of 3 minutes followed by being dipped water for 1 minute. The nuclei contained within the tissue were stained by being submerged in haematoxylin for 1 minute followed with a washing in water for 30 seconds. The tissue was then placed in a counter stain Eosin 1% for 10 seconds and washed in water for a further 30 seconds. The tissue was dehydrated in 95% and 100% ethanol for 1 minute each and cleared through histo-clear II 2 x 5 minutes. Finally the slides were left to air dry and then mounted with a cover slip and DPX in preparation of examination using microscopy technique.

Collagen staining

The first stage of this stain (Masson's trichrome protocol A) the slides were put through the oven station (13.5 minutes) and then in two pots of histo-clear II (5

minutes each) to de-paraffinise the tissue samples. They were then rehydrated by dipping them in 100%, 95% and 70% ethanol for 1 min 30 sec each. Once finished the slides were taken from the rack and placed into pre-heated (56°C) bouins solution for 1 hour; to re-fix the tissue samples that improves staining quality. The slides were then transferred back into the auto stainer rack and put through the Masson's trichrome protocol B. The slides were washed in water 10 minutes to remove yellow colour of the bouins solution. To stain the nuclei they were placed through weigert's iron hematoxylin for 10 minutes, followed by washing in water for a further 10 minutes and distilled water for 30 seconds. The cytoplasm contained within the tissue was then stained by placing through biebrich scarlet-acid fuchsin for 10 minutes, then the mordant phosphomolybdic-phosphotungstic acid for 10 minutes and finally stained for collagen by submerging in aniline blue for 5 minutes. The slides were washed briefly by dipping in distilled water for 10 seconds and differentiated in acetic acid 1% for 4 minutes. The tissue was then quickly dehydrated in 95% ethanol for 1 minute and then cleared by placing through two pots of histo-clear II for 5 minutes each. Finally the slides were left to air dry and then mounted with a cover slip and DPX in preparation of examination using microscopy technique.

2.1.12 Microscopy Imaging

Brightfield images were captured from the stained/immune-stained tissue using the x20 objective lens on a Nikon Eclipse 50i microscope combined with AxioCam ICc1 digital camera. The image analysis software AxioVision LE 4.8.2 (Zeiss) allowed computer controlled image acquisition. Five contiguous framed images were taken of each slide capturing the same lung structures for each sample set between markers; which was white balanced and averaged to minimise noise. The resulting images obtained (24 bit and 1388 x 1038 pixels) were subsequently labelled and placed in dedicated project folders until analysed.

2.1.13 Image analysis

Images were analysed with ImageJ (Rasband WS, NIH, Bethesda, MD). All images had background subtracted to correct any shadowing or colour effects obtained during the imaging process. Following this the image was segmented (separate stains) to avoid cross contamination that may affect the quantification of the individual stains.

Colour Deconvolution

The image analysis technique used is based on converting the images into a format that allows maximal separation of collagen/DAB-stained pixels from background tissue. Each original 24 bit image was split into 3 8 bit images (red, green and blue that form conventional digital imaging), determined as colour deconvolution (CD). CD was developed by Ruifrok and Johnston 2001 through deconvolution mathematics that determined the relative contributions of each of the RGB colour channels to the collagen/DAB staining. It utilises the following vectors for the RGB channels: for colour Blue (channel 1) haematoxylin, 0.65, 0.70 and 0.29; for colour Red (channel 2) DAB 0.27, 0.57 and 0.78; and for colour green (channel 3) 0.71, 0.42 and 0.56. Thus in the example of staining with a single antibody and chromogen, the un-mixing of chromogen from the counter stain generates a partition of DAB and haematoxylin signals, (Krajewska et al 2009).

The imaging software was then used to set the thresholds used for automated DAB selection and quantification of percentage area stained. Once determined (see methodology below) the threshold selects the area of tissue that falls within the set threshold optical density allowing this area to be measured. The results were then recorded in excel spreadsheet. Thirty six slides were analysed per marker resulting in 1620 total images analysed in this study. Positive leukocyte staining was analysed by counting cells stained and total cells present; results were expressed as percentage of cells present.

Thresholding

Threshold values were set after examining preliminary images of tissue stained at the same time as the slides used in this study; S100A4 positive controls, five slides equalling twenty-five images. The determined threshold values were then held at a constant in the analysis of all relevant images.

Analysis

Positive controls

Using the set threshold values the percentage area stained was determined for each of the positive control images. These were used to statistically determine if the experimental repeatability was robust, allowing statistical comparison between markers in the patient groups.

Manual selection

Manual selection is a technique widely used in the field of IHC assessment and is accepted in the scientific community as accurate for the classification of an area stained positively with the DAB chromogen.

For confirmation that the method of CD is accurate and robust to use, the positive control images were double checked using the manual selection methodology. To allow for any variations in counting of positively stained areas in the tissue, this method was repeated on 3 different days.

These values were then compared values acquired by CD computer assisted analysis, allowing determination of accuracy of this method.

2.2. IHC Statistical Analysis

2.2.1 Cell counts

Manual cell counts were conducted for the leukocyte markers CD45, CD68 and NE using image J software.

2.2.2 Manual counting versus Colour Deconvolution

The mean (\pm SEM) of percentage area stained was determined of each image for both techniques. These results were compared and the closer the values indicated exact agreement with manual analysis. The closer the values are to zero, the more accurate the method. Difference testing was performed using a paired student's t-test. Statistical significance was defined as $p \leq 0.05$. Analysis was carried out using GraphPad InStat version 3.06 (GraphPad Software, Inc., San Diego, CA, USA).

2.2.3 Analysis of Patient samples

Data is not normally distributed. Between overall demographic group samples (COPD vs. Healthy) a Mann-Whitney U test was performed and between individual demographic group samples (COPD current smoker, COPD ex-smoker, healthy current smoker, healthy ex-smoker and healthy non-smoker) comparisons were assessed by one way Kruskal-Wallis ANOVA. Where significant, Mann-Whitney U tests were performed for two-way comparisons. $p \leq 0.05$ was considered significant for all analysis. Analysis was carried out using GraphPad InStat version 3.06 (GraphPad Software, Inc., San Diego, CA, USA).

2.3 Laser Capture Microdissection (LCMD)

LCMD is a method used for the isolation of microscopic cells/tissues from one another. In this study it has been used to isolate epithelial and fibrotic regions from the same lung tissue for downstream qRT-PCR analysis to identify the differential EMT and pro-inflammatory gene expression between the two groups.

2.3.1 Cryosectioning

Tissue used for this study was from APG group catalogue; these samples had been snap frozen within approximately 1 hour of patient's surgery and therefore had the best chance of higher quality non-degraded RNA. The samples were removed individually from -80 °C storage and placed within the cryostat to acclimatise to -20 °C for 10 minutes prior to O.C.T embedding and subsequent sectioning. Snap frozen tissue was orientated in a plastic mould and O.C.T cryo-compound was enfolded around it; a chuck was placed onto the top and the assembly was left at -20 °C to set.

Using a cryostat microtome the selected lung patient's samples was sectioned at -20°C. The tissue was cut to 7µm thick (6 per patient) where each individual section was carefully mounted on a pre-UV treated (slide sterilisation, 30 minute treatment) steel frame slides with PET membrane (1.4 µm, Lecia microsystems, Milton Keyens, UK). These were stored at -80°C and transferred to Wythenshawe hospital on dry ice). Prior and in between sectioning patient samples, the disposable blade was changed, gloves changed and all equipment was sterilised using 70% ethanol.

2.3.2 Rapid IHC

Fibrotic areas were identified using a modified rapid immunoperoxidase immunostaining method Fend *et al* (1999), Simpson *et al* (2011) and Lecia protocols.

Individually the mounted frozen tissue sections (7 µm), were taken from -80 °C and immediately fixed in ice cold methanol for 3 minutes, blocked with 1.5% Vectastain® Goat normal serum (Elite, PK-6102 Rabbit IgG, Vectastain® ABC Kit; Vector, Peterborough, UK) made in PBS for 3 minutes, and incubated with the primary antibody S100A4 (Dakocytomation) diluted 1:2500 in blocking serum for 10 minutes on ice. The sections were washed briefly with TBS with tween, incubated with 5% Vectastain® Anit -Rabbit IgG Biotinlayted secondary antibody made in normal blocking serum and PBS for 3 minutes on ice followed by being washed briefly with TBS with tween. Any endogenous peroxidise was blocked by adding 0.3% hydrogen peroxide in 0.3% normal serum in PBS to the lung tissue and incubated on ice for 3

minutes. After this the slides were placed DEPC-water for 30 seconds followed by washing in TBS with tween for a further 30 seconds. The pre-made (in PBS) Elite Vectastain® ABC A&B reagent was added to the slides and incubated on ice for 3 minutes, followed by brief washing in TBS with tween. The samples were then visualised using DAB (ImmPACT™ peroxidase substrate kit, SK-4105; Vector, Peterborough, UK) on ice for a maximum of 3 minutes. The positive staining were monitored under light microscope, when there were sufficient staining the reaction was stopped by immersing the slides in a coplin jar filled with cold deionised DEPC-H₂O. Sections were dehydrated in a graded series of ethanol 70% (10 seconds), 95% (10 seconds), and 100% (5 minutes). Then cleared through two stages of histoclear (3 and then 5 minutes) and then air-dried. Sterile solutions made with diethyl pyrocarbonate (DEPC)-treated water and RNase-free conditions (RNaseZap® and autoclaved treated) were used throughout this protocol.

2.3.3 Lazer Capture Microscope Dissection (LCMD)

Once dried the slides were mounted into a slide holder compatible with the laser capture microscope (LCM). Brightfield images were captured to create a slide overview from the immune-stained tissue using the x5 objective lens on the LCM (DM6000B) combined with Camera -Lecia DFC300FX; this was done by utilising the LCM software Lecia LMD 6000 Laser micro-dissection version 6.5.0 that allowed computer controlled image acquisition as well as full microscope and laser control. Either fibrotic tissue (indicated by brown staining) or epithelial tissue (non-stained tissue) was selected by computer assisted drawing around the tissue (faint blue line in, Figure 2.1), being careful to leave a wide margin around the cells. Using 40x/0.60 XT CORR objective lens specific tissue was cut out using the Laser – Crylas FTSS 355-50 (Fig 2.2) and the specimen dropped into the pre-selected eppendorf below (Fig 2.3). Each tissue slice was worked on for a maximum of 30 minutes after staining. Once finished the relevant eppendorfs was carefully removed from the system and 20µl of extraction buffer (Arcturus® Picopure® RNA isolation Kit, Applied Biosystems, Life Technologies Corporation, Carlsbad, USA) was added to each cap and heated to 42°C for 30 minutes to solubilise capture material, then

stored at -80°C before transportation on dry ice back to the University of Salford - 80°C freezer.

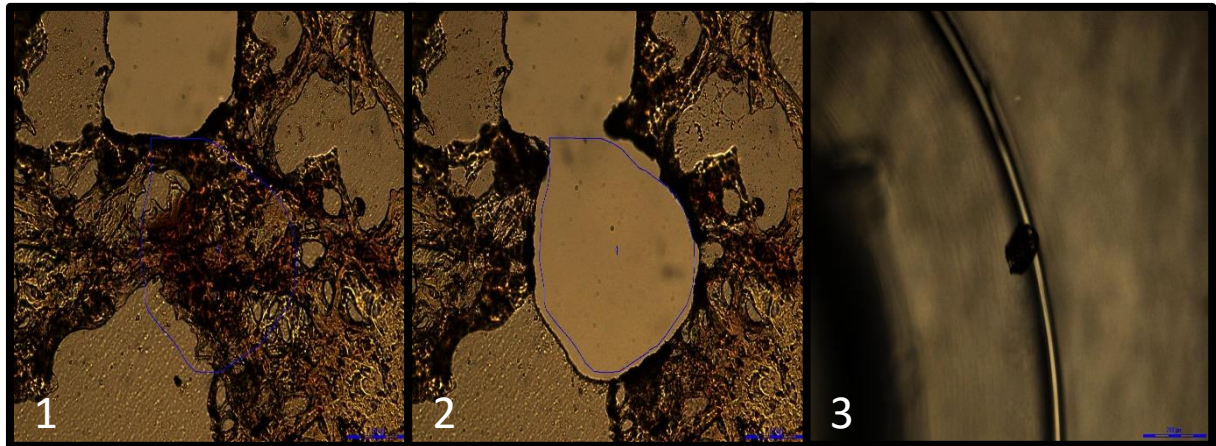


Figure 2.2 Image depicts example of fibrotic tissue isolation via LCMD, LP431. Image 1&2 x400, image 3 x50.

2.4 QRT-PCR

2.4.1 RNA isolation

The following RNA isolation procedure was conducted at room temperature (unless otherwise stated) under RNase-free conditions, using the Arcturus® Picopure® RNA isolation Kit, (Applied Biosystems, Life Technologies Corporation, Carlsbad, USA).

The LCM isolations as well as whole tissue serial sections (adjacent to sections used for LCM) solubilised in extraction buffer, were quick thawed by placing in a 37°C dry bath then homogenized by vortexing for 30 seconds to 1 minute, ensuring all tissue is lysed and to disrupt genomic DNA by mechanical shearing. The multiple eppendorfs per sample were collected into one eppendorf and these were centrifuged at 3000xg for 2 minutes and avoiding any pelleted material the supernatant was transferred to a new eppendorf containing an equal amount of 70% EtOH. This was mixed well by shaking vigorously for 30 seconds and quick spun to

get the entire sample to the bottom. The sample was added to pre-conditioned (according to manufacturer's instructions) purification columns and left to stand for 2 minutes for RNA binding, before centrifugation at 100xg for 1 minute immediately followed by 2 minutes at 13,000xg. The flow through was carefully discarded using a pipette. Wash buffer 1 (W1) was then added to the column and centrifuged for 1 minute at 8000xg. To minimise genomic DNA contamination, a DNase digestion step (using RNeasy - free DNase set (50) Qiagen, Hilden, Germany) was incorporated conducted according to manufacturer's instructions. After the DNase treatment 40µl W1 was pipetted onto the membrane and centrifuged at 8000xg for 15 seconds. A 100µl of Wash buffer 2 (W2) was added to the column and using a fresh collection tube the purification column was inverted and rolled between the fingers for 2 minutes to eliminate residual salts stuck to the tube. The assembly was centrifuged at 8000xg for 1 minute followed by a further 100µl of W2 added and subsequent centrifugation for 3 minutes at 13,000xg. The column was transferred to a kit-provided 0.5mL eppendorf and 11µl of elution buffer added directly to the membrane then incubated for 1 minute before centrifugation at 2000xg and 13,000xg for 1 and 2 minutes respectively. The elution step was repeated using the 11µl flow through. Samples were transferred to ice and the purity and concentration of the RNA was assessed using a NanoDrop 1000 spectrophotometric analyser. The isolated RNA was then stored at -80°C prior to downstream applications.

2.4.2 RNA Gel Electrophoresis

This technique was used for RNA detection and quality assessment by looking for clear 18s and 28s bands. A sample of the RNA was taken and placed into a gel that is placed under an electric current. RNA is negatively charged and travels towards the anode through the gel; the gel acts as a sieve which impedes the migration of the RNA in proportion to its mass (its mass is generally proportional to its charge). The length of the RNA is generally determined by its migration (against a known size RNA ladder) as mass is approximately related to chain length.

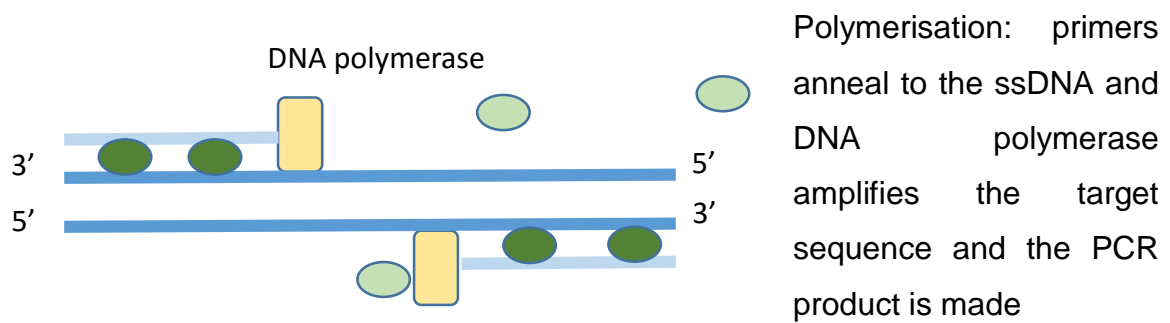
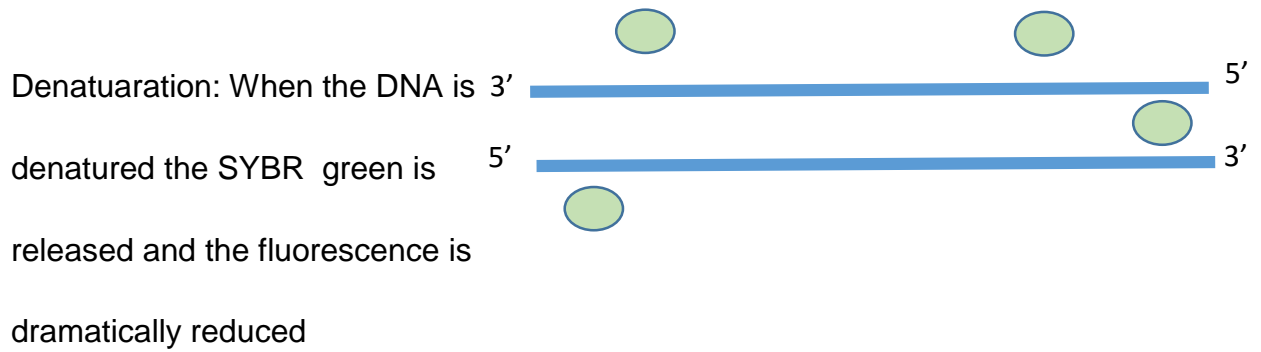
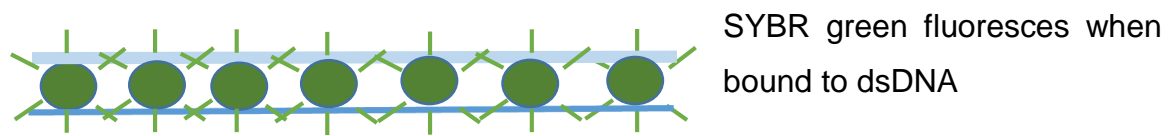
A denaturing gel was made for this technique to assist the unfolding of RNA allowing for RNA migration through the gel. The 1.5% formaldehyde-agarose gel was made as follows: 0.6g of agarose was dissolved in 33.5mL ddH₂O in a microwave using a conical flask with cotton wool bung for 30 second bursts. The conical flask was gently swirled ensuring all agarose was dissolved, following this 5mL of 10x MOPS buffer (MOPS 200mM, Sodium acetate 50mM, EDTA 10mM dissolved in 0.1% ddH₂O and adjusted to pH7) was added and mixture swirled. Mixture was then transferred to a fume hood and 9mL of formaldehyde was added to the cooling molten agarose. The RNA detection solution GelRed 10,000x (Biotum Inc.) was added at 1:10,000 and mixed thoroughly. The gel was then poured into a casting tray and taped to remove any bubbles. A comb was then placed into the gel and left to set at room temperature for a minimum of 30 minutes. Whilst waiting for the gel to set the samples were prepared. Equal volumes of the RNA samples and 2x RNA loading Dye (Thermo Scientific™, Leicestershire, UK) were mixed and heated to 70°C for 10 minutes using a dry bath. These were then transferred to chill on ice until ready to load into the gel. Once the gel was set the comb was removed and gel transferred to the electrophoresis tank filled with 1x MOPS buffer. The samples and RNA hyperladder (Thermo Scientific™, Leicestershire, UK) were added in equal volumes and gel ran at 100 volts for 1 hour or until loading dye had travelled 2/3 of the gel. Once finished the gel was transferred to UV trans-illuminator for gel visualisation.

Sterile solutions made with diethyl pyrocarbonate (DEPC)-treated water and RNase-free conditions (RNaseZap® and autoclaved treated) were used throughout this protocol.

2.4.3 Two Step Quantitative reverse transcriptase- polymerase chain reaction (qRT-PCR)

QRT-PCR is a technique that is commonly used to detect gene expression. It allows for the comparison of gene expression between groups i.e. healthy vs. diseased tissues or treated vs. non-treated samples, enabling people to get a better understanding of how cells/tissues react and open up potential targets or cellular mechanisms to for disease treatments. There are a few different types of fluorescent

DNA probes that can be used in qRT-PCR such as SYBR green, TaqMan and Molecular beacons. The probe used in this study was SYBR green it utilises the unspecific binding to double stranded DNA and emits light upon excitation. The more dsDNA produced has a higher amount of SYBR green bound giving a higher intensity of fluorescence upon excitation (Fig2.2).



When polymerisation is complete the SYBR green attaches to the dsDNA, resulting in a net increase in fluorescent intensity.

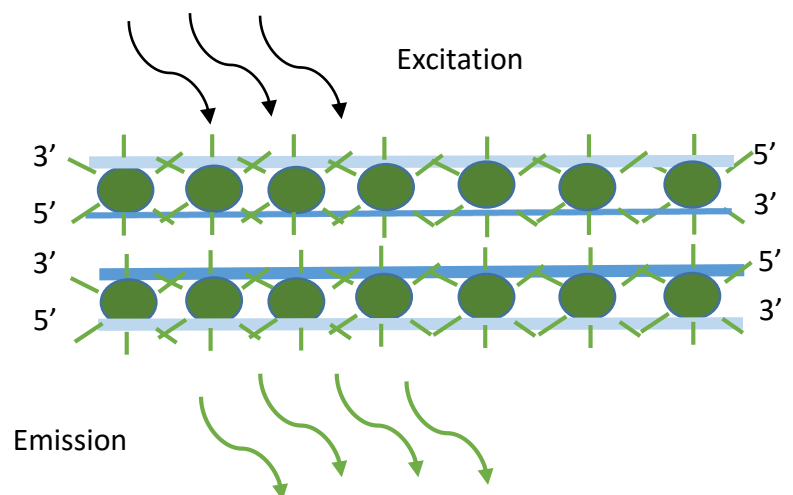


Figure 2.3 Overview of Syber-Green qPCR

Primers targeting expression of TGF β 1, IL-6, SMAD3 and SNAI1 were obtained from Primerdesign Ltd, Southampton, UK, GAPDH and 18S was selected as the housekeeping gene for normalization of results and both used in all real-time analyses.

First step Reverse Transcriptase Reaction

Reverse transcription assays were performed manually using a dry heat block using total RNA that was isolated as methodology above. Conducted using nanoscript™ 2 reverse transcriptase kit (Primerdesign Ltd, Southampton, UK). This methodology itself uses a two-step system. Doing it in two steps reduces the formation of secondary structures within the RNA template thus allowing the reaction nanoscript enzyme to move freely along the RNA template.

The first is the annealing step in which the RT primer is annealed to the denatured RNA; a 1:1 mixture of both Oligo-dT primers and Random nonamer primers and 1 μ l was added 9 μ l of the RNA template in a thin walled PCR tube and heated to 65°C for 5 minutes then immediately transferred to ice to cool.

The second step is the reverse transcription of RNA into cDNA called the extension step. cDNA synthesis is initiated at the primer binding sites, creating a budding cDNA strand whilst simultaneously degrading the original RNA template, (Primerdesign LTD, 2014). A master mix was made following manufacturer's instructions and 10 μ l was added to the samples on ice. This then was vortexed and pulse spun before incubated at 25°C (room temperature) for 5 minutes then 42 °C for 20 minutes. The reaction was then heat inactivated by heating to 75°C for 10 minutes. Once complete the synthesised cDNA was made to 0.8ng/ μ l by the addition of the relevant volume of RNase- DNase free H₂O and stored at -20°C until needed for real time PCR.

Second step

The second step RT-PCR was performed using the Precision™ 2x qPCR mastermix kit with SYBR® green & low Rox (Primerdesign Ltd, Southampton, UK) which was used in conjunction with primers that were designed by Primerdesign Ltd. All samples and PCR reagents were defrosted and prepared on ice. For each 20µl real-time PCR reaction 4ng * of cDNA (5µl) template was added relevant wells of a MicroAmp® Optical reaction96 well plate and 15µl of the relevant mastermix made from manufacturer recommended quantities of Precision™ 2x qPCR mastermix 10µl, Primer (300nM) 1µl and RNase/DNase free water 4µl. the plates were sealed using optical adhesive films and centrifuged at 3500rpm for 5 minutes to ensure all reaction mix was at the bottom of each well. For every plate run two controls were also included per primer these were no template controls (NTC) water added instead of cDNA and No –reverse transcription control (No-RT) control without the addition of reverse transcriptase to the RNA template, to remove and possible residual genomic DNA contamination.

The PCR products for the chosen targets were amplified using Applied biosystems 7500 fast system & 7500 fast software v2.0.6 with amplification protocol settings of an enzyme activation hot start, 95°C for 10 minutes then 50 cycles of 15 second denaturation 95 °C, and data collection at 60°C for 60 seconds with post PCR run melt curve to prove primer specificity.

The Genbank accession numbers and forward (F) and reverse (R) primers are as follows:

TGFβ1 (NM_000660)	F-CACTCCCACTCCCTCTCTC R-GTCCCCTGTGCCTTGATG;
IL-6 (NM_000600)	F-GCACAAAACAACCTGAACCTT R-ACCTCAAACCTCCAAAAGACCA
SMAD3 (NM_005902)	F–GGCTGCTCTCCAATGTCAAC R- ACCTCCCCTCCGATGTAGTA;
SNAI1 (NM_005985)	F- GGCAATTTAACAATGTCTGAAAAGG R- GAATAGTTCTGGGAGACACATCG;

The internal controls used Homo sapien glyceraldehyde-3-phosphate dehydrogenase (GAPDH) and Homo sapien 18S genes also provided by Primer design Ltd, Genbank accession number not provided.

(4ng*) detection limits determined from A549 and NHLF positive control total RNA dilutions primer qPCR efficiencies. The above experimental procedure was carried out using a 6 point dilution range of initial RNA concentration 50, 25, 10, 5, 4 and 2ng.

2.5 Cell culture

2.5.1 Isolation of fibroblasts lung resection biopsies

Working in aseptic conditions (Cellbind class II safety cabinet); lung tissue was sliced into small pieces (~2mm x 2mm) using forceps and scalpel. The pieces of lung tissue was then washed in sterile PBS, drained (excess PBS via gently squeezing each piece on the side of the bijou) and transferred into a T25 cellbind flask. The lung pieces where gently pressed into flask ~10mm apart and left for ≥3 minutes to adhere to the plastic. A small amount (generally 3ml) of supplemented RPMI was added to the flask, just enough to cover the lung tissue, and was incubated 37°C, 5% CO₂. Supplemented (10% (v/v) foetal calf serum, 2mM L-glutamine, 100U/mL penicillin, 100µg/mL streptomycin and 0.25µg/mL Amphotericin B (Fungizone) (Thermo Fisher Scientific Inc) RPMI 1640 (Lonza, Biowhittaker®) was changed every 2-3 days to replenish nutrients and to reduce infections. Fibroblasts were observed to be growing from the lung tissue which could range from 6- 8 days to 4 weeks, dependant on fibrotic state of the lung tissue being used. The flasks then became 100% confluent within a further 2 weeks. When cells where 70-90% confluent, the lung tissue was removed and destroyed in Virkon; the remaining Fibroblasts where trypsinized and frozen for future experiments.

2.5.2 Growing cell lines

Working in aseptic conditions (Cellbind class II safety cabinet); the NHLFs and A549s defrosted (as mentioned above) and were added to a 550mL tissue culture flasks with filter lid (CellStar) with sufficient (25mL) supplemented RPMI and swirled gently to ensure an even spread of cells around the lower flask surface. They were incubated for several days (with supplemented RPMI changed every 2-3 days) at 37°C, 5% CO₂ for growth. Once 70 -90% confluent the cells were trypsinized (split). Trypsin-EDTA (GIBCO, Invitrogen™, Paisley, UK) was applied to the cells as in method below to dissociate cells from flask.

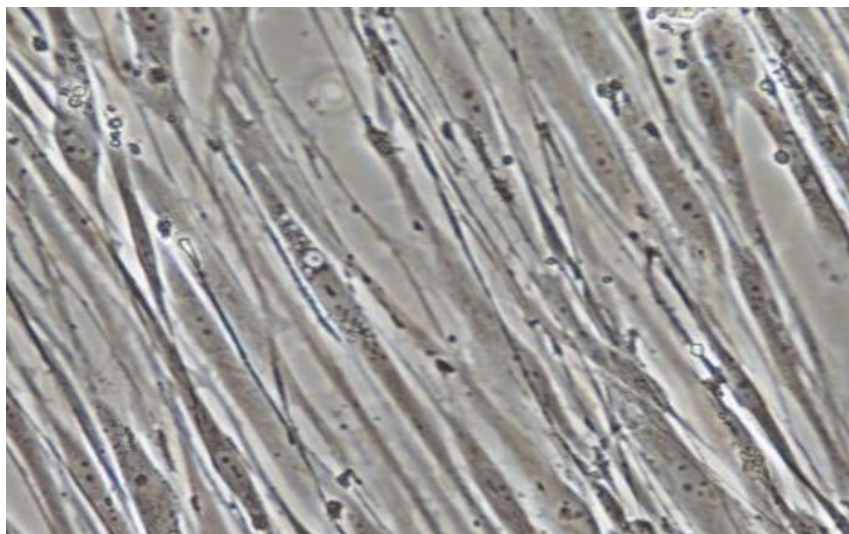


Figure 2.4 depicts NHLFs at 70% confluence grown in 550mL tissue culture flask. X200 magnification

2.5.3 Trypsinization

Supernatant (supplemented RPMI) was removed using a 10mL plastic strippette. To remove residual RPMI the cells were then washed by gently adding pre-warmed sterile PBS. Carefully all of the residual RPMI and PBS were removed as any residual FCS in the supplemented RPMI would have deactivated the Trypsin. 5ml of Trypsin-EDTA was added to the flask and incubated at 37°C, 5%CO₂ for 5 minutes. The flask was gently tapped to dislodge the monolayer of cells and 5ml

(equal amount) of supplemented RPMI was added to neutralise the Trypsin - stopping all enzymic reactions. The cell suspension was transferred into a 50ml falcon and centrifuged for 10 minutes at 400g. The supernatant was discarded and cells re-suspended in ≥ 1 ml of supplemented RPMI for counting, using trypan blue and a haemocytometer.

The cells either went into cryopreservation (stored in liquid nitrogen), were plated on collagen coated plates for the required experiment/s or reseeded in flasks for farming up the numbers. Plated and reseeded cells were incubated at 37°C with a 5% CO₂ atmosphere for a minimum of 2 hours for cell adherence but generally left overnight.

2.5.4 Collagen coating of plates

This procedure was used for primary cell cultures to prevent the cell contracting into sphere structures.

Under sterile conditions the 96 flat bottom plates were coated 50 μ l/well, using collagen type I; from rat tail (Sigma Aldrich) of 100 μ g/mL dissolved in 0.01M HCL. The plates were incubated for a minimum of 1 hour at room temperature in a Class II cabinet, the remaining fluid was carefully aspirated off and each well was rinsed three times with sterile PBS. The plates were kept at 4°C for a maximum of 12 hours before seeding of cells.

2.5.5 Cell Cryopreservation

Once the cells have been counted they were re-pelleted by centrifugation, 400g for 10 minutes. The RPMI was removed and the cells were re-suspended in freezing mix (FCS with 10% DMSO) at $\leq 10 \times 10^6$ /mL. Quickly the cell-freezing mix mixture was transferred to a pre-labelled cryotube (1mL per tube), which were then placed into a cryo 1°C freezing container “Mr Frosty” containing isopropyl alcohol, allowing a -1°C/min cooling rate required for successful cell cryopreservation. The Mr frosty was placed into -80°C for 24 hours and then the cryotubes were transferred into a liquid nitrogen cryobank, for long term storage.

2.5.6 Immunocytochemistry to characterise cell lines

Using cytopins and IHC methodologies previously explained; cytopins were made of a select group of the primary cells to look at the marker expression of the isolated cells to compare against the NHLF and A549 cell lines.

2.6 Cell culture experiments

2.6.1 Generation of Cigarette Smoke Extract

The apparatus was set up as illustrated in (Figure 2.4). To produce 100% Cigarette Smoke Extract (CSE), one IR3F Kentucky research cigarette was burned and the cigarette smoke was bubbled through 25mls of supplemented RPMI, (held in a 50ml falcon tube) and exhaust fumes were passed through a 2% Savlon solution. The cigarette was burnt for approximately 5 minutes at 15rpm until it reached ~2mm from filter tip. The optical density of each CSE produced was measured at an absorbency of 320nm using a Jenway Genova spectrophotometer, for monitoring smoke batch generation.

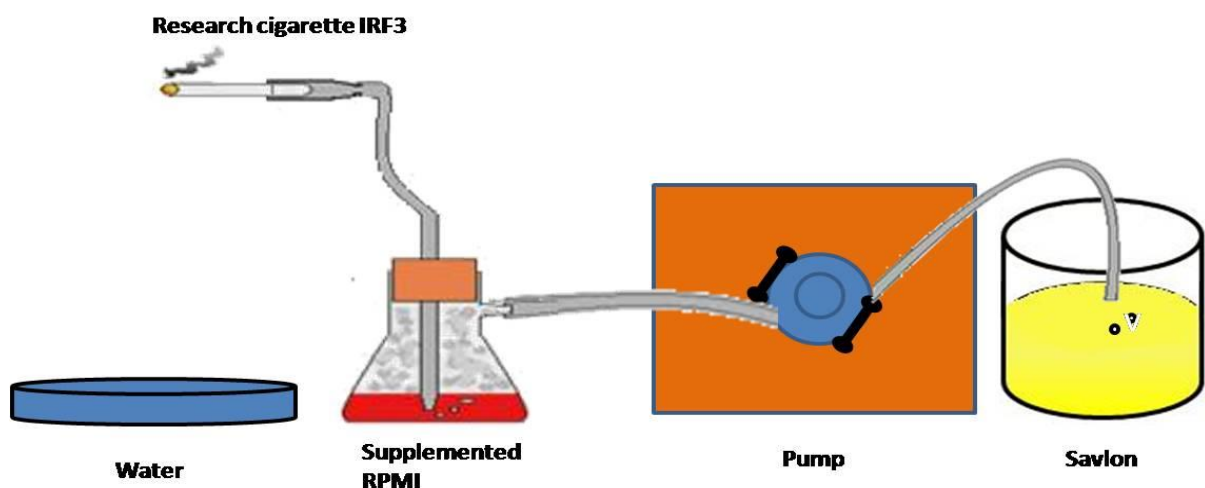


Figure 2.5: Illustration of production of CSE. This was achieved by bubbling cigarette smoke of 1 research cigarette (IRF3) through 25mL of supplemented RPMI. Suction via pump and exhaust fumes passed through a 2% savlon solution.

The first cell culture experiments, was exposing the NHLF, 16HBE140 and A549 cell lines and primary fibroblasts to CSE over a set time course, determined by experiments previously done by the FIR group. The cells were plated out at 100,000 cells/well on a 96 well plate, incubated overnight at 37°C and 5% CO₂ for cell adherence. Before experiment the cells were washed with 100µl of pre-warmed RPMI to remove any non-adherent cells. The 100% CSE was generated as stated in the above method and a serial dilution was performed to produce a range of concentrations 1-50%. The CSE (200µl) was added to the cells, (0 % (RPMI), 1%, 5%, 10%, 20% and 50%) and incubated for 4, 6, 24 and 48 hours. At the set time points supernatants (190µl or 100µl with subsequent MTT experiments) were removed and stored at -80°C prior to analysis.

2.6.2 Exerting stretch forces on Cultured Cells

The second stage of the experiments was exposing some primary cells to 10% CSE in the addition to 20% stretch. The cells were plated out at 800,000 cells/well and incubated overnight as stated previously; they were exposed to four conditions 0% CSE with no stretch, 0% CSE with stretch, 10% CSE with no stretch and 10% CSE with stretch. Cells were seeded on a Bioflex collagen 6 well plate was attached to the circular shaped loading posts on the FX-4000T™ FlexerCell® Tension Plus™ which is a computer-regulated bio-receptor that applies strain to cultured cells, (Ning and Wang 2007; Ochoa *et al* 2008). “Strain is the measure of the degree of stretch and is expressed as the percentage of the change of the cell length to resting cell length” (Ochoa *et al* 2008).

Stretching imposed was cyclic of 30 cycles/ minutes with 1:1 stretch/relaxation ratio had triangular waveforms and biaxial elongations (stretching) of 20% (frequency of 0.5Hz) that was applied to the cells cultured under incubated conditions (37°C and 5% CO₂) for 4, 6, 24, and 48 hours. Supernatants were collected at specific time points and stored at -80°C prior to ELISA analysis.

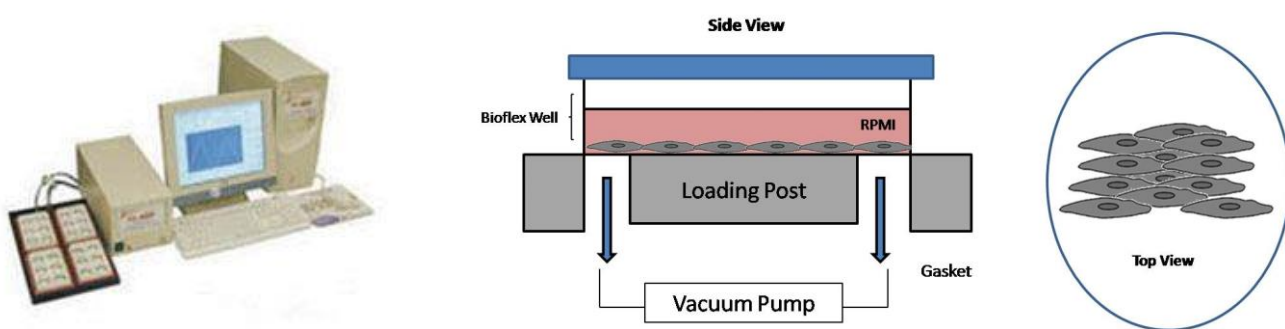


Figure 2.6: Image to the left is the FX- 4000T FlexerCell Tension plus system.

Diagram to the right shows the principles of operation of the FX- 4000T FlexerCell Tension plus system Picture adapted from Ning and Wang 2007.

2.7 MTT Assay for cell viability

A 3-[4,5-dimethylthiazol-2-yl]-2,5diphenyl tetrazolium bromide ((MTT)Life Technologies, Paisley, UK) assay is a colourmetric analysis experiment for determination of cell viability. It works by the cells ability to reduce the yellow tetrazolium ring via activity of mitochondrial dehydrogenase and convert into insoluble purple formazan crystals, (Ahmed et al 2013). This experiment was used to determine whether there was a reduction in formazan crystal formation after exposure to CSE over time and/or concentration.

After the specific time point removal of supernatant, from the CSE experiments 50µl of MTT solution (3mg/mL in sterile PBS) was added to the remaining 100µl of supernatant. The plates was then re-turned to the incubator 5% CO₂ and 37°C for a further 3 hours. The MTT-supernatant mixture was then aspirated from each well and 200µl of DMSO added to dissolve the formazan crystals that have formed. The optical density of each well was read using a microplate reader set to 540nm with wavelength correction set to 690nm.

2.8 Bender 11plex assay

The levels of Interferon- γ (IFN γ), Interleukin-1 β (IL-1 β), Interleukin-2 (IL-2), Interleukin-4 (IL-4), Interleukin-5 (IL-5), Interleukin-6 (IL-6), Interleukin-8 (IL-8), Interleukin-10 (IL-10), Interleukin-12 p70 (IL-12 p70), Tumor Necrosis Factor alpha (TNF α) and Tumor Necrosis Factor alpha beta (TNF β) from a selection of early cell culture CSE and CSE with stretch experiment supernatants (NHLF, A549, 16HBE140, LP#624 and LP#635) were measured using a Human TH1/TH2 11plex kit (BMS810FF, Bender Medsystems GmbH, Vienna, Austria) a quantitative bead based analyte detection system achieved by flow cytometry. This was conducted to determine the best targets to study on a larger scale via sandwich ELISA.

The test procedure was conducted following manufacturer's experimental procedure using cytometer tubes. All assay buffers, biotin-conjugate, bead mixtures and standards were prepared according to manufacturer's instructions. Standards were reconstituted with dH₂O giving a concentration of 400ng/mL for all except IL-8 that was 200ng/mL. A seven point serial dilution of the kit standards was prepared by diluting the top standard 1:20 with 1%BSA in PBS buffer giving a top standard of 20,000pg/mL and 10,000pg/mL for IL-8; followed by 1:3 serial dilutions.

FACS bead mixture was prepared in reagent dilution buffer (RDB) and the working concentration of 11 primary antibodies was added; 25 μ l of the bead mixture was added to 25 μ l of each sample, standards and blank tubes. Following this 50 μ l of the biotin-conjugate mixture was added to all tubes, thoroughly mixed and incubated at room temperature for 2 hours, being protected from light by being covered with aluminium foil. All tubes were washed twice by the addition of 1mL of assay buffer and spun down at 200xg for 5 minutes and the careful discardure of supernatant leaving 100 μ l of liquid in each tube. Following this 50 μ l of the streptavidin-PE solution was added to all of the tubes and incubated for 1 hour covered at room temperature. Washing procedure was repeated and 500 μ l of assay buffer was added to each tube then taken for Facs analysis running standards and blacks first using linear scales. Flow cytometric analysis was conducted on BD Canto with Diva software.

2.9 Enzyme-Linked Immunosorbent Assay (ELISA)

In response to external stimuli such as being exposed to CSE (pathological stimuli) or stretch (physiological stimuli), cells release a cocktail of cytokines and chemokines in response to the injury, to initiate a rapid repair response. These responses can be affected by a number of factors such as disease state or previous exposure to the external stimuli. ELISAs are used to measure the amount of specifically chosen analytes (Cytokine/chemokine) released by the cells, they work on the premises that a surface bound specific antibody binds to the specific antigen (e.g. IL-6) in the supernatant and through the binding of an enzyme linked secondary antibody and with the addition of a substrate a colour change is formed directly proportional to the amount of cytokine present in the sample, with quantity determined by comparison to known standards.

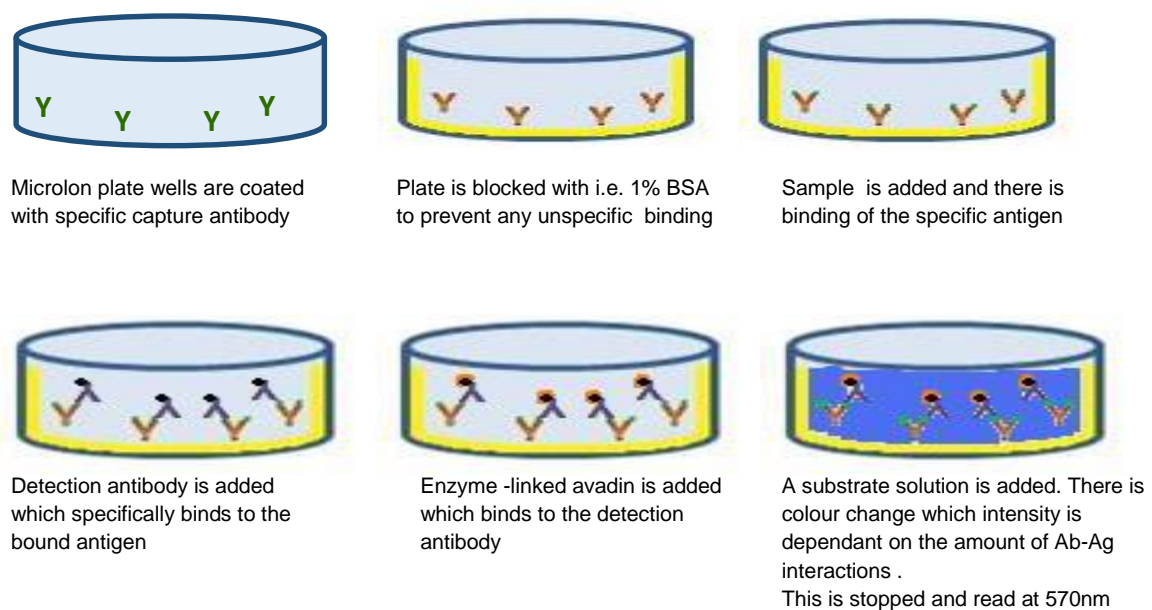


Figure 2.7 ELISA assay based on the antibody sandwich principle: Capture antibody is coated onto the well surface which captures the biomarker in the supernatant being tested. After washing a secondary antibody conjugated to detection system and enzyme causes a colour change when the substrate is added. This is read against a standard curve of known protein concentrations to quantify the biomarker in the supernatants.

The levels of IL-6, IL-8 and TGF- β 1 in the collected supernatants from the above cell culture experiments were measured using duoset ELISA development system kits from research and development systems (R&D Systems; Abingdon, UK). The assays were conducted according to manufacturer's instructions. Firstly 50 μ l/well of the working concentration of specific capture antibody (either IL-6, IL-8 or TGF- β 1) was applied to a microtiter plate and incubated at room temperature overnight; creating a solid phase. The plate was then washed 3 times with wash buffer (0.005% Tween®20) removing any unbound antibody, inverted and blotted against clean tissue paper to remove any remaining washing buffer. The plate was then blocked with 150 μ l/well of the ELISA specific Reagent Diluent (RD) and incubated at room temperature for 1 hour, to reduce nonspecific binding. Depending on specific cytokine/chemokine being assessed the samples were diluted (to avoid antibody saturation) and activated (in the case of TGF- β 1) before being added to ELISA plate. After repeating the wash step the sample, controls and standard (7 point standard curve produced using 2 fold serial dilutions) was added and incubated at room temperature for 2 hours. Following this the plates were washed as above to remove any unbound analyte and 50 μ l/well of specific detection was added and again incubated for 2 hours at room temperature. After washing the plate to remove any unbound detection 50 μ l/well of the working concentration of detection reagent (streptavidin -HRP) was added and incubated at room temperature for 20 minutes. The plate was washed as mentioned above and 50 μ l/well of a substrate solution (1:1 mixture of H₂O₂ and Tetramethylbenzidine) was added to the wells and incubated at room temperature for 20 minutes, avoiding direct light. The colour development was stopped by adding 50 μ l/well of a stop solution (1M H₂SO₄) and the optical density of each well was read and compared to the standard curve using a microplate reader set to 450nm with wavelength correction set to 570nm. Figure 2.7 gives specific conditions and ELISA high and lower limits of standards.

ELISA	Reagent Diluent pH7.2-7.4, 0.2µm filtered	Sample activation	High standard limit pg/mL	Lower standard limit pg/mL
IL-6	1% BSA in PBS	N/A	600	9.375
IL-8	0.1% BSA, 0.05% Tween 20 in TBS	N/A	2000	31.25
TGFβ1	1.4% delipidised BSA, 0.005% Tween®20 in PBS	Activated with 1:5 1N HCL for 10 minutes, then neutralisation with equal amount of 1.2N NaOH/0.5M HEPES	2000	31.25

Table 2.3 Summary of ELISA sensitivity ranges for each biomarker and the required reagent diluents needed for each assay.

Chapter 3

Investigation of EMT in human lung tissue via immunohistochemistry

3.1 Background

IHC is an important technique that is readily used across the world for research, diagnostics (D'Amico *et al* 2009) and tracking progress not only in humans but across veterinary science too. It is used for the identification of location, frequency and/or structure of amino acids, proteins, individual cells, tissues and infectious agents of interest (Matos *et al* 2010). It is achieved by the specific binding of antibodies to the antigen of interest for example E-cadherin on epithelial cells, HER2 on breast cancer biopsies allowing the interpretation of distinct observations and diagnostics that are undeterminable by simple conventional stains such as haematoxylin and eosin. The strength of using IHC over other techniques is that it allows the study and observation of biomarkers within intact tissue; whereas biomarker study using westerns, flow cytometry and PCR require disruption to the tissue, (Matos *et al* 2010).

Tissue fixation prevents the autolysis and degradation of tissues and its components and essentially is the foundation step behind the study of pathology, (Howat and Wilson 2014). Due to the tissue freezing or wax embedding preparation steps additional steps of epitope retrieval, to a standard IHC protocol, is sometimes necessary. It is used to unmask antigens of interest that have either been masked through methylene bridge crosslinking/damage by neutral buffered formalin fixation (Paavilainen *et al* 2010; Howat and Wilson 2014; Warford *et al* 2014) or they fall within tight junctions, proteins are coiled or are intercellular; all of which cause the reduction in immune-reactivity of the intended target, in the case of this study E-cadherin. Epitope retrieval techniques can significantly increase target detection that can parallel the sensitivity achieved in immunohistochemical staining of fresh or frozen tissue but provides better morphological detail, (D'Amico *et al* 2009). The most commonly used epitope retrieval methods is a combination of heat mediation, first described by Shi *et al* 1991 (cited in Warford *et al* 2014), via either a microwave, pressure cooker, autoclave or water baths in addition to a retrieval solution such as sodium citrate pH6, EDTA pH8 or Tris-ETDA pH9. Some antigens can be retrieved

by any pH, others can prefer either a higher or lower pH and this plays an important role in the epitope reformation, via generation of hydrophobic and electrostatic forces that can also play a critical role in antigen/antibody binding (D'Amico *et al* 2009). In some cases it has protein digestion has been used for antigen epitope retrieval however it can cause destruction of some epitopes and tissue morphology, (Warford *et al* 2014). These methods were utilised in optimisation of these studies chosen antibodies to determine the best parameters for IHC staining of FFPE human lung tissue.

This part of the study was to further develop the understanding of fibrotic processes in the human lung especially associated with cigarette smoking and COPD. The focus was mainly driven on the determination of EMT presence in the lung via using well-established fibrotic antibodies S100A4 and Desmin or if structural fibroblasts α SMA are the main factor in lung fibrosis. These were looked at in combination with epithelial markers cytokeratin and E-cadherin. In addition to this WBC markers CD45, CD68 and NE, were assessed

Previous studies (De Vriese *et al* 2006) conducted on tissue injury related EMT, showed double positive staining of α SMA and cytokeratin in fibrotic lesions of rats with chronic uraemia. Also in relation to lung diseases as well as lung fibrosis, immunohistochemically it has been found that there is double stained cytokeratin and S100A4 of cells (13.8%) in the basal epithelium ((CCS n=6) Sohal *et al* 2011) with an increased amount of S100A4 inversely correlated with airflow limitation when comparing CCS, CEX to NS (Sohal *et al* 2010) and S100A4 positive cells in areas with morphology consistent with tissue damage from donor lung tissue epithelial after transplantation (Forrest *et al* 2005). Tanjore *et al* (2009) conducted *in vivo* experiments on rat lungs and found that only 1/3 of S100A4 positive cells were derived from epithelium post-injury and only a minority of these stained double positive for both S100A4 and α SMA, supporting hypothesis that injury induced fibrosis is derived from multiple sources and not EMT alone.

Karvonen *et al* (2013) immunohistochemically assessed α SMA on a cohort of 101 patients (CCS, CS and ns) and interestingly found that the number of α SMA positive alveolar tips with smoking is decreased when compared to non-smokers, when overall it has been seen that there is an increase of α SMA in large airways of COPD

patients when compared to controls (n=20 COPD, n=13 CS n=14 NS), (Löfdahl *et al* 2011). Santos *et al* (2002) showed that there was similar levels of α SMA and desmin expression in smokers and COPD patients.

As would be expected Santos *et al* (2002) and Kranenburg *et al* (2006) concluded that there was an increase in collagen deposition in sites of lung damage and there was higher deposition in patients with COPD when compared with controls

E-cadherin down regulation is linked to EMT in the lungs (Yao *et al* 2014) and Nagathihalli *et al* (2012) have shown that there is a direct correlation of E-cadherin downregulation with increased PYH in lung cancer patients (n=310). Supporting this Ohbayadhi *et al* (2014) showed with post-methotrexate induced injury on primary mouse epithelial and A549 cell lines there was a down regulation of E-cadherin and up regulation of α SMA, as well as co-localisation of E-cadherin and α SMA positive cells in the fibrotic foci, supporting the drive for injury induce EMT in the lungs.

In a review conducted by Barnes (2004) it states that the analysis of the inflammatory cell profile of alveoli and the small airways of COPD patients shows an increase of all the cell types implicated in COPD including macrophages, lymphocytes and neutrophils. These inflammatory cells were targeted in this study as numerous studies have been conducted looking into the pathological hallmarks of leukocytes in COPD, (Caramori and Adcock 2003; Todd *et al* 2012) and were used to validate previous studies however the main reason was to normalise any EMT staining on inflammatory cells so that the EMT markers we report are EMT derived only, reducing any false positives given by WBC staining.

My study expands on previous studies done due to larger number of EMT biomarkers used in one study, further we have used a more diverse set of patient groups; enabling us to assess links with smoking history in addition to airway obstruction.

3.1.1 Aims

The aim of this body of work was to further develop the understanding of lung fibrotic processes by assessing evidence for EMT in control subjects (non-smokers and smokers) and COPD patient lung resection tissue, using immunohistochemical techniques.

3.2 Methods

Table 3.1 Patient Demographics for immunohistochemistry study

Variables	COPD											Healthy			
	Total				Current Smoker				Ex-Smoker			Total	Current Smoker	Ex-Smoker	Non Smoker
GOLD Stage	ALL	3	2	1	ALL	3	2	1	ALL	2	1	0	0	0	0
Subject numbers	12	2	8	2	6	2	3	1	6	5	1	25	9	9	7
Sex	M=10 F= 2	M=2 F= 0	M=6 F= 2	M=2 F= 0	M= 5 F= 1	M=2 F= 0	M=2 F= 1	M=1 F= 0	M= 5 F= 1	M= 4 F= 1	M=1 F= 0	M=9 F=16	M= 4 F= 5	M= 4 F= 5	M= 1 F= 6
Age (years)	66.75 ±6.84	68 ±9.9	68.38 ±6.14	59 ±2.83	68.17 ± 7.5	68 ±9.9	72 ±2.65	57	65.33 ± 6.47	66.2 ±6.83	61	66.72 ±13.09	59.11 ±10.2	69.89 ±13.83	72.43 ±12.3
Pack year history	51.83 ±26.26	49 ±12.73	50.69 ±21.95	59.25 ±62.58	62.75 ±21.33	49 ±12.73	58.33 ±2.89	103.5	40.92 ±27.86	46.1 ±27.73	15	23.64 ±24.78	39.11 ±24.52	26.56 ±21.74	0
FEV₁ % Predicted	66.75 ±9.32	76.5 ±3.54	63.9 ±7.76	68.4 ±16.12	72.35 ±7.91	76.5 ±3.54	67.1 ±8	79.8	61.15 ±7.29	61.98 ±7.82	57	91.96 ±16.18	84.44 ±19.27	93.56 ±16.1	99.57 ±7.12
FEV₁/FVC ratio, %	56.41 ±10.65	50.28 ±6.66	55.31 ±11.31	66.93 ±0.3	56.67 ±9.78	50.28 ±6.66	57.57 ±11.14	66.75	56.15 ±12.4	53.94 ±12.47	67.17	74.33 ±11.22	70.95 ±13.6	77.17 ±9.74	75.12 ±10.1

3.2.1 IHC standard single label immunoperoxidase

All antibody optimisation was conducted from lung patient (LP#624) whose demography is COPD ex-smoker. Once pre-treatment and antibody dilutions were determined, all positive controls and study lung tissue were stained using the same timings and procedure.

Immunohistochemistry (IHC)

IHC is a biochemical assay that enables the detection of antigens (proteins) present within cells of a tissue section; this is achieved by antibodies binding specifically to the antigen of interest. A peroxidase enzyme bound secondary antibody general to all antibodies of the same species as the primary, binds to the untagged primary antibody. A coloured product forms at the antibody binding site when a chemical reaction occurs catalysed by the peroxidase enzyme.

The first step of this procedure was to determine the correct pre-treatment for each of the selected antibodies on the sectioned lung tissue samples to provide optimum membrane staining.

The buffers made and used for pre-treatment were:

- No pre-treatment
- Citrate buffer pH 6.0
- 1mM EDTA buffer pH 8.0
- Tris- EDTA buffer with Tween-20 pH 9.0

The optimal staining dilution and conditions was achieved for all of the antibodies, this can be seen in table 3.2. These conditions were used for subsequent staining of the relevant lung tissue and positive controls, method same as in Methods and materials chapter.

Table 3.2 Table of optimal dilution and staining conditions for each antibody

Primary Antibody	Mono-clonal	Clone / Cat No	Source	Dilution	Pre-treatment	Cell target and Localisation
E-cadherin	Mouse	G10	Insight Biotech	1:100	Tris-EDTA	Epithelia: Membrane
Cytokeratin	Mouse	AE1/AE3	Dako	1: 200	-	Epithelia: cytoplasmic
Desmin	Mouse	D33	Dako	1:100	-	Mesenchymal cells: cytoplasmic, may show fibrillar aspect
S100A4	Rabbit	A5114	Dako-cytomation	1:2500	-	Mesenchymal cells: nuclear, cytoplasmic and/or membrane staining
Alpha Smooth Muscle Actin	Mouse	61001	Progen	1:100	-	Mesenchymal Cells: cytoskeleton
CD68	Mouse	PG-M1	Dako	1:500	-	Macrophages: cytoplasmic
CD45	Mouse	2B11+ PD7/26	Dako	1:300	-	Lymphocytes: Membrane but some cytoplasmic may occur
Neutrophil Elastase	Mouse	NP57	Dako-cytomation	1:500	-	Neutrophils: cytoplasmic

3.2.2 Imaging

Brightfield images were captured from the stained/immune-stained tissue using the x20 objective lens on a Nikon Eclipse 50i microscope combined with AxioCam ICc1 digital camera. The image analysis software AxioVision LE 4.8.2 (Zeiss) allowed computer controlled image acquisition. Five contiguous framed images were taken of each slide capturing the same lung structures for each sample set between markers; which was white balanced and averaged to minimise noise. The resulting images obtained (24 bit and 1388 x 1038 pixels) were subsequently labelled and placed in dedicated project folders until analysed.

3.2.3 Image analysis

Images were analysed with ImageJ (Rasband WS, NIH, Bethesda, MD). All images had background subtracted to correct any shadowing or colour effects obtained during the imaging process. Following this the image was segmented (separate stains) to avoid cross contamination that may affect the quantification of the individual stains.

Colour Deconvolution

The image analysis technique used is based on converting the images into a format that allows maximal separation of collagen/DAB-stained pixels from background tissue. Each original 24 bit image was split into 3 8 bit images (red, green and blue that form conventional digital imaging), determined as colour deconvolution (CD). CD was developed by Ruifrok and Johnston (2001) through deconvolution mathematics that determined the relative contributions of each of the RGB colour channels to the collagen/DAB staining. It utilises the following vectors for the RGB channels: for colour Blue (channel 1) haematoxylin, 0.65, 0.70 and 0.29; for colour Red (channel 2) DAB 0.27, 0.57 and 0.78; and for colour green (channel 3) 0.71, 0.42 and 0.56. Thus in the example of staining with a single antibody and chromogen, the un-mixing of chromogen from the counter stain generates a partition of DAB and haematoxylin signals, (Krajewska *et al* 2009).

The imaging software was then used to set the thresholds used for automated DAB selection and quantification of percentage area stained. Once determined (see methodology below) the threshold selects the area of tissue that falls within the set threshold optical density allowing this area to be measured. The results were then recorded in excel spreadsheet. Thirty six slides were analysed per marker resulting in 1620 total images analysed in this study. Positive leukocyte staining was analysed by counting cells stained and total cells present; results were expressed as percentage of cells present.

Thresholding

A set of five individual control slides (all LP#624) were stained alongside project samples, in different processing runs of the antibody S100A4. Five contiguous framed images were taken from each slide (equalling 25 images) capturing the same lung structures. Minimum and Maximum threshold values were recorded of the manually adjusted (determined positively stained area) computer automated DAB selection and the means were used for analysis of all subsequent images.

3.2.4 Analysis

Positive controls

Using the set threshold values the percentage area stained was determined for each of the positive control images. These were used to statistically determine if the experimental repeatability was robust, allowing statistical comparison between markers in the patient groups.

Manual selection

Manual selection is a technique widely used in the field of IHC assessment and is accepted in the scientific community as accurate for the classification of an area stained positively with the DAB chromogen.

For confirmation that the method of CD is accurate and robust to use, the positive control images were double checked using the manual selection methodology. To allow for any variations in counting of positively stained areas in the tissue, this method was repeated on 3 different days.

These values were then compared values acquired by CD computer assisted analysis, allowing determination of accuracy of this method.

Cell counts

Manual cell counts were conducted for the leukocyte markers CD45, CD68 and NE. They were also conducted for taking into account of the positive S100A4 staining of alveolar macrophages (AM). All cells positively stained (area determined by CD)

were manually counted and any positively stained AMs (determined by morphology and CD68 serial section comparison) were deducted from the total value, giving solely lung parenchyma results.

$$\text{Corrected CD value} = \text{CD value} - \left(\frac{100\% - \text{AM positive \%}}{\text{CD value}} \right)$$

3.2.5 Statistical Analysis

Manual v CD

The mean (\pm SEM) of percentage area stained was determined of each image for both techniques. These results were compared and the closer the values indicated exact agreement with manual analysis. The closer the values are to zero, the more accurate the method. Difference testing was performed using a paired student's t-test. Statistical significance was defined as $p \leq 0.05$. Analysis was carried out using GraphPad InStat version 3.06 (GraphPad Software, Inc., San Diego, CA, USA).

Patient samples

Data is not normally distributed so analysed non-parametrically. Between overall demographic group samples (COPD vs. Controls) a Mann-Whitney U test was performed and between individual demographic group samples (COPD current smoker, COPD ex-smoker, current smoker, ex-smoker and non-smoker) comparisons were first assessed by one way Kruskal-Wallis ANOVA. Where significant, Mann-Whitney U tests were performed for two-way comparisons. $p \leq 0.05$ was considered significant for all analysis. Analysis was carried out using GraphPad InStat version 3.06 (GraphPad Software, Inc., San Diego, CA, USA).

3.3 Results

3.3.1 Antibody optimisation

The first step was to optimise all of the antibodies that had been chosen for this study. Selected epithelial markers were: E-cadherin and Cytokeratin

Selected EMT markers were: Desmin, S100A4 and α SMA

Each antibody was tested on a lung patient sample of a known demography (COPD ex-smoker). The starting antibody concentrations were determined by manufacturer data sheets supplied with the antibodies and concentrations used by previously cited studies. Each antibody was optimised by doing serial dilutions of antibody i.e. 1:100, 1:200 (suggested dilution on the data sheet) and 1:300. The set of dilutions would then be used in the 4 different pre-treatment options to determine the ideal dilution for human lung tissue.

The following pages show example images of the IHC optimisation staining. Figure 3.3.1 shows the optimisation of E-cadherin. With no-pre-treatment there is little to no staining evident in the lung tissue; suggesting that there was a need for epitope retrieval via pre-treatment. The sectioned lung tissue was then processed through the three different pre-treatments, (these are standard buffers used and recommended by our collaborating colleagues at UHSM and general IHC-Paraffin methods Abcam®) before the addition of the serial dilutions the negative controls had no non-specific antibody binding to the lung parenchyma. A small amount of tissue antigen retrieval occurred with the citrate buffer and there was a weak positive reaction for the 1:50 and 1:100 dilutions. With the EDTA pre-treatment again there were some antigen retrieval across the serial dilution range, but this was very weak positive staining with no clear membrane or structural (specific areas in lung tissue) patterns. Finally it could be seen in the lung tissue pre-treated in Tris-EDTA buffer, which was definitive antigen retrieval with clear membrane staining. It also can be seen that the epithelial cells form the alveolar sacs (1:100 image) and they also seem to be present on the outer rings of thickened airways (1:200 image).

The ideal pre-treatment and dilution chosen for this was Tris-EDTA at a dilution of 1:100 based on staining pattern observed in previous journals, the darkest and clearest specific colouration in the test condition and a colourless negative control.

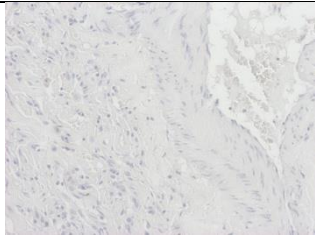
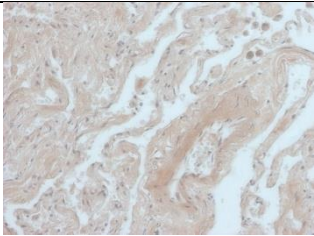
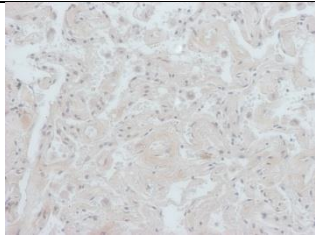
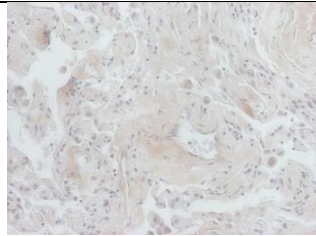
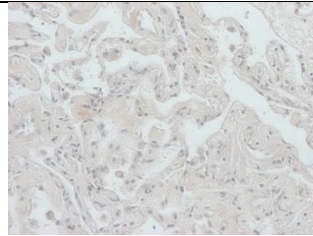
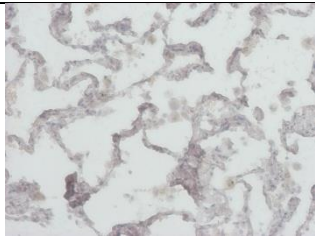

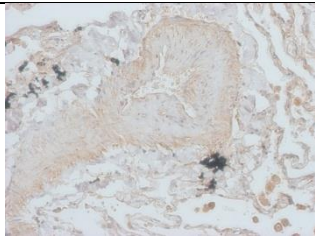
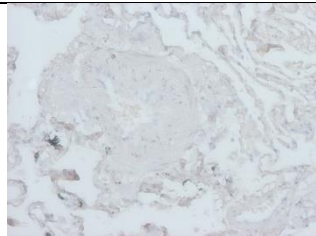
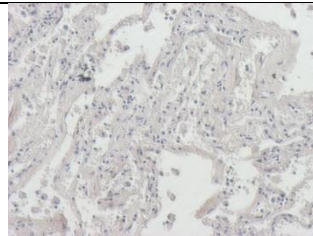
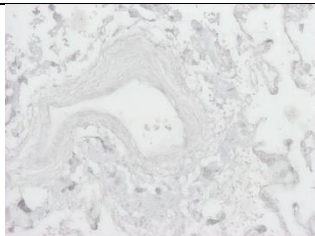
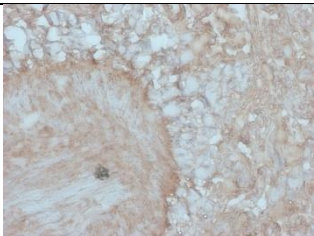
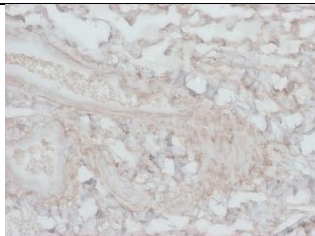
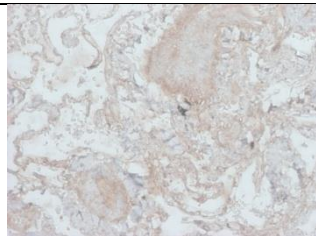
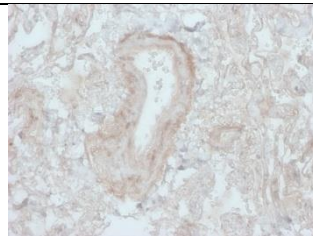
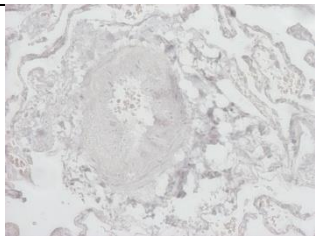
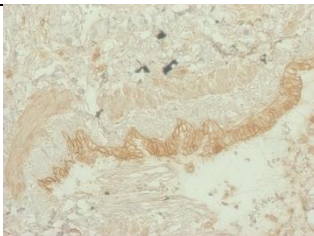
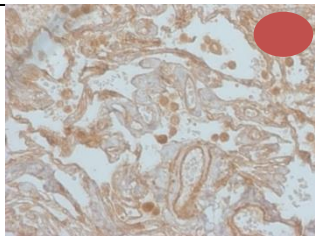
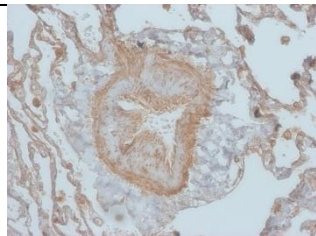
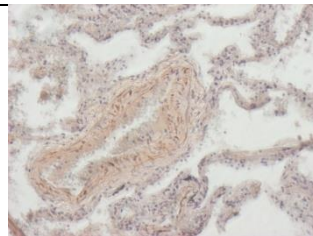
E-cadherin	Negative Control	1 in 50	1 in 100	1 in 150	1 in 200
No pre-treatment					
Citrate pH 6					
EDTA pH 8					
Tris-EDTA with tween pH 9					

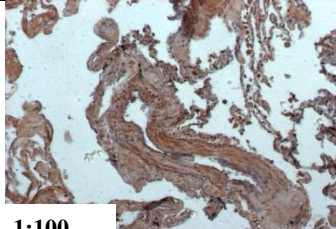
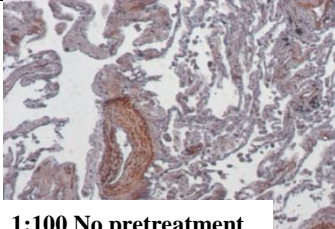
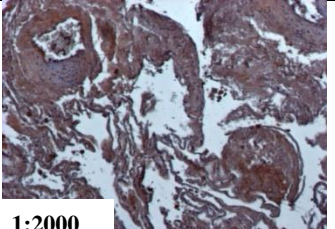
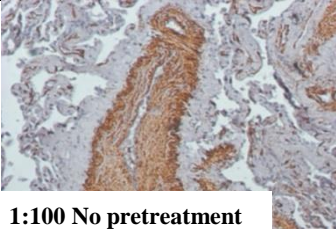
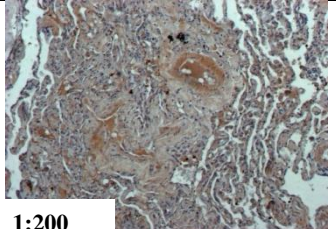
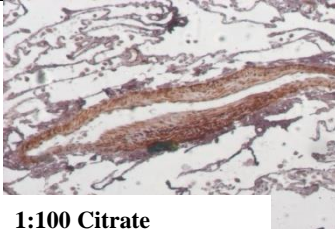
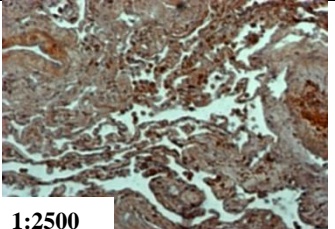
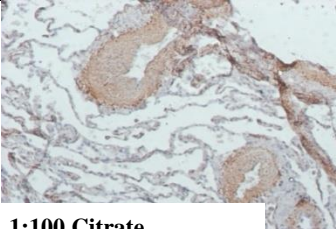
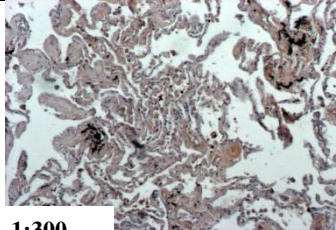
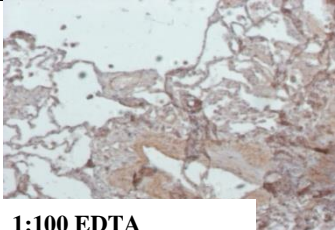
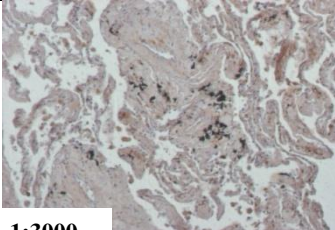
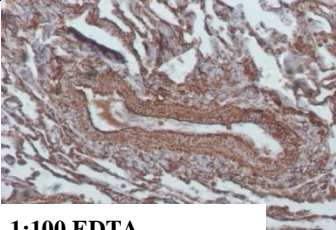
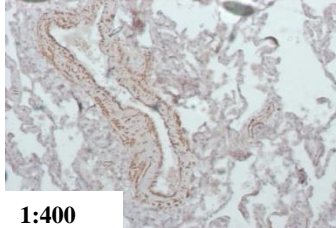
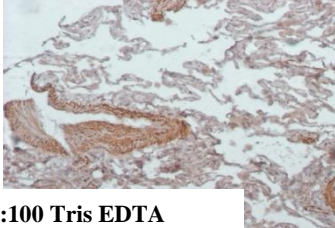
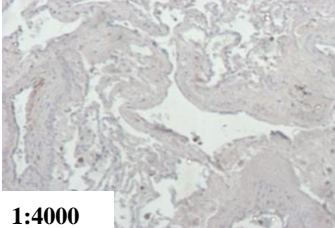
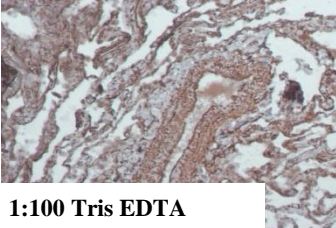
Figure 3.3.1: IHC optimisation: Sample images depicting staining that was achieved during E-cadherin optimisation preformed on LP#624; used to determine the optimal dilution and pre-treatment condition (red spot), for the samples used in the study; images x200 magnification.

As for E-cadherin optimisation, the same optimisation procedures were performed for the following antibodies cytokeratin, desmin, S100A4 and α -SMA, shown in Figure 3.3.2.

The images for the antibodies cytokeratin and S100A4 shows a range of antibody dilutions for no-pre-treatment only and the images antibodies desmin and α -smooth muscle actin show the same dilution (both 1:100) across the range of all four pre-treatment options.

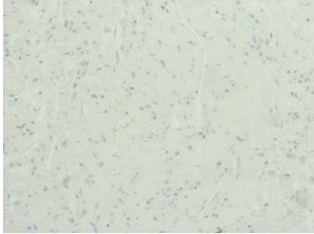
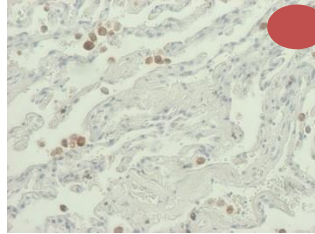
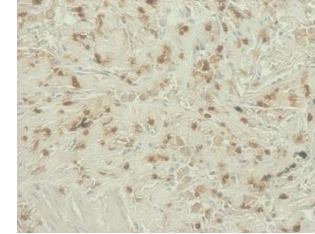
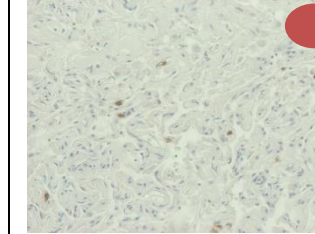
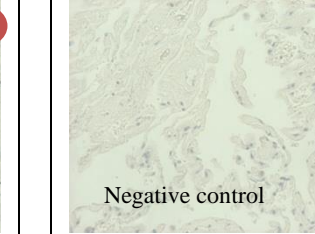
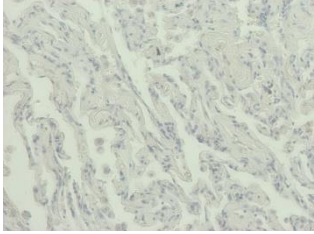
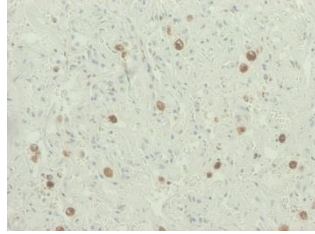
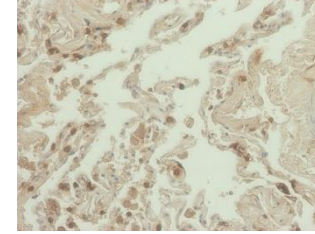
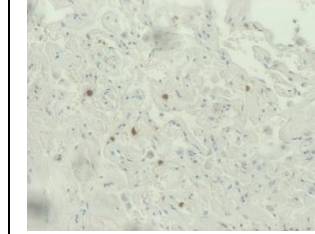
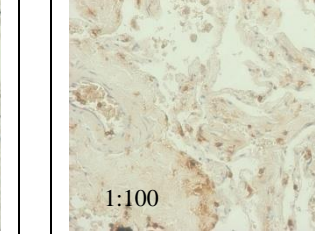
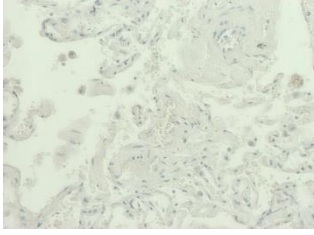
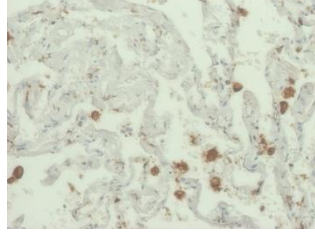
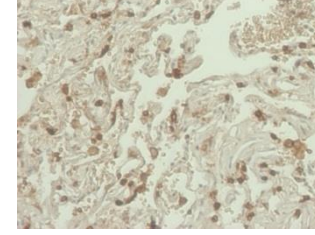

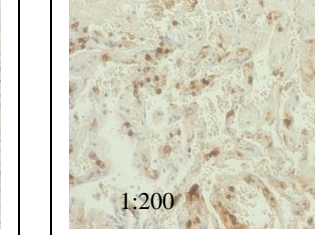
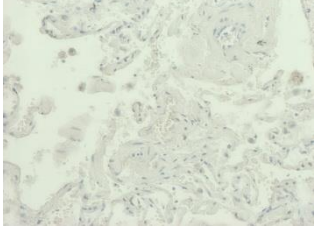
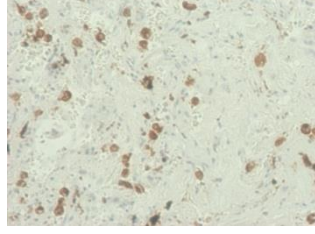
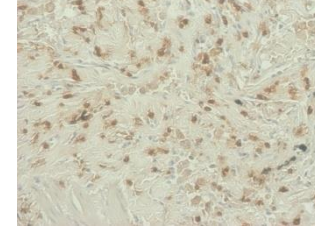
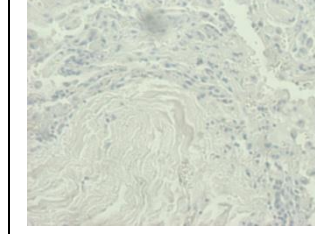
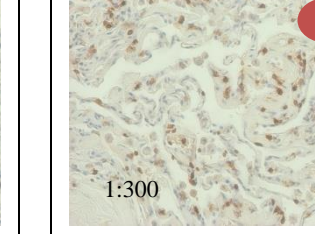
For each of the shown antibodies, a range of antibody dilutions and the common IHC pre-treatment buffers were tested. We verified that no pre-treatment conditions were needed as the clearest positive staining was observed without it. (Indicated by the red dots). The antibody dilutions for cytokeratin and S100A4 decided by optimisation were 1:200 and 1:2500 respectively. As can be seen in both cases the lower dilutions produced large undistinguishable areas of staining and the higher dilutions achieved little to no positive staining.

Figure 3.3.2: EMT markers Optimisation pictures for cytokeratin, S100A4 (no pre-treatment only) and desmin and α -SMA (1:100 across all pre-treatment options). Optimal conditions marked with red spot Images x100 magnification.

Cytokeratin	Desmin	S100A4	Alpha smooth muscle Actin
 1:100	 1:100 No pretreatment	 1:2000	 1:100 No pretreatment
 1:200	 1:100 Citrate	 1:2500	 1:100 Citrate
 1:300	 1:100 EDTA	 1:3000	 1:100 EDTA
 1:400	 1:100 Tris EDTA	 1:4000	 1:100 Tris EDTA

As found with antibodies in figure 3.3.3, sufficient staining was achievable by using the no pre-treatment option. There was little to no difference in the leukocyte staining between the four pre-treatments for CD45 and CD68. Yet no staining occurred with neutrophil elastase for EDTA and tris-EDTA pre-treatments suggesting that the alkalinity of these buffers has destroyed the neutrophil elastase antigenic epitope. Further dilutions of the CD45 antibody were required as background staining is evident therefore this was done under no pre-treatment; concluding that the best dilution is 1:300

Figure 3.3.3: Leukocyte Markers optimisation of the CD68, CD45 and NE. Optimisation through pre-treatments using the manufacturer recommended dilutions. The last column shows further dilutions of CD45 in no pre-treatment. Optimal conditions marked with red spot. Images x200 magnification.

Leukocytes	Negative Control	CD68 1:500	CD45 1:75	Neutrophil Elastase 1:500	CD45 no pre-treatment
No Pre-treatment					
Citrate pH 6					
EDTA pH 8					
Tris-EDTA with tween pH 9					

Marker	Antibody	Dilution	Pre-treatment
Epithelial	E-cadherin	1:100	Tris-EDTA pH9
	Cytokeratin	1:200	No
Fibrotic	Desmin	1:100	No
	S100A4	1:2500	No
	A-SMA	1:100	No
Leukocyte	CD45	1:300	No
	CD68	1:500	No
	Neutrophil Elastase	1:500	No

Table 3.3: Shows a summary of all optimal dilution and pre-treatment options

3.3.2 LP#624 Positive Control

Whilst staining batches of patient samples, a positive control (S100A4) was run in parallel. As lung patient 624 was used during the optimisation process, this patient was selected as an additional positive control throughout the cohort study.

The images captured from these slides have been used to determine the threshold parameters for ImageJ analysis. In addition to this they were also used to assess if there was a difference in **percentage** area stained between batches of slides that were stained on different days, which could be caused by day to day temperature variations and any subtle changes in reagents used, thus may effect DAB development.

Figure 3.3.4 gives example images taken from the positive control slides that had been stained with different batches of sample slides over a three week period. Visually it is apparent that there are slight differences in staining intensity however the calculated percentage area stained is very similar between all slides.

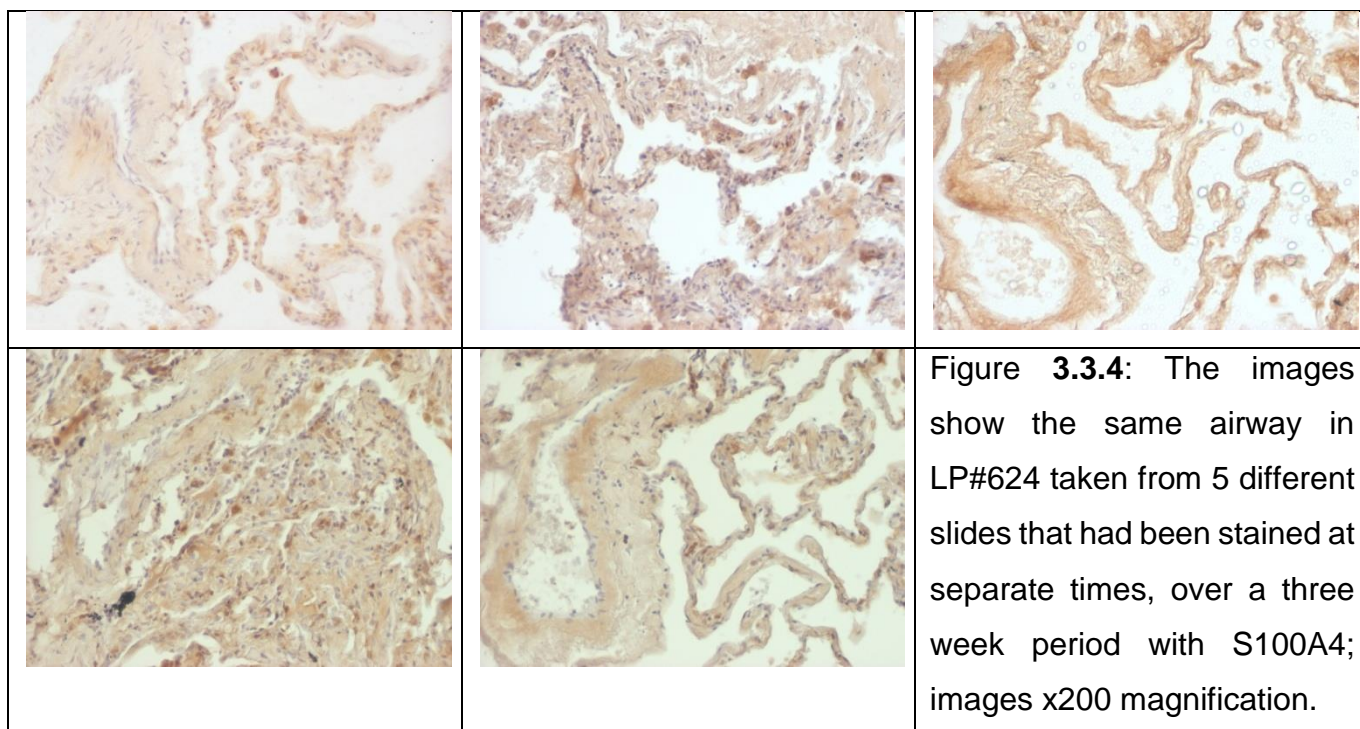


Figure 3.3.4: Example of the images used for threshold determination and percentage area stained analysis.

The figure 3.3.5 A, shows an example of threshold determination from one of the S100A4 positive control images. It can be seen that the light brown areas (image C) had not been selected reducing the initial 240 very weak positive threshold value (image E); which allows the exclusion of image noise from the analysis. As conducted by Krajewska *et al* 2009 in their sample analysis. This was repeated for all positive control images providing the results (figure 3.3.5 B) for determination of threshold to be used in sample analysis.

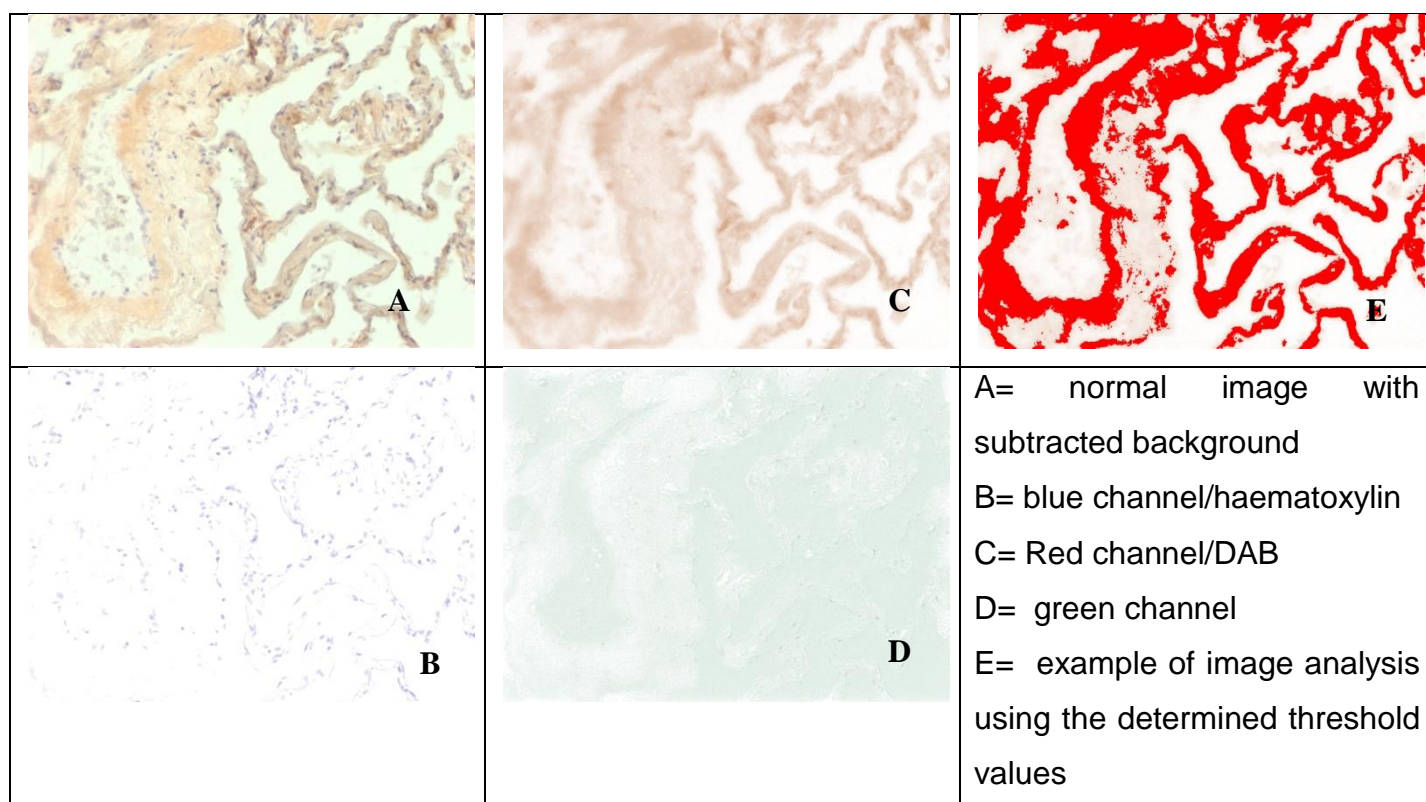


Figure 3.3.5 A: Example of threshold determination analysis upon image **A** DAB positive staining, by colour deconvolution **B**, **C**, **D** and threshold selection **E**.

Figure 3.3.5B shown below depicts the weak, moderate and strong positive thresholds that conformed to intensity ranges on a scale of 0 to 255 (black to white), that was achieved by computer assisted analysis of the images taken from the S100A4 positive control slides. The black line in each grouping indicates the mean threshold values (96 and 198 respectively) that were then used for all DAB stained sample analysis.

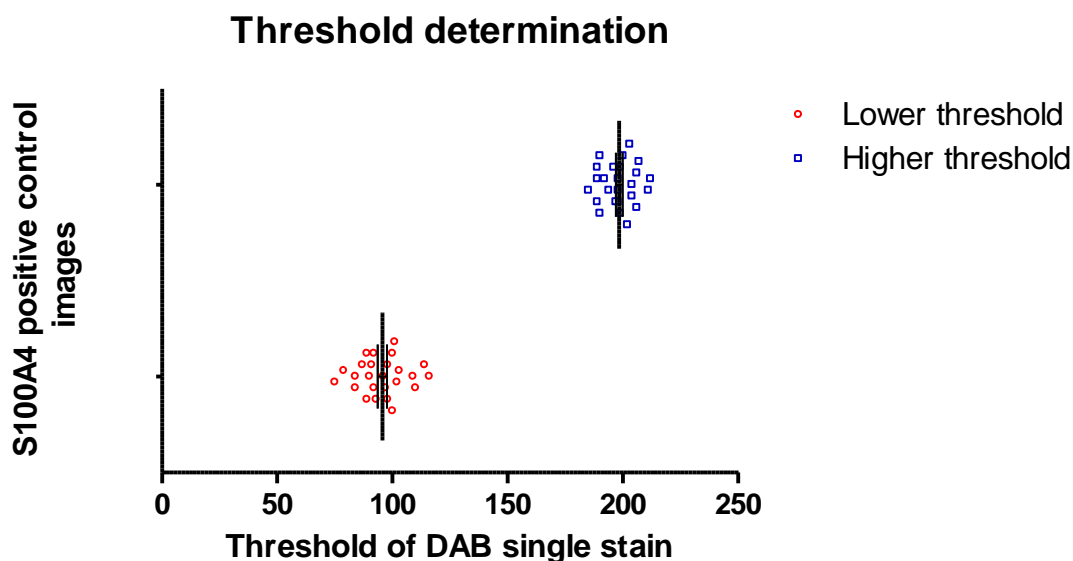


Figure 3.3.5B: depicts the lower and higher optical density thresholds achieved from images taken from the positive control slides.

The determined threshold values were applied to all of the positive control images, (by adjustment of threshold parameters), to determine the results for the percentage area stained between batches assessment. Results can be seen in the following graphical data, figure 3.3.6A. A repeated measures ANOVA was conducted on the data giving a p value of 0.329 and a variation of less than 3% indicates that there was no significant difference in the mean values of percentage area stained. Suggesting that the external variables such as room temperature and varying batches of reagents had little effect on the percentage area of tissue stained (range of 10.52%) between the batches of slides stained.

It had been noticed that the S100A4 marker is strongly expressed by alveolar macrophages (AMØ) present in the samples. Therefore in each slide the total positive stained cells and positive stained AMØ (determined by cell size and morphology) were counted manually; from this the percentage area positively

stained by AMØ was calculated and subtracted from the total percentage area positively stained. This has been deemed as the correction factor. This was implemented on an individual sample basis, due to variation in AMØ numbers between controls, COPD and between the progressive states of each patient group; in attempt to determine the true percentage area stained in each sample.

Figure 3.3.6A was achieved by computer assisted analysis, a computerised form of image analysis as traditional methods relied on manually assessing images by determining positive stained areas by visualisation of trained professionals alone. Therefore to determine that the methodology chosen for this study was reliable, the level of concordance between manual and computer assisted analysis was assessed. In the assessment of concordance (Figure 3.3.6B) between the results of manual and computer assisted analysis a two tailed paired students t test was conducted and it was found that there were no significant ($p=0.2567$) difference in comparison of the means and the pairing of the data was significantly effective ($p=0.0132$). Concluding that the use of computer assisted analysis in the single antigen staining by DAB is reliable.

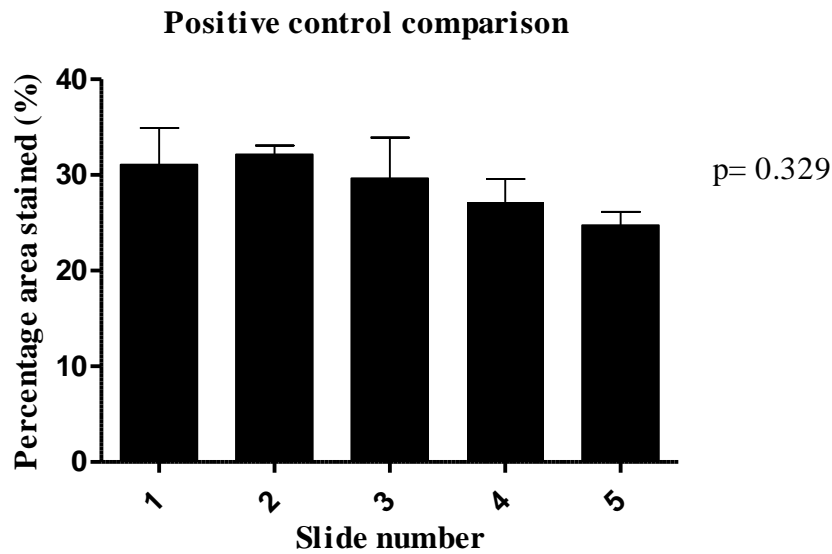


Figure 3.3.6A: Shows the mean +SEM of percentage area stained (minus correction factor) of 5 positive control slides stained with S100A4, stained over a 3 week period, $p=0.329$

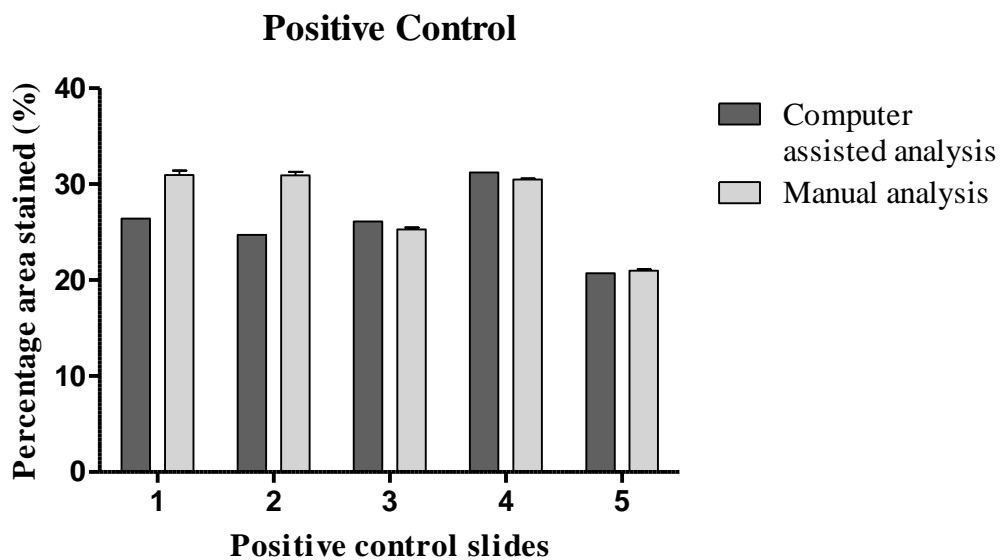


Figure 3.3.6B: depicts the concordance between the results of manual and computer assisted analysis. Comparison of the means $p = 0.2567$ and pairing effectiveness $p = 0.0132$.

3.3.3 Tissue structures: example of sample stains

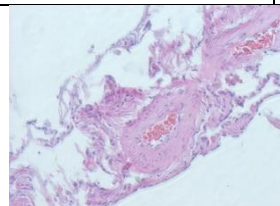
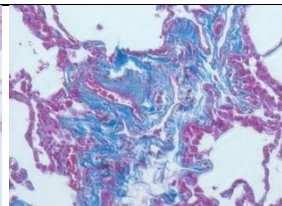
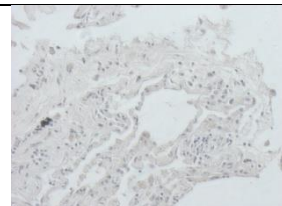
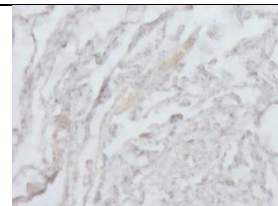
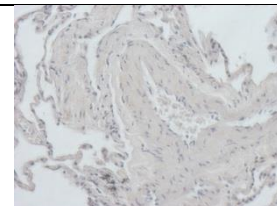
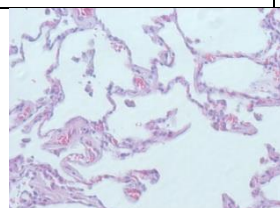
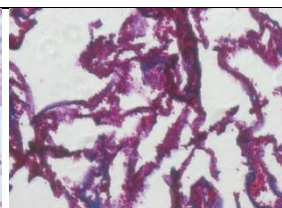
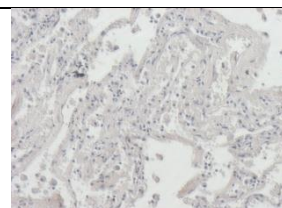
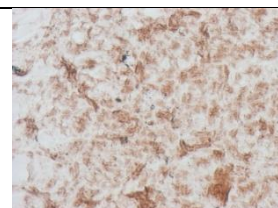
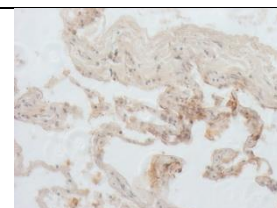
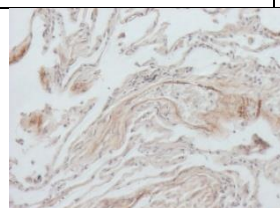
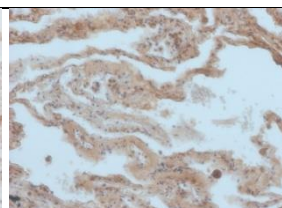
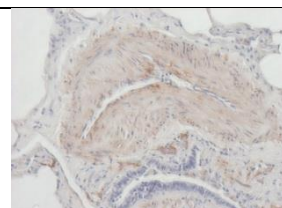
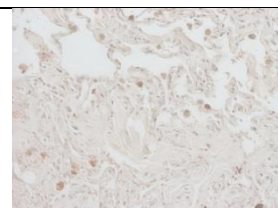
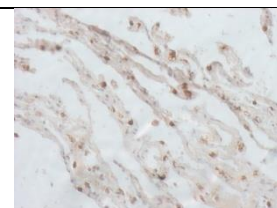
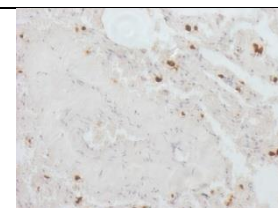
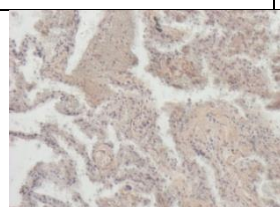
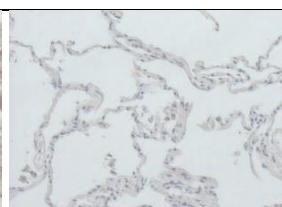
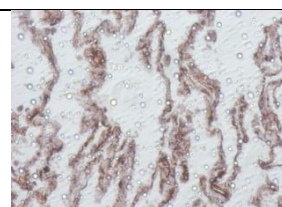
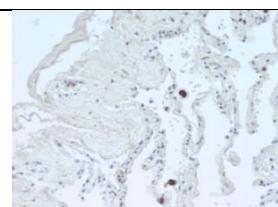
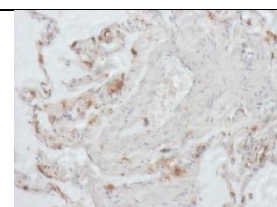
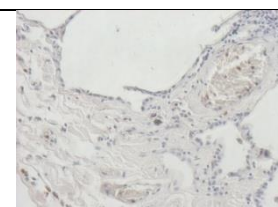
The following two figures (3.3.7A + B) depict examples of basic (H&E and Masson's trichrome) and antigenic staining on two lung patient samples. The samples shown are one patient with worst prognosis (COPD) and the patient with best prognosis (in regards to COPD) to show the contrast in staining patterns between the two groups.

In figures 3.3.7A +B it can be seen that in the COPD patients lung tissue there is extensive areas of broken down lung tissue (example is 'wispy' material in H&E image) and large areas of alveolar wall thickening. There are also large areas of ECM overproduction and deposition - depicted by positive blue collagen staining in MT image- which would be causing a reduction in surface area for gas transfer and destruction of normal lung architecture. There is no evident lung thickening in the control patient and no sign of excessive deposition of collagen.

There is a clear difference in the epithelial markers present between the two lung patients. It is evident that they are present in lung tissue of the control subject but there is very little evidence (no staining) of them present in the lung tissue of the COPD patient, suggesting either extensive EMT occurring in this section of the patient's lungs or evidence of cellular loss.

By comparing the two patients above it can be seen that the proteins linked with EMT/fibrosis are raised in the COPD patient. It can also be observed that the leukocyte numbers are increased in the COPD patient compared with the control subject.

Interestingly as seen with the positive controls it can be seen that the fibrotic marker desmin is present in both images. Suggesting that desmin is being expressed by these epithelial cells.

A	Lung Patient	H&E	Collagen	Negative control	E-cadherin	Cytokeratin	
	617 (COPD)						
	650 (Control patient)						
B	Lung Patient	Desmin	S100A4	Alpha smooth muscle actin	CD68	CD45	Neutrophil Elastase
	617 (COPD)						
	650 (Control patient)						

Figures 3.3.7A + B: Examples of both COPD (LP#617) and control (LP#650) lung tissue and their staining patterns in regards to collagen, epithelial fibrotic and leukocyte antigenic markers; Images x200 magnification.

3.3.4 Positive Controls: Cell lines

To further validate the antibody specificities, we used cell lines of established phenotype (Epithelia and Fibroblasts); to observe antibody binding i.e. the A549 (epithelia) and NHLF fibroblasts were used as positive control samples. This also ensured that cellular fixation used did not block the immunoreactivity of the antigens.

To match experimental conditions used for lung resections, initial attempts were made to mount the cell lines controls into agarose so enabling them being embedded into paraffin wax. After many attempts of a published protocol (Morgan 2001), this proved to be challenging as during the staining procedure the cells that were adhered to the polysine slides, disassociated from them at various points. After several weeks and failed attempts to prepare positive controls in this manner, it was decided to work with cytopins of the cell lines for the positive controls of each antibody.

The H&E stain was performed to compare cell size and morphology, of the two cells lines. It can be seen that the fibroblasts are larger than the epithelial cells. The epithelial cells are clustered together in no particular formation and possess the typical flatten morphology expected, whereas the fibroblasts that are touching are taking on the typical parallel formation and had begun to spread themselves in order to achieve the spindle shape normally associated with inactive cells.

The Masson's trichrome stain shows that there is no collagen present or surrounding any of the epithelial cells but there is the beginnings of collagen production by the fibroblasts (blue staining) seen on the membrane of some of the cells, pointed out by the arrows. The NHLFs used for the cytopins were in an inactivated form hence pale collagen staining; possibly intracellular.

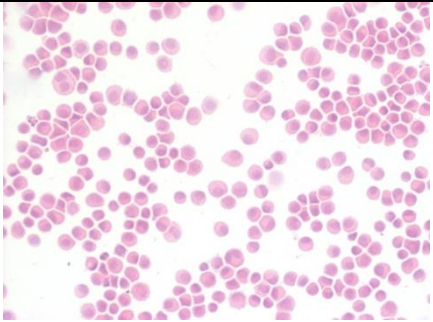
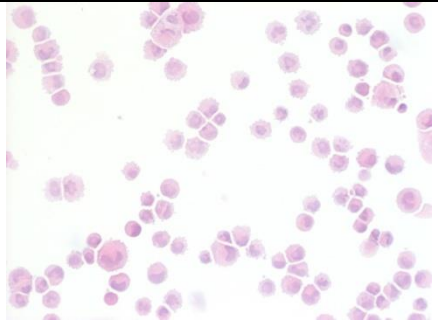

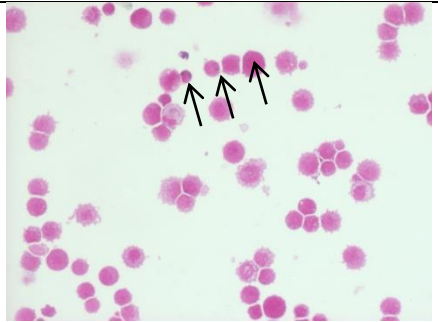
Stain	A549	NHLF
Haematoxylin and Eosin		
Masson's Trichrome (Collagen)		

Figure 3.3.8: Images of H&E and Masson's trichrome staining on cytopins of A549 and NHLF cell lines, being used as positive controls; images x200 magnification.

In the epithelial cell line it can be seen that there is a strong positive surface staining for E-cadherin with light cytoplasmic staining for all cells present in the image. The cytokeratin stain isn't as strong showing a very light cytoplasmic staining on the majority of cells, some of which have a darker membrane staining. The fibroblasts possess no E-cadherin staining as expected but do show a light cytoplasmic stain of cytokeratin in almost 50% of the cells present.

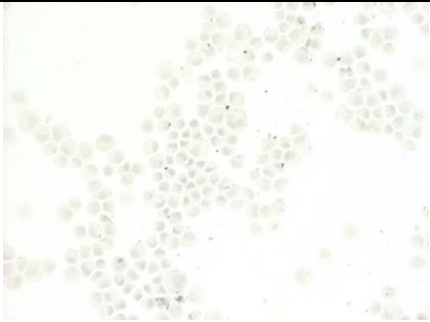
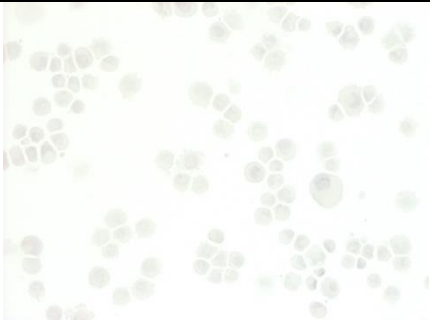
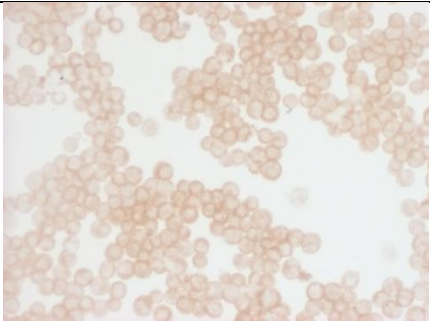

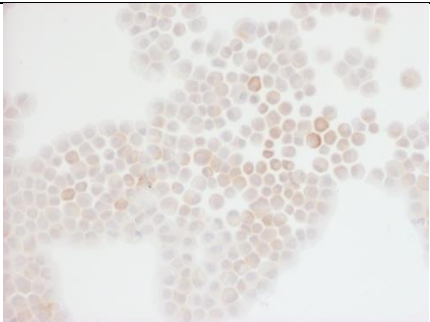
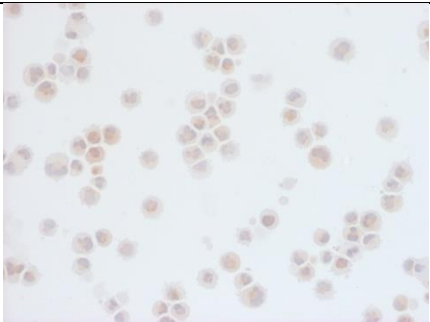
Antibody	A549	NHLF
Negative Control		
E-cadherin		
Cytokeratin		

Figure 3.3.9: Positive controls for epithelial markers demonstrated on A549 and NHLF cell line cytopins; images x200 magnification

The epithelial cells show no staining for the fibrotic markers S100A4 and α -SMA but do show significant cytoplasmic staining for the fibrotic marker desmin (figure 3.3.10). The fibroblasts show a strong positive membranal stain for α -SMA for some of the cells. There is also positive membrane and cytoplasmic stain for S100A4 and a positive cytoplasmic with some nuclear staining in the case of desmin.

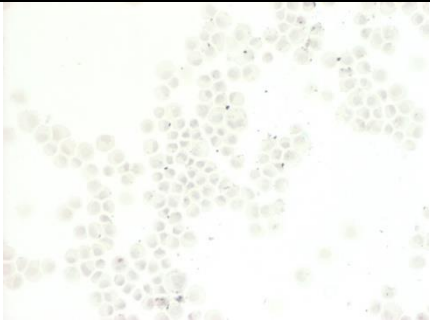
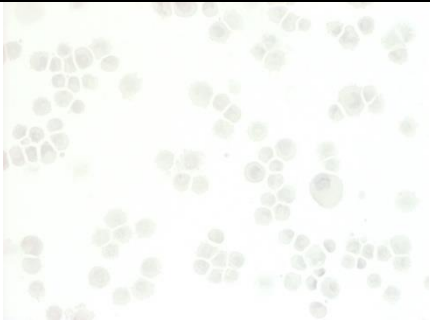
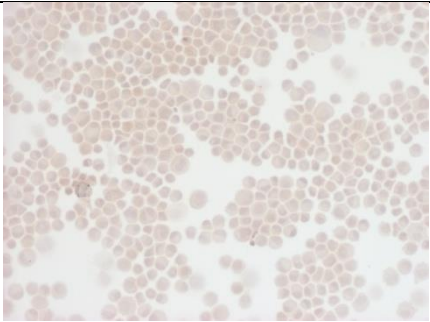
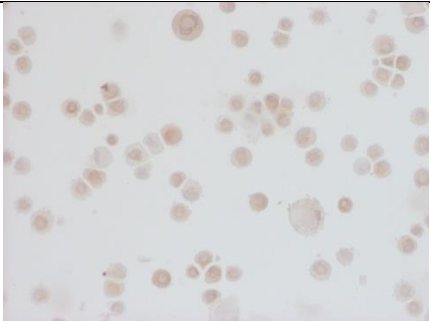
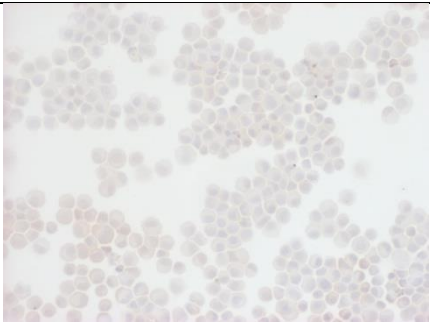
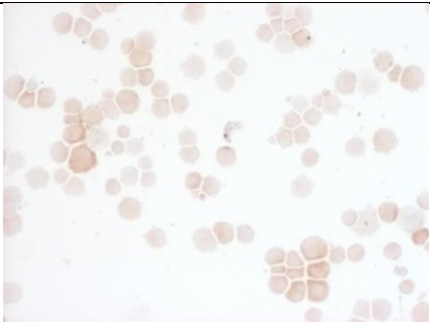
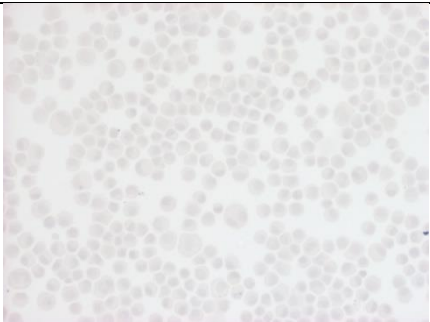
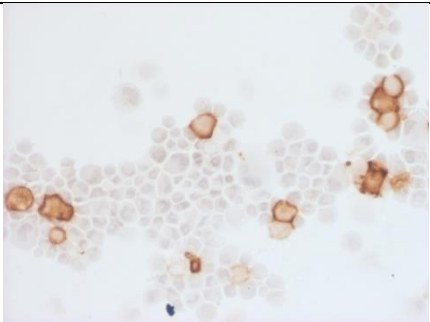
Antibody	A549	NHLF
Negative Control		
Desmin		
S100A4		
Alpha smooth muscle actin		

Figure 3.3.10: Positive controls of the fibrotic markers conducted on A549 and NHLF cell line cytopins; images x200 magnification.

As can be seen by the following images (figure 3.3.11), none of the leukocyte markers are expressed in both the epithelia and fibroblasts.

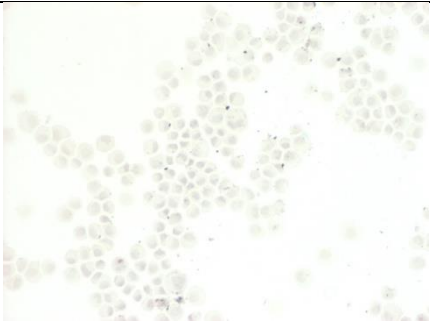

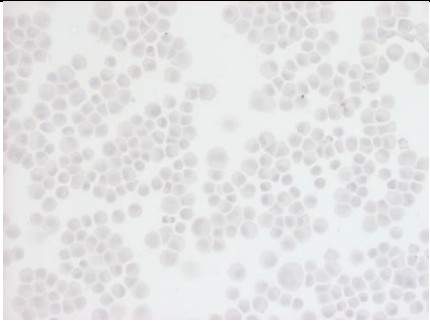
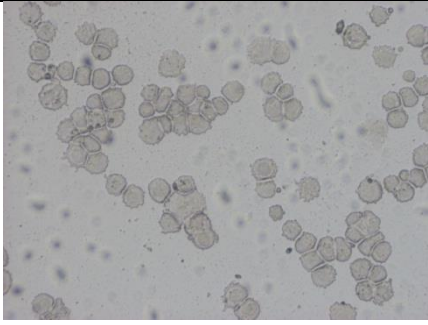
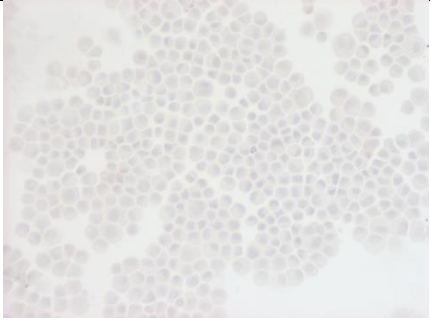

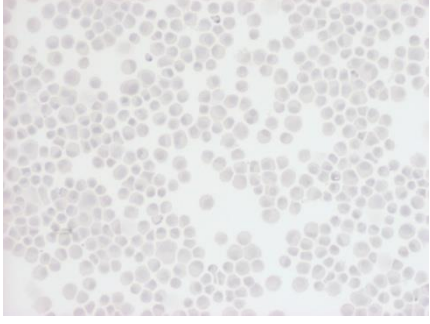

Antibody	A549	NHLF
Negative Control		
CD68		
CD45		
Neutrophil Elastase		

Figure 3.3.11: Positive control of leukocyte markers preformed on A549 and NHLF cell lines; images x200 magnification.

3.3.5 Patient Group Data (Lung sample IHC)

For each of the stains assessed, a comparison was conducted between all the COPD patient study group and all the control subjects. The groups were further split into separate patient demographics (COPD current smoker (CCS), COPD ex-smoker (CEX), current smoker (CS), ex-smoker (EXS) and non-smoker (NS)) to determine if there were significant differences between individual demographic groups. To assess the effects of current smoking versus previous smoking patients were split into current (COPD and controls) smokers, Ex (COPD and controls) and non-smokers for data analysis. This allowed us to ascertain if EMT effects are reversible or not.

Correlation graphs of EMT biomarkers with subject demographics were made.

Separate patient group analysis is shown in (Figure 3.3.12A-I). A one way Kruskal-Wallis ANOVA was conducted for all graphs and there were no significant difference in sample means found for the epithelial markers E-cadherin ($p=0.3270$) and cytokeratin ($p=0.2279$). In our patient cohort we observed cytokeratin was expressed more readily within the COPD tissue and there was more expressed within the ex-smokers than in the non-smokers group.

There was no significant difference for the EMT biomarkers S100A4 ($p=0.1043$) and α SMA ($p=0.1118$) between the patient groups. A non-significant higher expression of S100A4 trend was observed in COPD patients compared to controls. . It was also notable that there was a higher mean within the current smokers than both of the ex-smoker categories. There was no significant variation of α SMA between the 5 subject groups. The fibrotic marker collagen (figure 3.3.12D) showed a very significant, ($p=0.0015$) difference between the groups sample means. Very pronounced raised collagen levels were evident in current smokers when compared to ex or non-smokers. These results follow what was expected with the fibrotic markers and interestingly even though not significant S100A4 results follow the group collagen trend. There were no other significant differences found between any other data set combinations.

In line with previous literature leukocyte markers (3.3.12 G-I) present significant differences between the overall demographic groups, CD45 ($p=0.0005$), CD68 ($p=0.0013$) and NE ($p=0.0362$), determining that the tissue assessed follows the same pattern as tissue previously assessed. The CD45 graph (figure 3.3.12G) displays that there is very, significant and extremely significant differences between COPD current, ex and ex-smokers vs. the non-smokers. Interestingly the current smokers have the highest percentage of CD45 presenting cells; showing the same trend as the percentage area stained for both α SMA and desmin. This trend is also seen in the CD68 figure (3.3.12H) with very significant difference between COPD current and ex-smokers vs. non-smokers. The percentage of CD68 cells are raised in current smokers, compared to COPD ex-smokers. NE (figure 3.3.12 I) numbers vary between the 5 groups but there are no significant differences between two individual patient groups. Their numerical trend matches that of CD45 and CD68, with the exception of not having higher percentage of cells in the current smokers.

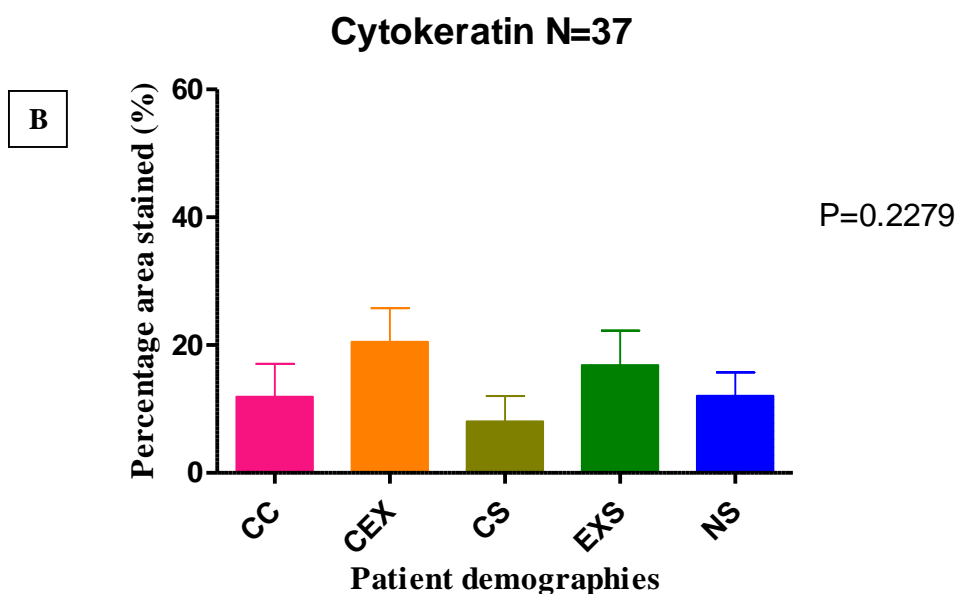
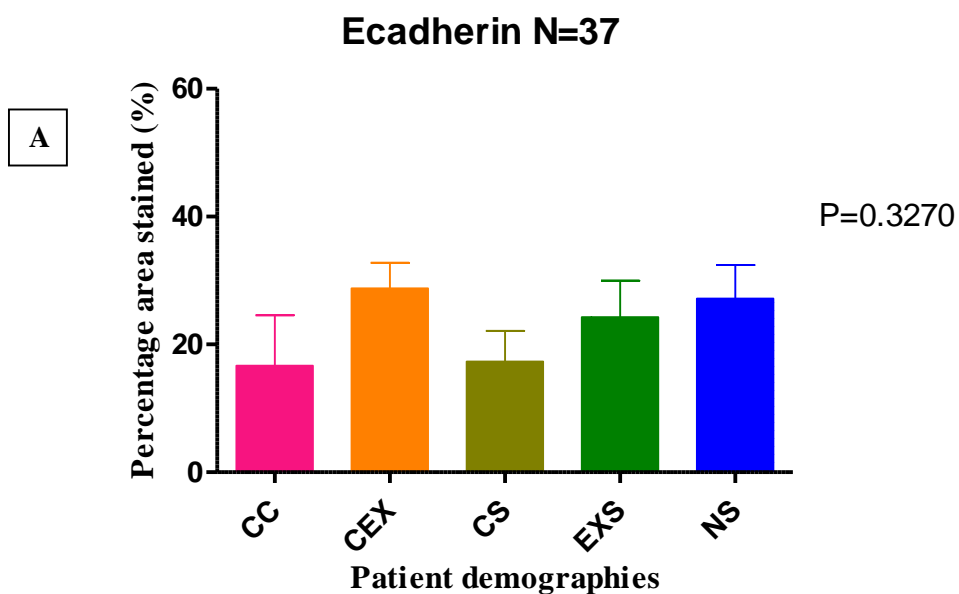


Figure 3.3.12 A+B Comparison of positive percentage area stained for epithelial markers E-cadherin (A) and Cytokeratin (B) between the separate patient groups COPD current smoker (CC) n=6, COPD ex-smoker (CEX) n=6, Current smoker (CS)n=9, ex-smoker (ExS) n=9 and non-smoker (NS) n=7. A one way Kruskal-Wallis ANOVA showed there was no significance was found for either marker, E-cadherin p=0.327 and cytokeratin p=0.2279.

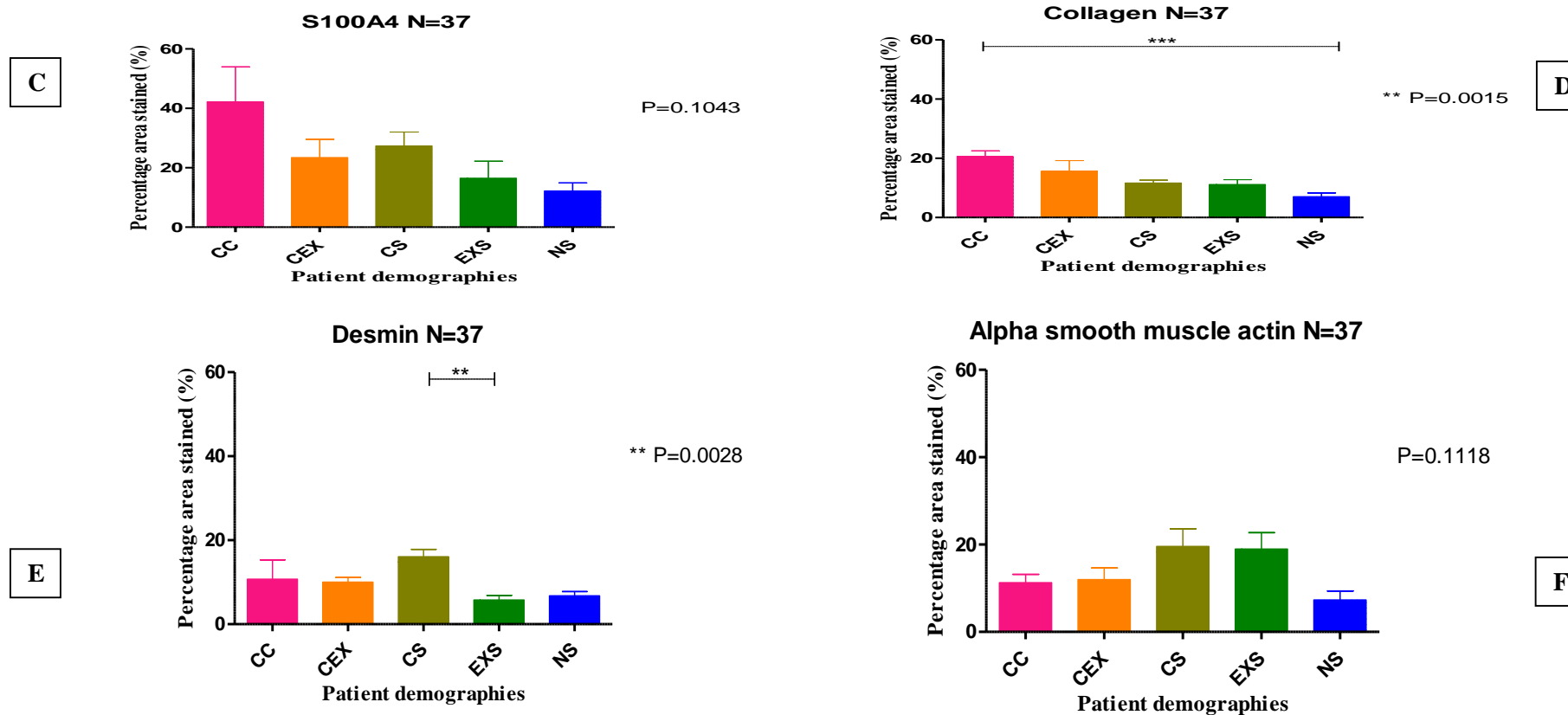


Figure 3.3.12 C-F Comparison of positive percentage area stained for fibrotic markers S100A4 (C), Collagen (D), Desmin (E) and α SMA (F) between the separate demographic datasets, COPD current smoker (CC) n=6, COPD ex-smoker (CEX) n=6, current smoker (CS) n=9, ex-smoker (EXS) n=9 and non-smoker (NS) n=7. A one way Kruskal-Wallis ANOVA showed that there was no significance for S100A4 ($p=0.1043$) and α SMA ($p=0.1118$). Post two way Mann-Whitney U tests show that there is extremely significant difference between CC and NS ($p=0.0001$) in percentage area stained of collagen and a very significant difference between CS and EXS in desmin.

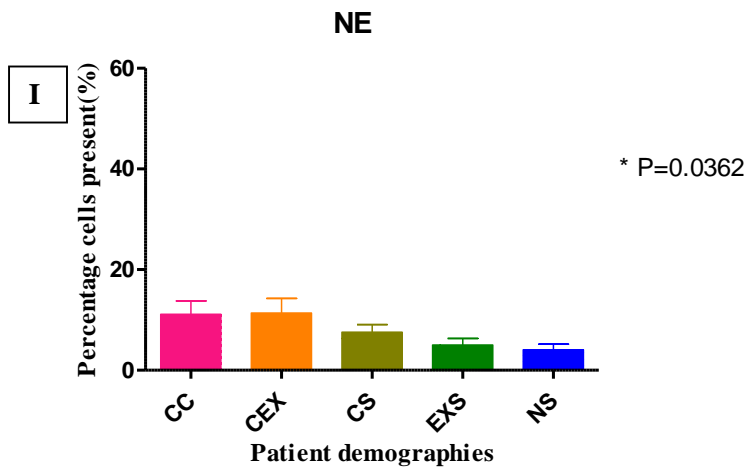
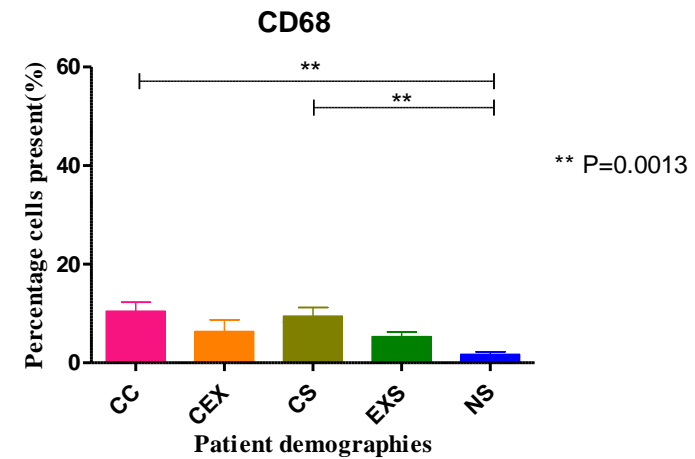
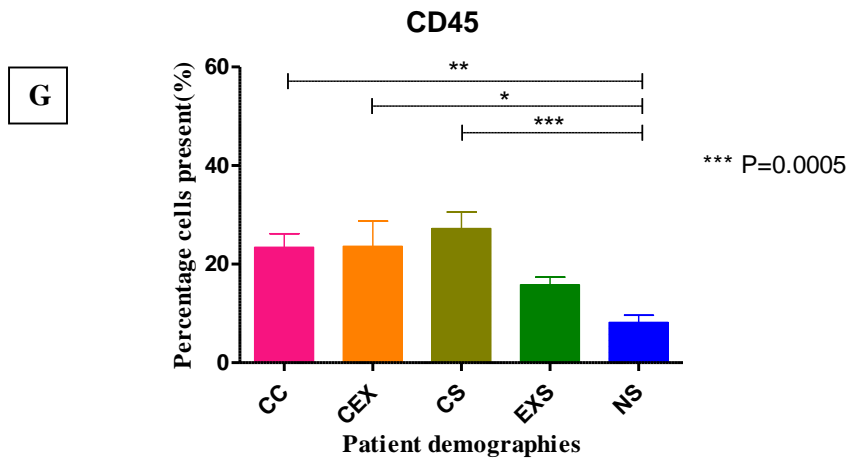


Figure 3.3.12 G-I Comparison of positive percentage cells present for leukocyte markers between the separate demographic data sets; COPD current smoker (CC) n=6, COPD ex-smoker (CEX) n=6, Current smoker (CS)n=9, ex-smoker (ExS) n=9 and non-smoker (NS) n=7. All markers have an overall significance with CD45 and CD68 showing varying degrees of significance between COPD smokers (Ex and current for CD45) and smokers against non-smokers. A one way Kruskal-Wallis ANOVA showed that there was significance for CD45 (p=0.1043), CD68 (p=0.0013) and NE (p=0.0362). Post two way Mann-Whitney U tests show that there is extremely significant difference between CC & CS against NS for both CD45 and CD68, with CEX and NS for CD45.

3.3.6 EMT Reversibility

To investigate if smoking cessation allowed reversion of EMT changes, patient groups were analysed as follows.

There is no significant difference between the groups for both of the epithelial markers, E-cadherin and cytokeratin. (Figure 3.3.13 A+B) Visually it can be seen that there is a higher amount of the epithelial markers present in the ex vs. current smokers, indicating it is possible that EMT may reversible within the lungs. As there is no significance within this data the assessment of more samples, especially in the COPD current category would add power to this analysis.

There is a significant difference of means for the fibrotic markers S100A4 (figure 3.3.13C) and desmin (figure 3.3.13F), with a very significant difference being shown within the collagen figure (3.3.13D); also mirrored between the current and non-smokers within this figure. All three graphs show that there is a high percentage of marker present in current smokers which drops with the ex-smokers. This again may indicate possible reversibility of EMT in the lung but further research will be required to fully confirm this. Another possibility is that the 'type' of COPD these patients have may be affecting the results on this part. There is no significant difference overall or between current and ex-smokers for α SMA (figure 3.3.13E) which have means around the same level, showing there is no difference in the expression of α SMA between current and ex-smokers. However it does follow the trends set by the other fibrotic markers in that the current and ex-smokers are higher than the non-smokers.

It shows in figure 3.3.13G-I that both CD45 (G) and CD68 (H) have extremely significant differences overall and between the current and non-smokers. There is no significant difference for NE (I) however it does follow the other leukocyte markers, in that there is more NE expressing cells for current over ex and more in ex than non-smokers. Linear regressions was plotted of NE vs all epithelial and fibrotic markers (data not shown) and there were no significance between the markers except for collagen that shown a very significant ($p=0.001$) positive correlation.

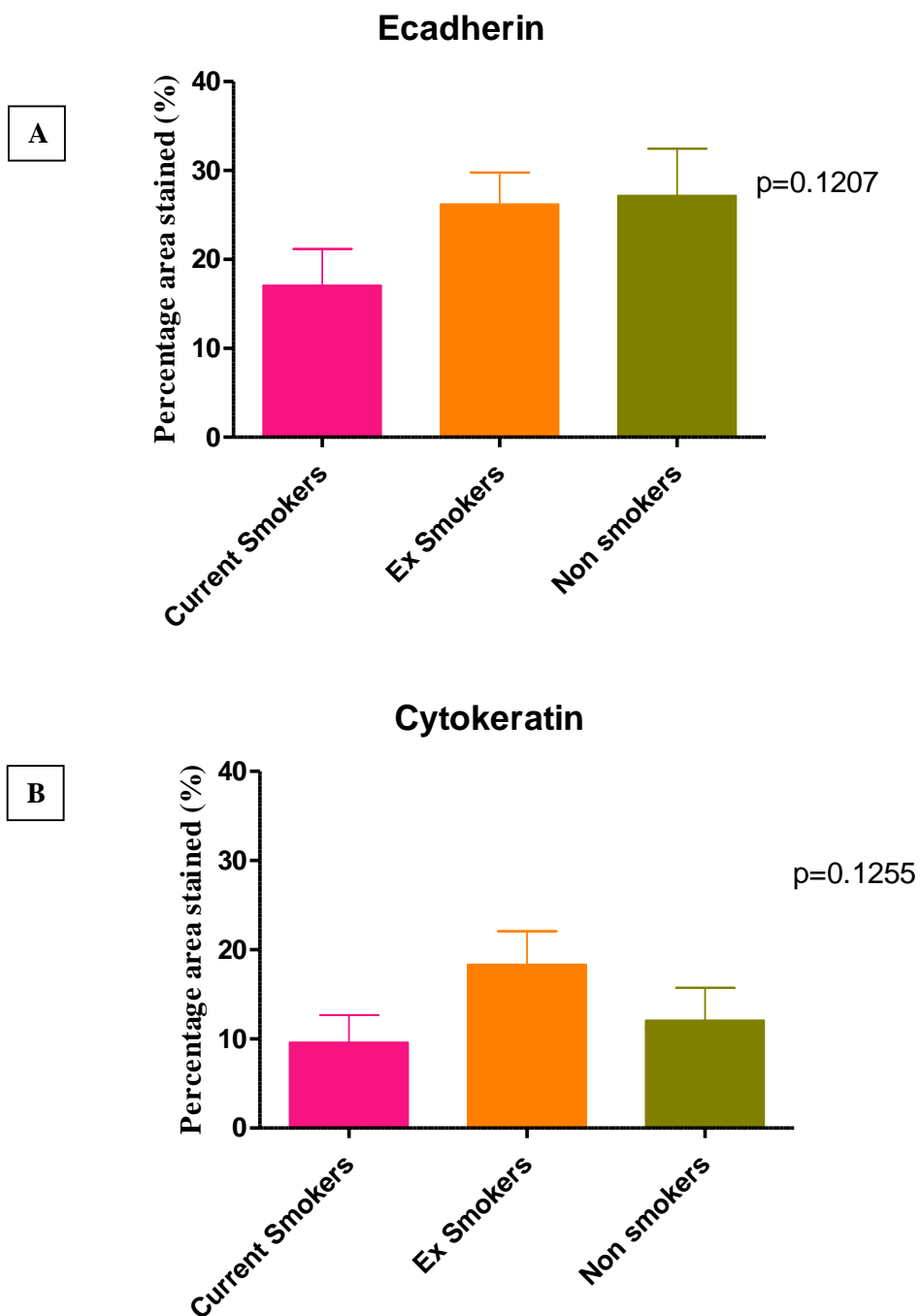
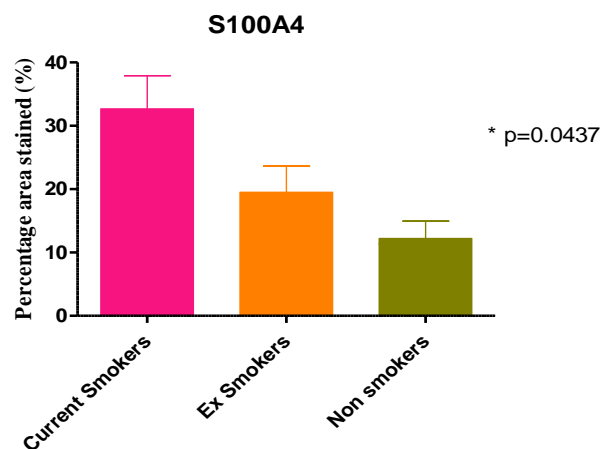
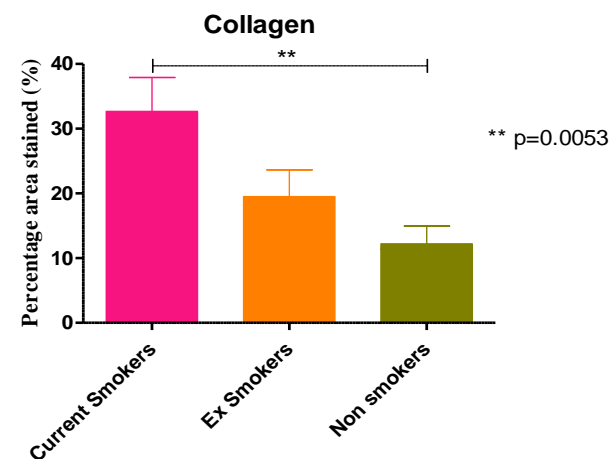


Figure 3.3.13 A+B Comparison of positive percentage area stained for epithelial markers split into smoking status. Total N=37, Current smokers N=15, Ex smokers N=15 and non-smokers N=7. A one way Kruskal-Wallis ANOVA showed that there was no significance between smoking status and percentage area stained of the epithelial markers ecadherin ($p=0.1207$) and cytokeratin ($p=0.1255$).

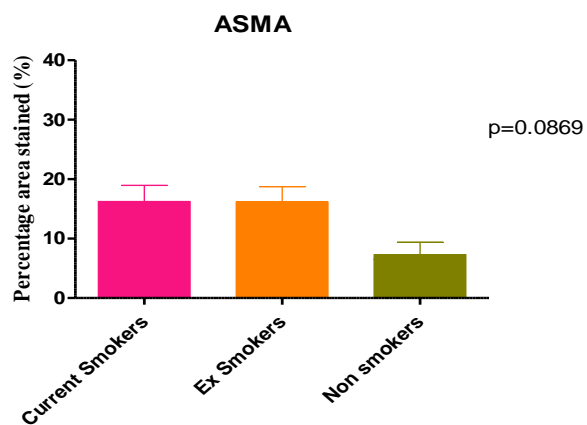
C



D



E



F

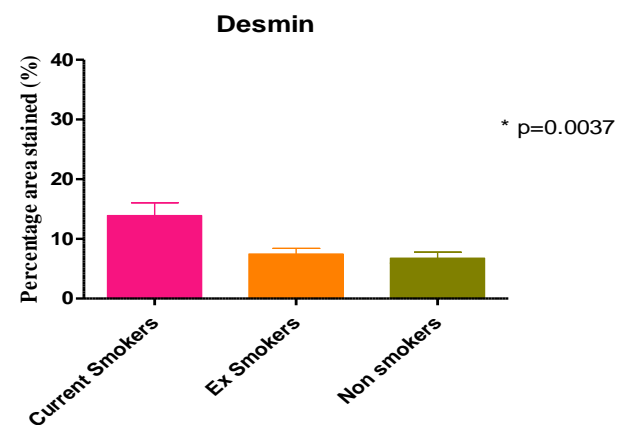
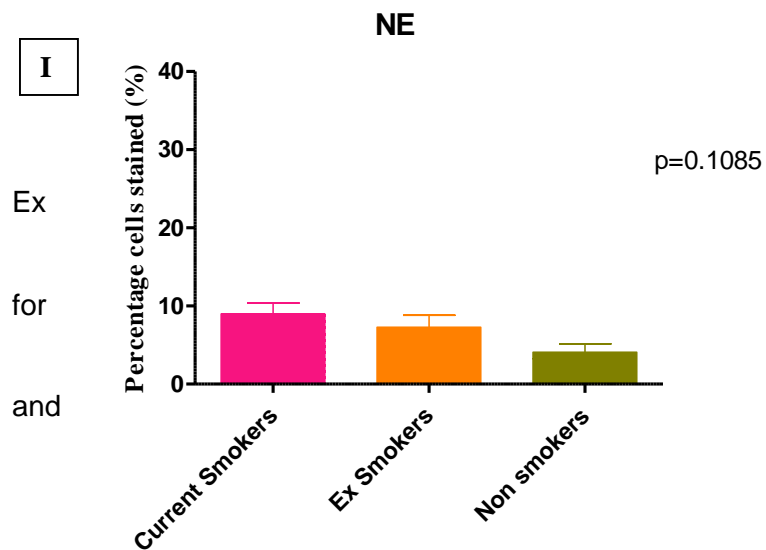
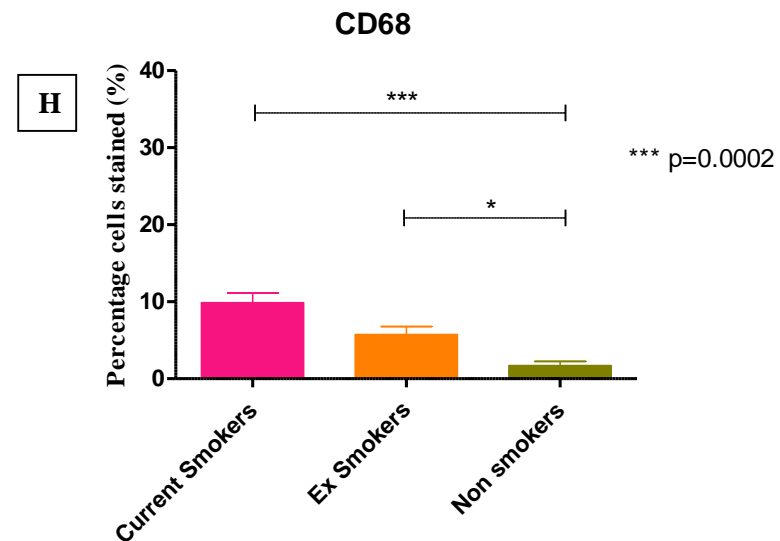
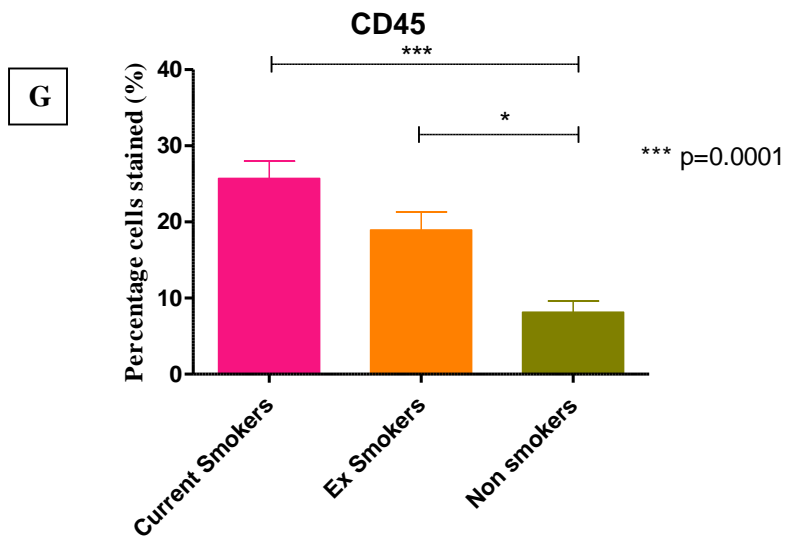


Figure 3.3.13C-F Comparison of positive percentage area stained for fibrotic markers between the split into smoking status: Total N=37, Current smokers N=15, Ex smokers N=15 and non-smokers N=7.. A one way Kruskal-Wallis ANOVA showed that there was no significant difference for ASMA (p=0.0869) but there was for S100A4 (p=0.0437), Desmin (p=0.0037) and collagen (p=0.0053) with a post two way Mann-Whitney U tests showing a significant difference between current smokers and non-smokers for the latter.



Figure

3.3.13

G-I Comparison of positive percentage area stained for leukocyte markers between the split into smoking status: Total N=37, Current smokers N=15, smokers N=15 and non-smokers N=7. A one way Kruskal-Wallis ANOVA showed that there was no significant difference for NE ($p=0.1085$) but there was CD45 ($p=0.0001$) and CD68 ($p=0.0002$) with a post two way Mann-Whitney U tests showing a significant difference between current smokers and ex-smokers non-smokers for both.

3.3.7 COPD patients versus Control subjects

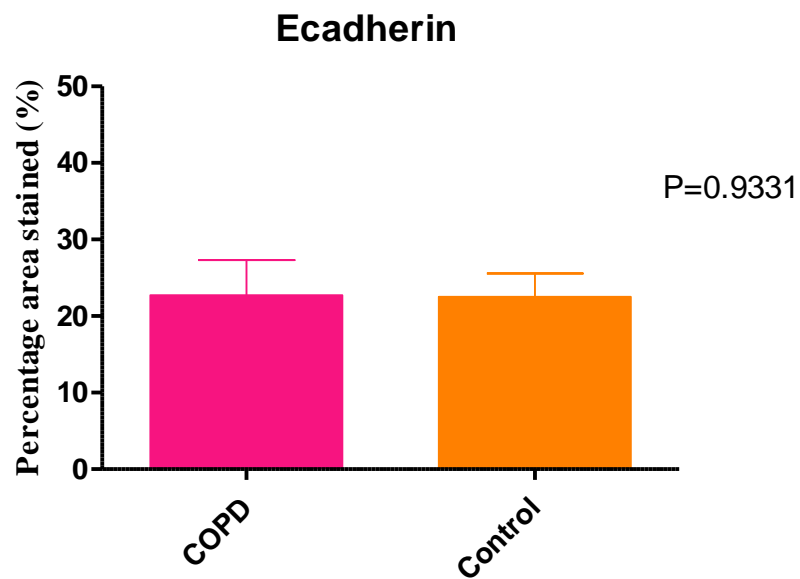
Patient groups were then split into two groups' total COPD patients and total control patients to determine if marker expression was linked to disease state.

The data shown in figures 3.3.14 A & B it can be determined that the epithelial markers E-cadherin and cytokeratin are expressed at similar levels in lung tissue of both COPD and control patients, as there is no significant difference ($p=0.9331$ and $p=0.2971$) between the two data sets.

As with the epithelial markers there was no significant difference in sample means found between the two data sets for S100A4, α SMA and desmin. Yet visually it can be seen that there is a larger (than cytokeratin) difference in S100A4 being expressed between the COPD and control patients. The final fibrotic marker assessed was collagen (3.3.14D) that show an extremely significant, ($p=0.0009$) difference between the sample means.

Figures 3.3.14G + H depict similar patterns that visually there is more CD45 and CD68 presenting cells present in COPD patients than in controls with CD45 not quite significant. With Figure 3.3.14I it can be seen that there is a higher percentage of NE expressing cells in COPD patients when compared to controls calculated as very significant ($p=0.006$)

A



B

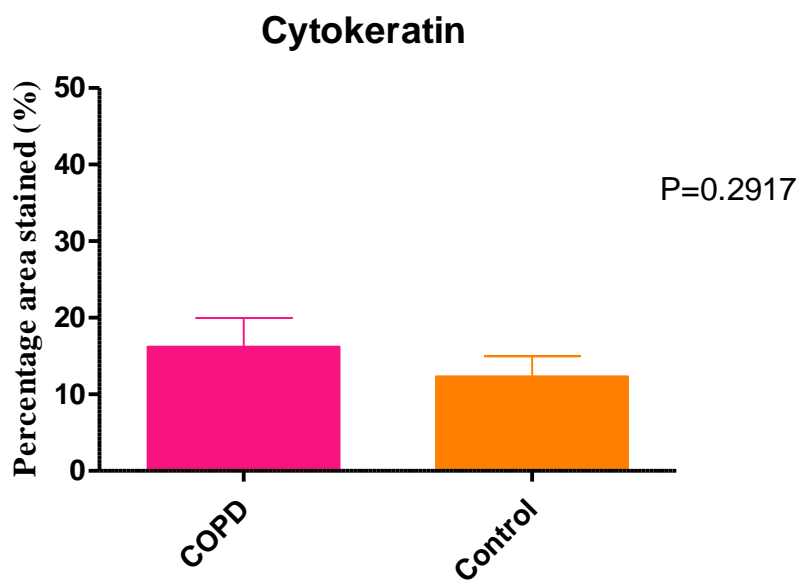


Figure 3.3.14A+B Percentage area stained comparison of epithelial markers between the total COPD and control patient data sets, Total N=37, COPD N=12 & control N=15. A Mann-Whitney U test showed that there was no significant difference between the groups for both Ecadherin and Cytokeratin.

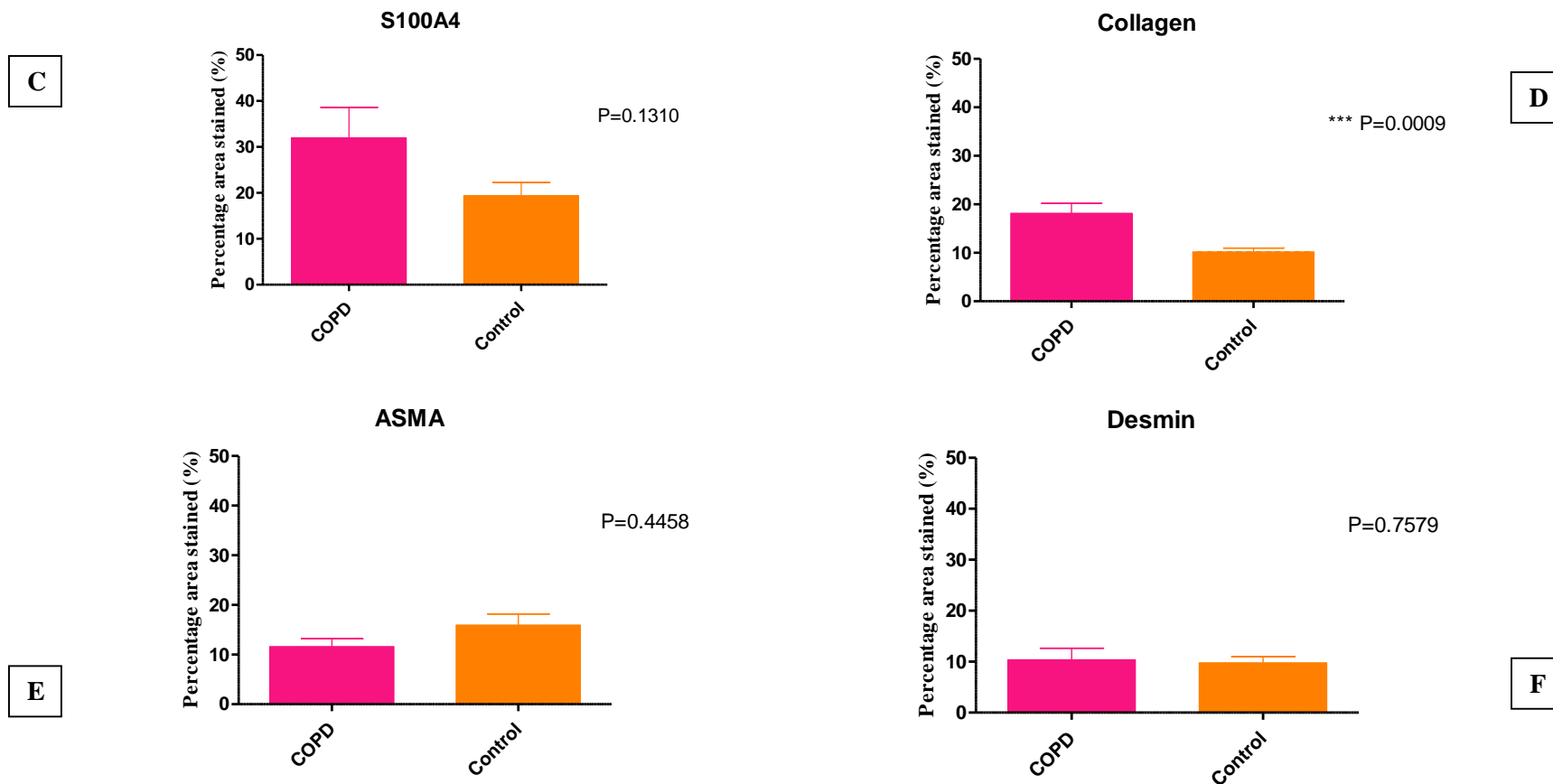


Figure 3.3.14C-F Comparison of fibrotic markers between the total COPD and Control patient data sets: Total N=37, COPD N=12 & control N=15. A Mann-Whitney U test showed there were no statistical significance between the two groups for S100A4, α SMA and Desmin. There was a statistical difference ($p=0.0009$) between the groups for the percentage area stained of collagen.

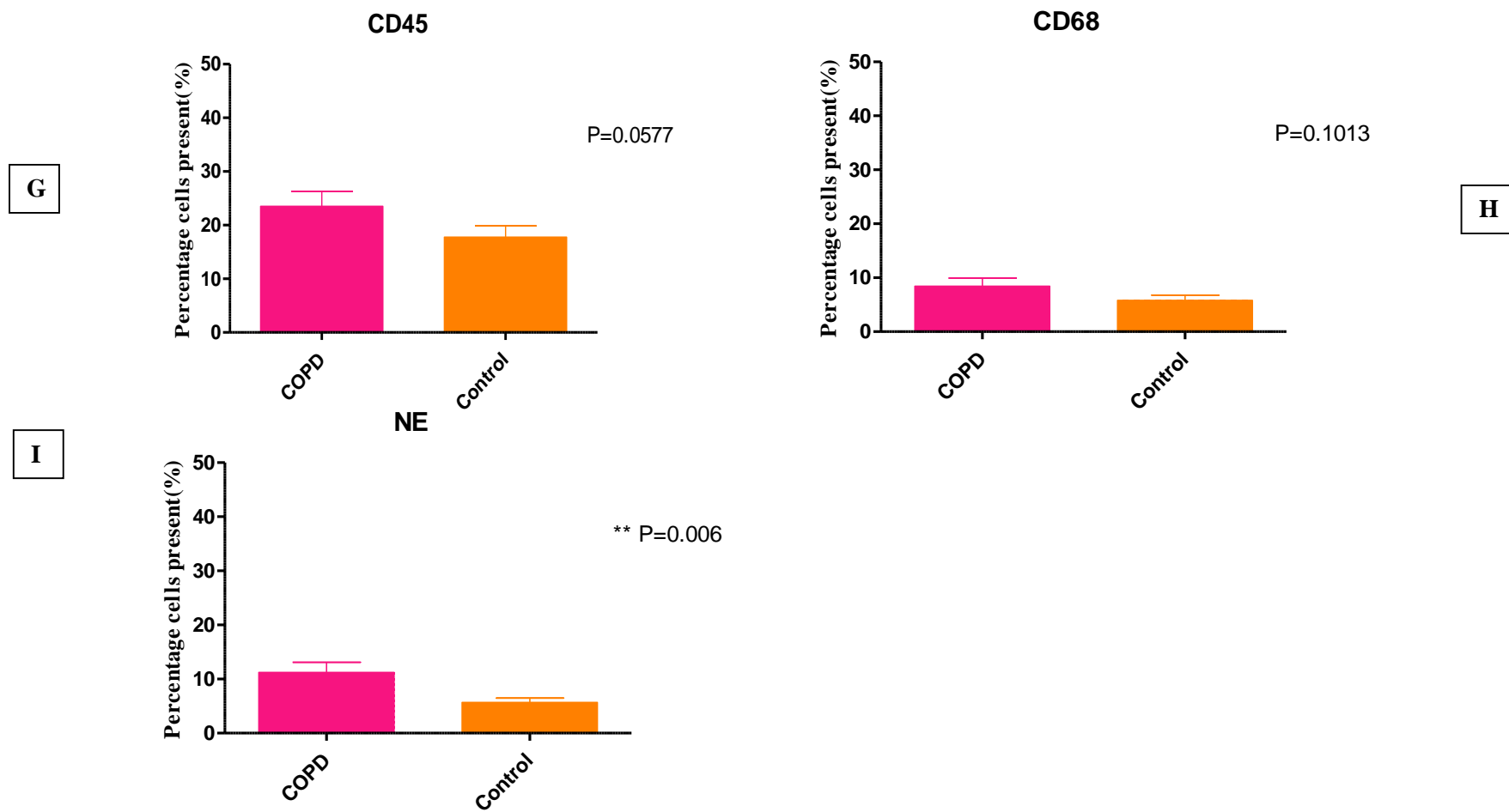


Figure 3.3.14G-I Percentage area stained comparison of leukocyte markers between the total COPD and control patient data sets: Total N=37, COPD N=12 & control N=15. A Mann-Whitney U test showed significance ($p=0.006$) between the data sets for NE.

3.3.8 Correlation of demographics to EMT biomarkers

To better understand the relationship between lung function (disease severity) and smoking history (pack year history (PYH)) with biomarker expression, dot plots were made for each marker with and added best fit linear regression line.

3.3.8.1 Lung function

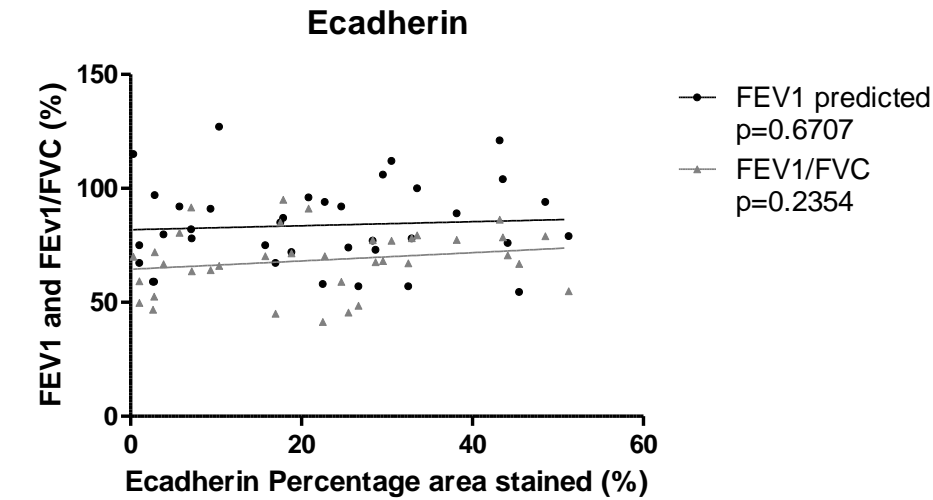
The figure 3.3.15A+B shows that there is no correlation between the percentage of lung tissue stained with either FEV1 or FEV1/FVC ratio. This indicates that there is no connection between lung function and the amount of expression of the epithelial markers, which matches histograms shown previously in this chapter.

There is a significant negative correlation ($p=0.0195$) between FEV1/FVC and percentage area stained of S100A4; meaning as lung function declines there is an increase in expression of the EMT/fibrotic marker. Figure 3.3.15D shows that there is no correlation between the total amount collagen present and lung function. The Masson's trichrome stain used for assessing the collagen content is a broad spectrum stain and stains all types of collagen. It would be interesting to see the results after doing a specific collagen stain i.e. type I collagen that is associated with tissue repair. When looking at the desmin figure (3.3.15F), even though not statistically significant ($p=0.0531$), there is a trend of a negative correlation FEV1/FVC and to a lesser extent FEV1. No correlations were formed between lung function and presence of α SMA.

There is a significant negative correlation ($p=0.0253$) between predicted FEV1 and the amount of CD45 cells present with a complementary insignificant trend against FEV1/FVC ratio. This means that as the predicted FEV1 decreases there is an increase in the amount of CD45 cells present, however this finding is not significant. There is also a negative correlation trend for both CD45 and CD68 when plotted against FEV1/FVC ratio. Again these results could have been affected by the residual blood in the tissue and or sample types – some have a large number of blood vessels within the sectioned tissue.

There is a significant negative correlation ($p=0.0303$) between predicted FEV1 and the amount of NE cells present with no correlation for FEV1/FVC ratio. This means that as the predicted FEV1 decreases there is an increase in the amount of NE cells present, however this result is not reflected in the lung function results the patients achieved, FEV1/FVC ratio.

A



B

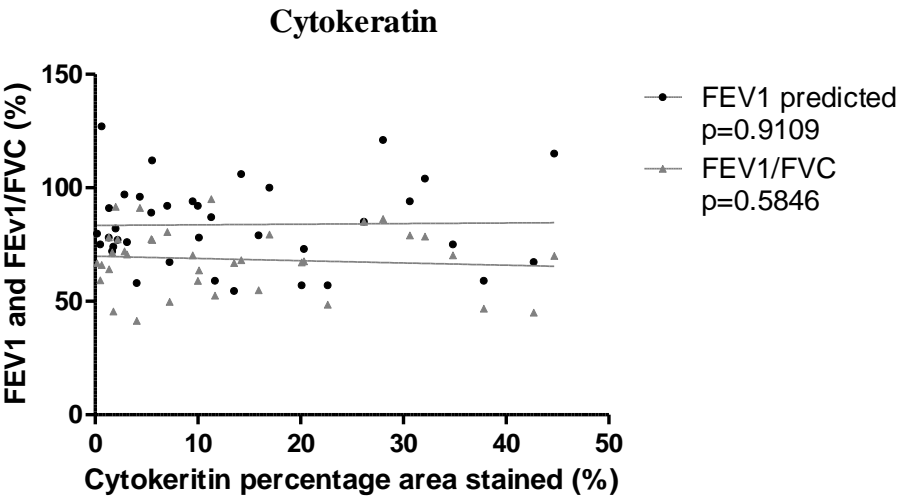
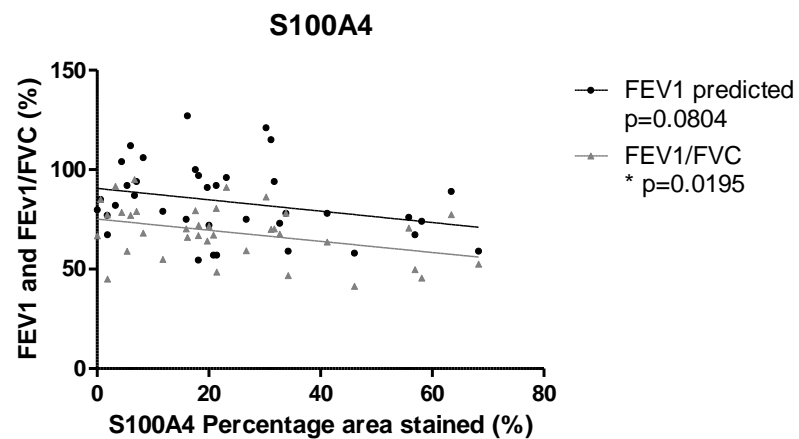
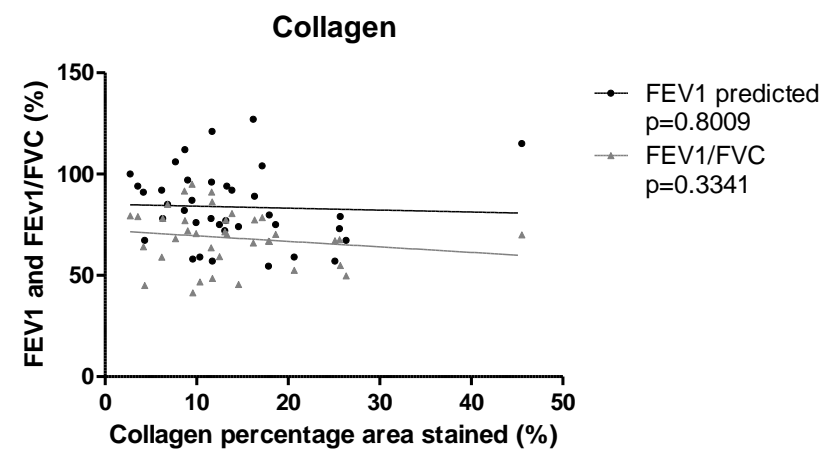


Figure 3.3.15 A+B Linear regression of lung function and percentage area stained of epithelial markers N=37. A Mann-Whitney U test showed no significant correlation for either marker in both FEV1 predicted and FEV1/FVC ratios.

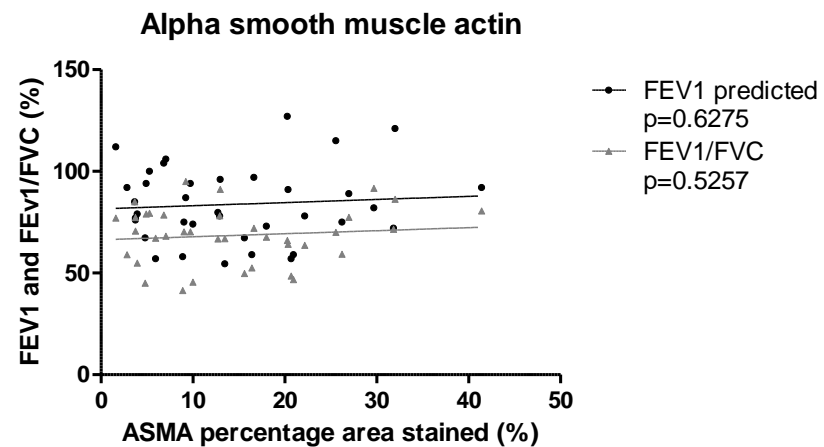
C



D



E



F

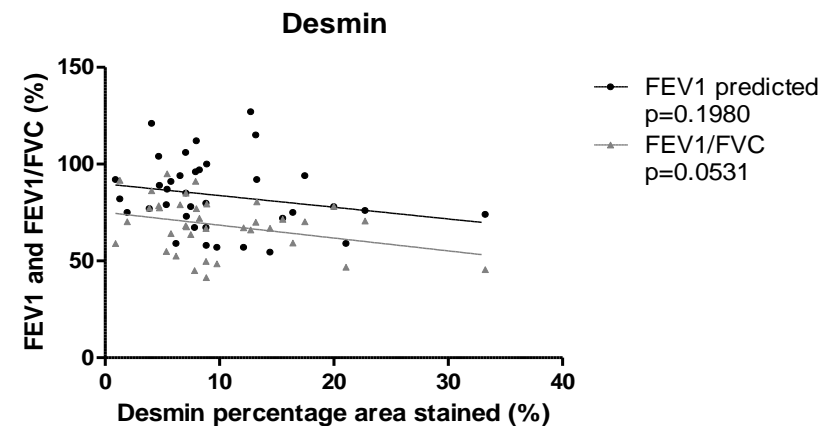


Figure 3.3.15C-F Linear regression of lung function and percentage area stained of fibrotic markers: N=37. A Mann-Whitney U test showed no significant correlation for any marker in both FEV1 predicted and FEV1/FVC ratios, except a significant ($p=0.0195$) negative correlation for FEV1/FVC in S100A4

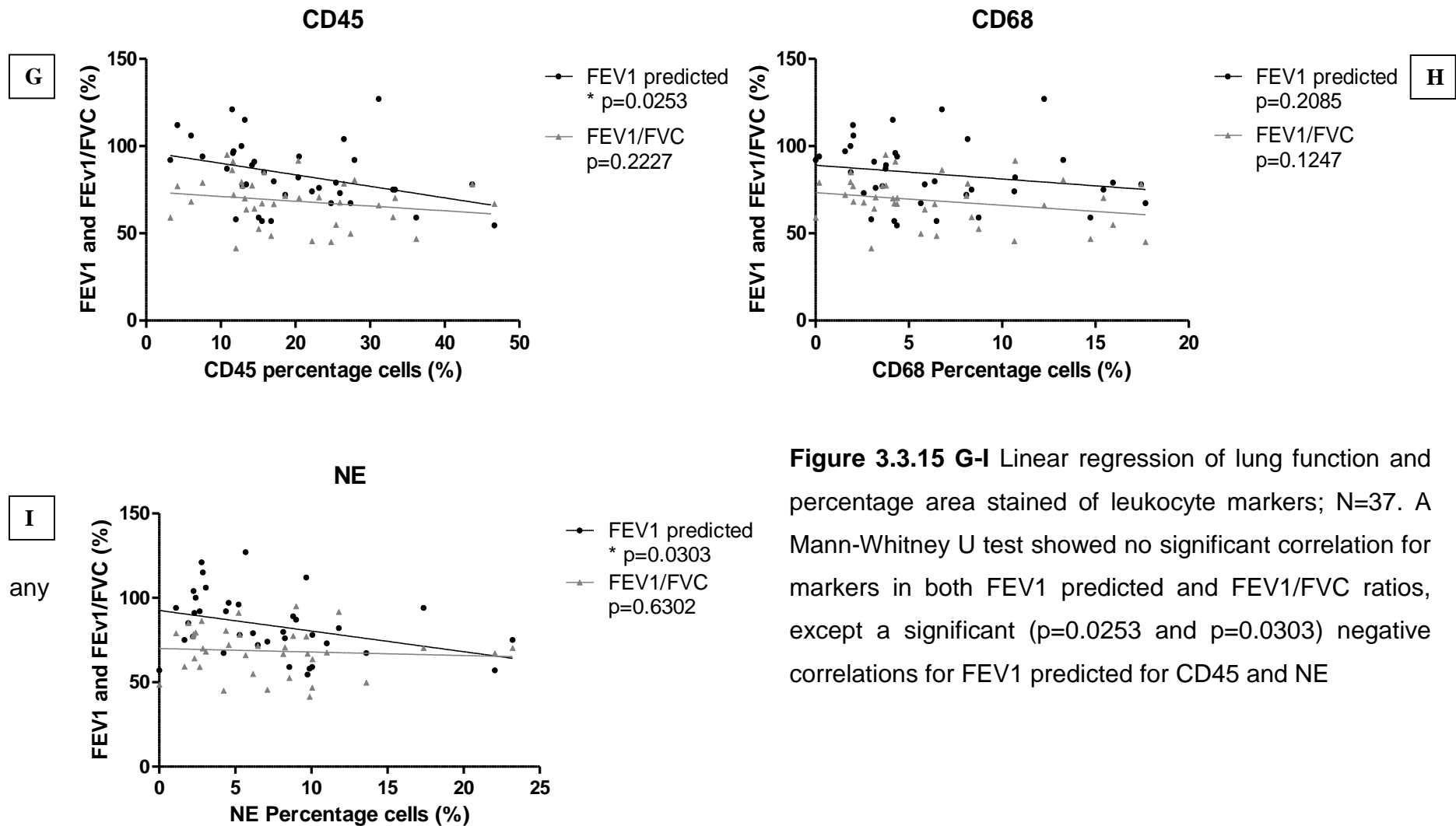


Figure 3.3.15 G-I Linear regression of lung function and percentage area stained of leukocyte markers; N=37. A Mann-Whitney U test showed no significant correlation for markers in both FEV1 predicted and FEV1/FVC ratios, except a significant ($p=0.0253$ and $p=0.0303$) negative correlations for FEV1 predicted for CD45 and NE

3.3.8.2 Pack year history

There is a significant negative correlation ($p=0.0308$) between the pack year history and the expression of E-cadherin (figure 3.3.16A); meaning the more the patient smokes the less E-cadherin is expressed in the alveolar tissue. These results follow the trends seen in the histograms. Cytokeratin also showed a non-significant negative correlation trend to lung function, (fig 3.3.16B) however there has been no significant evidence shown in the histograms therefore the data shows no clear link for smoking and reduction in cytokeratin present in the lung tissue.

There is a significant positive correlation between the pack year history and the percentage area of collagen present ($p=0.0405$) and S100A4 ($p=0.05$); meaning the more the patient smoked the more collagen and S100A4 marker are present within the tissue.

There is no significant correlation for the α SMA or Desmin graphical data shown in figures 3.3.16E+F. They do show positive correlation trends similar to the lung function linear regression graphs. The α SMA trend with PYH and histograms may be an early indicator of lung structure changes linked to active smoking but not linked with COPD.

There is a very significant ($p=0.0010$) positive correlation between PYH and percentage of CD45 expressing cells (Figure 3.3.16G) present in the lung tissue, meaning the more the patient smoked the more lymphocytes within the tissue. The trends for the entire leukocyte markers match the trends seen in the lung function linear regressions with the CD68 vs. PYH trend being much stronger linking the increase with active smoking more strongly than with lung function decline.

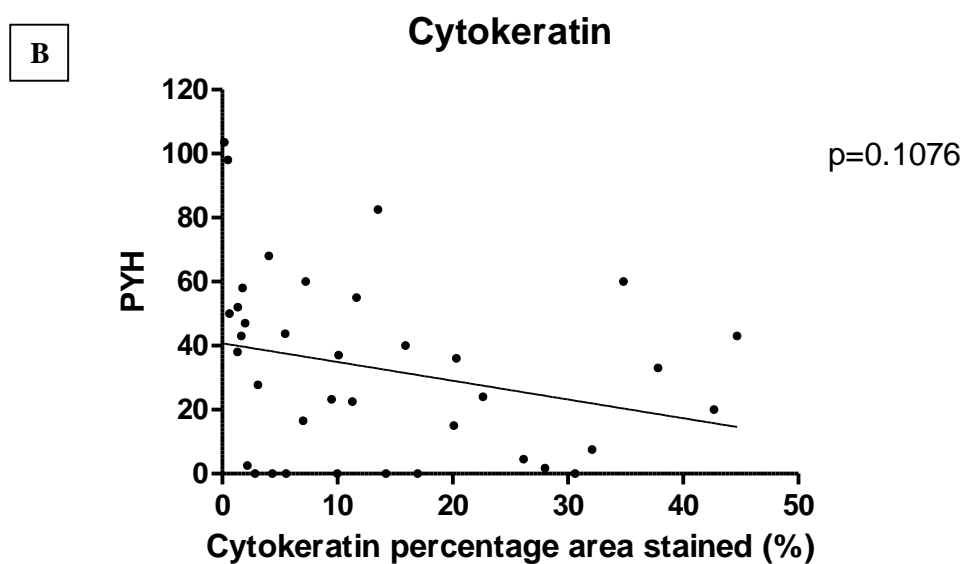
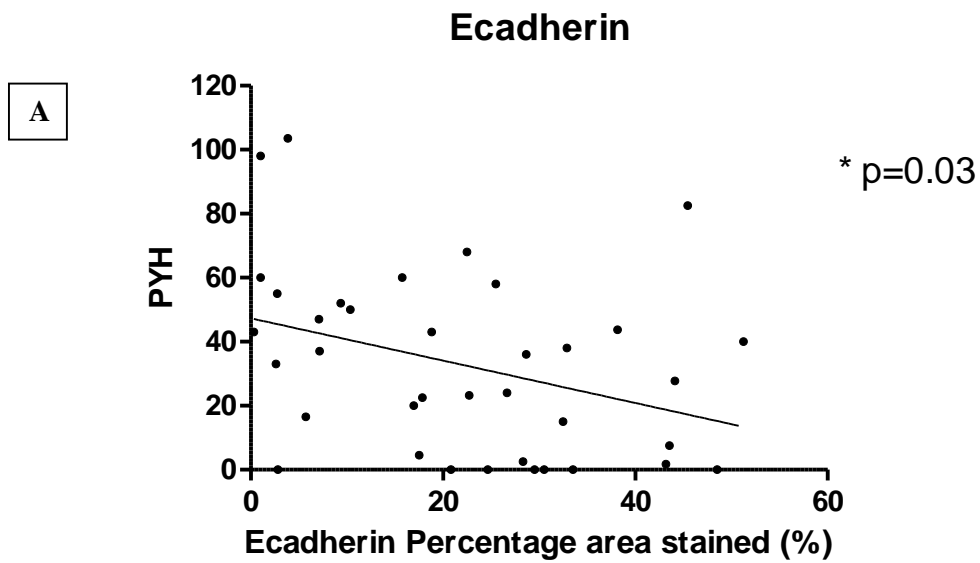


Figure 3.3.16 A+B Linear regression of PYH and percentage area stained of epithelial markers; $N=37$. A Mann-Whitney U test showed significant negative correlation for Ecadherin and pyh, $p=0.03$.

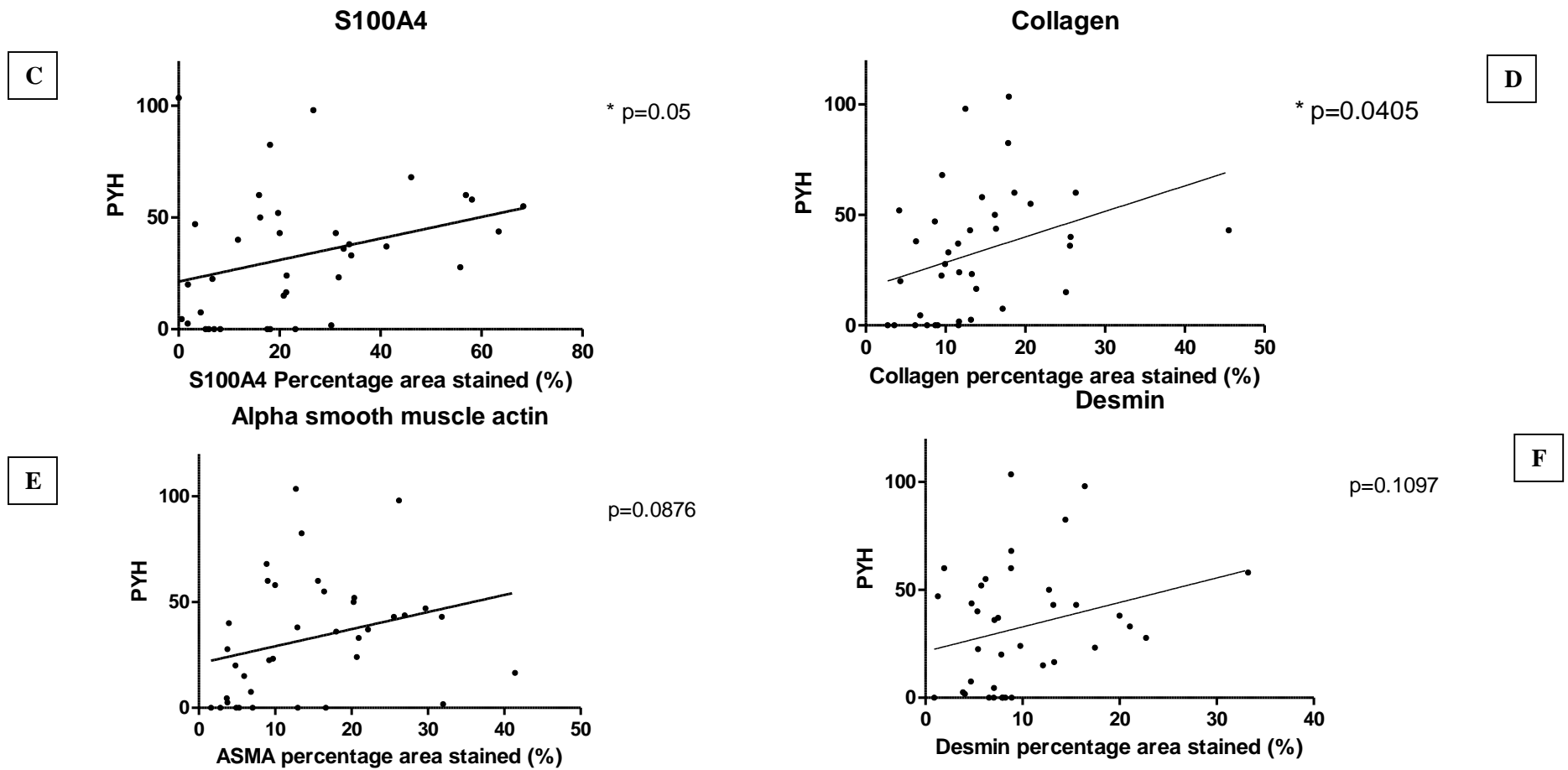


Figure 3.3.16C-F Linear regression of PYH and percentage area stained of fibrotic markers; N=37. A Mann-Whitney U test showed significant positive correlation for S100A4 ($p=0.05$) and collagen ($p=0.0405$) against pack year history.

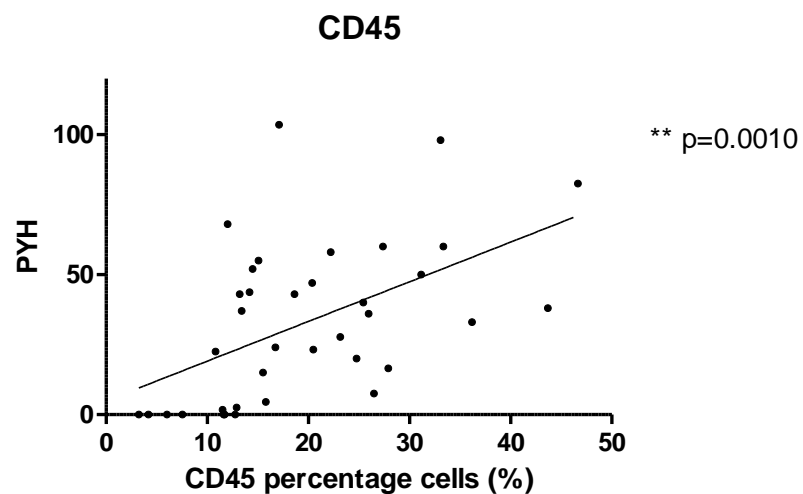
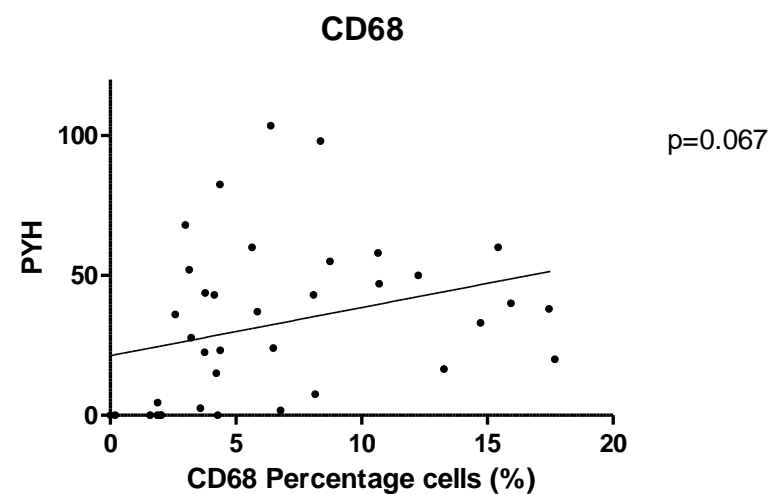
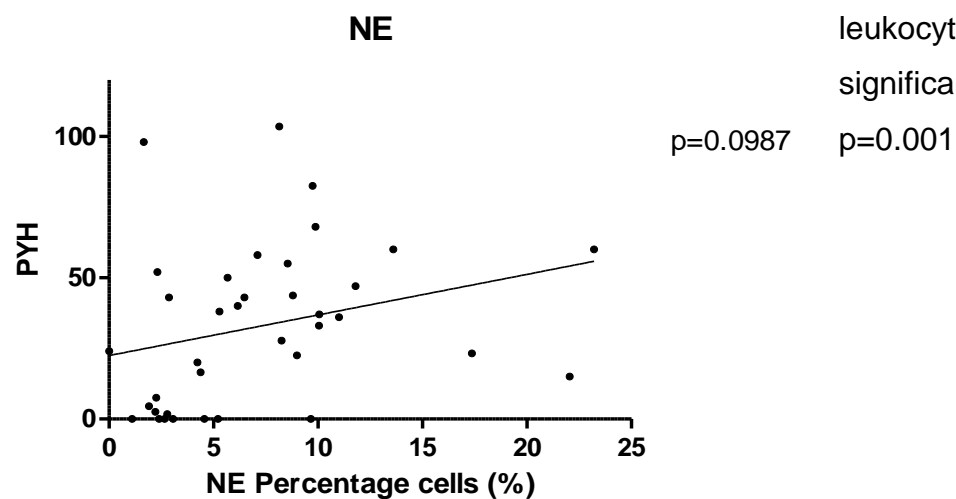
G**H****I**

Figure 3.3.16 G-I Linear regression of PYH and percentage of leukocyte cells present; N=37. A Mann-Whitney U test showed significant positive correlation for CD45 and pack year history, $p=0.001$

3.4 Discussion

IHC findings in this chapter report airway remodelling events relating to EMT/fibrotic processes in the COPD lung. This was achieved by studying the differences in epithelial, fibrotic (EMT) and leukocyte markers over a range of formalin fixed paraffin embedded human lung tissue samples with ranging demographics, from non-smokers to COPD current smokers.

3.4.1 Antibody optimisation: Positive controls

The first stage conducted was antibody optimisation of the selected pre-established epithelial and fibrotic markers. Preparing cell lines (A549 and NHLF as IHC staining controls) into paraffin fixed wax embedded proved to be very difficult due to cell detachment from the slides during staining. Our attempt to repeat the method of Morgan 2001, became overly time consuming for our overall aims; issues included (1) potential over dilution of the cells in the mixture therefore providing with sections with a very sparse distribution making it difficult to identify any cells that may have stained, or (2) the cell agarose mix may be improved with an alternative cell-agar mixture. Alternatively we elected to use cell cytospins for our IHC staining controls, accepting the limitations of them not being processed via wax as the lung samples. The cytospin technique works by drawing suspension fluid into a filter resulting in a deposited monolayer of cells onto a defined area of a slide; however this technique can cause pronounced changes to the cellular morphology, such as stretching and distorts cellular as well as nuclear appearance, it can change staining characteristics and possibly cause cellular destruction, (Morgan 2001). With this in mind the chosen methodology wasn't the best for the IHC controls and the alternative of growing the cells upon coverslips would be done in future studies.

3.4.2 Epithelial markers: optimisation

The E-cadherin antibody required heat induced epitope retrieval which was most optimal in pH9 tris-EDTA buffer; this worked in agreement with the experimental findings that a ph. change from 6 to 9 gives around a fourfold increase in staining

enhancement, (Nordi, 2005). It also followed the same pre-treatment patterns as Sawada *et al* 2008 seen with FFPE ovarian and peritoneal tissue as well as Beraki *et al* 2012 established on breast tissue fine needle aspiration fixed smears. A heat induced epitope retrieval expected as e-cadherin is an adheren junction protein that plays a critical role in homotypic cell-cell adhesion, formation of the paracellular barrier and maintenance in tissue architecture, (Naydenov *et al* 2012). E-cadherin is mainly expressed on cell membranes and due to its functionality will be localised to where cell membranes meet, (Didon *et al* 2010). Therefore without the epitope retrieval the e-cadherin protein being expressed would not be fully accessible for immune-staining; this is evident as there is little to no staining on the slides that had no pre-treatment. The positive staining achieved was mainly found in areas of the lung with reduced signs of remodelling, for example in control subject alveolar sac walls which was expected as these are primarily made by epithelia. E-cadherin staining was also found in the outer borders of thickened airways, this suggests that either not all epithelia in damaged areas undergo EMT (even though percentage area stained was much less evident in fibrotic areas), or the epithelial cells are in the process of undergoing trans-differentiation into mesenchymal cells but are yet to lose E-cadherin expression. This has also been noted in areas in proximity to the bronchioles of emphysematous mice, (Didon *et al* 2010).

Similarly to lung tissue E-cadherin staining patterns, there was a strong positive membrane staining for E-cadherin with light cytoplasmic staining in the positive control for all epithelial cells (A549s). There was no staining in the fibroblasts (NHLFs). Expected staining patterns of well characterised cells ensured optimal pre-treatment and dilutions were applied to the lung tissue.

Cytokeratin is widely known as a good epithelial marker and has been used to distinguish between fibrotic and non-fibrotic cells (Sohal *et al* 2011). In the optimisation images it can be seen that cytokeratin is wide spread throughout the lung tissue and it can also be observed in dense areas of thickened airways suggesting that it may be expressed in cells of a fibrotic lineage. Sohal *et al* 2011 observed dual positive staining for S100A4 and cytokeratin in epithelial cells in the reticular basement membrane of biopsies taken from 6 COPD current smokers. This

suggests that cytokeratin is still readily expressed in cells that of a fibrotic lineage or the cell type in the thickened alveoli may not just be fibroblasts but have a range of cells that have undergone “partial EMT” (Kalluri and Weinburg 2009).

With the positive controls the immune staining of cytokeratin is not as strong as the E-cadherin, showing a very light cytoplasmic staining on the majority of the A549 cells, some of which also have a darker intra-cellular membrane staining. The fibroblasts (NHLFs) unexpectedly showed a light cytoplasmic stain of cytokeratin in almost 50% of the cells present. This data is not supported by Pilling *et al* 2009 as they found no expression of cytokeratin present in both fibrocytes and fibroblasts they used. However with the data presented by Sohal *et al* 2011 shows that both S100A4 and cytokeratin can be dually expressed in epithelial cells, it would be interesting to see if this is the same for the NHLFs as this is not a normal characteristic expected of them; nevertheless this result supports the antibody optimisation, as cytokeratin was readily expressed throughout the lung parenchyma. Alternatively growing cells on coverslips rather than cellular cytopins may rectify this observation. As previously mentioned cells can become distorted and change staining patterns during this procedure.

3.4.3 EMT/Fibrotic marker optimisation

Desmin was expressed in dense quantities around large airways, thickened blood vessels and thickened alveoli. Additional small areas of expression may be due to formation of α -SMA and/or desmin positive fibroblastic spindle shaped cells in the lung periphery. Taking into account the data found by Lofdahl *et al* 2011 also found similar expression in human COPD patient lung tissue; supporting our findings.

The antibody used for the fibrotic marker S100A4 produced dark positive staining around thickened airways and blood vessels. It also became apparent that the resident alveolar macrophages also express S100A4, it has been observed by Pilling *et al* 2009 that it is expressed in macrophages and monocytes from peripheral blood. Presence of stained alveolar macrophages has been taken in to account when performing analysis of stained lung samples; the area of macrophage staining subtracted from the parenchymal staining. In addition to this, the α -SMA biomarker

was found in large fibrotic areas of the lung including thickened blood vessels and small areas of spindle shaped cells. Pilling *et al* 2009 showed variable S100A4 expression in both fibroblasts and fibrocytes. The possible different origins of the fibroblast cells could be a reason for the variable expression of both biomarkers desmin and α -SMA. This also may be due to a variation in patient types, as Lofdahl *et al* 2011 found that COPD patients had significantly higher α -SMA expression than smokers and non-smokers.

The positive control epithelial cells show no staining for the fibrotic markers S100A4 and α -SMA but do show significant cytoplasmic staining for the fibrotic marker desmin. Kalluri and Weinburg 2009 state that desmin has been used to identify epithelial cells of the kidney liver intestine and lung that are in the midst of undergoing inflammatory related EMT, suggesting the A549 cell line could have undergone stress during the cytopspin procedure; it is known that desmin is expressed early before cellular conversion to fibrotic lineage (in myogenic programme). Desmin has many attributed functions including cytoskeletal structure, cellular regulation and aiding cellular contractility, (Costa *et al* 2004) and so may be normally expressed at a residual background level.

NHLFs show a strong positive but patchy membranal stain for α -SMA for some of the cells. It would be expected to see a more uniform staining in all cells; this may be due to cell protein changes in the latent cells, or due to their naïve state. Activated cells with TGF beta may have provided a better positive control. There is also positive membrane and cytoplasmic stain for S100A4 and a positive cytoplasmic with some nuclear desmin staining. This is to be expected with fibroblasts and it conforms to the mesenchymal cellular characteristic that is expected to be observed in patient samples.

3.4.4 Leukocyte markers

Leukocyte markers CD45 the lymphocyte common antigen, CD68 a macrophage marker and neutrophil elastase are widely used to identify these cells residing in different tissues.

Neutrophils are the first cells recruited to the lung in response to cell injury they phagocytose apoptotic bodies and any residing cell debris. Then in turn activates the neutrophils causing cell degranulation, release of inflammatory and pro-fibrotic cytokines. Macrophages are then recruited via IL-8 and other chemokines, then extravade into the damaged tissues. Macrophages phagocytose and secrete fibrogenic cytokines; including TGF- β 1 in fibrosing organs. T and B lymphocytes are also recruited to the site of injury and further facilitate secretion of fibrogenic cytokines. (Barnes 2003; Barnes 2008; Kisseleva and Brenner 2008).

In the higher concentrations of CD45 there is some staining of the lung periphery evident this is due to fibrocytes and fibroblasts expressing this marker, (Pilling *et al* 2009) however once further dilutions of the antibody was made this reduced any lung periphery staining therefore avoiding high background parenchymal staining.

When tested on the positive control cells (A549 and NHLF) none of the leukocyte markers were expressed. This is as would be expected but it has been noted that CD45 and CD68 can be expressed in fibrocytes and fibroblasts, (Pilling *et al* 2009) therefore it was essential to take cell size and morphology into account when undertaking cell counts and staining quantification.

3.4.5 H&E and Collagen

The H&E stain was performed to compare cell size and morphology, of the two cells lines. It can be seen that the fibroblasts are larger than the epithelial cells. The majority of the lung tissue is comprised of epithelial cells and they were are clustered together and possess the typical flatten morphology expected, whereas the fibroblasts that are in contact with each other are taking on the typical parallel formation and had begun to spread themselves in order to achieve the spindle shape normally associated with inactive cells (Dalby *et al* 2005).

Observed shrunken cell morphology may be caused by cytopspining, fixing and dehydration of the cells. Other studies (Morgan 2001) have used gentler ethanol gradients to reduce this effect; however our study needed to match these control cells with staining conditions of the lung tissue.

The Masson's Trichrome stain shows that there is no collagen present or surrounding any of the epithelial cells which is to be expected as they are not collagen producing cells, when activated they recruit cells that do such as myofibroblasts (Hastie *et al* 2002; Pardo and Selman 2012). There is weak collagen staining in the NHLFs (blue staining), this is typical of collagen producing cells such as fibroblasts in response to environments that place them under stress, such as being deposited on hard surface, (Kisseleva and Brenner 2008).

3.4.6 Patient Examples (1 COPD and 1 control subject)

There is a clear difference in the epithelial markers expression between the two lung patients (LP#617 COPD patient and LP#650 Control subject). Epithelial markers are raised in control subject; compared to lower expression levels COPD patient, suggesting extensive EMT occurring in this section of the patient's lungs. In addition to this by comparing the two patients in figure 3.3.7 A & B, it can be seen that the proteins linked with EMT and fibrosis are raised in the COPD patient but not in the control subject. Leukocyte numbers are also increased in the COPD patient compared with the control subject; this is typical cell pathology of COPD patients as the disease is highly inflammatory driven causing the influx of leukocytes to areas of alveolar damage (Kisseleva and Brennan 2008). These preliminary results are what were hypothesised to be found between the two groups of the main' blinded' study.

Interestingly as with the control cell lines the fibrotic marker desmin was present in both subjects, although there was only a small percentage cover in the control subject compared to the COPD patient. Desmin has been found to be present in tissue that may have undergone partial EMT (Kalluri and Weinburg 2009), even though this particular subject is classified a non-smoker.

3.4.7 Validation of repeatability in the S100A4 positive control

Staining intensity showed modest variations in staining intensity on 5 independent occasions. Statistical analysis found this was not significant in the percentage area stained. This indicates that external variables such as room temperature and

varying batches of reagents had little effect on the percentage area stained over the course of the study.

Positive macrophage staining for S100A4 was subtracted from overall expression to adjust data to be specifically focussed on EMT related changes. All S100A4 results presented, takes this correction factor into account.

The images taken from the positive control slides had also been used to determine the DAB threshold parameters for ImageJ analysis (figures 3.3.5A&B), which has been applied to the analysis of all DAB chromogen stained samples.

As an additional determination that the computer assisted analysis was reliable the level of concordance between it and manual analysis was checked, figure 3.3.6B. It was found that there was no significant difference between the analysis means and that the data was significantly matched; concluding that this method of analysis is reliable for the study which matches conclusions reached by Brey et al 2003. It is now believed that the use of computer assisted analysis is far superior to traditional methods as low levels of stained antigen are difficult to separate from areas of dark counter stain. The difficulty in differentiating between these areas by manual analysis leads to variations in the results. Computer assisted imaging and analysis methods that reduce dependence on observer analysis decreases the overall time of analysis and lessens the variation in results among different laboratories and between day to day opinions of the observer (Ruifrok and Johnston 2001; Brey *et al* 2003; Sezgin and Sankur 2004; Levenson 2004 and Luongo de Matos *et al* 2010).

3.4.8 Group data findings

3.4.8.1 Epithelia markers

E-cadherin

Our cohort data showed no significant variation of E-Cadherin expression between subject groups or in relation to current or ex smoking status. Trends do show E-cadherin expression is lowest in current smokers in ex-smokers and again in non-smokers. Sohal and Walters 2013, state that they have observed an abundant amount of E-cadherin staining in conjunction with N-cadherin (fibrotic) expression within the same area (serial sections); this indicates the occurrence of EMT within

the small airways of smokers lungs. We observed E-Cadherin expression levels being reduced in current smokers inferring EMT processes are a consequence of active smoking.

Reduced E-cadherin expression in diseased lungs is not linked to the onset of COPD (airway obstruction), but may be linked to smoking. This data is supported by Nagathihalli *et al* 2012 who have shown that the down regulation of E-cadherin does correlate with the number of pack years in lung cancer patients via 'cigarette induced EMT'. Ohbayadhi *et al* 2014 show E-cadherin down regulation in epithelial cell lines post injury. It is also interesting to note that E-cadherin expression is linked with a tumour suppressor gene; down regulation of E-cadherin is linked with tumour progression and metastasis (Yao *et al* 2014). Noting this it would be interesting to relate E-cadherin expression data to cancer typography for possible future studies.

Cytokeratin

It is interesting to point out that the level of cytokeratin present is slightly higher in COPD over control lung tissue which arises from the COPD ex-smoker patients, Sohal *et al* 2011 suggest that cells undergoing active EMT are either derived from another origin or that they are can double express both epithelial and fibrotic markers in the airways of smokers and COPD. It is seen that active EMT is indicated by the degradation of underlying epithelial basement membrane and is mediated by the transition of epithelial cells into mesenchymal cells, which have migratory potential, meaning that they relocate from the epithelium in which they originated into deeper tissues.(Sohal *et al* 2011). This suggests that cytokeratin is still readily expressed in cells/tissue of a fibrotic lineage, or that the cell type in the thickened alveoli may not just be fibroblasts but have a range of cells that have undergone "partial EMT" as also noted in other lung studies (Kalluri and Weinburg 2009). Future studies using a dual stain, on a select set of patients, with cytokeratin and a fibrotic marker such as S100A4 would be able to confirm this. De Vriese *et al* 2006, describe a pronounced co localisation of cytokeratin and the fibrotic marker α -SMA in interstitial fibrotic tissue of rat uraemic peritonea, showing cytokeratin can still be present in fibrotic tissue as in our study.

S100A4

S100A4 expression did not significantly vary in our patient cohort between COPD and control subjects or with pack year history. However expression levels were numerically raised in COPD patients compared to controls

We assessed effects of current smoking (all current smokers) versus previous smoking (all ex-smokers) on EMT markers. Significantly raised expression was evident in COPD current smokers. Our findings are similar to Sohalet *al* 2011 who observed in airway biopsies, S100A4 is present in asymptomatic smokers with normal lung function but was most pronounced in COPD current smokers.

Our study also shows current active smoking in control subjects is significantly linked with raised S100A4 levels (Fig 3.3.13 C). This data shows EMT is evident in smokers' airways but further raised in current smoker COPD subjects indicating EMT signalling may require an ongoing persistent stimulating signal for example as S100A4 levels are high in current smokers but lower in ex this may suggest that there is some element of EMT reversibility and that EMT up regulation may require ongoing cigarette smoke stimulus. This is important to understanding the role of EMT contribution to the known irreversible nature of COPD pathology. If the driving factor (cigarette smoke) is removed, the cells may undergo mesenchymal to epithelial transition. The better understand the rate of this reversal process is very relevant to the survival chances of patients following quitting smoking.

Both our data and Sohal *et al* 2010 showed inverse correlation of S100A4 expression and airflow limitation. It is likely additional COPD current smokers in our study may strengthen this data. The above results and observations suggest that the level of S100A4 is not linked to the onset of COPD but it is linked to the smoking status of the patient with a possible element of reversibility of EMT. Reversibility of fibrosis has been studied in the liver and is associated with the withdrawal of chronic injury e.g. HBV, HCV this results in the reduced production of pro- inflammatory and fibrotic cytokines/chemokines with the loss of TGFβ1 signalling being critical, (Kisseleva and Brenner 2008) Less is known about the

reversibility of lung fibrosis and the loss of lung integrity may prevent any resolution of fibrosis.

A-SMA

There is no a significant difference or correlations between the amount of α -SMA expressed and any of the analytical categories, It is interesting to note that the expression of α -SMA is higher in control subjects compared to COPD and particularly higher in current and ex-smokers compared to the other groups, which is contrary to what was expected. Lofdahl *et al* 2011 describe COPD patients having significantly higher α -SMA expression than smokers and non-smokers which themselves had no difference. However data from this study is fully supported by Karvonen *et al* 2013 who report that peripheral specimens of COPD current smoker patients, have a lower area coverage of positively stained alveolar tips (free inter alveolar septa), than smokers with normal lung function. The difference between our data is that their non-smokers present a higher amount of α -SMA than other groups; they characterise their non-smokers as long life never smokers or ex-smokers who have less than a 10 pack year history (differently to our study using a cut-off of just one pack year). Karvonen's controls are therefore different to ours and may have been exposed to many more pack years of cigarette smoke. Rock *et al* 2011 propose that the expression of α -SMA in myofibroblasts is dynamic over the course of fibrosis, with higher levels early in progression which may help explain the data discrepancies. Variations may be further explained by α -SMA expression being located to large fibrotic areas of the lung including thickened blood vessels (Santos *et al* 2002 and Karvonen *et al* 2013). Some patients had increased numbers of blood vessels in the samples and larger airways such as bronchioles, (Karvonen *et al* 2013). Epithelial cells (alveoli) and endothelial cells (blood vessels) are located in very close proximity to one another and the injury of one often affects the other (Kisseleva and Brenner 2008).

Considering S100A4 and α -SMA data, it is possible we are observing a mixture of fibrotic areas derived from EMT and fibroblastic expansion and/or recruited fibroblasts. Rock *et al* 2011 observed that S100A4 cells did not co-localise with either stellate S100A4 positive cells located near vasculature and airways, and

other S100A4 positive cells were elongated and located within the interstitium, supporting my observation.

Pilling et al 2009 show that there is variable expression of α -SMA expressed in both fibroblasts and fibrocytes. This suggests that there can be a variation in α -SMA protein expressed on fibroblasts cells which could be due to deviation in fibroblast origins, which have been recruited to sites of lung injury. To determine the origin it would be interesting to conduct a dual fibrotic stains on COPD current smoker sections with desmin and α -SMA; this may indicate differences in stained areas, which could indicate that there are two different phenotypes of myofibroblasts (Löfdahl et al/2011; Skalli et al/ 1989 cited in Karvonen et al/ 2013).

Seemingly from my data the decrease in α -SMA expression is linked to COPD and its overall increase could be related to smoking but further studies need to be conducted to verify this.

Desmin

Desmin expression did not vary between COPD vs. controls however considering 5 groups revealed very significant differences between current and ex-smokers which we believe is a novel finding to the best of our knowledge from current literature. Even though desmin expression mirrors that of α -SMA in control smokers it is noted that most α -SMA expressing cells (either fibrotic lineage or smooth muscle cells) are negative for desmin (Santos et al 2002, Löfdahl et al/ 2011 and Karvonen et al/ 2013). In areas that do co-express the desmin positive cells were very few in numbers, (Löfdahl et al/ 2011). It is good to note that both of these markers are found in smooth muscle cell within pulmonary arteries, as some patients had an increase (compared to other samples) in blood vessels; this explains the high percentage area stained.

It is likely that desmin expression is not connected to COPD progression but has been used as a co-identifying marker for fibrotic cells or smooth muscle cells in pulmonary arteries in previous studies. Even though not quite significant there is an observational negative correlation between the FEV1/FVC and desmin expression. This explained staining patterns observed within the lung tissues, as desmin was seen to be expressed in dense quantities around larger thickened

airways, thickened blood vessels and thickened alveoli; suggesting that this marker is associated with obstruction of the airways. Pilling *et al* 2009 did not detect any desmin expression in fibrocytes derived from human peripheral blood or normal human dermal fibroblasts, interestingly these cells only had variable expression of α -SMA. Taking into account data found by Lofdahl *et al* 2011 our results are reasonable. On another point it has been shown that desmin knockout mice can go through myogenesis unaffected which suggests that once the fibrotic cells has used the desmin i.e. for cell contractility it may down regulate this marker and replace it with the other contractile protein α -SMA, (Costa *et al* 2004). This again ties in with the previously noted results from the antibody optimisation, positive controls and lung samples (LP#617 and 650) which supports the findings by Kalluri and Weinburg 2009.

Collagen

We found a significantly raised amount of total collagen deposition in COPD patients versus control subjects which is prominent in COPD current smokers compared to non-smokers. This is in agreement with published data that the total collagen is increased in COPD patient's lung periphery when compared to control subjects, (Kranenburg *et al* 2006). An increase in collagen in the lung periphery was expected to correlate with increasing disease progression/ inverse correlation with FEV1 as seen by Kranenburg *et al* 2006. As the more tissue injury occurred through smoking causes the recruitment of inflammatory leukocytes which in turn facilitates the process of EMT and excessive production and deposition of collagen, (Kisseleva and Brenner 2008; Tanjore *et al* 2009). However no significant correlation between lung function and collagen deposition was seen. Masson's trichrome stain is broad spectrum and stains all collagen, including existing ECM and collagen content in cytoskeletal structures of cells including RBCs in blood-filled samples. It is likely if the staining was repeated with collagen specific antibodies (beyond the scope of the current study), type I and III this would change to an inverse correlation of lung function and deposition of collagens associated with fibrosis. In addition to this it would be interesting to distinguish between the collagen positive fibrocytes from the collagen positive fibroblasts by using the expression of cellular fibronectin, HA-BP or TE-7 which is expressed on the fibroblasts but not fibrocytes, (Pilling *et al* 2009); this would give another clearer view on the origin of the collagen producing cells.

We observed raised levels of collagen in current smokers and a positive correlation with PYH. It has been suggested that cigarette smoke inhibits the growth and functionality of lung fibroblasts grown from patients with emphysema, (Nobukuni *et al* 2002) however more recently it has been found that CSE did not affect fibroblast activity to deposit collagen, (Larsson-Callerfelt *et al* 2013) which supports my data of the more the patient smokes the more collagen is present in the lungs. It is safe to say that collagen deposition is linked to both smoking and the onset of COPD.

3.4.8.3 Leukocytes

Numerous studies have characterised pathological hallmarks of leukocytes in COPD; characteristically linked with COPD progression are raised numbers of macrophages, neutrophils and lymphocytes within the airway mucosa and lung parenchyma when compared to control subjects, (Caramori and Adcock 2003; Hogg *et al* 2004 and Todd *et al* 2012).

CD45

Comparisons of 5 subject groups revealed current smokers have a higher amount of infiltrating CD45 presenting cells when compared to both ex and non-smokers. This suggests that there is a reversibility of the amount of infiltrating CD45 cells but not be mistaken with the un-reversible amount of damage already done.

COPD current smokers have the highest numbers of CD45 cells, indicating raised number of leukocytes have infiltrated into the lung tissue in COPD smokers. It is possible it also reflects altered numbers of blood vessels too.

There is also a significant negative correlation between the predicted FEV1 and CD45 positive cells showing that the poorer the lung function the more CD45 cells are present; linking these cells with disease progression. Supporting this data is a positive correlation with PYH (showing raised leukocytes with smoking duration.

CD68

Considering 5 groups, macrophages were strongly linked with current smoking but there were no significant differences between COPD vs. control subjects. Macrophages do not only phagocytose the products of cellular damage and degradation but provide key fibrogenic signals including TGF β 1, which in turn promotes the activation and proliferation of collagen producing cells (Kisseleva and Brenner 2008) therefore the more macrophages present the more tissue remodelling may occur; this finding thus supports our hypothesis of EMT as a mechanism of COPD progression.

NE

There is a very significant difference between the amount of NE cells present between COPD and control subjects. Similarly when considering 5 groups raised neutrophils are present in COPD current and ex-smokers compared to control current-smokers which is only slightly higher than ex and non-smokers. Broader comparisons of all current smokers versus all ex-smokers show no significant variations of neutrophil numbers; suggesting that once recruited, there is no decline or reversibility of neutrophil presence within the lung parenchyma. Neutrophil numbers are therefore linked to disease progression rather than smoking status and is supported by the lack of correlation between NE numbers and PYH. Once damaged the alveolar tissue releases stress signals in the form of cytokines/chemokines causing the mass recruitment of phagocytic leukocytes, macrophages (CD68) and neutrophils (NE) into the lung. Neutrophils release proteases which inadvertently causes destruction of ECM as the process progresses into chronic inflammation (repeated injury induced by smoking). Ordinarily protease levels are regulated by TIMPs, however in COPD it is likely this process is dysregulated. Overstimulation of the phagocytes can induce fibrogenesis; NE is also implicated in the activation of latent TGF β 1, (Kisseleva and Brenner 2008). Once this chronic inflammatory cascade has started neutrophils will continually be recruited to the lung as more inflammatory signals are perpetuated by positive feedback, (Overbeek *et al* 2013). There is a significant correlation

between FEV1 predicted and the amount of neutrophils present which is similar to previously reported findings (Balzano *et al* 1999).

We found a very significant correlation between the percentage area stained of collagen and NE positive cells. Overbeek *et al* 2013 proposes that neutrophils activated by cigarette smoke extract can breakdown collagen into chemotactic collagen fragments and that this can activate neutrophils, which may lead *in vivo* to a self-propagating cycle of neutrophil infiltration, chronic inflammation and lung emphysema. This indicates that the higher percentage of neutrophils present will be causing destruction to the lung periphery and ECM causing a cascade of further overproduction of ECM i.e. collagen.

Data in this report and from previous studies show increases in macrophages, neutrophils and lymphocytes within the airway mucosa and lung parenchyma as hallmark characteristics of COPD lung pathology. (Caramori and Adcock 2003; Hogg *et al* 04, Todd *et al* 2012). One interesting point is the patient with the highest PYH 103.5 (COPD current smoker) appears to be an outlier with all of the fibrotic and leukocyte markers; despite having COPD this patient has a reasonable FEV1/FVC ratio of 66.76%. This indicates that lung damage and subsequent remodelling is not exclusively linked to smoking but could also be linked to an unknown genetic mutation that itself has degrees of severity.

Throughout the IHC study each patient had only one lung section used per marker; this formed a limitation to the study and interpretation of the results as it was only an insight into a very small fraction of the patients' lung parenchyma. For example the data taken from 5 images of one section was assumed to be the standard parenchymal environment for the patient. However this would not be true as alveolar areas containing fibrotic tissue or not would change.

To expand on this study any future staining will start off using the cumulative frequency approach to determine the correct number of individual sections to be used per marker. Cumulative frequency is used to determine the analysis of the frequency of an occurrence of data values, in our case the percentage area stained of a particular marker, which is more or less than a reference value. Once data

analysed the correct number of patient sections pre marker would be sliced and stained giving a better overview of overall tissue structure in each individual patient. A reference lung block e.g. LP#624 would be used as a reference, then all residual patient tissue would be compared to this data. By adopting this approach it would make our data more robust and enable us to draw more concrete conclusions in regards to EMT in COPD.

3.4.9 Conclusion

Computer assisted analysis is reliable for the analysis of all DAB stained samples using the threshold determined by the positive controls but it is not suitable to measure collagen production stained via Masson's trichrome stain, to provide true reliable results manual counts were conducted.

It can be concluded that the epithelial marker E-cadherin down-regulation is not linked to COPD progression, however is linked to an increasing smoking history. Cytokeratin expression is not a reliable marker for EMT characterisation, as it can be readily expressed in both epithelia and fibroblasts. Interestingly the three fibrotic markers S100A4, α -SMA and desmin expression is not linked to COPD/airway obstruction progression, but the variable expressions are linked to increasing smoking history with possible EMT for S100A4 and desmin. Finally, matching previous literature both collagen deposition and leukocyte numbers is linked to both COPD and smoking.

From this study, it can be determined that depending on the location of fibrosis source, or possible severity of COPD (in the case of α -SMA) the fibroblasts may develop different cytoskeletal and protein expression features despite the fact they all have the same morphological appearance. This leads to being able to determine that fibrosis of the lung is not solely via the EMT process but it is consistent with the suggested model of where there are four possible sources endothelial - mesenchymal transition (EndMT), epithelial - mesenchymal transition (EMT), the increase in number of fibroblasts at fibrotic foci derives from circulating bone marrow-derived progenitors and fibrocytes attracted to regions of lung injury. As

noted the tissue for patients with lung cancer, the findings are in agreement with Sohal *et al* 2011 that EMT is smoking related and that it may lead to understanding of why lung cancer is so common in smokers but especially in those patients with COPD, where the lungs have a higher instance of injury and seemingly higher expression of some fibrotic markers in conjunction with the decrease of epithelial tumour suppressor marker E-cadherin, (Yao et al 2014).

Findings of this study support justification to continue with characterisation studies and do further investigations via LCMD and subsequent studies of looking at fibrosis related gene transcription factor expressions via QRT-PCR.

Chapter 4

Characterisation of signalling paths mediating EMT in human lung tissue:

Quantitative RT-PCR gene expression analysis of laser capture micro dissected tissue

4.1 Background

4.1.1 TGF- β is a key mediator of EMT

Trends found in chapter 3 indicated raised fibrotic biomarkers with smoking history for S100A4, collagen and desmin, and a clear trend for α SMA; which inversely correlated with raised E-cadherin expression in never smokers. These findings supported our hypothesis of EMT contributing to lung fibrosis in smoking related COPD.

Weaker data is seen when directly considering the airway obstruction of COPD patients, nevertheless, S100A4 was significantly raised in COPD patient tissue and E-Cadherin expression was again clearly raised in subjects with normal lung function compared to those with obstruction; again supporting our hypothesis.

Regulation of EMT is a key process to understand in order to develop novel treatments to intervene with its progression with a view to slowing or limiting lung fibrosis. Many triggers may induce EMT, however TGF- β in particular is well documented in driving EMT (Kalluri and Weinburg 2009) and some of the TGF- β mediated signalling paths are well described in other fibrotic conditions. Indeed TGF- β can induce fibroblasts to up regulate at least 150 genes; spanning functions from cell signalling (autocrine and paracrine), matrix formation, cytoskeletal reorganisation, cell proliferation and differentiation, survival gene transcription and metabolism, biosynthesis of proteins, apoptosis and ECM production (Wang *et al* 2012). More specifically to EMT, fibroblast trans-differentiation *in vitro* was observed via the SMAD3 (transcription factor) dependant mechanisms (Willis *et al* 2006), however SMAD3 independent mechanisms are also described in this review; shown in figure 4.1.

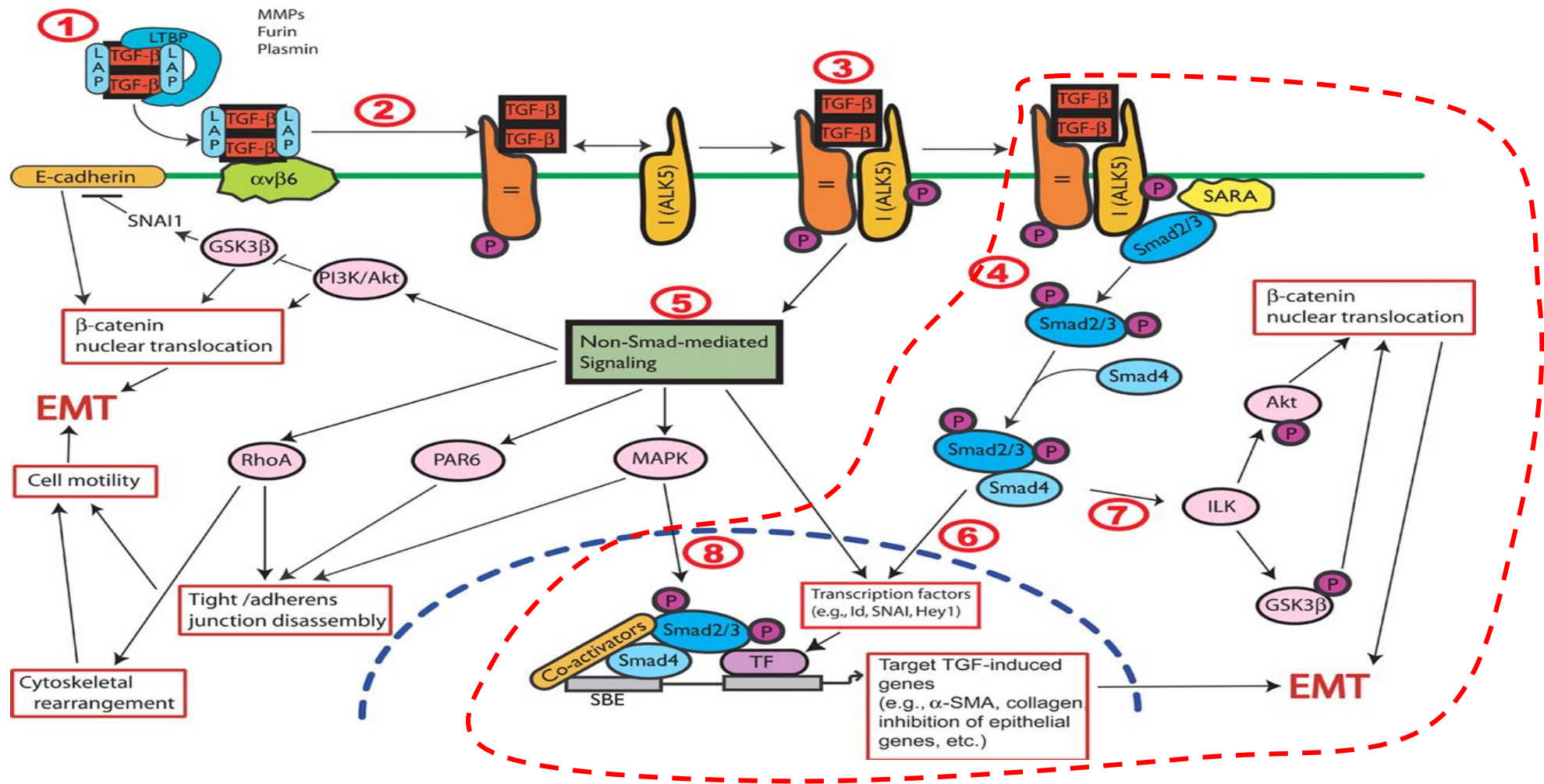


Figure 4.1. Proposed mechanisms of TGF- β regulation of EMT adapted from Willis and Borok 2007. SMAD3 dependent mechanisms are highlighted by the red dotted region and are the key focus of this chapter to identify TGFbeta mediated EMT in COPD lung tissue.

4.1.2 TGF- β signalling

TGF- β is inactive most of the time as it is presented in a latent form that prevents it binding to its receptors. It is bound to latency associated peptide (LAP), and by the latent TGF binding protein (LTBP) (1 in fig 4.1). Release by LTBP allows TGF- β LAP complex to be either stabilised by surface cadherins or freed by proteases such as plasmin. Free TGF- β heterodimers can bind to the TGF- β receptors (2 in fig 4.1).

TGF- β /type II receptor complexes may in turn associate with the type I TGF- β receptor (e.g., ALK-5) in a heterodimer (3 in fig 4.1). This receptor heterodimer becomes activated and can initiate several signalling pathways. Not all paths result in functional transcription; non-genomic signalling has also been described. It seems both Smad-mediated (Smad2 and Smad3) (4 in figure 4.1) and non-Smad-mediated (5 in fig 4.1) pathways are involved in either case.

Smad-mediated pathways are associated with activation of TGF- β -induced target genes such as α -smooth muscle actin, collagen, plasminogen activator inhibitor-1, and connective tissue growth factor. Also linked is the inhibition of epithelial genes (e.g., E-cadherin) (6 in fig 4.1) which is via activation/induction of and coassociation of transcription factors such as Snail1 and Snail2. This is followed by binding to Smad-binding elements.

EMT is also mediated by the non-genomic signalling molecules that are still Smad-mediated. These include ILK, which activates Akt and GSK3B and β -catenin nuclear translocation.

Non-Smad-mediated pathways can elicit a range of cell changes via activation of PI3K/Akt, RhoA, PAR6, and MAPK. EMT related changes include tight/adherens junction disassembly, and E-cadherin downregulation,

Also described are interactions of SMAD and non SMAD mediated mechanisms via MAPKinase activation (8 on fig 4.1).

Relating specifically to the lung, previous research by our group used the lung epithelia cell line A549 to investigate EMT and found supporting evidence for the role of TGF- β signalling via SMAD (Kasai et al 2005). More recently S100A4 a calcium binding protein has been characterised as a downstream Smad3 dependent mediator responding to TGF β 1 stimulation on fibroblasts in systemic

sclerosis (Tomcik *et al* 2013); further, expression of S100A4 is linked to the process of EMT of many fibrotic conditions including Kidney, cirrhosis, and cardiac hypertrophy (reviewed, Schneider *et al* 2008).

Given the EMT observations in lung tissue via IHC in chapter 3, we wanted to characterise EMT associated signalling mechanisms to investigate regulation of EMT in COPD lung tissue. We therefore selected likely candidate gene targets based on contemporary literature focussing on SMAD mediated paths that are regulated by TGF- β .

4.1.3 Rationale of Lazer Capture Microscopy Dissected Tissue (LCMD) followed by QRT-PCR technologies used in this chapter.

LCMD is now a wide and routinely used technique used for the direct visualisation and isolation of individual microscopic cells to whole areas of tissue of interest from heterogeneous tissue, (Fuke *et al* 2004; Nawshad *et al* 2004; Erickson *et al* 2009 and Percoco *et al* 2012). Specific regions of interest can be dissected without the disruption of *in vivo* cellular status for downstream applications such as RNA, DNA and protein analysis (Fuke *et al* 2004). LCM has been applied in a wide range of studies to examine varied cell types in both normal and diseased states, (Kinnecom and Patcher 2005), such as the isolation of endothelial and perivascular cells from brain micro vessels (Kinnecom and Patcher 2005), dermatological isolation of keratinocytes from skin biopsies, (Percoco *et al* 2012) and bronchiolar macrophage and epithelium to assess inflammatory chemokine expression of COPD patients, (Fuke *et al* 2004).

Formalin fixation limits quality of RNA and DNA available for extraction, as its crosslinking fixation action can directly react with the nucleotides (Howat and Wilson 2014) for this reason fresh-snap frozen lung tissue was used as the basis for this molecular study.

Sectioned snap frozen tissue that has either not been stained or stained with a routine dye such as H&E, shows a greatly reduced cellular detail without a cover slip, (Fend *et al* 1999); this can prove difficult for the specific isolation of the cells/tissue of interest from a complex mixture of cells with similar morphological

features. The use of IHC for cellular identification is ideal, however, the standard protocol used requires several hours of incubation periods, which results in the degradation of integrity with subsequent loss of RNA. Preservation of RNA quantity and quality is critical for RNA quantification analysis. Using methods from Fend *et al* 1999, Simpson *et al* 2011 and Lecia microscopy protocols, in this study I established a rapid immunostaining technique for S110A4 to enable precise isolation of epithelial and EMT regions in human lung tissue, when used in conjunction with LCM.

Various methods can be employed to quantify transcription factor and their downstream products, and western blotting is a popular option as this allows observation of post-translational modifications such as protein phosphorylation; indicative of component activation. Westerns typically require much larger amounts of starting tissue material so we selected the very sensitive technique of Q-PCR which we anticipated would be suitable for much small amounts of material generated from the LCMD technique.

Quantitative RT-PCR gene expression analysis was achieved by using SybrGreen. SybrGreen, employs one pair of gene specific primers while the fluorescent dye incorporates into the DNA during amplification which quantifies DNA amplification (Erickson *et al* 2009). Two 'housekeeping' or 'normalisation' controls were chosen; expression levels of singular HK genes have been shown to vary among different cell types, samples and environments (Erickson 2009). Obtaining the housekeeping gene average (Geomean) gives more robust data due to the reduction in variation of the data. In addition to using housekeeping genes, the RNA starting quantity was normalised (i.e. made equal) for all samples via quantification using a nanodrop followed by necessary RNA dilutions.

4.1.4 Chapter 4 aims

To characterise EMT associated signalling mechanisms in COPD lung tissue. In particular to identify expression of likely candidate gene targets of the SMAD mediated path that are regulated by TGF- β .

Specifically:

- To use immune-LCMD to identify and isolate epithelia, and regions undergoing EMT within the same patient lung to compare levels of: SNAI1 and SMAD3; also TGF β 1 and IL-6 (downstream products of SMAD).
- To use immuno-LCMD to compare the same series of SMAD3 mediated markers between the patients with COPD and the control groups.

At the time of writing we are not aware that this work has been published before and our findings are entirely novel.

4.2 Methods

Table 4.1 Demographics of lung patients used for immuno-LCMD study

Variables	COPD			Healthy		
	Current Smoker			Total	Ex-Smoker	Non Smoker
GOLD Stage	ALL	2	Unknown	0	0	0
Subject numbers	4	1	3	4	2	2
Sex	M= 2	M= 0	M= 2	M=2	M=1	M=1
	F= 2	F= 1	F= 1	F=2	F=1	F= 1
Age (years)	68.5	71	67.7	68.25	71	65.5
	± 4.12		±4.62	±6.85	±9.9	±3.54
Pack year history	52.2	56	50.93	11.23	22.47	0
	±4.98		±5.25	±21.77	±30.29	
FEV₁ % Predicted	60.2	63.7	59.03	106.88	102.5	111.25
	±3.17		±2.63	±5.17	±0.71	±1.77
FEV₁/FVC ratio, %	50.79	53.05	50.04	75.74	75.22	76.26
	±4.98		±5.82	±6.68	±0.43	±11.51

4.2.2 Tissue Preparation for Laser Capture Microscopy Dissection and Q-RTPCR

The selected snap frozen LP tissue was sectioned using a cryostat and mounted onto UV pre-treated PET membrane steel framed slides. Kept under cool conditions the tissue was stained by the fibrotic marker S100A4 using a rapid IHC protocol, and in quick succession epithelial and fibrotic tissue was isolated using LCM. Following tissue isolation, RNA was extracted for reverse transcription and cDNA synthesis prior to Q-RTPCR, performed on an Applied Biosystems 7500 Fast system. All solutions equipment and procedures used for this study were RNase/DNase free.

Three types of tissue was isolated using the same LCM technique; the individual fibrotic tissue indicated by brown staining and individual epithelial tissue deemed as non-stained tissue, as depicted in figure 4.2 below. Also whole tissue (everything disregarding any staining patterns) was isolated, this is tissue that has been sliced,

mounted, stained and stored in exactly the same manner as the individual isolated tissues. For full methodologies please refer to Chapter 2: Method & Materials.

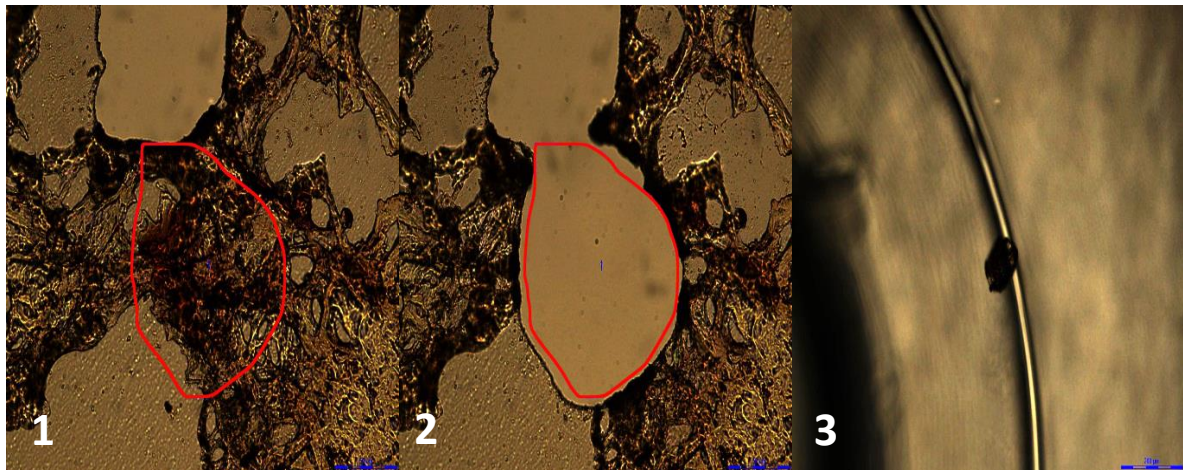


Figure 4.2 Image depicts example of fibrotic tissue isolation via LCMD, LP431. Image 1: Fibrotic area, identified by brown positive staining of S100A4, was selected and outlined utilising LCMD software. Image 2: the computer guided laser cut along selected tissue area which dropped below into a DNase RNase free eppendorf; image 3. Same repeated with non-stained epithelial tissue. Images 1&2 x400 magnification, image 3 x50 magnification.

4.2.3 Comparative C_t method ($2^{-\Delta\Delta C_t}$)

We adopted a cited method used to achieve relative quantification of gene expression by arithmetic formulas which is recommended for dissected cells assuming the efficiencies between the genes of interest are similar 100% \pm 10%, (Erickson et al 2009; Applied biosystems 2008)

To ensure $2^{-\Delta\Delta C_t}$ calculations are accurate, validation experiments were conducted; this was done using cDNA reverse transcribed from A549 and NHLF isolated RNA. These validation studies were conducted to determine if PCR efficiencies between the chosen targets IL-6, TGF β 1, SNAI1 & SMAD3 and endogenous controls GAPDH and 18S were relatively equivalent. The template cDNA was added to PCR

reactions to span 6 log concentrations (50, 25, 10, 5, 4, 2ng/uL of original RNA template as described Erickson *et al* 2009). Three replicates were performed for each standard curve point using 300mM of each primer as recommended by Primerdesign protocols.

Input Amount of Total RNA ng/uL	Log input Amount of Total RNA ng/uL	Average SNAI1 C _t of NHLF and A549 triplicates
50	1.69897	24.19635
25	1.39794	25.23671
10	1	26.65161
5	0.69897	27.9253
4	0.60206	28.21112
2	0.30103	29.32111

Table 4.2: Shows an example of the validated results for the SNAI1 target with result efficiency of 99.92%

From a combination of both NHLF and A549 data the target gene efficiencies were generated. These were then put into the 7500 fast software v2.0.6 for each plate run, which were used in the C_t value determination.

Gene Target	Efficiency %
IL-6	98.91
TGFβ1	94.73
SNAI1	99.92
SMAD3	99.76
GAPDH	99.86
18S	99.04

Table 4.3: Target efficiencies for all gene targets used

4.2.4 ΔC_t and $2^{-\Delta\Delta C_t}$ calculations

ΔC_t is the subtraction of the average endogenous control C_t value from the average C_t of the target gene. As two endogenous controls were used in this study the Geomean C_t (average of all endogenous controls) was used as the control values.

ΔC_t or otherwise known as gene expression shows the difference expression between two genes or in this case the Geomean of two housekeeping genes. This normalises all results allowing the comparison of data between two or more individuals.

$$\Delta C_t = C_t \text{ target} - C_t \text{ Geomean}$$

For the $\Delta\Delta C_t$ value the ΔC_t of EMT stained tissue was subtracted from ΔC_t of the epithelial tissue.

$$\Delta\Delta C_t = \Delta C_t \text{ epithelial tissue} - \Delta C_t \text{ EMT tissue}$$

To determine if EMT was more prominent in COPD patients compared to controls fold changes between the epithelial and EMT tissue were compared for each lung patient group. Fold change is used to calculate the quantity change from the initial value, in this case 'normal' epithelia tissue to the final value, in this case fibrotic tissue. This can only be done, in this case, on individual lung patient data sets.

$$2^{-\Delta\Delta Ct} = \text{Fold Change}$$

4.2.5 Statistical Analysis of PCR CT values

For control subjects versus COPD patients whole tissue ΔCt analysis, the data was unpaired therefore a Mann-Whitney test was performed.

For Epithelial tissue gene expression versus EMT tissue gene expression ΔCt the data was parametric so a paired t-test was used.

4.3 Results

4.3.1 Original cohort (n=12) Account and Overview of Study Limitations

This chapter originally set out to compare 12 patients (6 COPD and 6 controls) for any variations in EMT gene changes. After months of meticulous immuno-LCMD preserved samples in Trizol were prepared for RNA extraction. Unexpectedly all the samples were accidentally damaged beyond restoration by a catastrophic tube failure during centrifugation; which splintered and fractured all tube samples in the centrifuge and rendering all their contents mixed, contaminated and useless.

This was incredibly disappointing and frustrating, however immediate plans were made to do a scaled down study in the time left during my PhD and within the remaining budget. Therefore 8 more samples were used for LC tissue isolation as indicated in section 4.2.1. Due to the time constraints, smaller amounts of tissue were laser capture microscopy dissected which did impact on the yield of RNA recovered from them.

Nevertheless, data was collected from the RNA available and is presented in this chapter, however it is acknowledged further work would be needed to validate findings and raise patient numbers for publication.

RNA integrity and detection of intact 18S and 28S subunits was assessed by RNA gel electrophoresis. Results from an initial test sample (before the damaged main cohort), showed this method was useful in demonstrating we had successfully isolated RNA from the lazer captured tissue (data shown in figure 4.3.1 below). However on the repeat study, RNA yields were too low to view for assessment by this method.

Three RNA samples from validation subject LP#624, whose tissue was isolated using LCMD, were run on a denaturing RNA gel. In all three samples both rRNA subunits 28s and 18s can be seen, with sample 3 (whole tissue) having the best integrity. Samples 1 (epithelial tissue) and sample 2 (fibrotic tissue) both display band smearing, indicative of beginnings of RNA degradation.

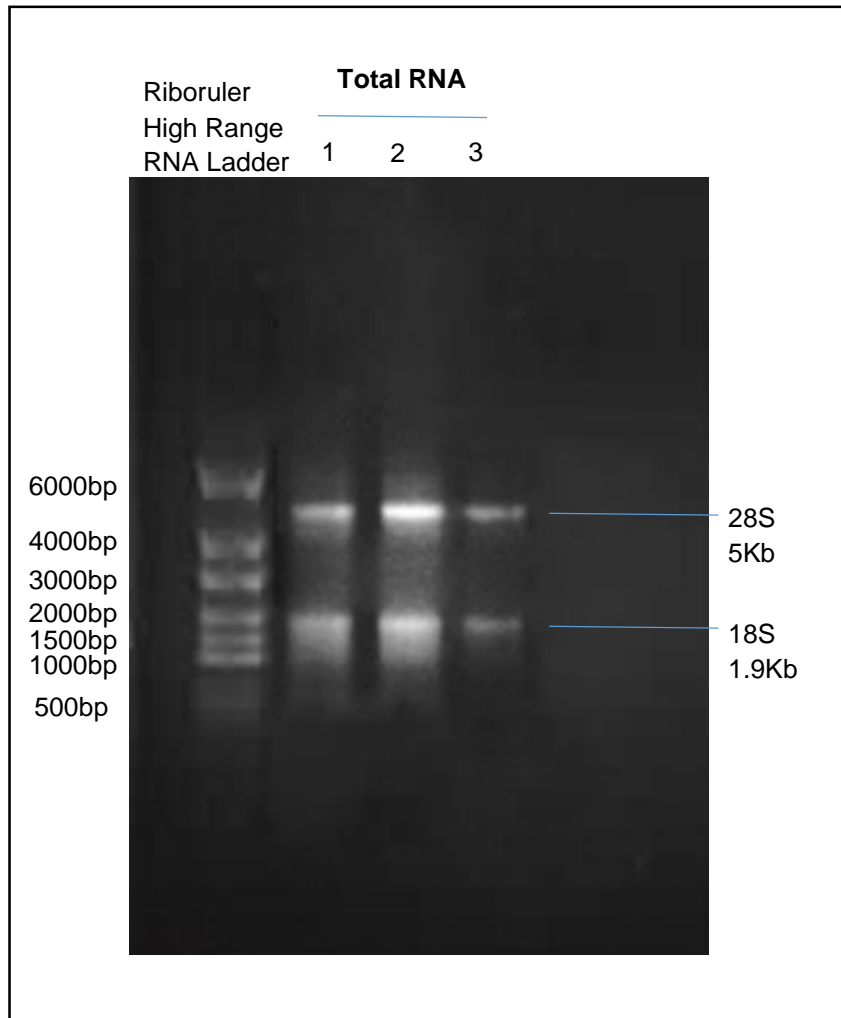


Figure 4.3.1. Denaturing RNA gel 1.5% electrophoresis of RNA isolations from LCMD tissue Image shows the results of 3 LCMD samples from a lung patient belonging to the original cohort, LP#624. Both 28s (5Kb) and 18s (1.9Kb) rRNA subunits were detected in all three samples. Samples 1 and 2 are LCMD epithelial and fibrotic tissue respectively whilst sample 3 is whole lung tissue dissected out using the same LCMD technique.

4.3.2 Validation of RNA yield was comparable between immuno-LCMD and LCMD without prior staining.

There was no statistically different C_t value difference between stained and non-stained tissue (data not shown) showing that the Rapid-IHC procedure did not affect downstream applications. In addition to this, sections of laser captured slide-

membrane alone had been isolated and no detectable RNA was isolated from this verifying there was no contaminating signal from the capture slides themselves.

Two negative controls per sample were run: no template control (NTC) and a no reverse transcription control (no RT). Each had ≥ 10 Ct difference to all amplified samples. One positive control per gene per plate was used which was cDNA from NHLF cell line. RNA isolated from these cells was put into RT-PCR in the same quantity as the RNA from the laser captured samples.

4.3.3 Group Data: Gene Expression from Whole Lung Tissue

Data in figure 4.3.2 represents the gene expression (Δ Ct values; normalised data allowing the comparison between the individual LP data) from whole LCMD lung tissue (tissue treated and dissected in same manner as individual epithelium and fibrotic tissues) for all 8 patients (4 control subjects and 4 COPD). Gene expression data was used for this assessment

By conducting Mann-Whitney U tests, the two tailed p values show that there were no statistically significant data for all tested genes. Regardless of this the COPD means are higher than the controls with the SEM being tight for TGF β 1 and SMAD3. The COPD SEM for IL-6 and SNAI1 is wider with the lower spread caused by the same single patient for both genes; indicated by the red circle in graphs A and C.

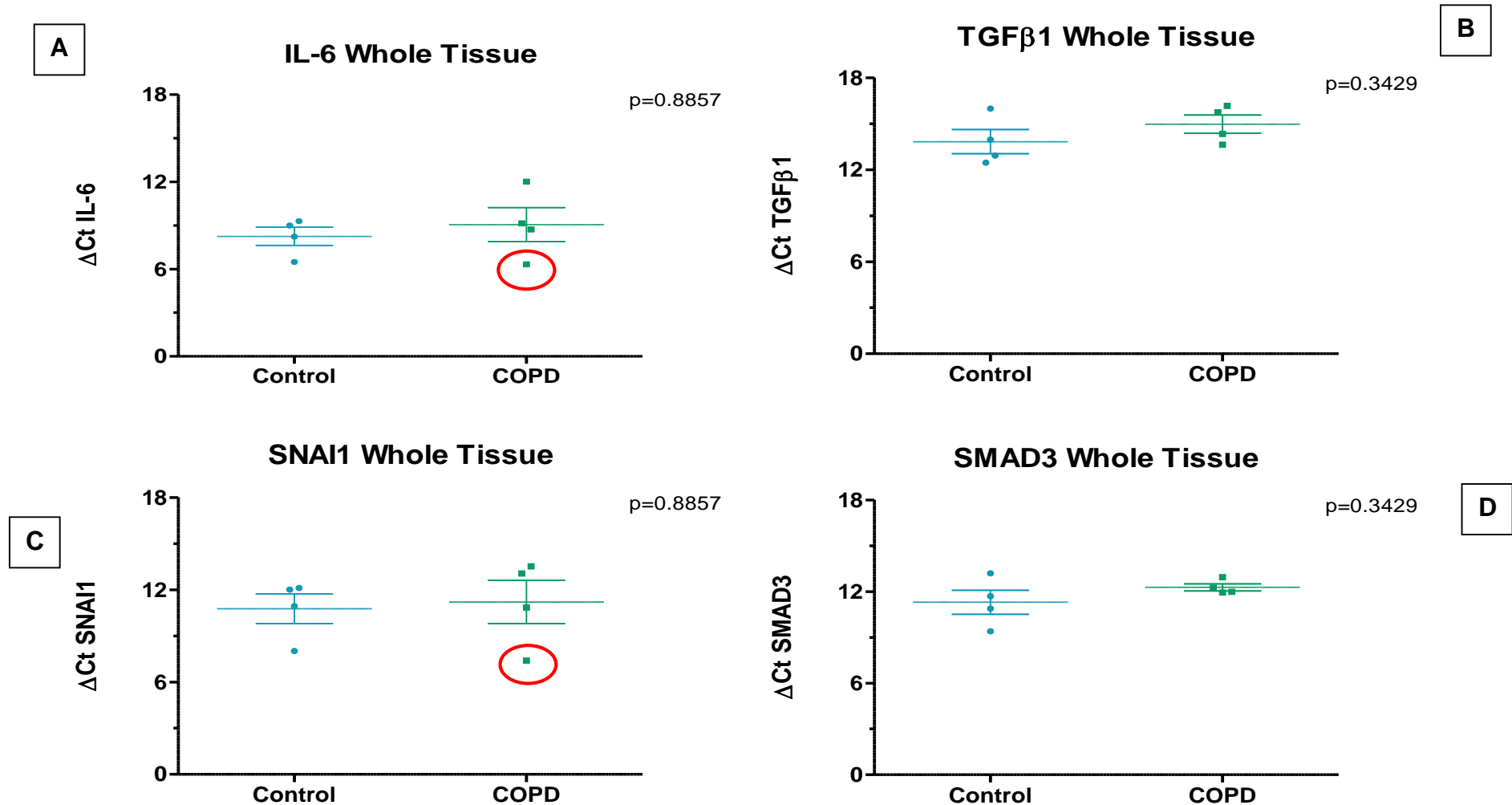


Figure 4.3.2 A-D: Q-RT-PCR gene expression of LCMD whole lung tissue. Gene expression (ΔCt) IL-6, TGFβ1, SNAI1 and SMAD3 ΔCt data of control (N=4) and COPD (N=4) groups on whole LCMD tissue (epithelium and fibrotic mix). Red circles indicate the same outlier COPD patient for IL-6 and SNAI1. Mann-Whitney U test resulted in no significant difference between groups for all genes assessed.

4.3.4 Group Data: Gene Expression from immune-LCMD: epithelia versus EMT regions.

There was no significant difference between any of the epithelial vs. EMT gene expression data (ΔCt values; normalised data allowing the comparison between the individual LP data) presented in figure 4.3.3 A-D. There is however a clear numerical increase in EMT ΔCt means against epithelial for the four genes represented.

In the EMT regions there was a wide distribution of the 7 plotted patient data, 1 patient yielded no results due to low RNA yield. Further inspection of this showed that the three highest EMT data points came from the following patients: LP# 507 of a never smoking history (NS), LP#497 a control ex-smoker (ExS) and LP#1024 a COPD current smoker. This shows that there is a mixture of patient demographics contributing to both the high and low gene expressions in these data sets.

The same three patients showed the highest ΔCt values in the epithelial tissue which were all numerically lower to those in the EMT tissue. The SEM was tighter despite clusters of points on either side of the mean for IL-6, TGF- β 1 and SNAI1; there was a more even spread for SMAD3.

Interestingly the CCS patient LP#1024 gene expression is within the highest ranges for all genes except TGF β 1. In complete reverse to this, gene expression for LP#431 (also a CCS) has the lowest ranges for both epithelial and EMT tissue for SMAD3 and TGF β 1 and low EMT tissue expression for SNAI1 and IL-6 but in mid ranges with the epithelial tissue. The low EMT tissue expression also applies to CCS patient LP248.

There were no clear correlations of smoking history (PYH) or lung function for any gene expression (not shown).

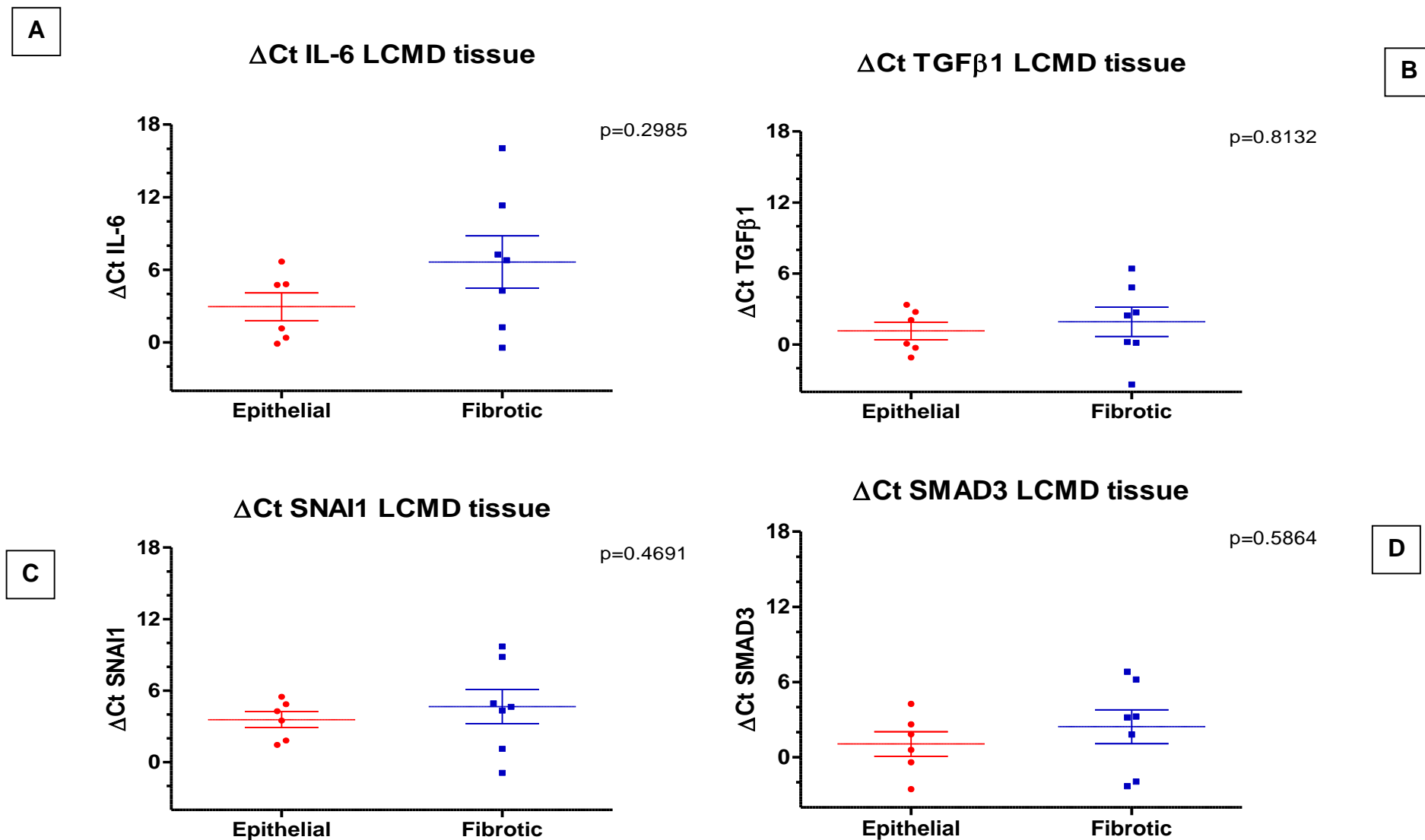


Figure 4.3.3 A-D: Q-RTPCR gene expression of Epithelial and Fibrotic LCMD lung tissue. All subject's data was grouped together then assessed for variations in gene expression between immune-LCMD epithelia (N=6) and regions of fibrotic (N=7) ΔCt gene expression IL-6, TGF β 1, SNAI1 and SMAD3. Mann-Whitney U tests performed with no significant difference found between the two tissue types.

4.3.5 Group Data: Fold changes of Gene Expression from immune-LCMD: epithelia versus EMT regions in COPD and control subjects.

Figure 4.3.3 showed raised EMT gene expression in the regions of EMT 'fibrotic' tissue. We attempted to assess if this raised gene regulation in EMT was aligned to either of the subject groups (controls or COPD) and therefore calculated fold change of epithelia to EMT for each individual patient and plotted them in the disease status groups shown in figure 4.3.4. Fold change (change in gene expression between epithelial and fibrotic tissue) is based on an individual lung patient basis. All data was normalised to the Geomean of housekeeping genes therefore data can be assessed on fold change in the disease state groups.

Due to the very limited amounts of RNA available, only a subset of matching patient data (both epithelial and fibrotic tissue gene expression for each patient) was obtained: controls n=3 and COPD n=2 meaning statistical analysis was not appropriate.

It is important to note that all graphs in figure 4.3.4 are not on the same scale, this is due to the larger fold changes in one patient IL-6 control group and one patient in the SNAI1 COPD group. This highest fold change result in the control group is due to the same patient, LP#497. Again one patient (LP#1024) provided the highest fold change for all genes in the COPD group.

For IL-6 and SMAD3, interestingly due to one patient (LP#497), there is a higher mean fold change for IL-6 and SMAD3 in the control group than the COPD group. The reverse is seen for TGF β 1 and SNAI1. A larger group size would be needed to draw meaningful conclusions from these findings.

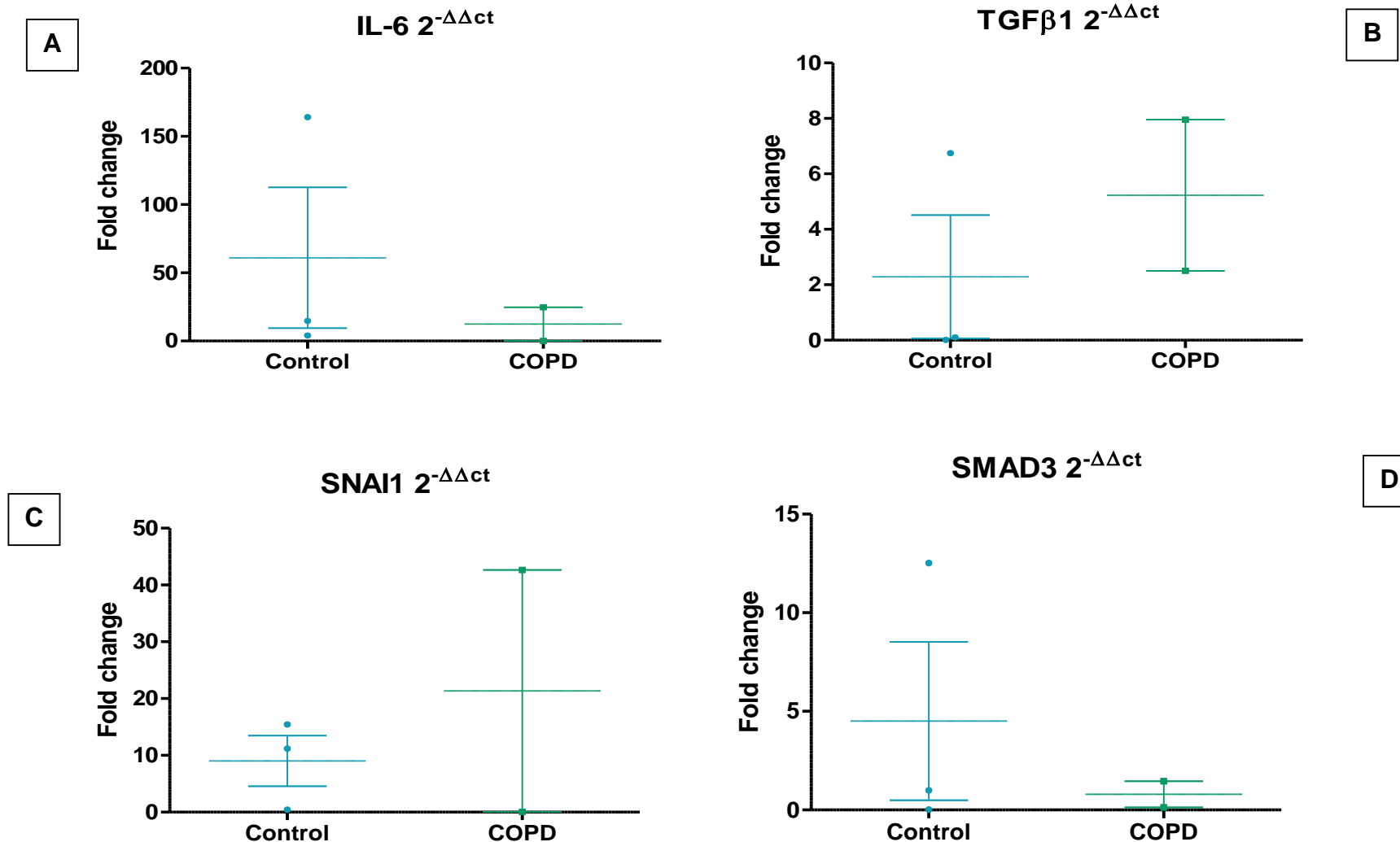


Figure 4.3.4 A-D: Q-RT-PCR fold change ($2^{-\Delta\Delta Ct}$) gene expression between epithelial and fibrotic LCMD tissue The fold change gene expression data of IL-6, TGFβ1, SNAI1 and SMAD3 assessing the gene expression change epithelial-to-fibrotic in individual patients; data groups to disease status. Control subjects (N=3) versus COPD patients (N=2). No statistical analysis conducted due to low subject numbers in each grouping.

4.4 Discussion

Q-RTPCR of whole lung tissue showed numerical increases of TGF β 1 and IL-6 gene expression in COPD tissue together with increased SNAI1 and SMAD3; this supports our hypothesis that EMT is progressed in association with COPD and that this is a SMAD3 mediated process, including the recruitment of SNAI1.

S100A4 calcium binding protein expression was most significantly linked with PYH and COPD in chapter 3 of this immunohistochemistry study; therefore this EMT associated marker was selected for fast immune-LCMD. Q-RTPCR of lazer captured tissue to enable analysis of gene expression changes in areas that were not S100A4+ve (deemed 'epithelial') and regions of S100A4+ve staining (deemed 'EMT') to gain information on associated signalling paths in EMT tissue in COPD lung tissue. To our knowledge this is the first study of this type in COPD tissue.

Comparisons of gene expression with EMT regions versus epithelial tissue for n=7 patients plotted, is indicative that EMT genes (downstream TGF β 1 and IL-6 and transcription genes SMAD3 and SNAI1), are more likely to be raised in the fibrotic S100A4 positive regions of lung tissue, which looks favourable on our hypothesis that EMT can be mediated by a SMAD3 dependent pathway in human lung tissue contributing to fibrosis in COPD; however more data is needed to reach a solid conclusion. Studies in breast cancer cell lines previously described binding of S100A4 to SMAD3 N terminal region (Schneider et al 2008). S100A4 binding the SMAD3 may potentiate its transcriptional capacity and we have shown for the first time this may also be the case in COPD lung tissue undergoing EMT.

The stimulus for this process is however, less clear as 3 very different patient histories contributed to the highest EMT Δ Ct values including a non-smoker. We cannot therefore conclude that EMT is solely initiated by cigarette smoking. We cannot rule out prior exposure of that patient to smoke or co-morbidities that may have contributed to that finding. Medications are also reported to regulate EMT progression; for example an anti-tumour drug Methotrexate, commonly used in cancer patients tested *in vitro* on cell lines induced large increases in IL-6 and TGF β 1 expression and EMT in A549 cells (Ohbayashi *et al* 2014).

In addition to signalling proteins, IL-6 and TGF β 1 are also raised in S100A4 tissue, implying their transcription in response to S100A4 activity and contribution to EMT.

Conversely, our COPD patients are commonly treated with steroids used for their anti-inflammatory properties: lung patient 431 a CCS was on seretide, Ventolin and Spiriva and the EMT genes were lower than all the other patients.

A control non-smoker (LP# 507) not receiving any medications had consistently high gene expression for IL-6, TGF- β 1 and SMAD3 in S100A4+ve tissue. Also noted for this patient they had prior dust exposure. Ideally a control patient would not have this history, however this is a limitation of the study as patients would not be having a lung tumour resection without some underlying cause.

Interpretations of the fold change data is very difficult due to the small number of patients assessed; however it is likely building this study would yield good information on the kinetics of EMT gene transcription on COPD patients compared to controls. For example in this small study we observed the COPD patient with the worst lung function/obstruction had the highest fold change for SNAI1 gene expression. SNAI1 can be linked with SMAD3 or operate independently, however the intensity of EMT signalling may be linked with the speed of COPD progression.

Reports however to offer precautionary advice over interpreting large fold changes as the most biologically more relevant; smaller differences in expression can still be important in disease progression, (Erickson *et al* 2009).

The lungs are anatomically complex organs, so rather than making gene expression observations from tissue homogenates to yield average expression levels of all the cells, the strength of this study is based on the ability to select regions of interest to perform Q-RTPCR. Combining LCM with immuno-staining enabled the most significantly associated EMT biomarker to guide our gene expression analysis to characterise signalling processes during EMT. Taking this study forward will enhance understanding of EMT pathology modulation in COPD.

Limitations of this study stem mostly to the technical challenges of preserving the tissue and RNA integrity following resection from the patient through to performing the laser capture and Q-RTPCR. Specimen related issues are numerous such as freezing times and methods used, ongoing patient medications/therapies, tissue acquisition and assay normalisation. Erickson *et al* 2009 report that snap-frozen samples provide the highest quality mRNA for analysis even though histological detail is inferior, as we have found in our study. Samples stored for a year or more

may have compromised RNA even when stored at -80; a limitation for a retrospective study but not for a prospective one providing time and resources allow for immediate analysis of each tissue at the time of resection from the patient.

Erickson *et al* 2009 found that using OCT–cryocompound in conjunction to RNA extraction prior to qRT-PCR analysis gives excellent results in downstream applications. The protocol used for RNA extraction eliminates the presence of any PCR inhibitors in the total RNA template.

The main limitation of this study was the tiny quantity of RNA yield from the LCMD material. The use of rapid immuno-LCM with intact RNA has been used by many groups (Fuke *et al* 2004; Kinnecom and Patcher 2005), who were able to do their RNA isolations immediately after tissue isolation; to suppress RNases and maintain acceptable integrity of nucleic acids. Our study was a retrospective study of snap frozen tissue archived in -80C over several years. Tissue was immediately snap frozen on the surgery day and archived to HTA standards in minus 80C, so to the best of our knowledge this was a feasible study. In spite of this I achieved successful amplification of the target genes without the employment of more sensitive techniques such as nested PCR using two or more sets of specific primers.

The second main technical issue was operation of the LCMD. During laser dissection of the second cohort (n=8), the laser operation only allowed for cutting on a high power setting. This was not the case for the first cohort that had initially shown good RNA yields in the trial sample. Using the higher power laser setting may have caused damage to isolated tissue RNA integrity before even the RNA isolation preparation. I found in agreement with work done by Kinnecom and Patcher 2005, that capture sessions that ran longer than 30 minutes drastically reduced the amount of RNA therefore in an effort to maximise the amount of RNA isolated I had to pool samples from multiple 30 minute sessions; again a consequence of the changed operation of the laser capture microscope.

Further improvements could make use of a dehumidifier to keep the room humidity constantly low (Kinnecom and Patcher 2005), this reduces chance of aqueous activation of endogenous RNases.

Fuke *et al* 2004 showed significant elevated GAPDH mRNA in smokers with airflow limitation/emphysema when compared to their control group smokers and non-

smokers with no airflow limitation. In our study it was also seen that numerically there were raised ΔCt levels in COPD compared to controls; though this was not significant and the causes may be simply from small patient numbers to the possibility that there are genuinely lower gene levels in the control group. Again expanding the patient group and assessing the fold changes would be interesting.

For detection of intact rRNA 18S and 28S subunits, RNA gel electrophoresis was performed. It can be seen from the initial results that the subunits can be detected in all three tissue isolations whole, fibrotic and epithelial however there is an element on RNA degradation, indicated by band smearing. This may be due to a few factors such as freshness of the snap frozen tissue, which includes time taken from patient to being snap frozen and the time the tissue is in storage, if these increase it heightens RNA degradation before experimental procedure. Also with this studies case, transporting the material between two sites could also give rise to possible areas of material degradation, such as freeze thawing. Ideally the whole procedure (tissue slicing, staining, LCMD and RNA isolation) would take place on a singular day to reduce this factor whereas due to equipment constraints in both laboratories this procedure was spread across 3 days, with -80°C storage in between.

This was also conducted on any remaining RNA from the samples however the levels were too low to detect. RNA quantification of total RNA from micro-dissected tissue samples yields quantities too small, especially from precious samples, to routinely use conventional gel electrophoresis to determine RNA integrity. Alternatively to gel electrophoresis, Erickson recommends using Agilent 2100 bioanalyser to provide RNA integrity number from 18S and 28S rRNA analysis. We did not have access to such a resource, but we may have got better information on the RNA quality if we had.

We elected use of SYBR green for economy reasons, however Taqman® chemistry based primer/probe sets may have been more sensitive. We used 4ng of total RNA which was sufficient in our efficiency experiments and also shown to work by Erickson et al 2009. Total RNA samples from LCMD tissues are precious this is why it was imperative for the validation experiments to ensure that they specifically amplify their intended target sequence linearly.

Despite the limitations, we were able to put 4ng RNA per well, into Q-RTPCR from LCMD material and have observed raised SMAD3, SNAI1, TGF β 1 and IL-6 in S100A4 tissue. The data show is suggestive that TGF β 1 gene expression levels showed the least difference in the LCMD isolated epithelial tissue; which may support previous reports of IL-6 initiating EMT via SMAD3 with TGF β 1 providing a later feature of fibrotic cell function.

Chapter 5

Investigation of cultured primary lung fibroblast cytokine and viability responses to cigarette smoke and stretch forces.

5.1 Background

5.1.1 *In vitro* models of COPD: What can it tell us?

A variety of cells such as epithelial cells, macrophages, leukocytes and fibroblasts can be explanted from lung tissue either from biopsies, bronchial alveolar fluid or as in our case from tissue resections. Human cells isolated in this manner have an important role when trying to identify differences in stimuli responses between patients with a disease such as COPD and controls, (Krimmer and Oliver 2011). They also are able to contribute a deeper understanding into the complexity of both cellular and molecular processes when compared to immortalised cell lines (e.g. A549, NHLF and 16HBE140) which retain many of the original characteristics and can provide a high level of reproducibility yet are often questioned when studying disease specific processes. The use of *ex vivo* human tissue models gives a much closer representation of what occurs within the human diseased state opposed to data generated using *in vivo* animal models.

The airway cellular micro-environment provides active defence mechanisms exerting important roles in coordinating local inflammation and immune responses through the generation of chemokines, cytokines and regulation of membrane components.

5.1.2 Cigarette Smoke Extract (CSE) *in vitro* studies

Cigarette-smoke induced lung damage has widely been studied in the combined effort to the understanding the pathogenesis of inflammation and fibrosis in COPD, (Nagigel *et al* 2013). The use of *in vitro* human lung cell models enables the direct exposure of specific stimulators such as the use of CSE, allowing the study of cellular processes affected by the exposure of such substances.

Cigarette smoke contains a highly complex mixture of over 4000 toxic chemicals and additives. All of these components are small enough to potentially reach the lower airways. Included in this is the TLR4 inducer lipopolysaccharide which has been shown to up regulate the release of growth factors from airway cells (Wang *et al* 2005) and is known to be increased in airways of COPD patients, inducing innate immune responses and activation of structural cells such as epithelial fibrotic and smooth muscle cells, (Krimmer and Oliver 2011). Indeed the authors state that nicotine alone can up regulate extracellular matrix deposition from murine fibroblasts.

The whole phase cigarette smoke extract model, is widely used for the study of cigarette smoke induced changes *in vitro* and has been confirmed that it has detrimental effects on cell growth, migration, proliferation, viability and ECM deposition; across a wide range of cell types. A selection can be seen in table 5.1 of the effects that have been seen on both human cell lines and primary cells.

Table 5.1 The effects of cigarette smoke (CSE) on human lung cells *in vitro*

Cell type	Effect of CSE	Reference
Fibroblast	Increased apoptosis	Baglole <i>et al</i> 2006
Fibroblast	Increased non-fatal DNA damage	Carnevali <i>et al</i> 2002
Fibroblast	Decrease in cell proliferation and migration.	Nyunoya <i>et al</i> 2006
Fibroblast	Increased ECM deposition	La Rocka <i>et al</i> 2007
Epithelial	Increased IL-6 + IL-8 expression and protein production	Beisswenger <i>et al</i> 2004
Epithelial	Increased TGF β responsiveness via decreased SMAD6	Springer <i>et al</i> 2004
Endothelial Cell line	Increased apoptosis with CSE dose and exposure time	Gornati <i>et al</i> 2013

Direct measurements of cytokine levels in COPD patient lung tissue and BAL are characterised by the cellular expression/ production of the IL6, IL8 and TGF β 1 amongst others. In smokers intracellular IL-8 is upregulated in epithelial cells from the small airways (Fuke *et al* 2004) and is prominently released by lung epithelial cells along with TNF α following exposure to cigarette smoke (Nadigel *et al* 2013).

While TGF β 1 is a key cytokine inducing EMT and a fibroblast growth factor, it was reported to be not constitutively expressed, but becomes strongly upregulated during injury and inflammation (Kisseleva and Brenner 2008), undoubtedly serving to activate myofibroblasts to contribute to the injury repair process. TGF β 1 is a multifunctional cytokine that in mammals is present in three isoforms; the active TGF β 1 as well as two latent inactive isoforms (L-TGF β 1) of TGF β 1 having proteins such as the latency associated peptide 1 (LAP-1) bound to it. These act as

extracellular store that can be activated by proteases such as plasmin, which cleave LAP-1 enabling TGF β 1 to act in an autocrine or paracrine manner, (Khalil *et al* 2001). It has been shown via IHC in IPF human lung tissue that the inactive L-TGF β 1 is present in all pulmonary cells except interstitial myofibroblasts, Khalil *et al* 2001).

TGF β 1 when applied *in vitro*, stimulates fibroblast ECM production, myofibroblast differentiation, promotes resistance to apoptosis and production of reactive oxidative species. Conversely, when applied to epithelial cells it can induce apoptosis and it has been seen in animal models that TGF β 1 overexpression/up-regulation induces severe lung fibrosis (Tod *et al* 2012). Methotrexate, an immunosuppressive drug used to treat cancer, may induce lung fibrotic processes: a 48hr treatment *in vitro* upregulated IL-6 and TGF β 1 in A549 cells, this may be an important and deleterious side effect causing methotrexate-induced pulmonary fibrosis (Ohbayashi *et al* 2014).

As considered in chapters 3+4, EMT is a process promoting mesenchymal cell differentiation from lung epithelia that may contribute to fibrosis pathology in COPD. Associated with the EMT process there is an enhanced secretion of a subset of inflammatory cytokines and chemokines that includes IL-6 and IL-8, (Reviewed, Palena *et al* 2012). Blocking experiments on colorectal cancer cell lines have shown that IL-8 is a critical part for SNAI1-mediated EMT (De Wever *et al* 2004) while purified IL-6 was sufficient to induce an EMT phenotype of a breast cancer cell line. These findings both suggest that raised IL-6 and IL-8 release by cells in response to injury could function in a paracrine function for the induction of EMT-like phenotypic switching.

Fibroblasts under stress, e.g. CSE exposure, can secrete further levels of IL-8 adding to the pro-inflammatory and ultimate emphysematous destructive environment in the lung. A very recent study isolated epithelial cells from large airway samples from 13 very severe COPD (Gold stage IV) patients. Authors observed an increased fibronectin release (ELISA readout) over a 5 week period in response to CSE. They also showed that the broncho-epithelial cells displayed de-differentiation/mesenchymal features that persisted for 2 weeks in their air-liquid interface culture system (Gohy *et al* 2015). The authors hypothesised that these

cells were induced by cigarette smoke *in vivo* to be primed to release more TGF β 1 than control cells hence maintaining the mesenchymal phenotype for two weeks in culture. They also speculated that CSE creates an early event of imprinting the EMT phenotype via TGF β B1 pathway and that it needs further study. Given the cytokine microenvironment governs the differentiation of lung epithelia in EMT, the functional role of pre-established fibroblasts is likely to be important. We set about a comprehensive study to ascertain primary fibroblast responses to CSE in 26 control and COPD patients.

While cytokine levels are well characterised in the lungs, and numerous studies have characterised cellular responses to smoke, relatively little attention is paid to the continuous mechanical stretch of alveolar epithelium by forced ventilation associated with emphysema; it is likely to contribute to the pulmonary injury and fibrosis (Kisseleva and Brenner 2008) and this process may be significantly increased with additional injury such as smoking. Using a plate based vacuum operated cell-flex system; we set up an *in vitro* fibroblast model to simulate this pathology to observe fibroblast responses to CSE.

Finally, in addition to EMT associated cytokines contributing to fibrosis, cellular apoptosis is thought to contribute to emphysematous lung destruction in response to cigarette smoke (Park et al 2013). In addition to assessing the cytokine responsiveness of the isolated fibroblasts we also assessed the possibility that CSE may induce fibroblast apoptosis via simple MTT cell death assays

5.1.3 Aims:

- This study aimed to establish an *in vitro* culture system of human lung fibroblasts to assess baseline and CSE induced cytokine levels (IL-6, IL-8 and TGF β) in order to characterise responses between subject groups: controls (non-smokers, ex-smokers and current smokers) and COPD patients (current smokers and ex-smokers).
- Using the same culture system, we also wished to assess cell death responses to CSE.

- In a subset of patients we also applied the use of stretch forces in our culture model to ascertain if emphysema is a contributing factor to lung fibrotic processes.

5.2 Methods

Table 5.2 Demographics of lung patients used for CSE and CSE with stretch study

Variables	COPD										Healthy			
	Total				Current Smoker			Ex-Smoker			Total	Current Smoker	Ex-Smoker	Non Smoker
GOLD Stage	ALL	2	1	Unknown	ALL	2	1	ALL	2	Unknown	0	0	0	0
Subject numbers	11	10	1	1	6	5	1	5	4	1	15	7	7	1
Sex	M=3 F= 8	M=3 F=7	M= 0 F= 1	M= 0 F= 1	M= 1 F= 5	M= 1 F= 4	M= 0 F= 1	M= 2 F= 3	M= 2 F= 2	M= 0 F= 1	M=7 F=8	M= 3 F= 4	M= 4 F= 3	M= 0 F= 1
Age (years)	66.45 ±7.41	67.33 ±7.98	63	62	67.33 ± 5.09	68.2 ±5.17	63	65.4 ± 10.11	66.25 ±11.47	62	70.43 ±8.09	63.57 ±10.06	71.43 ±8.1	85 ±0
Pack year history	43.14 ±18.65	37.39 ±11.84	50	88	45.92 ±7.85	45.1 ±8.49	50	39.8 ±27.7	27.75 ±7.41	88	39.79 ±25.55	40.43 ±19.02	42.44 ±28.76	0
FEV₁ % Predicted	65.17 ±10.23	63.1 ±10.07	71	78	66.65 ±7.4	65.78 ±7.92	71	63.4 ±13.65	59.75 ±12.63	78	97.97 ±17.82	96.29 ±21.2	103.66 ±17.86	97 ±0
FEV₁/FVC ratio, %	56.49 ±9.53	54.34 ±6.93	54	78.31	55.58 ±5.94	55.9 ±6.58	54	57.85 ±13.43	53.4 ±7.84	78.31	74..22 ±12.01	72.88 ±16.52	74.99 ±6.89	72.02 ±0

5.2.1 Primary cell expansion, cell culture and cytopins

Primary fibroblasts were isolated from human lung biopsies over a 6 week period as described in the methods chapter, 2.5.1. Once grown and harvested, a small sample of cells were then cytopun onto glass slides (2.1.8) and stained for e-cadherin S100A4 and α SMA using the standard immunohistochemical methodology (2.1.9); for cellular identification. The cells were plated on collagen coated 96 well and 6 well plates prior to experimentation.

5.2.3 CSE exposure versus CSE with Stretch Experiments with ELISA readout

One 1R3F Kentucky research cigarette was burned and smoke bubbled through 25ml supplemented RPMI media to produce '100% CSE'. This was subsequently diluted to a range of concentrations, 1-50% and added to the re-washed cells and incubated for 4, 6, 24 and 48 hours. At the set time points supernatants (190 μ l or 100 μ l with subsequent MTT experiments) were removed and stored at -80°C prior to analysis. Parallel experiments exposed the same primary cells to 10% CSE and cyclic 20% stretch using Flexercell® Tension plus™. Again the supernatants were collected at 4, 6 24 and 48 hour time points and stored at -80°C prior to ELISA analysis. The levels (pg/mL) IL-6, IL8 and TGF- β 1 in the collected supernatants were measured using 'Duoset' Sandwich ELISA development kits (R&D systems; Abingdon, UK) all procedures were conducted to manufacturer's instructions and the well optical densities were read using a microplate reader set to 450nm with a wavelength correction set to 570nm. Sample ODs were converted to pg/mL against the standard curve.

Table 5.3 Demographics of lung patients used for MTT study

Variables	COPD							Healthy			
	Total			Current Smoker			Ex-Smoker	Total	Current Smoker	Ex-Smoker	Non Smoker
GOLD stage	ALL	2	1	ALL	2	1	2	0	0	0	0
Subject numbers	6	5	1	3	2	1	3	7	3	3	1
Sex	M=3	M=3	M=0	M= 1	M=1	M=0	M= 2	M=3	M= 1	M= 2	M= 0
	F= 3	F= 2	F= 1	F= 2	F= 1	F= 1	F= 1	F=4	F= 2	F= 1	F= 1
Age (years)	65.33	65.8	63	66	67.5	63	64.67	64.28	57.67	64	85
	±9.65	±10.71		± 7	±9.19		± 13.51	±12.27	±12.34	±4.36	
Pack year history	33.42	30.1	50	42.17	38.25	50	24.67	28	22.67	42.67	0
	±11.77	±9.53		±9.57	±9.54		±5.03	±25.13	±7.51	±32.88	
FEV₁ % Predicted	62.17	60.4	71	70.67	70.5	71	53.67	102.99	104	103.67	
	±10.78	±11.03		±7.51	±10.61		±4.16	±20.7	±26.66	±23.51	97
FEV₁/FVC ratio, %	53.15	52.98	54	57.67	59.5	54	48.63	71.9	70.39	22.67	
	±5.61	±6.25		±3.22	±0.71		±2.64	±4.69	±2.15	±7.5	72.02

5.2.5 MTT 3-(4,5-dimethylthiazol-2-yl)-2,5-diphenyltetrazolium bromide assay for cell viability

The colour metric analysis MTT assay was used to assess cell viability of the primary fibroblasts post CSE exposure. At the relevant time points 3mg/mL of MTT solution was added to the remaining cells/supernatant and was returned to the incubator for a further 2 hours. Any formazan crystals that had formed after this time period was dissolved in DMSO and the optical density of each well was read using a microplate reader set to 540nm with a wavelength correction set to 690nm.

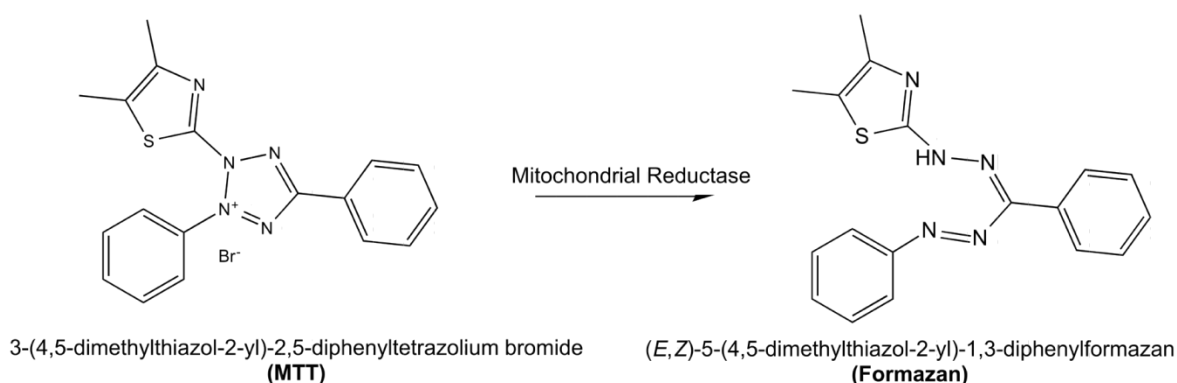


Figure 5.1: Mitochondrial reduction of MTT into formazan

5.2.6 Statistical Analysis of Cytokine responses between subject groups

All comparisons were between more than two groups therefore a repeated measures ANOVA followed with post-test was used for parametric data and Friedman test with post test was conducted for non-parametric data. A p-value of <0.05 was considered statistically significant and data is expresses as mean \pm standard error of mean.

5.3 Results

5.3.1 Cytospins

To determine the primary cell composition the prepared cytopins of the primary cells were stained using the same procedure seen in chapter 3. Randomly selected images were used for the table below (5.4), showing a representative for each demographic group.

There were no apparent staining visible in any of the negative controls resulting in any staining present being genuine for the specific markers. Cellular morphology as with the NHLFs in chapter 3 is not as expected with them possessing a more rounded feature expected with epithelial cells, however this may be a consequence of the cytospin process.

E-cadherin was expressed heavily in the NS subject, moderately in the current smokers and very little in the ex-smoker groups. α SMA was expressed throughout all samples to varying degrees with the COPD patient and NS subject expressing it more heavily. Finally the EMT marker S100A4 was expressed by all subjects but again to varying degrees among patient groups with most interestingly being expressed the highest in the NS subject.

The cytopins were also stained with the leukocyte markers CD45, CD68 and neutrophil elastase subjects produced no positive staining for these, data not shown.

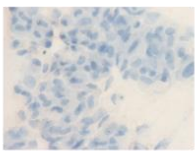
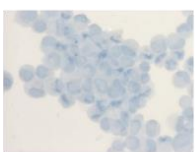
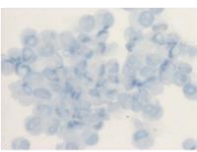
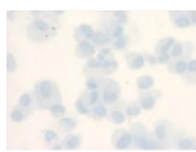
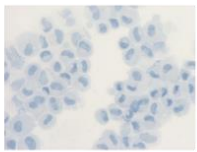
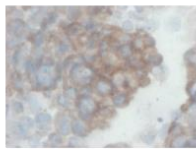
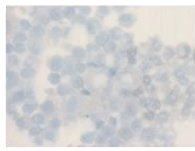
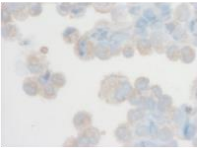
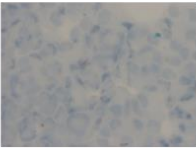
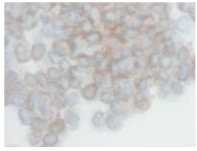
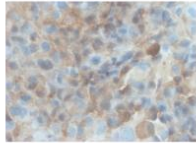
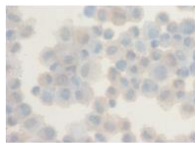
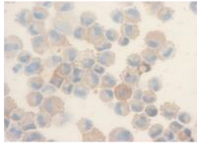
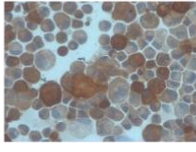
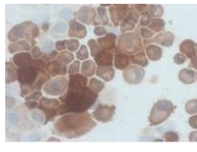
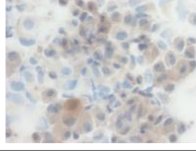
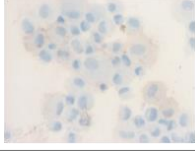
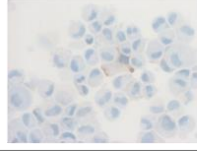
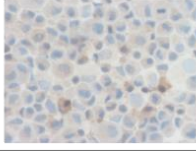
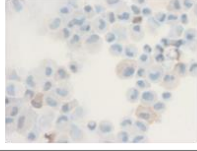
	NS	ExS	CS	CEx	CCS
LP#	676	2056	1018	681	2041
Negative					
E-Cadherin					
α SMA					
S100A4					

Table 5.4 Depicts staining of cytospin primary fibroblast isolations stained with the epithelial marker e-cadherin, fibrotic marker α SMA and EMT marker S100A4.

5.3.2 Bender 11plex

As described in chapter 2 an initial bender 11plex assay was conducted to determine the potential targets for ELISA. IL-6 and IL-8 elicited the highest response to CSE with this mode of assessment therefore these type 2 cytokines were chosen. TGF- β 1 was not in the 11plex however this is a well-documented fibrotic marker so we selected this as an indicator of fibroblast function. The 11plex data was useful for guiding this study but as it was generated by a study team (including myself and others) the data is not shown in this thesis.

5.3.3 ELISA

5.3.3.1 Grouped Data: all patients

The absolute levels of TGF β 1 released are lower than the amount of IL-6 or IL-8 (~1000pg/mL vs. ~2000pg/mL) released from the primary fibroblasts. At the 4, 6 and 24 hour time points for TGF β 1 there is limited evidence of a dose response to CSE with an overall significant ($p=0.0443$) for the 48 hour time point. The baseline level (0% CSE) for TGF β 1 is high. For IL-6 and IL-8 dose responses to CSE are evident particularly at 24 and 48 hour time points (Fig 5.3.1). For all three cytokines overall there is a significant ($p<0.0001$) increase of cytokine present in relation to both time and CSE concentration.

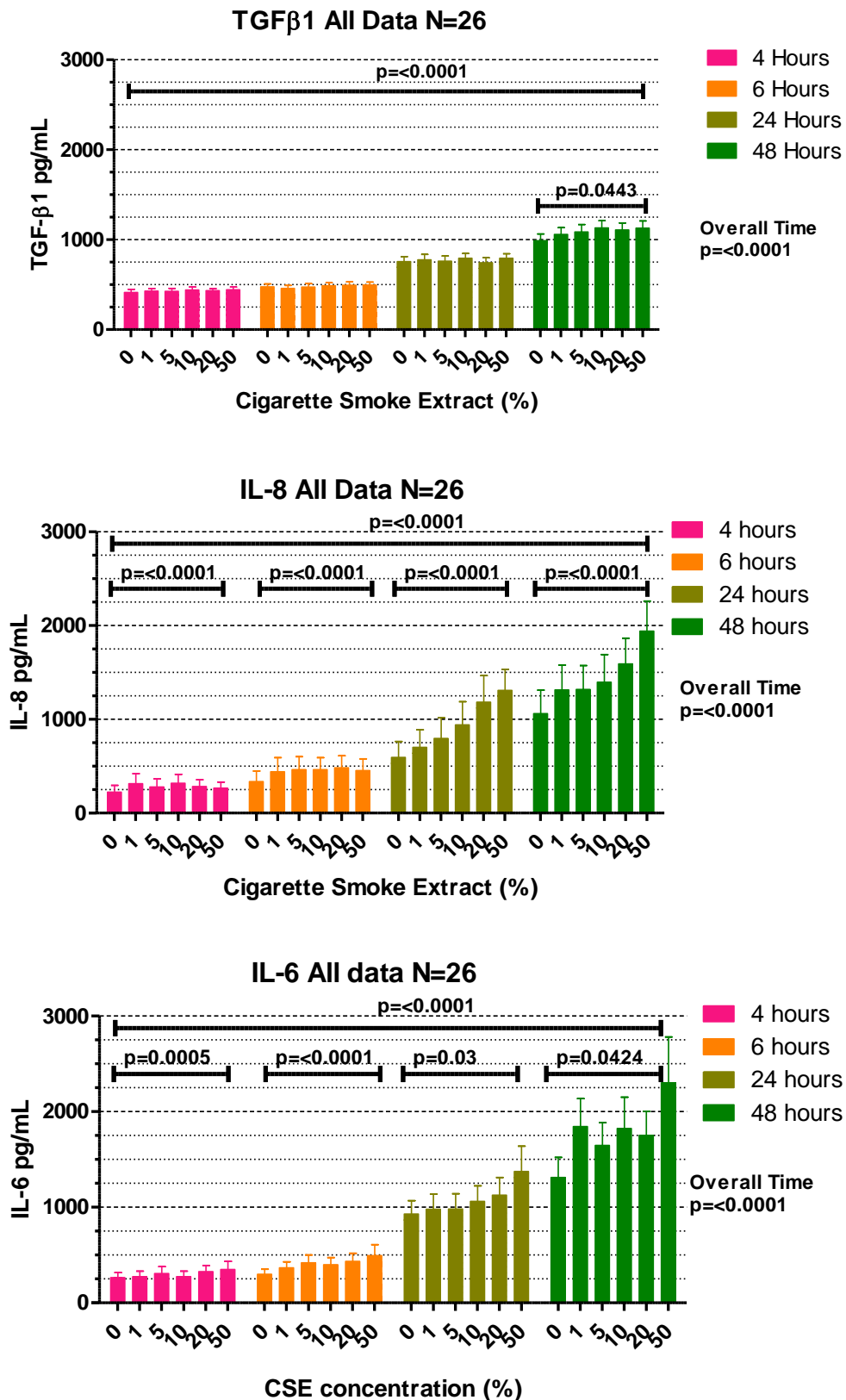


Figure 5.3.1 ELISA results of ALL primary fibroblast data. Shows the graphical representation (mean \pm standard deviation) of the cytokine/chemokines released, (pg/mL) from all primary fibroblast assessed, all graphs have n=26. TGFβ1, IL-8, and IL-6pg/mL. Repeated measures ANOVA with post t test was used for parametric data and Friedman test with post t test was conducted for non-parametric data. Statistical bars indicate significance of CSE concentration with overall time extremely significant ($p < 0.0001$) for all cytokines

5.3.3.2 IL-6 Responses individual groups

The 4 subject groups: COPD (current and ex-smokers) and controls (current and ex-smokers) show low level release (pg/mL) at 4 and 6 hours, rising sharply at 24 and 48 hours in all except the COPD current smokers; where the IL-6 responses remain relatively blunted at 48 hours for COPD current smokers. Overall there is a significant ($p < 0.0001$) increase of total IL-6 release from baseline when comparing data to both time and CSE concentration for all subject groups. (Fig 5.3.2)

To remove time as a contributing factor, cell responses were normalised at each time point. This was done by calculating the percent (%) change response to CSE compared to baseline (0% CSE) values. Dose responses are generally seen except at 48 hours where responses are universally raised.

To assess if current smoking is a contributing factor to fibroblast responses, data was split into current verses ex-smokers. There are no clear differences between current and ex-smokers though a clearer dose response is seen at 4 hours in current smokers and ex-smokers at 24 hours (Fig 5.3.3). Considering the control smokers only; current smokers had heightened responses compared to ex-smokers at 4 and 6 hours, with a sudden reduction for the following time points. Whereas ex-smokers responded in a dose dependant manner with an increase in IL-6 production at 50% CSE for 4-24 hours with a drop at 48 hour time point (Fig 5.3.5).

To assess if airway obstruction is linked with fibroblast responses, data was split into COPD versus controls (without airway obstruction). The control group in figure 5.3.4 had significant dose responses at 4, 6 & 24 hours; when comparing the COPD patients the IL-6 production was more sporadic and had no significant changes across all time points.

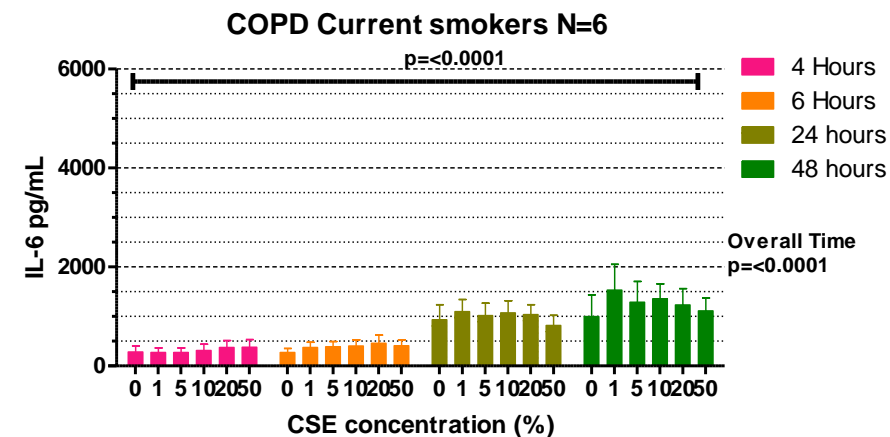
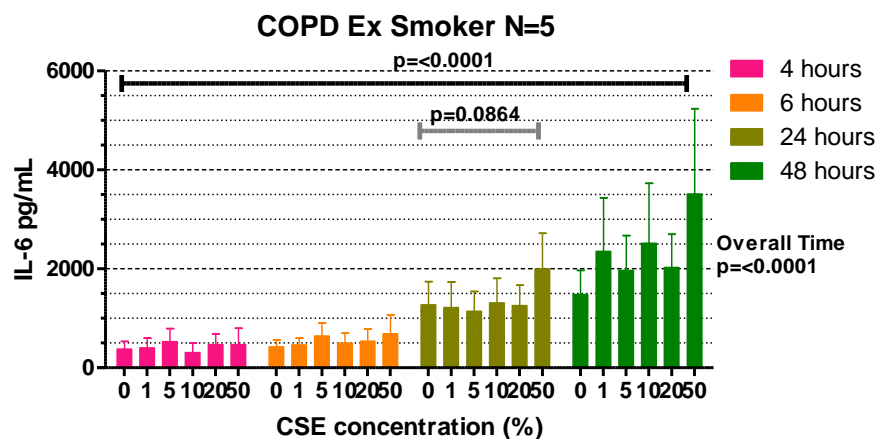
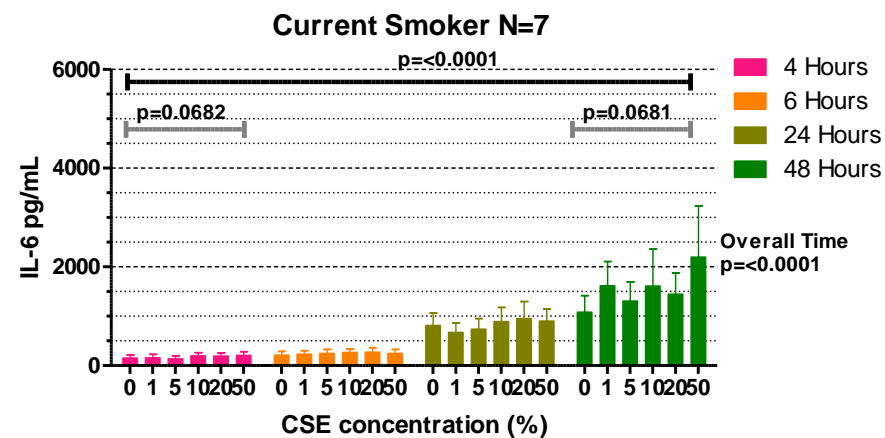
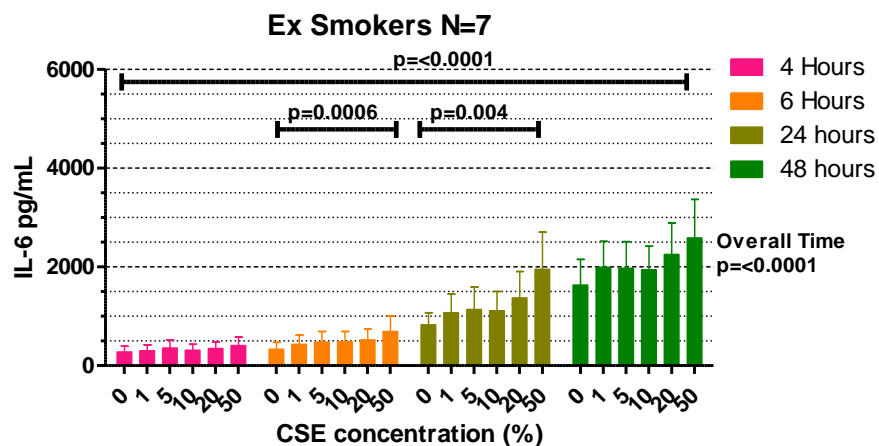


Figure 5.3.2 ELISA IL-6 responses (pg/ml) to CSE over time in 4 subject groups: ex-smokers N=7, current smokers N=7, COPD ex-smokers N=5 and COPD current smokers N=6. ANOVA with post t test was used for parametric data and Friedman test with post t test was conducted for non-parametric data. Black statistical bars indicate significance of CSE concentration with grey indicating almost significant. Overall CSE concentration (ANOVA) and time factor extremely significant ($p < 0.0001$) for all groups.

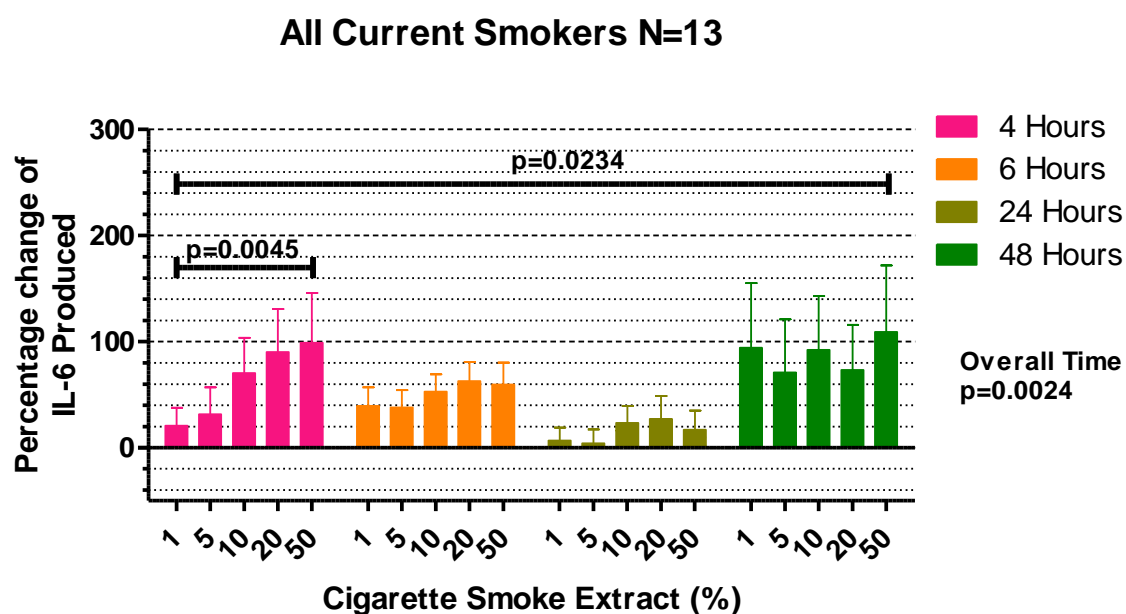
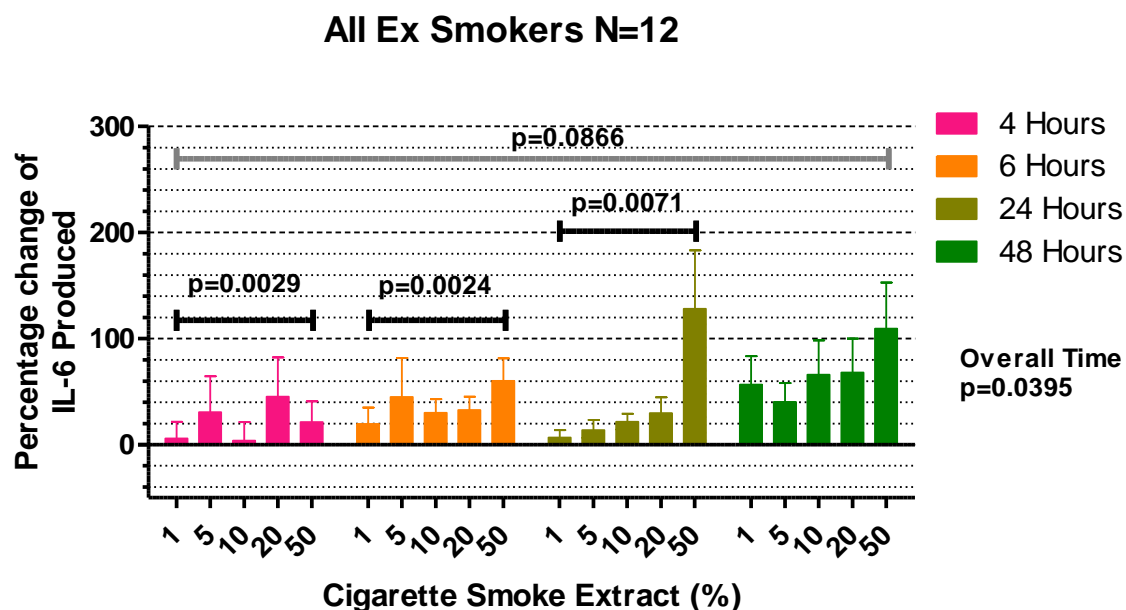


Figure 5.3.3 ELISA IL-6 responses (% change) to CSE over time in 2 subject groups: all ex-smokers (normal subjects + COPD patients) N=12, and all current smokers (normal subjects + COPD patients) N=13. ANOVA with post t test was used for parametric data and Friedman test with post t test was conducted for non-parametric data. Black statistical bars indicate significance of CSE concentration with grey indicating almost significant. Significance of time indicated at side of each chart.

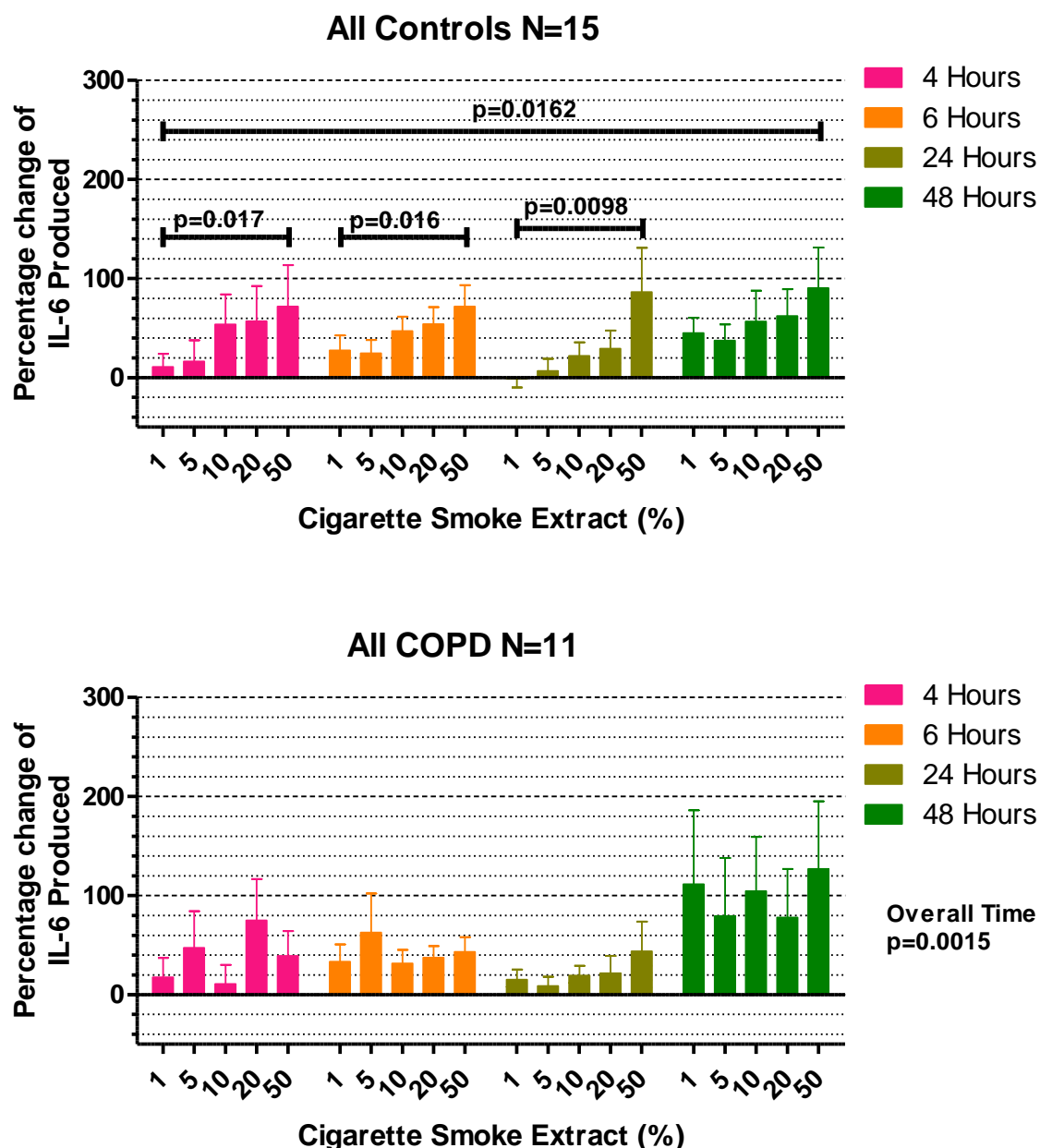
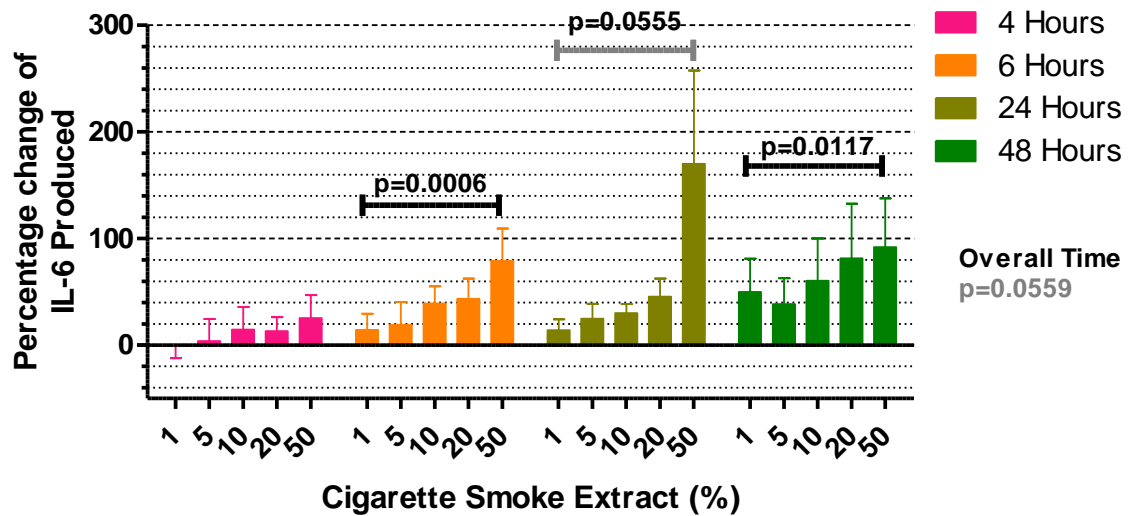


Figure 5.3.4 ELISA IL-6 responses (% change) to CSE over time in 2 subject groups: all control subjects (non-smoker, smokers and ex) N=15 and all COPD patients (smokers and ex) N=11. ANOVA with post t test was used for parametric data and Friedman test with post t test was conducted for non-parametric data. Black statistical bars indicate significance of CSE concentration. CSE concentration overall is a contributing factor to IL-6 release from All controls with significance at 4, 6 and 24 hours. Time was not a contributing factor for all controls whilst it was very significant ($p=0.0015$) for all COPD, with no significance CSE concentration.

Ex Smokers N=7



Current Smoker N=7

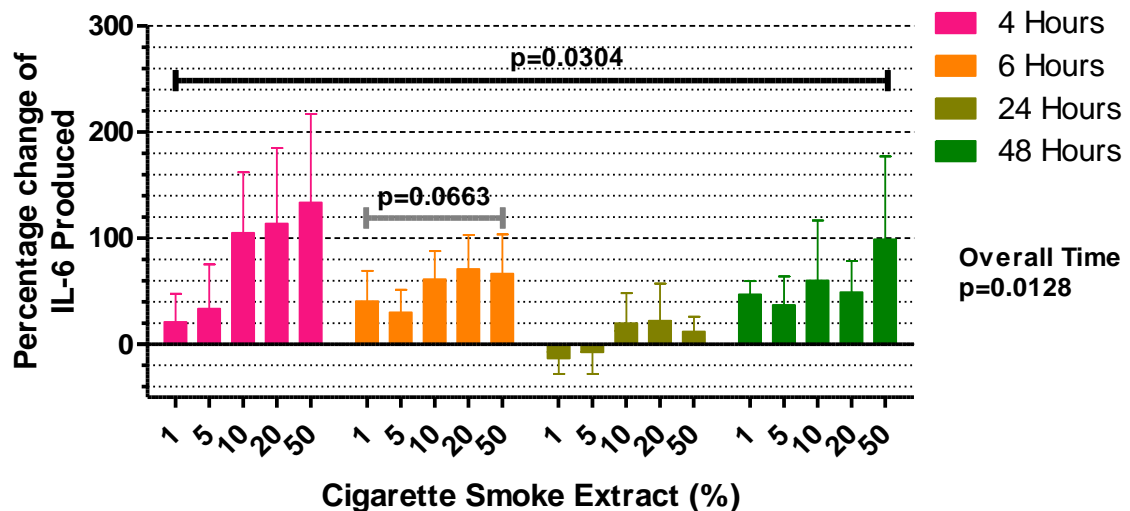


Figure 5.3.5 ELISA IL-6 responses (% change) to CSE over time in 2 subject groups: 'normal' ex-smokers N=7 versus 'normal' current smokers' n=7. Repeated measures ANOVA with post t test was used for parametric data. Black statistical bars indicate significance of CSE concentration with grey indicating almost significant. Overall CSE concentration was a contributing factor to IL-6 release for current smokers, where ex-smokers reacted in a dose dependant manner for 6, 24 and 48 hours.

5.3.3.3 IL-8 Response

The 4 subject groups show low level release (pg/mL) at 4 and 6 hours for all groups except COPD ex-smokers that had highest levels, double to triple of the other groups. Levels rise sharply at 24 and 48 hours in all groups dose dependently to CSE for all groups bar 48 hour in COPD ex-smokers (Fig 5.3.6).

To remove time as a contributing factor, cell responses were normalised at each time point. This was done by calculating the % change response to CSE compared to baseline (0%CSE) values. To assess if current smoking is a contributing factor to fibroblast responses, data was split into current verses ex-smokers. Clear dose responses are seen at all time points particularly at 48 hours for IL-8. There are no clear differences between current and ex-smokers (Fig 5.3.7).

Considering the current smokers only; COPD current smokers had heightened responses compared to normal current smokers at 4 and 6 hours and all time points show a dose dependant manner with 24 and 48 hours being the most significant (Fig 5.3.9). The normal current smokers responded in a dose dependant manner also at the 24 and 48 hour time points yet did not produce the same yield of IL-8 as the COPD patients.

To assess if airway obstruction is linked with fibroblast responses, data was split into COPD versus controls (without airway obstruction). There are no clear differences in IL-8 responses between COPD and controls. Clear CSE dose responses are seen at all-time points for both groups (Fig 5.3.8).

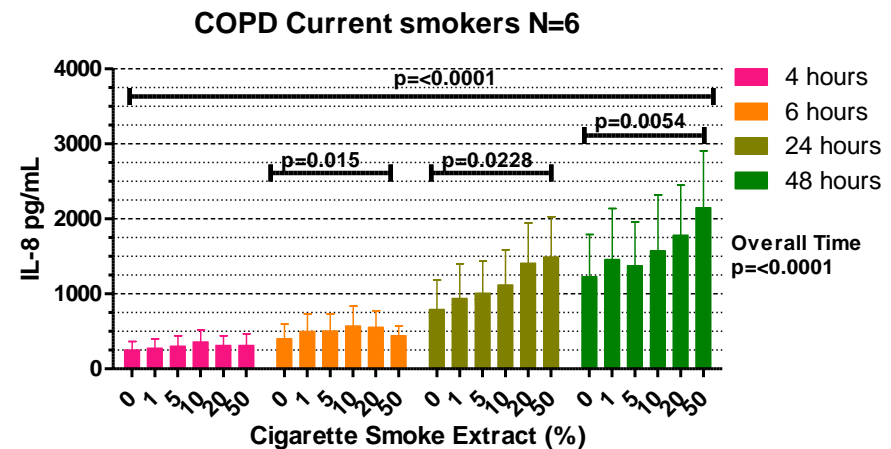
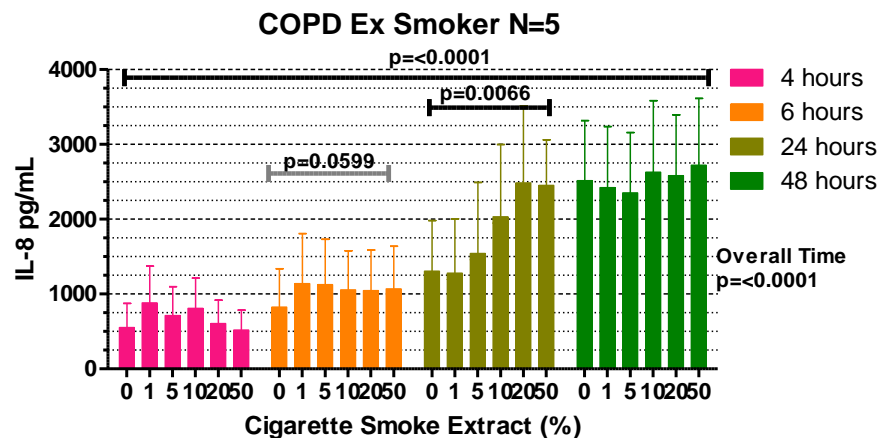
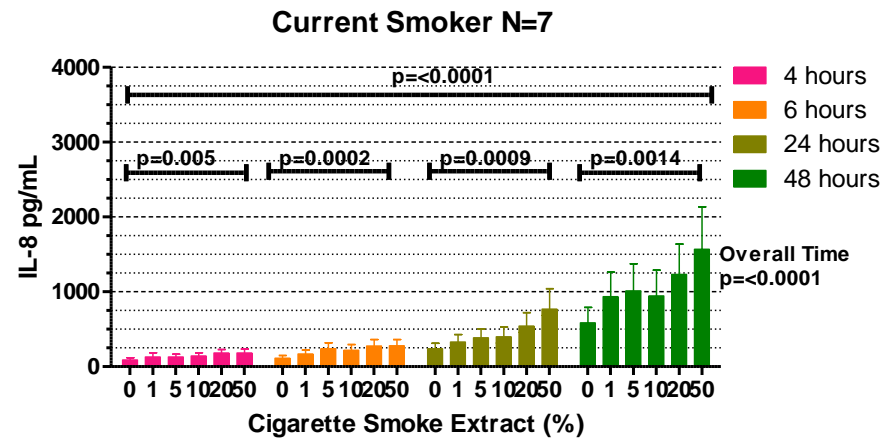
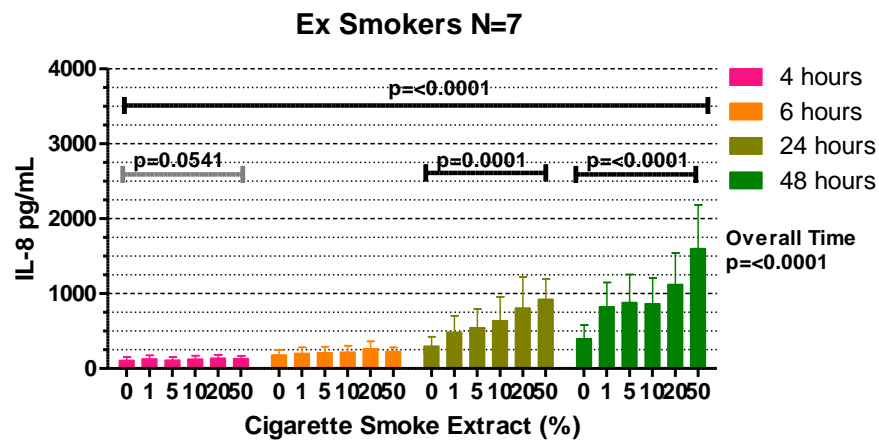


Figure 5.3.6 ELISA IL-8 responses (pg/ml) to CSE over time in 4 subject groups: ex-smokers N=7, current smokers N=7, COPD ex-smokers N=5 and COPD current smokers N=6. Repeated measures ANOVA with post t test was used for parametric data and Friedman test with post t test was conducted for non-parametric data. Black statistical bars indicate significance of CSE concentration with grey indicating almost significant. Overall CSE concentration (ANOVA) and time factor extremely significant ($p < 0.0001$) for all groups. Mainly IL-8 released in a dose dependant manner for all subject groups with larger SEM for COPD ex-smokers

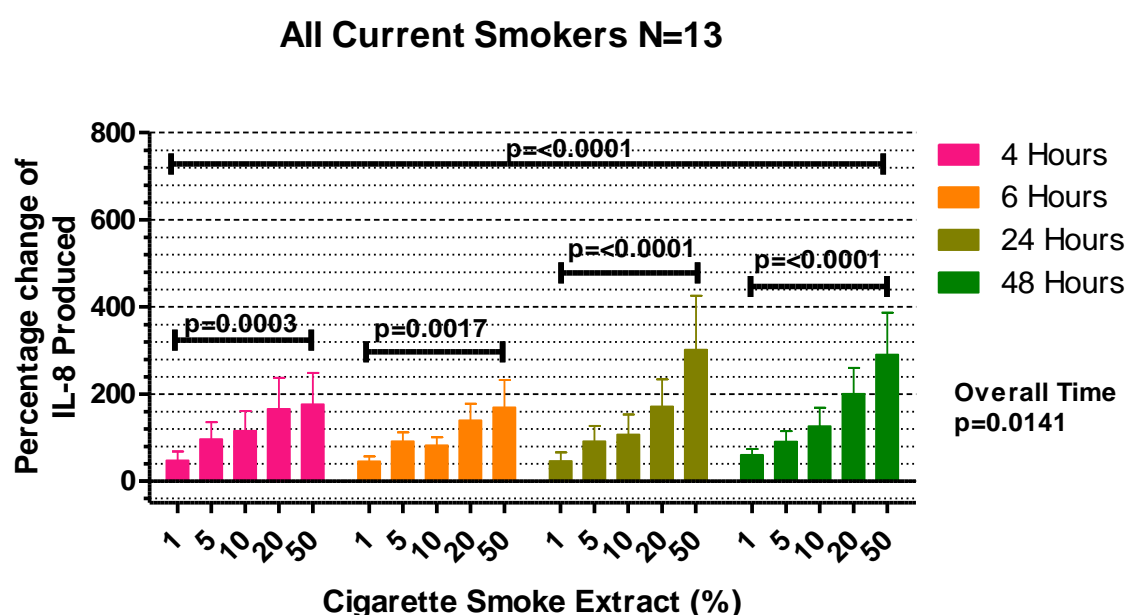
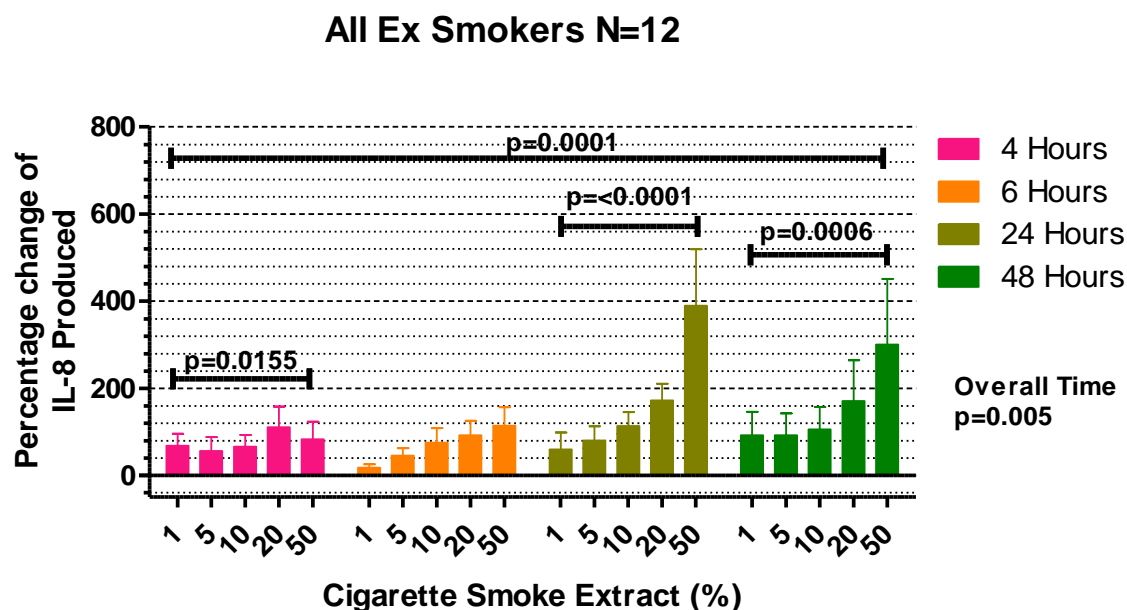


Figure 5.3.7 ELISA IL-8 responses (% change) to CSE over time in 2 subject groups: all ex-smokers (normal subjects + COPD patients) N=12, and all current smokers (normal subjects + COPD patients) N=13. ANOVA with post t test was used for parametric data and Friedman test with post t test was conducted for non-parametric data. Black statistical bars indicate significance of CSE concentration. Overall for both subject groups CSE significant and Significance of time indicated at side of each chart. IL-8 release increase in dose dependant manner at all time points for current smokers and 24 and 48 hours for ex-smokers.

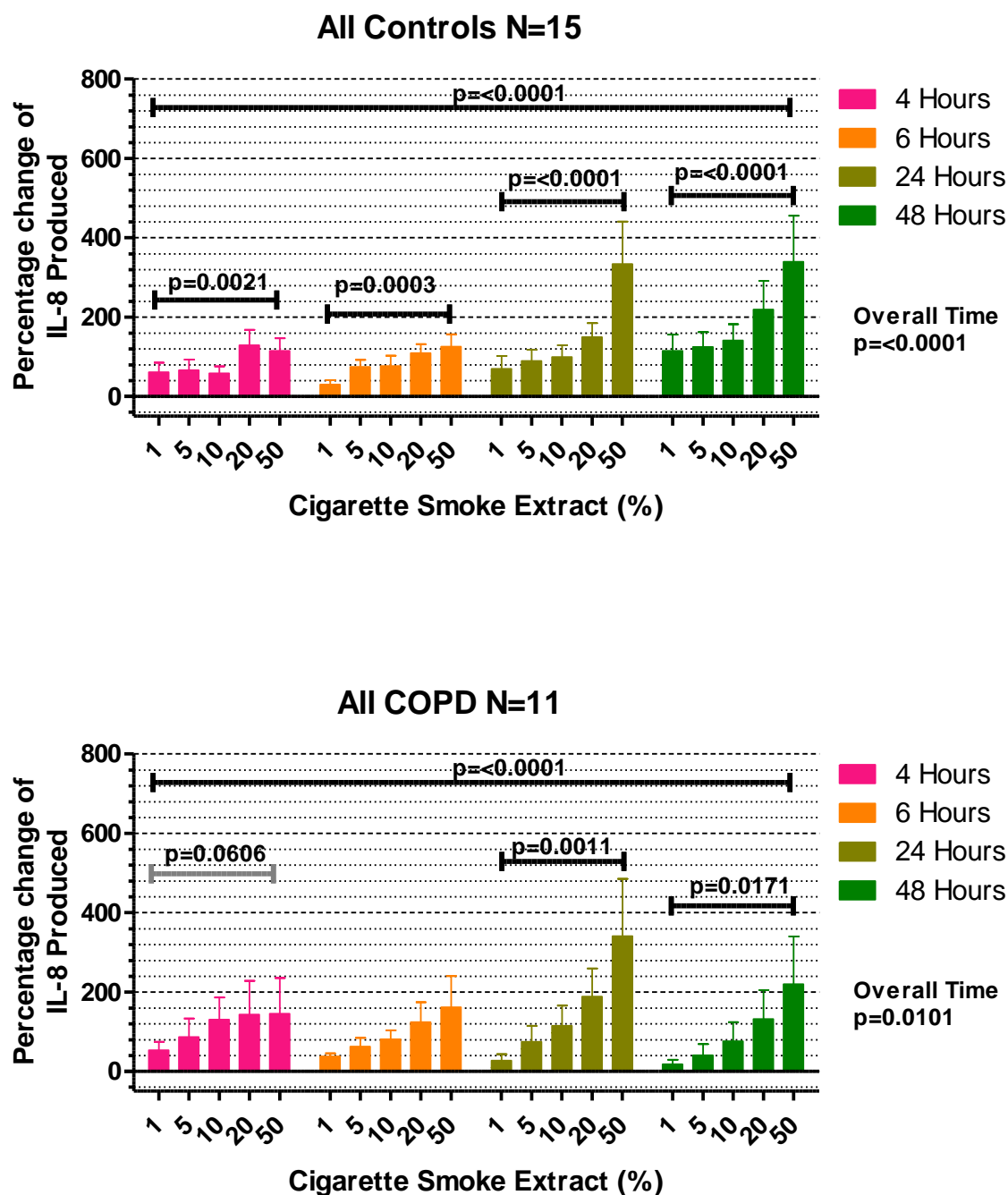


Figure 5.3.8 ELISA IL-8 responses (% change) to CSE over time in 2 subject groups: all control subjects (non-smoker, smokers and ex) N=15 and all COPD patients (smokers and ex) N=11. Repeated measures ANOVA with post t test was used for parametric data and Friedman test with post t test was conducted for non-parametric data. Black statistical bars indicate significance of CSE concentration whilst grey represents almost significant. CSE concentration overall is a contributing factor to IL-8 release from All controls with significance at 4, 6, 24 and 48 hours, in a dose dependant manner; mirrored at 24 and 48 hours in COPD patients . Time was a contributing factor for both subject groups.

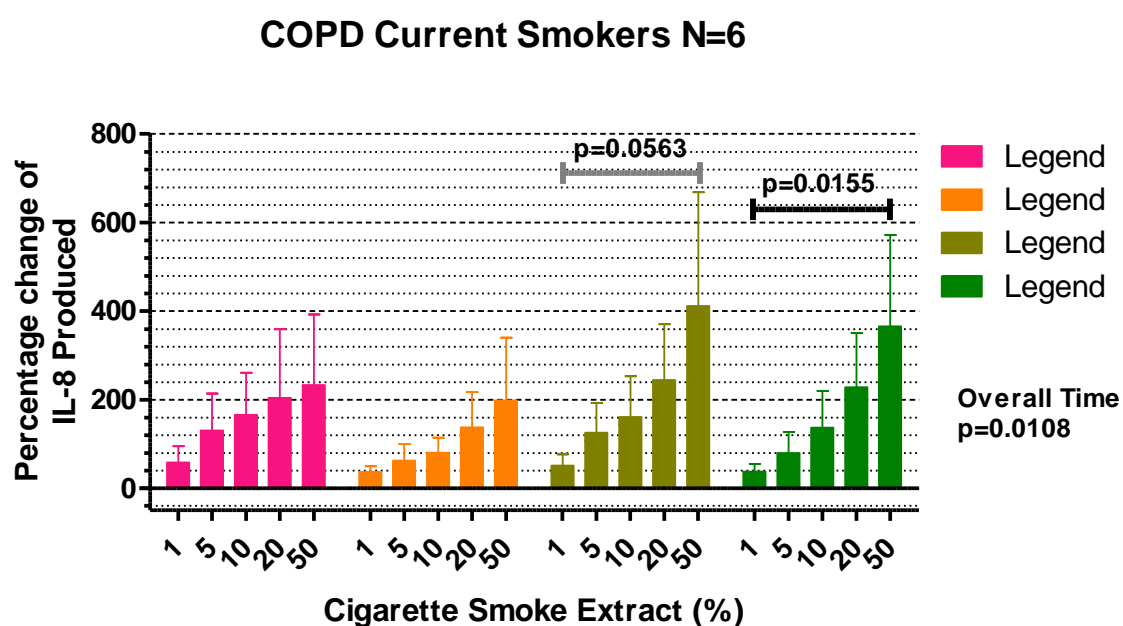
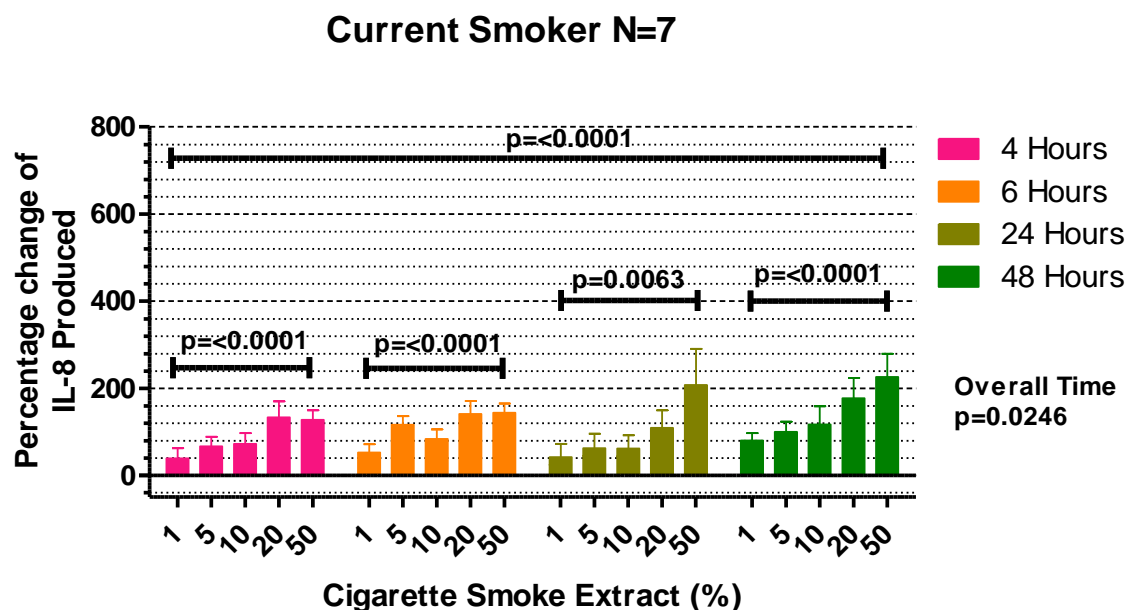


Figure 5.3.9 ELISA IL-8 responses (% change) to CSE over time in 2 subject groups: control current smokers N=6 versus COPD current smokers' n=6. Repeated measures ANOVA with post t test was used for parametric data. Black statistical bars indicate significance of CSE concentration with grey indicating almost significant. Overall CSE concentration was a contributing factor to IL-8 release for current smokers, where ex-smokers significantly reacted in a dose dependant manner at 48 hours.

5.3.3.4 TGFβ1 Responses

All 4 subject groups show double absolute TGFβ1 release (~500pg/ml) at 4 and 6 hours compared to IL-8 and IL-6 (~250pg/ml) for all groups. Levels rise sharply at 24 and 48 hours in all groups. Responses are not dose dependent to CSE at any individual time point for any group except control current smokers at 6 and 48 hours. (Fig 5.3.10). Overall both time and CSE concentration ($p < 0.0001$) contributed to total TGFβ1 release for all subject groups.

To remove time as a contributing factor, cell responses were normalised at each time point. This was done by calculating the % change response to CSE compared to baseline (0%CSE) values. To assess if current smoking is a contributing factor to fibroblast responses, data was split into current verses ex-smokers. There are no dose responses for the early time points (4, 6 and 24 hours), with an emerging CSE dose response at 48 hours in both groups. There is no difference in the proportion of response between the two groups (Fig 5.3.11).

To assess if airway obstruction is linked with fibroblast responses, data was split into COPD versus controls (without airway obstruction). Controls have modestly higher TGFβ1 levels than COPD patients that fail to respond to CSE doses at any time point. Dose response trends are seen at 4 and 48 hours for control subjects (Fig 5.3.12). Two groups from these control subjects (current and ex-smokers) revealed that the observed raised total TGFβ1 dose response is from the current smokers not the ex-smokers (Fig 5.3.13)

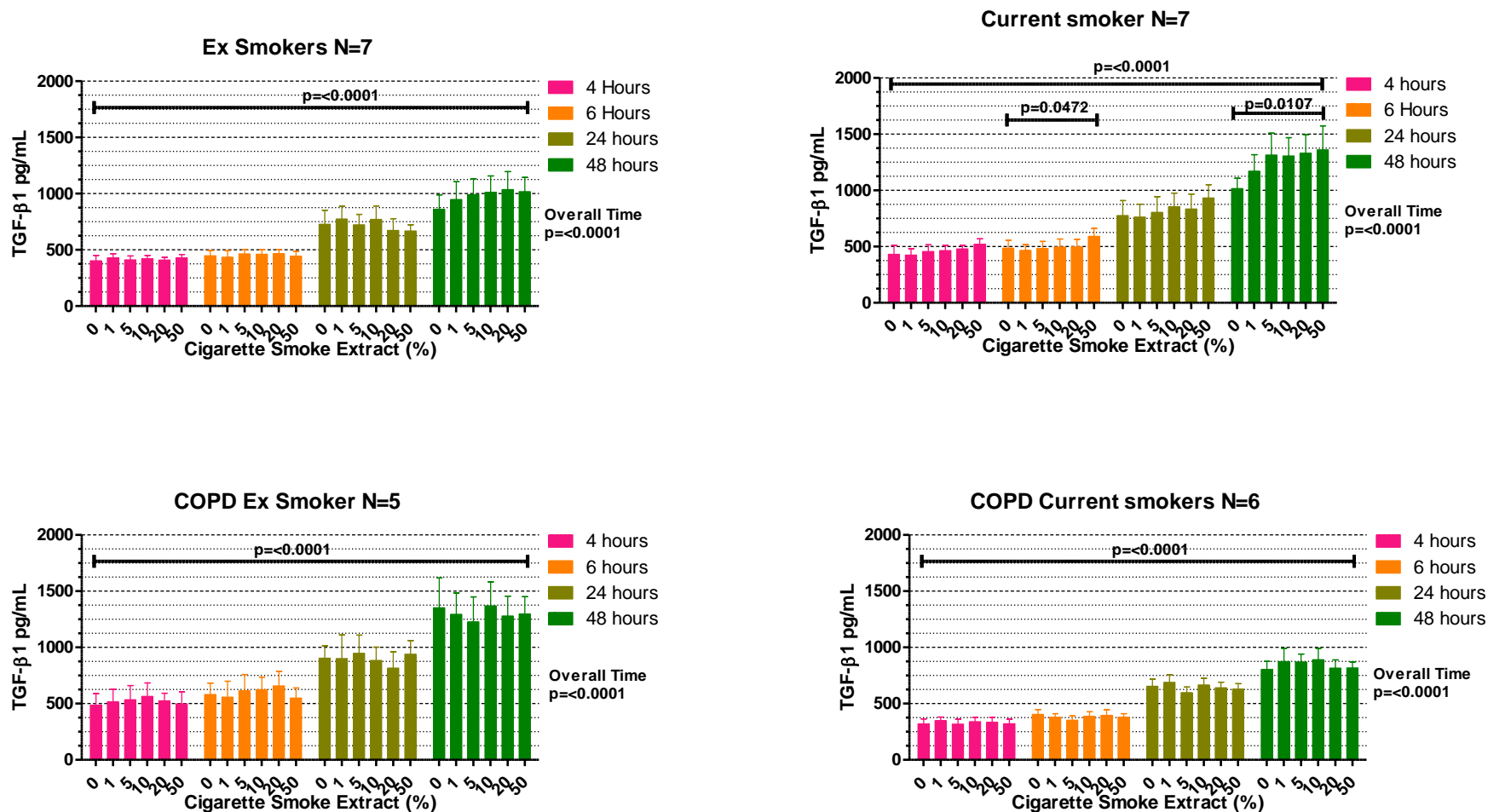


Figure 5.3.10 ELISA total TGFβ1 responses (pg/ml) to CSE over time in 4 subject groups: ex-smokers N=7, current smokers N=7, COPD ex-smokers N=5 and COPD current smokers N=6. Repeated measures ANOVA with post t test was used for parametric data and Friedman test with post t test was conducted for non-parametric data. Black statistical bars indicate significance of CSE concentration. Overall CSE concentration (ANOVA) and time factor extremely significant ($p < 0.0001$) for all groups. Total TGFβ1 released in a dose dependant manner at 6 and 48 hours in current smoker group.

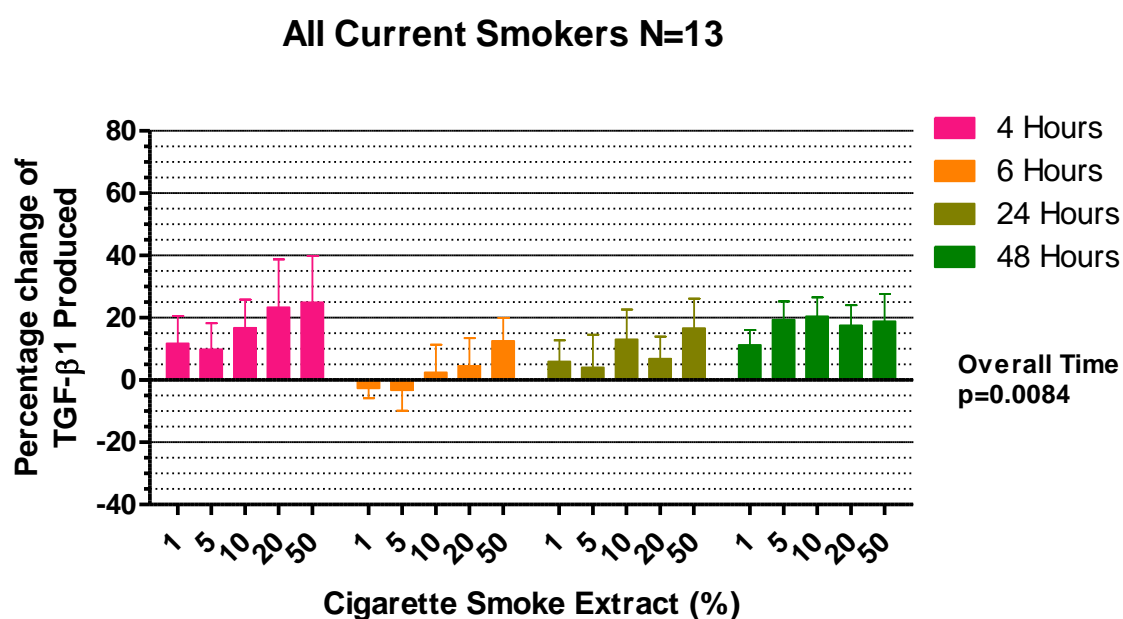
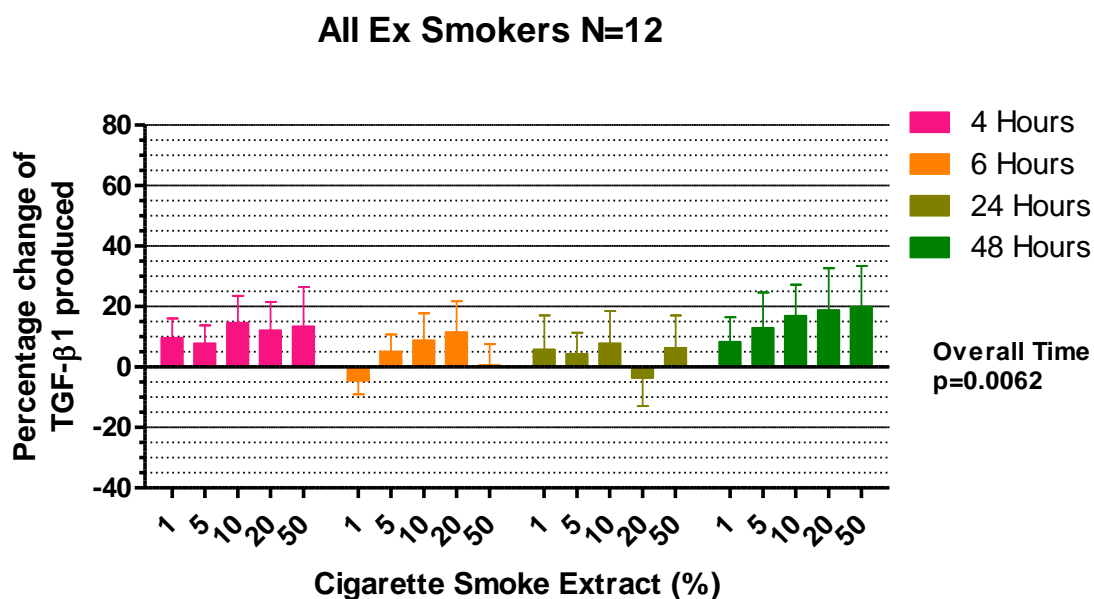


Figure 5.3.11 ELISA total TGF β 1 responses (% change) to CSE over time in 2 subject groups: all ex-smokers (normal subjects + COPD patients) N=12, and all current smokers (normal subjects + COPD patients) N=13. Repeated measures ANOVA with post t test was used for parametric data and Friedman test with post t test was conducted for non-parametric data. Significance of time indicated at side of each chart.

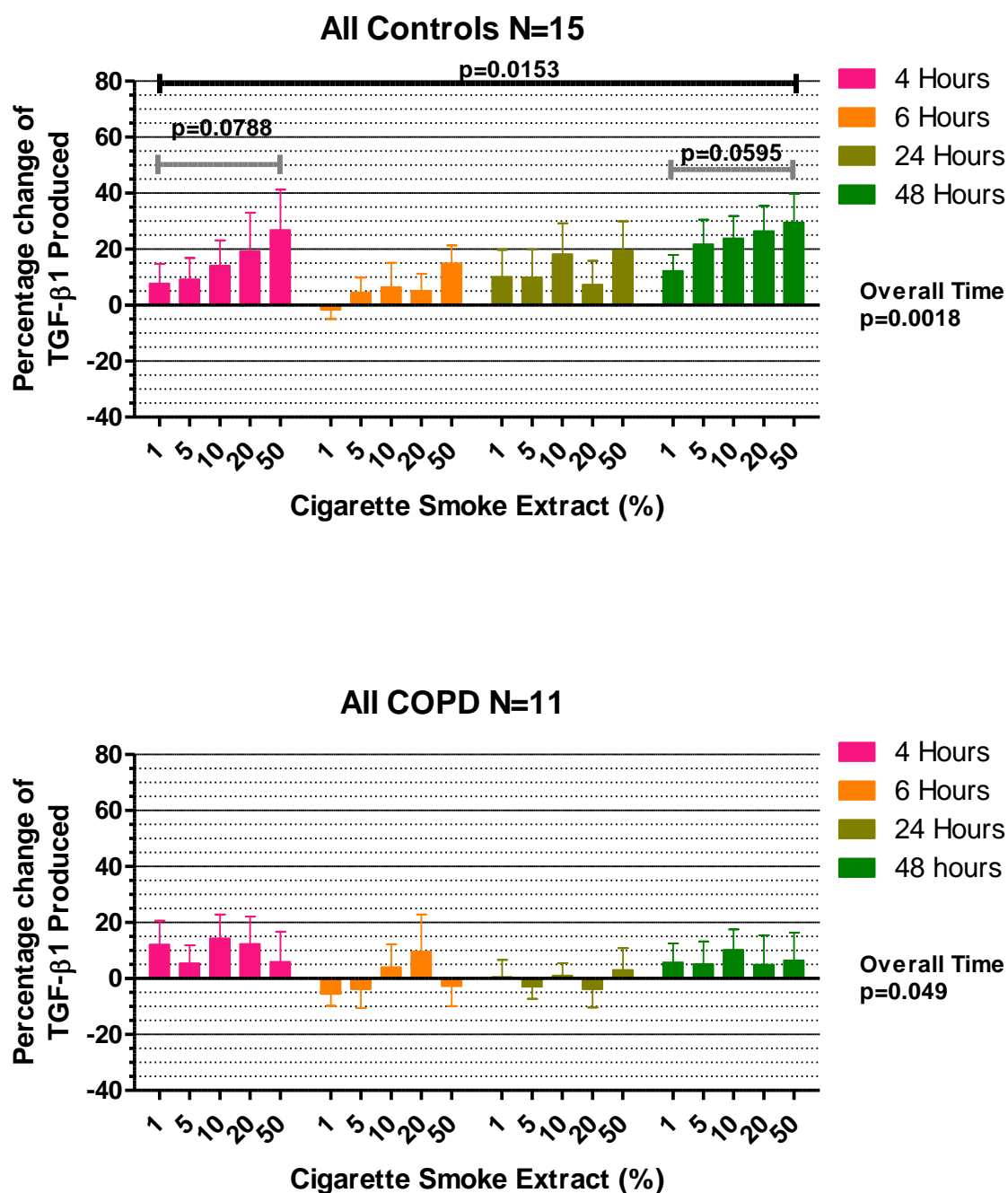


Figure 5.3.12 ELISA total TGFβ1 responses (% change) to CSE over time in 2 subject groups: all control subjects (non-smoker, smokers and ex) N=15 and all COPD patients (smokers and ex) N=11. Repeated measures ANOVA with post t test was used for parametric data and Friedman test with post t test was conducted for non-parametric data. Black statistical bars indicate significance of CSE concentration whilst grey represents almost significant. CSE concentration overall is a contributing factor to total TGFβ1 release from All controls. Time was a contributing factor for both subject groups.

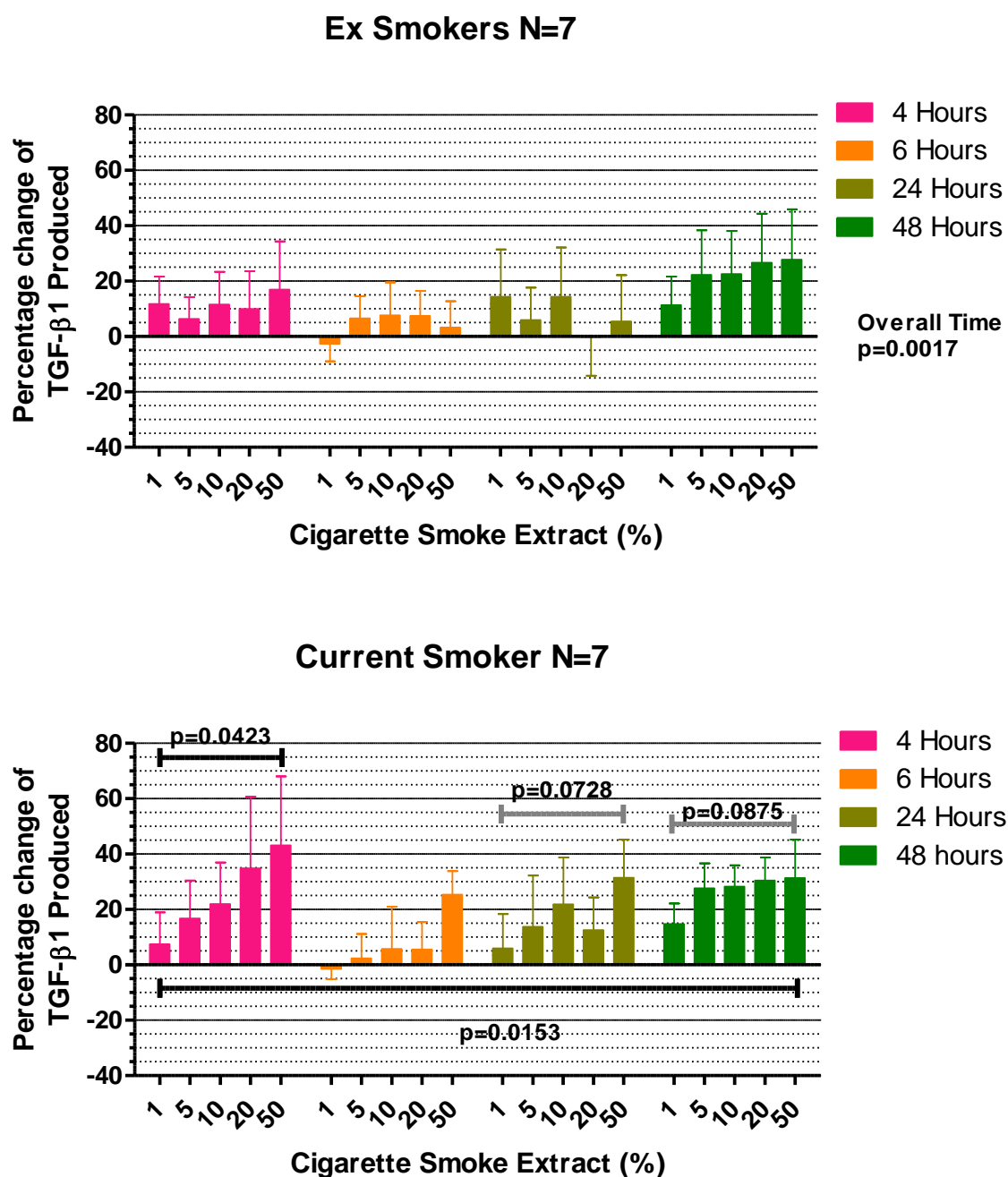


Figure 5.3.13 ELISA total TGFβ1 responses (% change) to CSE over time in 2 subject groups: ex-smokers N=7 versus current smokers' n=7. Repeated measures ANOVA with post t test was used for parametric data. Black statistical bars indicate significance of CSE concentration with grey indicating almost significant. Overall CSE concentration was a contributing factor to total TGFβ1 release for current smokers, with a dose dependant increase at 4 hours. Overall time was a significant contributing factor to release of total TGFβ1 with ex-smokers.

5.3.3.5 Comparing data between groups 24 hours

The absolute levels of IL-6 IL-8 and total TGF β 1 were compared between the data groups, Controls vs. COPD and all patient groups, at a chosen 24 hour time point only. There was no significant difference between all controls and all COPD patients for the release of absolute IL-6 and total TGF β 1. There were a significant ($p=0.028$) difference between the groups for IL-8, with a significant difference ($p<0.05$) between 20% CSE in both groups. As previously seen overall exposure to CSE causes a significant rise in IL-6 and IL-8 release, (Figure 5.3.14).

Comparing 24 hour data for the individual groups, Non-smoker, Ex-smoker, current smokers, COPD Ex-smokers and COPD Current smokers raised no significant difference. IL-8 released in a CSE dose dependent manner for all groups where as TGF β 1 appears to be sporadic as well as non plus current smoker groups in IL-6, with ex-smoker groups also reacting in a dose dependent manner.

.

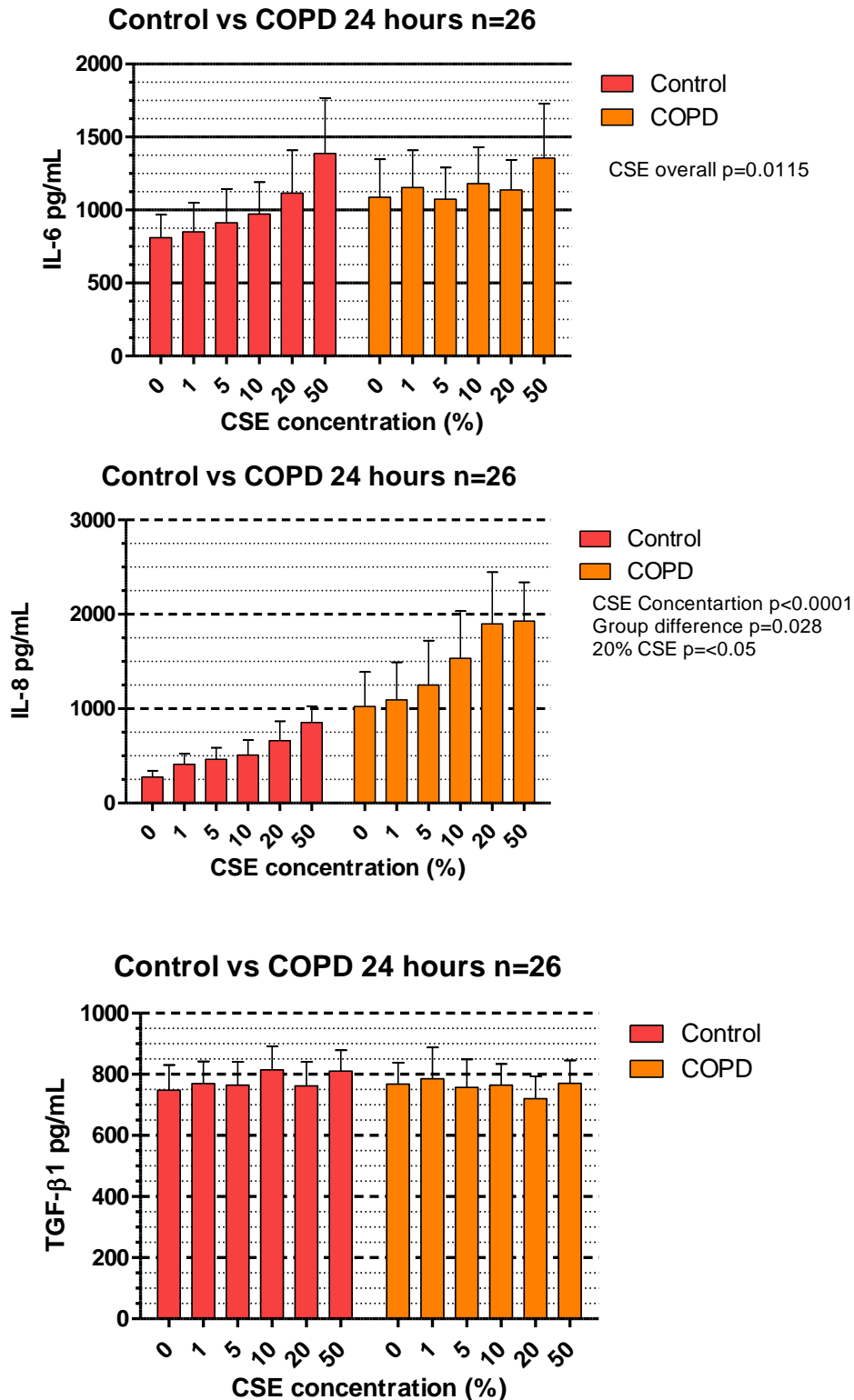


Figure 5.3.14. Absolute IL-6, IL-8 and total TGFβ1 (pg/mL) measure by ELISA. Comparison between All control N=15 and All COPD N=11, 24 hour time point. Repeated measures AVOVA with post t test was used for parametric data. No significant difference between groups TGFβ1 and IL-6. P=0.028 significant difference between IL-8 group data. CSE contributing factor to absolute IL-6 and IL-8 cytokine release. Graphs not on same scale

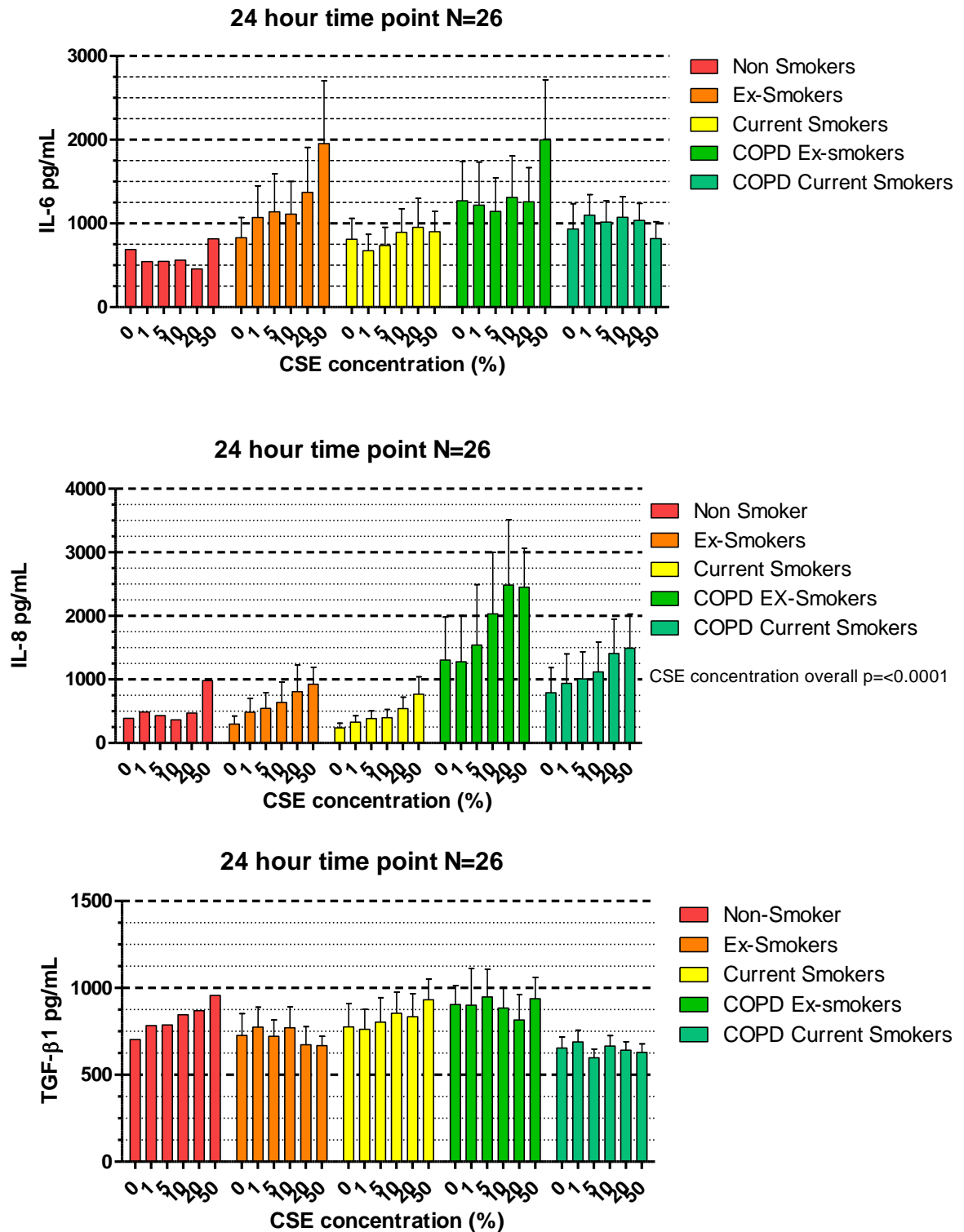


Figure 5.3.15. Absolute IL-6, IL-8 and total TGFβ1 (pg/mL) measure by ELISA. Comparison between Non smoker N=1, Ex-smoker N=7, Current Smoker N=7, COPD Ex-smokers N=5 and COPD current smokers N=6. 24 hour time point. Repeated measures AVOVA with post t test was used for parametric data. No significant difference between groups for all cytokines. CSE contributing factor to absolute IL-8 cytokine release. Graphs not on same scale

5.3.3.6 Cytokine Responses to Stretch Forces

To assess if stretch forces mediated additional responses from the primary human fibroblasts, cells were seeded into wells that were exposed to vacuum suction at regular intervals to exert stretch forces. IL-8 levels: were raised in response to stretch compared to without at 4, 6 and 24 hours in the absence of CSE. In the presence of CSE there was no difference in response +/- stretch forces at any time point. Total TGF β 1 levels: did not alter in the presence of stretch or in the presence of CSE (Fig 5.3.16).

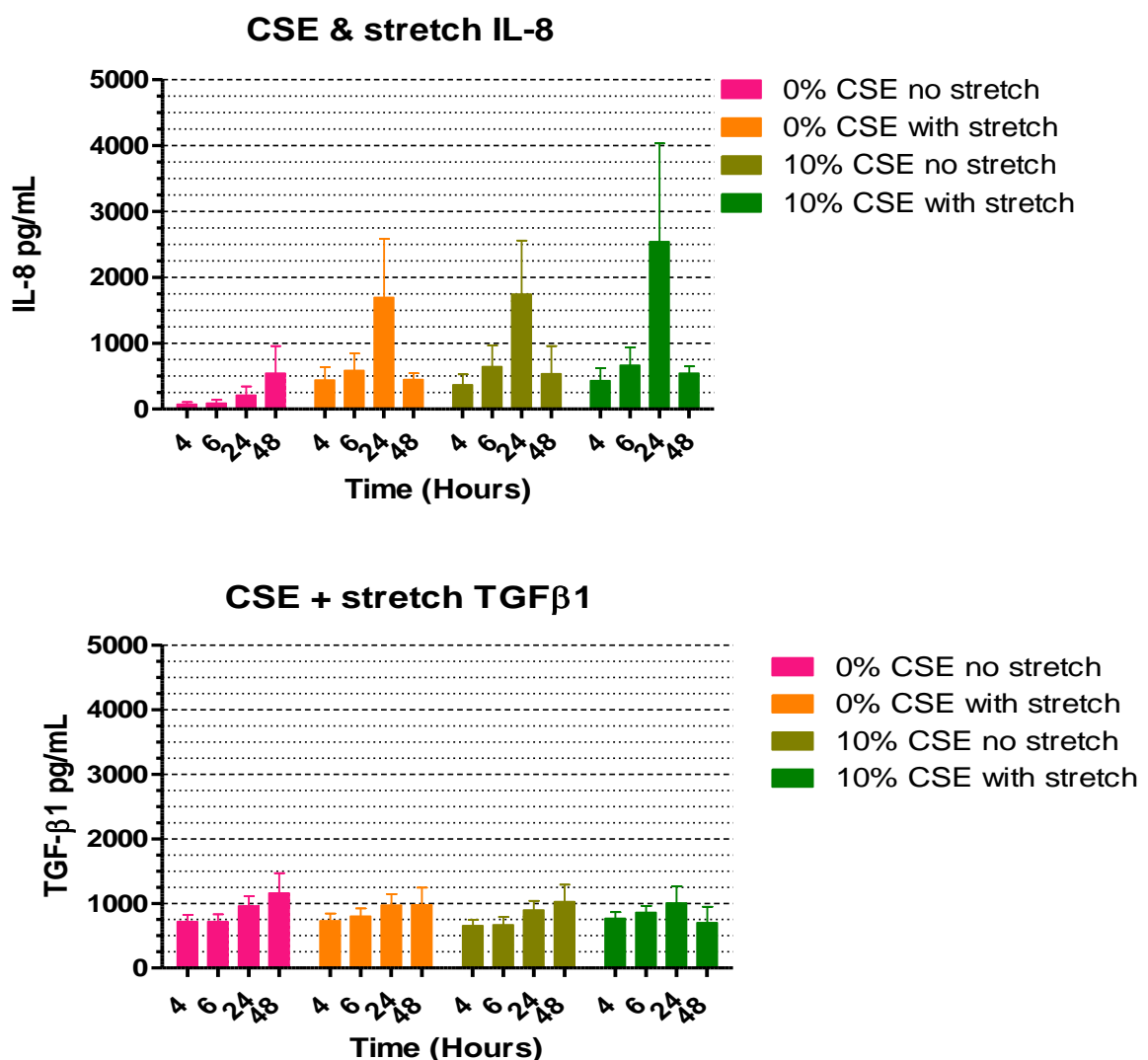


Figure 5.3.16 ELISA results for IL-8 and total TGF β 1 release (pg/mL) from primary fibroblasts (N=4) to stretch forces and/or 10% CSE over time. A repeated measures ANOVA with post t test revealed no significant change in cytokine release. IL-8 levels: were raised in response to stretch compared to without at 4, 6 and 24 hours in the absence of CSE

5.3.4 Cell Viability MTT assays

Considering group data (n=15) for all patients tested, COPD (N=6 smokers and ex) and control subjects (N=9 smokers and ex), starting viability was good >95% for all time points. Viability decreased modestly (up to 5%) in a dose dependent manner to CSE. The sharpest decline in viability is seen at 50% CSE, particularly at 48hours.

COPD patients (n=6 current at ex-smokers) starting viability was equal to the controls at the early time points ~4,6 and 24 hours) but was ~5% less than the control group at 48hours; this decrease also proceeded to decline more sharply to 80% viable at the highest CSE dose of 50% (Fig 5.3.17).

Dividing data into 5 groups: controls non-smokers current smokers and ex, and COPD current smokers and ex, revealed the current smokers in both control and COPD groups had a wider variation of responses with some individual patients showing marked decreases in viability particularly at the 48hour time point, except for the non-smoker group which only had a slight decline (Fig 5.3.18 & Fig 5.3.19).

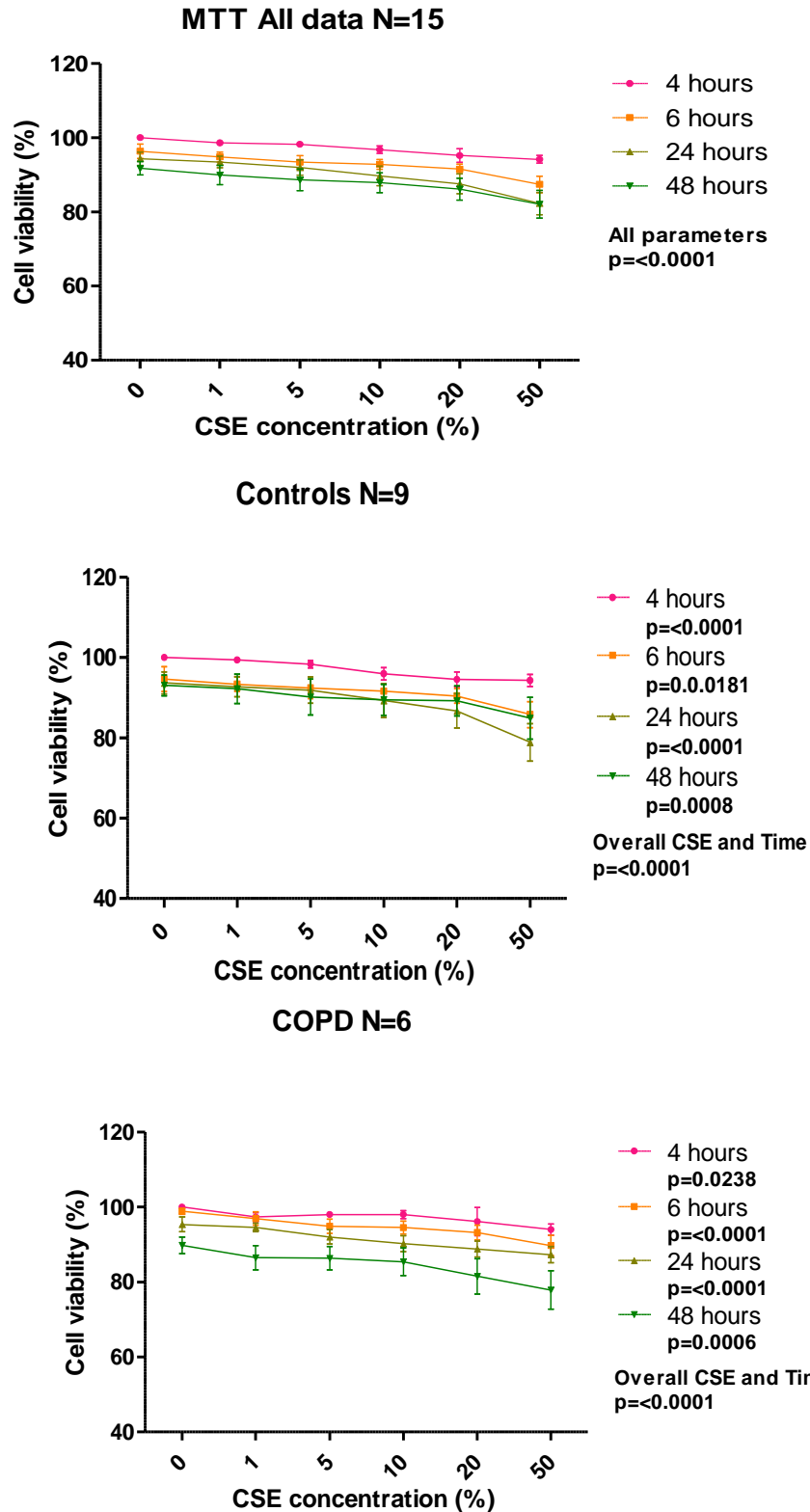


Figure 5.3.17 Primary human Fibroblast viability responses to doses of CSE measured by MTT assay: for group data (n=15), control subjects (smokers and ex n=9) and COPD patients (smokers and ex n=6). Repeated measure ANOVA with post t test revealed that cell viability decline was linked to both CSE concentration and time expose for all parameters, in all subject groups.

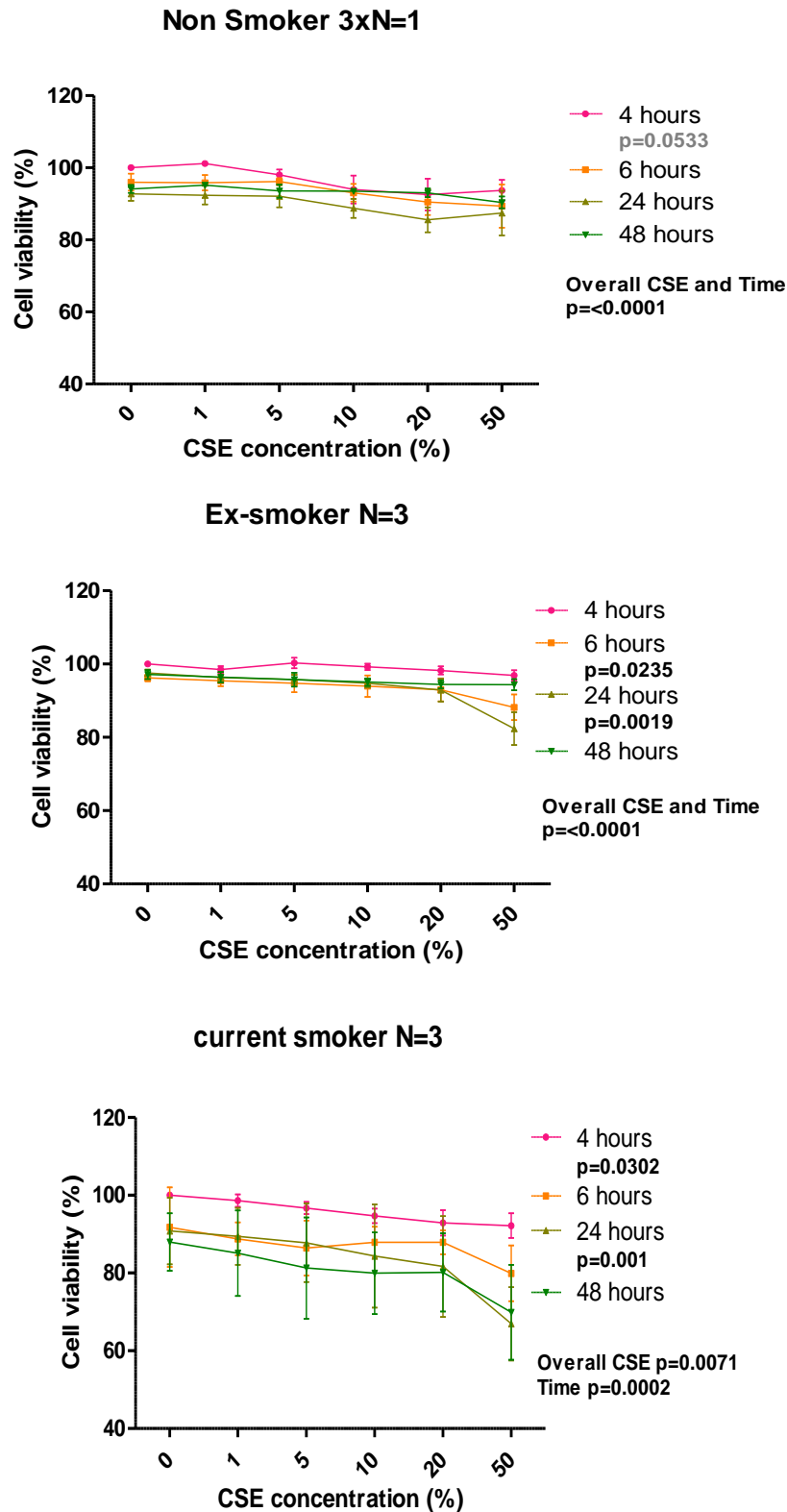


Figure 5.3.18 Primary human Fibroblast viability responses to doses of CSE measured by MTT assay: Non-Smoker 3xn=1, Ex-Smokers n=3 and Current Smokers n=3. Repeated measures ANOVA with post t-test revealed that overall time and CSE concentration affected cell viability for all subject groups with varying significant declines at 4, 6 and 24 hours for ex and current smokers.

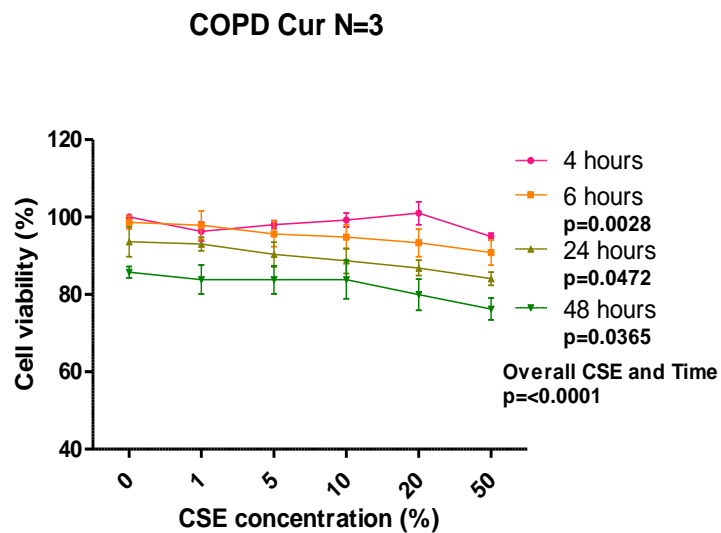
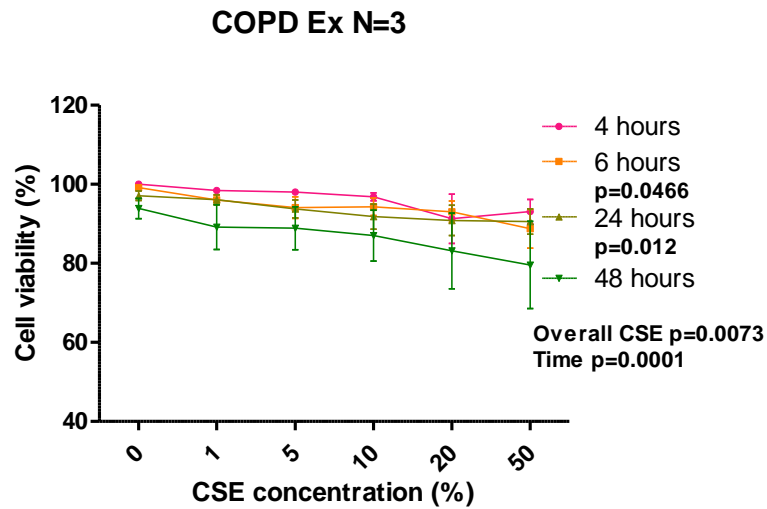


Figure 5.3.19 Primary human Fibroblast viability responses to doses of CSE measured by MTT assay: COPD Ex-smokers $n=3$ and COPD Current Smokers $n=3$ Repeated measures ANOVA with post t-test revealed that overall time and CSE concentration affected cell viability for all subject groups with varying significant declines at 6, 24 and 48 hours for COPD ex and current smokers.

5.4 Discussion

Our IHC characterisation of the primary fibroblasts indicated that they exhibit some typical mesenchymal characteristics including α SMA expression. Quite surprisingly, fibroblasts from control group (ex-smokers) appeared to have a more epithelial phenotype; lower α SMA expression while current smokers ('normal and COPD) have raised α SMA expression. Although this is almost a 'circumstantial look' at 1 patient in each group, these findings indicate that current smoking promotes continual EMT differentiation, while fibroblasts in ex-smoker lungs may be reverting to a less fibrotic phenotype. As mentioned in chapter 3, unfortunately we cannot use cell morphology as an indicator of cell differentiation after a cytopspin due to the process itself altering the cell shape. Future IHC staining on fibroblasts grown on coverslips in wells would better preserve cellular morphology. An example of fibroblast morphology expected is in chapter 2 figure 2.5 showing NHLFs at 70% confluence.

It is important to mention that there would have been an element of selection occurring whilst explanting and establishing cultures of the primary fibroblasts. Only 30-40% of all attempted primary fibroblast explants worked, initially within 2-5 days of tissue manipulation, a proportion of the intended culture would be infected with either a bacterial or fungal infection. As the same media and reagents were used across all experiments we were able to rule out laboratory contamination and deduced that they were growing from any existing cultures within the patient lung tissue itself. This was not deemed as unusual as the patients would have been immune compromised due to lung cancer and it is not unusual for the patients with COPD to have recurrent chest infections, (Barnes 2008; Kisseleva and Brenner 2008). Following this some explants failed to establish any form of cellular growth and tissue detached from the cellbind flasks and finally in a few individual cases multiple cell types established growth within the flasks, in one case both epithelial and fibroblasts grew in colonies side by side and another cells presenting a squamous cell morphology also grew. In all of these cases the cells were not used for any experiments in this study. As can be seen be this short explanation producing the primary fibroblast cell lines was itself very challenging.

With the remaining primary fibroblasts it took between 4 to 6 weeks to establish the primary cell cultures with enough cells to conduct the experiments in this study. This itself is a major unintended selection process. It was noticed (when presented with patient demographics) that the COPD explants (especially the current smoker group) would establish the fastest which could indicate that the cells were favourable of a fully mobile mesenchymal phenotype, whereas the non-smoker group was the group in which there was the most difficulty in producing a primary cell line from, which may indicate the cells are less mobile or active than the CCS cells. By growing the cells in normal plastic culture flasks it may have also had a selective process on the type of fibroblasts that survived, it has been suggested in previous studies that exposing/growing fibroblasts on ridged plastics can cause cell activation and in turn differentiation of the resident fibroblast into myofibroblasts, (Zhaodong *et al* 2007). These cells then would proliferate and become the more predominant cell type in culture. As this realisation came to light post experiments any future explant work would be conducted on collagen coated culture flasks.

As discussed this form of *in vitro* culture work is very selective, it is optimised and driven to the fast growth of cells to allow for the next experiment and only produces a singular cell type (dedifferentiation and select for mutations and subpopulations which grow faster) over a long period of time. Therefore it is also reasonable to mention that the cells isolated would have most likely changed phenotype and cellular activity to what they were *in situ*, prior to patient lung resection. They also do not have the multiple mechanisms and different cellular activities reducing the physiological reactions and interactions among the cells and tissues, meaning the exposure system in place is not an exact representative of action and reaction that would be seen *in situ*, (Hartung and Daston 2009). It has been suggested that in monolayer culture the cells have only 15% of normal cellular contacts, with cell densities $\leq 1\%$ of tissue situation, which impairs on intracellular signalling (Coecke *et al* 2006). In addition to this the continuous change to culture conditions i.e. depletion of nutrients accumulation of waste products and the sudden exchange of culture media, results in non-homeostatic conditions.

To overcome these problems found with *in vitro* work would be to move to *in vivo* work, as it is unethical to conduct human experiments the work is conducted in animal models e.g. mice as they have a high level of concordance with humans providing

the extensive interactions between cells and tissues as well as the test subject (lung fibroblast) being in its true form. In spite of this, *in vitro* work is cheaper with set ups being small allowing for a high number of replicates it also allows a reductionist approach to the bigger picture, allows for the testing of the specific material (in our case the primary cell lines) at all times and eases interpretation. COPD is caused by long term exposure to irritants, with a suspected undetermined genetic predisposition; even though chronic lung damage can be replicated within animal models e.g. mouse, there are species differences in responses that ultimately hinder the ability of using direct comparisons to predict and surmise human responses, (Hartung and Daston 2009).

There are respective advantages and limitations for both approaches however using a combined approach gives stronger argument much more than either alone. With the key characteristics (working with specific diseased tissue) of *in vivo* tests provides a simplistic framework to initially assess which can direct and further explain outcomes from follow on *in vivo* work. With this in mind the results from our cell culture experiments are the first stepping stone in assessing fibroblast reactions to CSE in a mono-cellular environment which could lead to future *in vivo* animal multicellular environmental studies.

All of the measurements in this study have been made on the understanding of the limitations (as previously mentioned) of the *in vitro* cell based assay; cells are removed from their native environment where they would have been directly interacting with ECM and other cell types. *In vitro*, cells are subjected to a simpler environment lacking other confounding factors in the lung. Cell phenotypic changes were minimised by restricting primary cell passages to P5 and inspecting cell morphology via light microscopy regularly.

Our comprehensive study of human lung primary fibroblast responses to CSE showed cytokine specific responses: IL-6 and IL-8 levels overall rose dose dependently whilst total TGF β 1 levels did not. This indicates that CSE does not directly stimulate total TGF β 1 transcription or release, rather, that IL-6 and IL-8 transcription occurs much earlier and is more sensitive to compounds in the smoke. This is somewhat surprising, however does absolutely support previous reports of

early IL-6 responses promoting an EMT phenotype and subsequent TGFβ1 release. This has been described for epithelia undergoing mesenchymal differentiation, however we were surprised to see this also true for mature fibroblasts.

It is important to mention at this stage that the all of the cell supernatants were activated during the TGFβ1 ELISA procedure. This cleaved off the LAP1 peptide from the latent TGFβ1 produced, allowing for the measurement of total TGFβ1 (both active and latent forms) in the samples. It was noted that the baseline 0% CSE and 4 hour time point for total TGFβ1 measure was high. This could be caused by any pre-existing latent TGFβ1, present extracellular matrix of the primary fibroblasts, which in turn was activated by the ELISA kit. It has been reported in Vehviläinen *et al* 2009, that after a short period of culture (1-2 days) L-TGFβ1 was present in the ECM. Future studies will assess both latent (by activating the samples) and active forms of TGFβ1. It was seen in BAL from IPF patients that in areas with no noticeable inflammation or fibrosis contained higher amounts of TGFβ1 in latent form compared to the active TGFβ1 form which was found in areas with fibrosis and inflammation, (Khalil *et al* 2001). It would be interesting to apply a similar hypothesis to cells from control and COPD groups to determine which isoform of TGFβ1 is produced and if the ratios change with disease or not.

By dividing subjects into 4 groups COPD and controls (current and ex-smokers in each) we were able to observe IL-6 responses in COPD current smokers at 48 hours were blunted compared to the other time points and other patient groups. It could be the fibroblasts are unable to keep transcribing the cytokine due to viability issues. Given that this does not also apply to IL-8 or TGFβ1 levels (as levels remain high at 48 hours) this is not likely to be the case, supported by modest viability declines at 48 hours in MTT assay; future PCR studies could add clarity to this. It more likely that preformed IL-6 protein has already been released due to IL-6 being an early indicator of EMT/fibrosis and ongoing heavy smoking would provide continued stimulus for an EMT phenotype.

Two group comparisons show current smokers (COPD and controls) exerted a more pronounced IL-6, IL-8 and TGFβ1 dose response to CSE compared to ex-smokers (COPD and controls), particularly at the early time points (4 and 6 hours).

This early release of cytokines would be from pre-formed lysozymes with further transcription occurring at the later time points, 24 and 48 hours. Clearly current smoker cytokines are being released in immediate response to the CSE, and similar responses in the later time points indicate cellular activation and gene transcription is ongoing throughout the exposure times. The ex-smoker responses for all cytokines are blunted at the early time points then rise dose dependently at 24 and 48 hours. This implies that the current smoker cells by comparison are in a heightened activated state producing early responses, while ex-smoker cells are more quiescent; requiring longer to synthesise and release their cytokine responses. This is an important finding and suggests that inflammation and fibrotic conditions require continued CSE stimulation and that by quitting smoking, subjects may slow or revert inflammatory processes in their lungs. Literature has considered an autoimmune component in COPD where inflammation continues beyond smoking cessation, indicated by previous studies from our group for lymphocytes (Smyth 2007 and Agusti 2003) however, in my hands, primary human lung fibroblasts do not exhibit such properties.

Dividing data into COPD verses control groups did not reveal any significant differences for IL-6 or IL-8 assessed but total TGF β 1 is raised somewhat in the control group. As shown by the 24 hour direct comparisons of all control and all COPD data there were no significant differences between the groups for IL-6 and TGF β 1 yet there was for IL-8. Müller *et al* 2006 describe primary human lung fibroblasts from emphysema patients having a senescent phenotype via the upregulation of senescence-associated markers IGFBP-3 and IGFBP-Rp1 suggesting that these cells have a reduced response to external stimuli. Nadigel *et al* 2013 describe higher IL-8 levels to CSE from control HBE cells compared COPD over 24 hours where we saw the opposite in the primary fibroblasts in agreement with Schulz *et al* 2003 who saw marked increase in IL-8 release from COPD patients when compared to non and current smokers. This could indicate that the cells from COPD patients are already pre-primed and ready to release IL-8 for its role in chemotaxis of neutrophils in the lung. In addition to this 24 hour data was compared for all 5 patient groups, this also shown there were no significant differences in cytokine release from the groups. Indicating that fibroblast cytokine release is not disease dependent overall.

We did not have access to blood gas diffusion test results so cannot be certain if any of our patients have emphysema, however the average lung function of the group (table 5.2) is 65% FEV1 putting them in COPD GOLD stage II (moderate) therefore they are not likely to have emphysema. Further, IL-8 and IL-6 responses were not blunted in our COPD cohort; so in earlier stages of COPD we can state that primary fibroblasts are not senescent.

In COPD clear dose responses to CSE can be seen for IL-6 and IL-8 at all time points except IL-6 at 48 hours where responses are uniformly high. Our data indicates that pro-fibrotic conditions alone are not sufficient pathology to cause airway obstruction; as COPD is an umbrella term for a range of conditions, it seems that assessing lung fibroblast responses to CSE would be insufficient to predict disease outcome. Taking this data into context with the current and ex-smoking data, it seems clear that ongoing cigarette smoking is a strong contributing factor to generating pro-fibrotic conditions which may be one contributing factor (among other pathologies) to COPD development; the risk rising with accumulating pack year history.

Some patients in our study were inhaled corticosteroid users prior to the lobectomy; steroids may modify some of the inflammatory and pro-fibrotic processes in the lung; we did not test fibroblast steroid sensitivity in our assay, or if cell express the steroid receptor. A growing body of evidence indicates steroid resistance in COPD at a cellular level in lymphocytes and macrophages (e.g. Kaur 2012, Barnes 2004); our culture system would be ideal to take this area of research forward for fibroblasts. Other medications may influence cell responses to external stimuli: e.g. B2 agonists can induce epithelial cells (A549s) to release IL-6 and IL-8 (Strandberg *et al* 2007).

It would be interesting to look at other functions of fibroblast behaviour in response to CSE, including fibronectin and other extracellular matrix (e.g. collagen) release. The IHC study (chapter 3) showed correlation with collagen deposits with airway obstruction, so making observations of the kinetics of this occurring with pack year history and airway obstruction would be valuable information from the primary cell culture system.

Viability of the cells used in our culture system overall was good >90%. In control current smokers viability decreased to ~60% at the highest CSE dose at 48 hours;

cytokine release for this particular time point may be as a result of cell lysis, however the morphology of the cells at the end of the experiment was good and did not indicate this may be the case. Studies using epithelia find higher losses of viability e.g. Gornati *et al* 2013 found a loss of cell viability (ECV-304 cell line) with increasing CSE concentration down to 70% viability after 1 hour with 10% CSE, which further decreased to 50% after 6 hours. Comparisons of this type indicate it is important to include such validation tests to take into consideration with the cytokine data.

We went to considerable trouble and expense to introduce stretch forces to simulate emphysema in addition to the CSE environment. Our data show modest rises in IL-8 release in response to CSE alone (as shown in previous figures) and to stretch alone compared to baseline (0% CSE). However there was no additive effect when both CSE and stretch forces were applied. Stretch forces did not change TGF β 1 release over baseline. This data implies that having emphysema during lung fibrosis would not be a predisposing factor to fibrosis acceleration. However by having emphysema, potentially exerting stretch forces in the lung, this may be sufficient to initiate pro-fibrotic conditions (rising IL-8) and potentially initiating EMT processes. As TGF β 1 levels seem to indicate a function of fibroblasts rather than being pro-mesenchymal, IL-8 rises may be sufficient to initiate EMT.

The Kentucky research grade cigarette is a well cited research tool however we accept that CSE media may not fully simulate smoke passage and particulate deposits in the lung via active smoking. Our studies have focussed on small airway/parenchymal fibroblasts that may be exposed to smaller particulates compared to in the large airways where the majority of smoke would normally arrive. Nevertheless, proof of principle understanding key events in response to CSE is useful.

To better characterise the primary fibroblast phenotype and behaviour, flow cytometric analysis/cell sorting could identify and isolate: S100A4/Vimentin +ve or double +ve cells to identify EMT derived cells, from α SMA –ve that may represent blood vessel structural cells, from E-cadherin +ve cells to identify lung epithelia. Sufficient cell numbers in each population would enable functional fibroblast responses to CSE / novel drugs to be assessed; either by QRT-PCR or protein assays.

Since starting my study e-cigarettes have become increasingly popular and are self-advertised as “safe” yet they are not regulated. There are many different types, strengths and flavours of the vapour liquids. It would be interesting to investigate these in the same manner as I have conducted with the CSE. To do this it would be useful to determine how much ‘e-vapour’ liquid would equal 1 cigarette and then make this in supplemented RPMI to be equal to 100% CSE. Experiments could be conducted on both cell lines and then progress on to the primary cells that have been isolated. To summarise, this research has helped pave the way for planning future studies that will be considered in chapter 6.

Chapter 6

6.1 Discussion and Conclusions for future work

COPD is a disease of the lungs that is one of the largest causes morbidity and mortality throughout the world (Mannino 2002), it is predicted by 2020 that it will be the third most prevalent diseases worldwide, (Sarir *et al* 2008; Cosio *et al* 2009; Smith *et al* 2001 cited in Rangasamy *et al* 2009). With this it is clear that the economic burden of COPD is considerable, not only in the UK but globally and it will continue to grow considerably, as the number of people surviving longer continues to increase, (Bousquet and Khaltayev 2007). Therefore it is clear that there is a need for better understanding of the cellular pathology to provide more cost effective and beneficial to patient health treatments.

During normal repair of a lung injury epithelia respond by rapid proliferation to cover the wound and release mediators into the wound space to facilitate further repair processes. It is understood fibroblasts are recruited and respond by differentiation into myofibroblasts that contract to draw together the margins of the wound to reduce its size and aid re-epithelialisation. Ordinarily the myofibroblasts disappear and the repair process ends following suitable wound recovery. In fibrotic conditions this repair process continues and the myofibroblasts may be derived from EMT processes. EMT is now a recognised process contributing to fibrosis of various diseases including renal and liver fibrosis. EMT markers and cellular signalling components are characterised in various fibrotic conditions and in lung cell lines, however, this study set out to gain new information about EMT in *primary* human lung isolates.

Typical indicators of EMT include membrane-associated adherens junctions and desmosomes being dissociated followed by upregulation of intermediate filament proteins and cytoskeletal re-arrangement. E-cadherin adhesion protein becomes down regulated thus altering polarity and reducing epithelial tightness. This process is also a key indicator of epithelia tumour metastasis. Loss of E-cadherin expression during EMT is usually accompanied by α -SMA expression, a myofibroblastic morphology and extracellular matrix production.

Our group previously showed the A549 lung epithelial line adopts a mesenchymal phenotype when exposed to pro-fibrotic conditions (TGF β 1). Cells lost their cobblestone morphology and took on a fibroblast spindle shape; they also adopted fibroblast functions including collagen I and III and MMP9 (protease) release. Further, EMT characteristics of A549 were shown to signal via a SMAD pathway, as MEK inhibitors did not reduce SMAD2 phosphorylation. SMAD2 siRNA suppressed SMAD2 phosphorylation and reduced the EMT-mediated effects on the expression of epithelial and mesenchymal markers. Our group's previous data added to the growing body of evidence that TGF- β 1 can induce EMT in A549 cells, by a process involving SMAD signalling, (Magee *et al* 2008).

This study (chapters 3+4) have suggested that EMT is an important contributing process to fibrosis in COPD, particularly evidenced by the patients with a high pack year history. With further studies into this it may reveal that EMT is a potential therapeutic target to treat lung fibrosis with applications for COPD patients. We didn't see EMT processes in all COPD patients so it may be important to determine the mechanism of ongoing disease in patients to provide individual therapies effectively. This may be done by means of bronchoscopy and biopsy to reliably observe lung EMT via histochemistry studies. Recent clinical trials have proved encouraging using Pirfenidone, an agent that exhibits anti-inflammatory and anti-fibrotic properties (Costabel 2011).

Very recently published findings in ERJ 2015 (Gohy *et al* 2015) observed EMT changes in COPD lung tissue by IHC; they observed increases in vimentin levels in COPD lungs. The authors provide demographics for (n=62) COPD patients compared to control subjects (n=42) however the number of patients assessed by IHC was smaller and very comparable to our study.

The contribution of inflammation to EMT is controversial; in fibrotic areas there is little evidence of inflammatory cells and standard anti-inflammatory steroid treatments are largely ineffective for treating COPD. Nevertheless IL-6 is reported to initiate EMT processes with TGF β 1 being a key mediator later on; further, inflammatory cytokines are likely to be responsible for failed epithelial repair. Other authors have used A549 cells and found that TGF β 1 mediated EMT could be enhanced with a 'cytomix' of IL1 β , IFN γ and TNF α which upregulated the TGF β 1 receptor expression (Liu *et al* 2008).

TNF α can enhance TGF β 1-induced contraction in cells that have undergone EMT (Yamauchi 2010). Similar studies done on human bronchial epithelial cells also found that TNF α enhances TGF β 1 effects on EMT (Camara *et al* 2010; Kamitani *et al* 2011). From all these studies we clearly had a valid rationale for researching EMT in human lung samples with a view to developing drugs that may reduce both inflammatory and fibrotic cellular activities during EMT.

Our evaluation of inflammatory (IL-6) and fibrogenic (TGF β 1 and IL-6) responses to primary lung fibroblasts time in culture, CSE and stretch has yielded valuable information on relevant stimuli for disease progression. All patient cells exerted large increases in IL-6 and IL-8 release over time, and to a smaller extent in response to CSE and to stretch forces. Particularly, time was a key factor for cytokine rises, and this may implicate an autoimmune aspect of the fibrotic process or simply a highly active state of the isolated cells. Extent of fibrosis and myofibroblast induction depends upon the level of TGF- β present (Gauldie *et al* 2002) so clearly, the mature fibroblasts may have a dominant role in creating pro-inflammatory micro-environment in the lung to promote further EMT processes. IHC characterisation of the fibroblasts (one patient from each category; NS, ExS, CS, CEx and CC) used in culture experiments (via cytopins and DAB IHC staining) showed they were differentiated fibroblasts expressing S100A4, alpha smooth muscle actin and reduced E-cadherin.

In my hands the fibroblasts were relatively easy to expand from lung tissue resections; not requiring any invasive processes that may activate the cells, or many passages to develop large stocks. Within the time of these PhD studies a model for assessing cellular responses to CSE and stretch forces to simulate emphysema was developed. This model can now be applied for a range of further lung fibrosis studies to observe effects of new potential therapies that may block or reverse inflammatory or fibrotic processes in the lung.

Previous studies in our lab have investigated the use of omega-3-poly unsaturated fatty acids (Ω -3 PUFAs) from fish oils as a potentially useful 'nutriceutical' and have demonstrated their use in regulating muscle wasting (Magee *et al* 2008). EPA (omega 3 fatty acids) but not omega 6 fatty acids (linoleic acid) were effective at blocking damaging effects of TNF α in their skeletal model. Furthermore, EPA was equally effective when applied as a pre-treatment or co-treatment and could be delivered at

concentrations that can be achieved *in vivo* (Magee *et al* 2008). This work also indicated that PUFAs may work via a peroxisome proliferator-activated receptor PPAR γ dependent pathway. Magee *et al* found that TNF α treatment increased NF- κ B activity and reduced expression and activation of PPAR γ and that EPA activity appeared to upregulate PPAR γ which was blocked by a specific PPAR γ inhibitor. Magee *et al* also showed omega-3 but not omega 6 PUFAs also inhibited TNF α -mediated transcription and secretion of IL-6; a key target gene of TNF-mediated NF- κ B transcriptional activity, and a key cytokine released from primary fibroblasts observed in this study in chapter 5.

Given that steroids are so poorly effective in treating COPD patients, it would be of great interest to apply this nutraceutical approach to our fibroblast model to see if pro-inflammatory and pro-fibrotic conditions (released cytokines) could be regulated or reversed, and to progress this research via a similar route to Magee *et al* 2008 to ascertain the mechanisms by which the PUFAs may be working. This study has suggested that EMT is occurring in human lung COPD tissue via TGF β 1 mediated mechanisms (raised levels of SMAD3, SNAI1, IL-6 and TGF β 1 in S100A4+ve tissue) so it would also be reasonable to investigate if PUFAs can interfere with TGF β 1 signalling. Using relevant specific inhibitors the involvement of SMADs, PPAR γ , sphingosine kinase and glucocorticosteroid receptors involvement in fibrosis and inflammation can all be investigated using this model system.

Future work

Throughout the writing process of my thesis I have been made aware of limitation to the study I conducted. If I was able to continue the research in this field I would attempt to re-address some of the limitations to make the studies data more robust. For example I would return to the IHC part of this study and pre-form additional staining of each individual lung patient with each marker and adopt the cumulative frequency approach as for mentioned I chapter 3.

I would also expand on the preliminary LCMD work (chapter 4) achieved in this study. To ensure best chances for RNA integrity more vigorous sample selection would take place, to ensure the tissue is as fresh as possible and hasn't been stored for an

extended period of time. Following this a change in experimental procedure would be fundamental, meaning sectioning, stain, LCMD, RNA isolation and quality assessment (Agilent Bio-analyser) would occur on the same day; again this is to ensure the best possible RNA yield and integrity. Following the patient expansion of the original study I would be inclined to further assess extra signalling components such as RAGE, the extracellular ligand SPHK1 and intracellular mediators S1P1 +3 of TGF β 1 signalling, as well as the NF-KB transcription factor Twist within the S100A4 positive fibrotic tissue and compare it to the S100A4 negative epithelial tissue.

In addition to this if I were to have unlimited resources I would reduce assumptions on primary fibroblast cellular identities by employing fluorescence activated cell sorting (FACS), which would not only identify specific markers but allow for heterogeneous population selection and sorting. This technique would enable us to compare further downstream experimental results directly without assumptions that the primary fibroblast samples are homogeneous. These sorted cells would then be applied to assessing novel inflammatory and anti-fibrotic drug actions with the addition of CSE stimulus, assessing enzymic activity via western blots and assess their mechanisms including the blockade of PPAR γ , GR and SMAD signalling via QRT-PCR.

Summarised in figure 6.1 is an overview of where this thesis work has fitted into EMT research, and how the outcomes may steer and influence future research to pave the way for better treatments of COPD and lung fibrosis.

Reflective comments: Undertaking this work has enabled me to develop my technical expertise in areas of primary tissue preparation for sectioning, microtomy, cryostat sectioning, immunohistochemistry, microscopy/imaging/quantification, statistical analysis, primary human cell tissue culture, ELISA, laser capture microscopy, and Q-RT-PCR. Many of these techniques required working SOPs to be developed which I needed to write and so have included them in the appendix. Working with human tissue has also raised my awareness of the need to respect the source of tissue and comply with the ethical approval from the South Manchester Regional Ethical approval committee; this committee approval is referenced in the subsequent Salford University ethical approval; included in the appendix. We needed to comply with the Human Tissue Act and have detailed records tracking all samples from source to disposal (or storage). Undertaking this work has given me opportunity to design and develop new areas of research and contribute to helping patients with respiratory disease; a hugely rewarding experience.

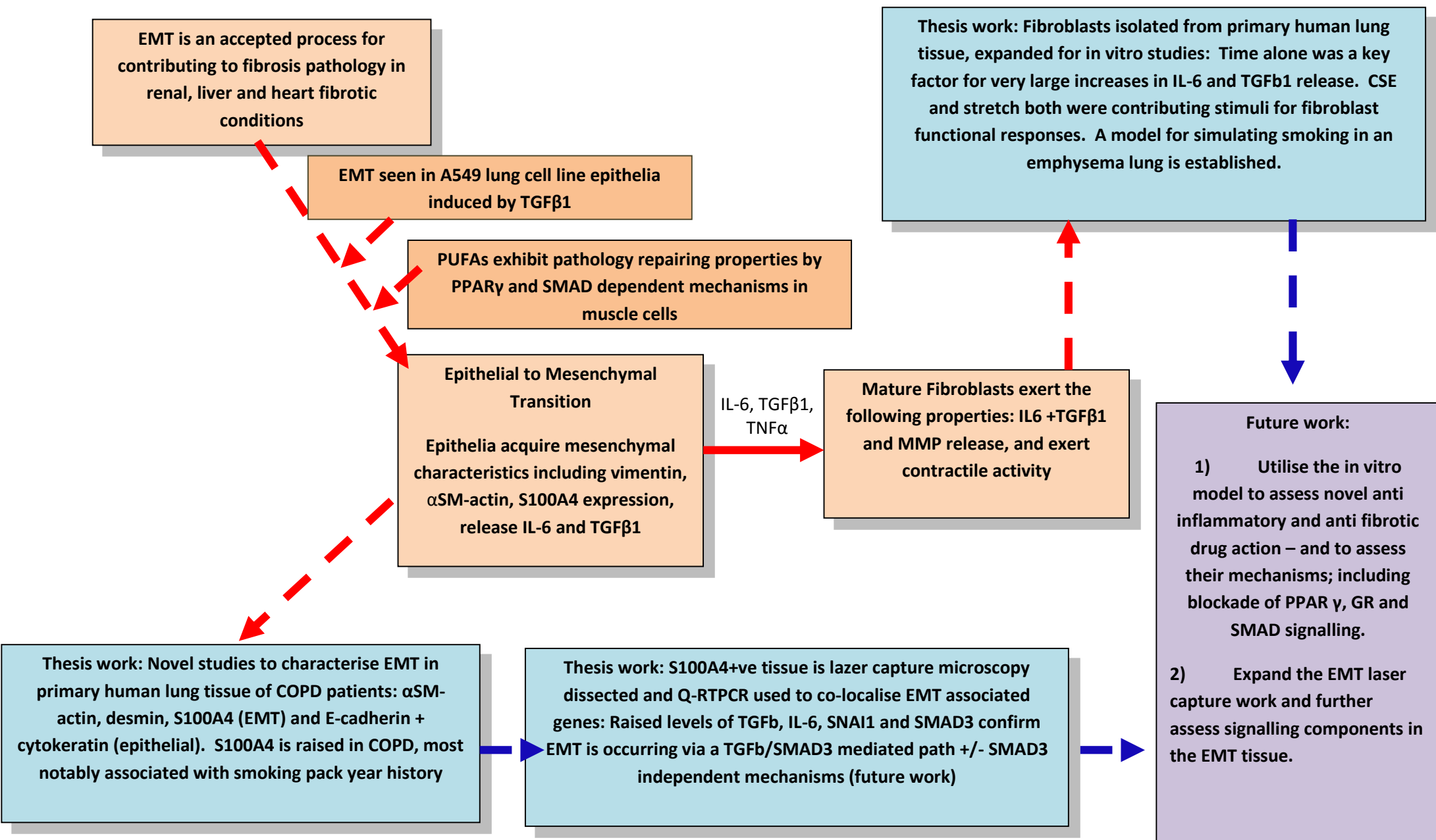


Figure 6.1: Overview of where this thesis work sits in current research and how it directs future research

Understanding of the processes of EMT are summarised in the pink boxes and information flow by red arrows. The darker orange boxes summarise previous findings of colleagues in my research group. The blue boxes summarise my thesis findings and the flow of this information contributing to future research; purple box.

References

Abcam® (1998-2015) IHC buffers and epitope recovery/tissue pre-treatments, [Accessed June 2015] Available from: [http://www.abcam.com/index.html?pageconfig=resource&rid=12854&source=pag etrap]

Abcam®, IHC-Paraffin protocol IHC-P, [Accessed June2015] Available from:[http://www.abcam.com/ps/pdf/protocols/ihc_p.pdf]

Agusti A, MacNee W, Donaldson K, Cosio M. (2003). Hypothesis: Does COPD have an autoimmune component? *THORAX*, **58**:832-834

Alberts B, Johnston A, Lewis J, Raff M, Roberts IC, Water P, Molecular biology of the Cell, 4th Edition, New York: Garland Science, 2002, Chapter 19.

Alder JK, Guo N, Kembou F, Parry EM, Anderson G, *et al* (2011) Telomere length is a determinant of emphysema susceptibility, *American Journal of Respiratory Critical Care Medicine*, **184**(8):904-12

Allen JT, Spiteri MA. (2002). Growth factors in idiopathic pulmonary fibrosis: relative roles. *Respiratory Research*, **13**:3

Alstead S, Badenoch AW, Bateman GH, Biggart JH, Bishop MF *et al*, (1989) Butterworths Medical Dictionary Second Edition, *Butterworth & Co (publishers) Ltd*

Applied Biosystems, (2008) Guide to Performing Relative Quantitation of Gene Expression Using Real-Time Quantitative PCR, [Accessed may 2014] Available from: [http://www3.appliedbiosystems.com/cms/groups/mcb_support/documents/generaldocuments/cms_042380.pdf]

Baglole CJ, Bushinsky SM, Garcia TM, Kode A, Rahman I, Sime PJ, Phipps RP, (2006), Differential induction of apoptosis by cigarette smoke extract in primary human lung fibroblasts strains: Implications for emphysema, *American Journal of Physiology, Lung Cellular and Molecular Physiology* **291**: L19-L29

Barnes PJ, (2000), Mechanisms in COPD: Differences from Asthma, *CHEST*, **117**:105-145

Barnes PJ, (2002), Asthma and COPD: basic mechanisms and clinical management, *Academic press*, pgs. 135, 171-172

Barnes PJ, (2003), New concepts in Chronic Obstructive Pulmonary Disease, *Annual Review of Medicine*. **54**:113-129

Barnes PJ (2004) Corticosteroid Resistance in Airway Disease. *Proceedings of the American Thoracic Society*; **1**:264-268.

Barnes PJ, (2004), Mediators of Chronic Obstructive Pulmonary Disease, *Pharmacological Reviews*, **56**:515-548

Barnes PJ, (2008), The cytokine network in asthma and chronic obstructive pulmonary disease, *The Journal of Clinical Investigation* **118**(11): 3546-3556

Barnes PJ, (2009), The cytokine network in Chronic Obstructive Pulmonary Disease, *American journal of Respiratory Cell and Molecular Biology* **41** (6): 631

Battaglia S, Mauad T, Van Schadwijk AM, Vignola AM, Rabe KF, Bellia V *et al* (2007), Differential distribution of inflammatory cells in large and small airways in smokers, *Journal of Clinical Pathology*, 60:907-911

Balzano G, Stefanelli F, Iorio C, De Felice A, Melillo EM *et al* (1999) Eosinophilic inflammation in stable chronic obstructive pulmonary disease: Relationship with Neutrophils and Airway function, *American Journal of Respiratory and Critical Care Medicine*, **160**:1486-1492

Beraki, Olsen TK, Sauer T, (2012) Establishing a protocol for immunocytochemical staining and chromogenic in situ hybridization of Giemsa and Diff-Quick prestained cytological smears, *CytoJournal*, **9**:8

Blaauboer ME, Smit TH, Hanemaaijer R, Stoop R, Everts V, (2011) Cyclic mechanical stretch reduces myofibroblast differentiation of primary lung fibroblast, *Biochemical and Biophysical Research Communications*, **404**:23-27

Blanco D, Vicent S, Elizegi E, Pino I, Fraga MF *et al* (2004) Altered expression of adhesion molecules and epithelial-mesenchymal transition in silica-induced rat lung carcinogenesis, *Laboratory Investigation*, **84**: 999-1012

Bousquet J, Khaltaev N, editors. World Health Organization (WHO) Global Surveillance, Prevention and Control of Chronic Respiratory Diseases: A Comprehensive Approach. Geneva: WHO; 2007. [Accessed august 09, 2012]. Available from: [\[http://www.who.int/gard/publications/GARD%20Book%202007.pdf.\]](http://www.who.int/gard/publications/GARD%20Book%202007.pdf)

Brey EM, Lalani Z, Johnston C, Wong M, McIntire LV, et al (2003) Automated Selection of DAB-Labelled Tissue for Immunohistochemical Quantification, *Journal of histochemistry and Cytochemistry*, **51**:575

Câmara J, Jarai , (2010), Epithelial-mesenchymal transition in primary human bronchial epithelial cells is Smad-dependant and enhanced by fibronectin and TNF- α , *Fibrogenesis & Tissue Repair*, **3**(2): 11 pages

Caramori G, Adcock I, (2002), Pharmacology of airway inflammation in asthma and COPD, *Pulmonary Pharmacology and Therapeutics*, **16**:247-277

Carnevali S, Petruzzelli S, Longoni B, Vanacore R, Barale R, Cipollini M *et al*, (2003) Cigarette smoke extract induces oxidative stress and apoptosis in human lung fibroblasts, *American Journal of Physiology, Lung Cellular and Molecular Physiology* **284**: L955-L963

Challa AA and Stefanovic B, (2011) A novel role of vimentin filaments, binding and stabilization of collagen mRNA's, *Journal of Molecular and Cell Biology*,

Chen J, Li H, Sundorraj N, Wang JHC, (2007) Alpha smooth muscle actin expression enhances cell traction force, *Cell Motility and the Cytoskeleton*, **64**:248-287

Chilosi M, Poletti V, Rossi A, (2012) The pathogenesis of COPD and IPF: Distinct horns of the same devil?, *Respiratory Research*, **13**:3

Coecke S, Ahr H, Blaauwer BJ, Bremmer S, Casati S *et al* (2006), A bottleneck in *in vitro* toxicological test development. *Altern. Lab. Anim.*, **34**:49-84

Cosio M, Majo J, Cosio M, (2002), Inflammation of the Airways and Lung Parenchyma in COPD: Role of T cells, *CHEST*, **121**:1605-1655

Cosio MG, Sietta M, Agusti A, (2009), Immunologic Aspects of Chronic Obstructive Pulmonary Disease, *Medicine*, **360**(23):2445-2454

Costa ML, Escaleira R, Cataldo A, Oliveira F, Mermelstein CS, (2004), Desmin: Molecular interactions and putative functions of the muscle intermediate filament protein, *Brazilian Journal of Medical and Biological Research*, **37**(12): 1819-1830

Costabel U. Emerging potential treatments: new hope for idiopathic pulmonary fibrosis patients? *Eur. Respir. Rev.* 2011;20:201-207.

Currie GP, (2009), the facts: Chronic Obstructive Pulmonary Disease, Oxford University Press, Page 11-21

Curtis JL, Freeman CM, Hogg JC, (2007), The Immunopathogenesis of Chronic Obstructive Pulmonary Disease, *American Thoracic Society*, **4**:512-521

Dalby MJ, Riehle MO, Sutherland DS, Agheli H, Curtis ASG, (2005), Morphological and microarray analysis of Human Fibroblasts Cultured on Nanocolumns produced by Colloidal lithography, *European Cells and Materials*, **9**:1-8

De Matos LL, Trufelli DC, De Matos MGL, Pinhal MADS, (2010) Immunohistochemistry as an Important Tool in Biomarkers Detection and Clinical Practice, *Biomarker Insights*, **5**:9-20

D'Amico F, Skarmoutsou E, Stivala F (2009) State of the art in antigen retrieval for immunohistochemistry, *Elsevier Journal of Immunological Methods*, **341**:1-18

De Vriese AS, Tilton RG, Mortier S, Lameire NH, (2006) Myofibroblast transdifferentiation of Mesothelial Cells is mediated by RAGE and contributes to peritoneal fibrosis in Uraemia, *Nephrology Dialysis Transplantation*, **21**:2549-2555

De Wever O, Westbroek W, Verloea A, Bloeman N, Bracke M *et al* (2004) Critical role of N-cadherin in myofibroblast invasion and migration in vitro stimulated by colon-cancer-cell-derived TGF- β or wounding, *Journal of Cell Science* **117**: 4691-4703

Didon L, Roos AB, Elmberger GP, Gonzalez FJ, Nard M, (2010), Lung-Specific Inactivator of CCAAT/enhancer binding protein & causes a pathological pattern characteristic of COPD, *European Respiratory Journal*, **35**:186-197

Domagala-Kuawik J, (2008) Effects of cigarette smoke on the lung and systemic immunity, *Journal of Physiology and Pharmacology*, **59**(6):19-34

Erickson HS, Albert PS, Gillespie JW, Rodriguez-Canales J, Lineham WM *et al* (2009) Quantitative RT-PCR gene expression analysis of laser microdissected tissue samples, *Nature Protocols*, **4**(6):902-922

Fend F, Emmert-Buck MR, Chuaqui R, Cole K, Lee J *et al* (1999) Immuno-LCM: laser capture Microdissection of Immunostained Frozen Sections for mRNA Analysis, *American Journal of Pathology*, **154**(1):61-66

Feng Z, Marti A, Jehn B, Altermatt HJ, Chicaiza G, Jaggi R, (1995), Glucocorticoid and pergesterone inhibit involution and programmed cell death in mouse mammary gland, *Journal of Cell Biology*, **131**(4): 1095-1103

Fuke S, Betsuyaku T, Nasuhara Y, Morikawa T, Katoh H, Nirshimura M, (2004) Chemokines in Bronchiolar Epithelium in the Development of Chronic Obstructive Pulmonary Disease, *American Journal of Respiratory Cellular and Molecular Biology*, **31**:405-412

FX- 4000T FlexerCell Tension plus system Image, <http://day-moon.com/store/product>

_info.php?products_id=5684 Updated 2007 [Accessed on 3.4.2011]

Gál K, Cseh Á, Szalay B, Rusai K, Vannay Á *et al* (2011), Effect of Cigarette Smoke and Dexamethasone on Hsp72 System of alveolar epithelial cells, *Cell stress and Chaperones*, **16**:369-378

Gauldie J, Kolb M, Sime PJ, (2002) A new direction in the pathogenesis of idiopathic pulmonary fibrosis? *Respiratory Research* **3**:1

Green CE, Turner AM, (2013) Role of chronic obstructive pulmonary diseases in lung cancer pathogenesis, *World journal of Respirology*,**3**(3):67-76

Gohy ST, Hupin C, Fregimilicka C, Detry BR, Bouzin C, (2015) Imprinting of the COPD airway epithelium for dedifferentiation and mesenchymal transition, *European Respiratory Journal*, **45**:1258-1272

Gornati R, Colombo G, Clerici M, Rossi F, Gagliano N *et al* (2013) Protein carbonylation in human endothelial cells exposed to cigarette smoke extract, *Toxicology Letters*, **218**:118-128

Hartung T, Daston G, (2009), Are *in vitro* test suitable for Regulatory use?, *Toxicological Sciences*, **111**(2):233-237

Hasday JD, Bascorn R, Casta JJ, Fitzgerald T, Dubin W, 1999, Bacterial endotoxin is an active component of cigarette smoke, *American college of Chest physicians, chest*, 115: 829-835

Hastie AT, Kraft WK, Nyce KB, Zangrilli JG, Musani AI, *et al* (2002), Astmatic epithelial cell proliferation and stimulation of collagen production: Human Epithelial Cells Stimulate Collagen Type III production by Human allergen challenge, *American Journal of Respiratory and Critical Care Medicine*, **165**(2): 266-272

Herrera I, Cisneros J, Maldonado M, Ramirez R Ortiz-Quintero B *et al* (2013) Matrix Metalloproteinase (MMP)-1 Induces Lung Alveolar Epithelial Cell Migration and Proliferation, Protects from Apoptosis, and Represses Mitochondrial Oxygen Consumption, *Journal of Biological Chemistry*, **288**(36):25964-25975

Hinz B, Celetta G, Tomasek JJ, Gabbiani G, Chaponnier C, (2001), Alpha-smooth muscle actin expression upregulates fibroblast contractile activity, *Molecular Biology of the Cell*, **12**:2730-2741

Hinz B, Phan SM, Tannickal VJ, Galli A, Bochaton-Piallat ML *et al* (2007) The Myofibroblast: One Function, Multiple Origins, *The American Journal of Pathology*, **170**: 1807-1816

Hogg JC, Chu F, Utokaparch S, Woods R, Elliott WM, Buzatu C, (2004), The Nature of Small-Airway obstruction in Chronic Obstructive Pulmonary Disease, *The New England Journal of Medicine*, 350(26):2645-2653

Hong KO, Kim JH, Hong JS, Yoon HJ, Lee J, *et al* (2009). Inhibition of Akt activity induces the mesenchymal- to- epithelial reverting transition with restoring E-cadherin expression in KB and KOSCC-2SB oral squamous cell carcinoma cells, *Journal of Experimental and Clinical cancer research*, **28**:28

Howart WJ and Wilson BA (2014), Tissue fixation and the effect of molecular fixatives on downstream staining procedures, *Elsevier Methods*, **70**:12-19

Ishikawa N, Ohlmeier S, Salmenkivi K, Myllärniemi M, Rahman I, Mazur W, Kinnula VL, (2010), Hemoglobin α and β are ubiquitous in the human lung, decline in Idiopathic pulmonary fibrosis but not COPD, *Respiratory Research*, **11**(1):123-135

Kalluri R (2009) EMT: When epithelial cells decide to become mesenchymal-like cells, *The journal of Clinical Investigation*, **119**(6):1417-1419

Kalluri R, Neilson EG, (2003), Epithelial-mesenchymal transition and its implications for fibrosis, *The Journal of Clinical Investigation*, **112**(12):1776-1784

Kalluri R and Weinberg RA, (2009), The basics of epithelial-mesenchymal transition, *The Journal of Clinical Investigation*, **119**(6): 1420-1428

Kamitani S, Yamauchi Y, Kawasaki S, et al. Simultaneous stimulation with TGF- β 1 and TNF- α induces epithelial mesenchymal transition in bronchial epithelial cells *Int. Arch. Allergy Immunol.* 2011; 155:119-128

Kang MJ, Lee CG, Lee JY, Dela Cruz CS, Chen ZJ, Enclow R, Eilas JA, (2008), Cigarette smoke selectively enhances viral PAMP- and virus-induced pulmonary innate immune and remodelling responses in mice, **118**:2771-2784

Kapanci Y, Burgon S, Pietra GG, Conne B, Gabbiani G, (1990), Modulation of isoform expression in Alveolar Myofibroblasts (contractile interstitial cells) during pulmonary hypertension, *American Journal of Pathology*, **136**(4):881-889

Karvonen HM, Lehtonen ST, Haiju T, Sormunen RT, Lappi-Blanco E *et al* (2013) Myofibroblast expression in airways and alveoli is affected by smoking and COPD, *Respiratory Research*, **14**:84

Kaur, M & Smyth, LJC, Cadden, P & Grundy, S & Ray, D & Plumb, J & Singh D, (2012), 'T-lymphocyte insensitivity to corticosteroids in COPD, *Respiratory Research*, **13**:1-9.

Khalil N, Parekh TV, O'Connor R, Antman N, Kepron W *et al* (2001) egulation of the effects of TGF- β 1 by activation of latent TGF- β 1 and differential expression of TGF- β receptors (T β R-I and T β R-II) in idiopathic pulmonary fibrosis, *THORAX*, **34**:907-915

Kim S, Coulombe PA, (2007) Intermediate filament scaffolds fulfil mechanical, organisational and signalling functions in the cytoplasm, *Genes & Development*, **21**:1581-1597

Kinnecom K and Pachter JS, (2005) Selective capture of endothelial and perivascular cells from brain microvessels using laser capture microdissection, *Brain Research Protocols*, **16**:1-9

Kisseleva T, Brenner DA, (2008), Mechanisms of Fibrosis, *Experimental Biology Medicine*, **233**:109-122

Knight D, (2001), Epithelium-Fibroblast interactions in response to airway inflammation, *Immunology and Cell Biology*, **79**:160-164

Krajewska M, Smith LH, Rong J, Huang X, Hyer ML, *et al* (2009), Image Analysis Algorithms for Immunohistochemical Assessment of Cell Death Events and Fibrosis in Tissue Sections, *Journal of Histochemistry and Cytochemistry*, **57**(7):649-663

Kranburg AR, Williams-Widyastuti A, Moori WJ, Sterk PJ, Alagappan VKT *et al* (2006) Enhanced Bronchial expression of extracellular matrix proteins in chronic obstructive pulmonary disease, *American Journal of Clinical Pathology* **126**:725-735

Krimpenfort PJ, Schaart G, Pieper FR, Ramaekers FC, Cuypers HT, (1988) Tissue-specific expression of vimentin-desmin hybrid gene in transgenic mice, *The EMBO Journal*, **7**(4):941-947

Larsson-Callerfeit A, Hallgren O, Anderson-Sjolan A, Thiman L, Bjorklund J *et al* (2013) Defective alterations in the collagen network to prostacyclin in COPD lung fibroblasts, *Respiratory research*, **14**:21

Laurent GJ, McAnulty RJ, Hill M, Chambers R, (2008), Escape from the Matrix: Multiple mechanisms for Fibroblast Activation in Pulmonary Fibrosis, *American Thoracic Society*, **5**:311-315

Leask A and Abraham DJ, (2004) TGF- β signalling and the fibrotic response, *The Journal of the Federation of American Societies for Experimental Biology*, **18**: 816-827

Levenson RM, (2004) Spectral imaging and Pathology: Seeing More, *Laboratory Medicine*, **4**(35):244-251

Löfdahl M, Kaarteenaho R, Lappi-Blanco E, Tornling G, Sköld MC, (2011) Tenascin-C and alpha smooth muscle actin positive cells are increased in the large airways in patients with COPD, *Respiratory Research*, **12**:48

Lomas NJ, Watts KL, Akram KM, Forsyth NR, Spiteri MA. (2012). Idiopathic pulmonary fibrosis: Immunological analysis provides fresh insights into lung tissue remodelling with implications for novel prognostic markers, *International Journal of Clinical and Experimental Pathology*, **5**(1):58-71

Liu X, (2008) Inflammatory cytokines augments TGF- β 1-induced epithelial-mesenchymal transition in A549 cells by up-regulating T β R-I *Cell Motil. Cytoskeleton* 2008; **65**:935-944

Luogo de Matos L, Trufelli DC, Luogo de Matos MG, Aparecida da Sliva Pinhal M, (2010), Immunohistochemistry as an Important Tool in Biomarkers Detection and Clinical Practice, *Biomarker Insights*, **5**:9-20

MacNee W, (2008), Update in Chronic Obstructive Pulmonary Disease 2007, *American Journal of Respiratory Critical Care Medicine*, **177**:820-829

Maillé E, Trinh NTN, Privé A, Bilodaeu C, Bissonnette É et al (2011) Regulation of normal and cystic fibrosis airway epithelial repair processes by TNF- α after injury, *American Journal of Lung Cell Molecular Physiology*, **301**:L945-L955

Magee P, Pearson S, Allen J. (2008) The omega-3 fatty acid, eicosapentaenoic acid (EPA), prevents the damaging effects of tumour necrosis factor (TNF)-alpha during murine skeletal muscle cell differentiation. *Lipids Health Dis.* 2008; **7**:24

Marmai C, Sutherland RE, Kim KK, Dolgonov GM, Fang X *et al.* (2011). Alveolar epithelial cell express mesenchymal proteins in patients with idiopathic pulmonary fibrosis, *American Journal of Physiology Lung Cellular and Molecular Physiology*, **301**(3):L71-L78

Midgley C, Heller T, Davey B, Smart L, Mackintosh B, (2008), *Introducing Health Sciences, Chronic Obstructive Pulmonary Disease: A Forgotten Killer*, Oxford University Press, Pages 70-71

Morgan JM, (2001), A Protocol for preparing cell suspensions with formalin fixation and paraffin embedding which minimises the formation of cell aggregates, *Journal of Cellular Pathology*, **5**:171-180

Muller KC, Welker L, Paasch K, Feindt B, Erpenbeck VJ *et al* (2006) Lung fibroblasts from patients with emphysema show markers of senescence *in vitro*, *Respiratory research*, **7**:32

Nadigel J, Audusseau S, Baglole CJ, Eidelman DH, (2013) Il-8 production in response to cigarette smoke is decreased in epithelial cells from COPD patients, *Pulmonary Pharmacology & Therapeutics* **26**:596-602

Nagathihalli NS, Massion PP, Gonzalez AL, Lu P, Datta PK, (2012), Smoking induces epithelial-to-mesenchymal transition in non-small cell lung cancer through HDAC-media of E-cadherin. *Mol Cancer Ther.* **11**(11):2362-72

Naydenov NG, Brown B, Harris G, Dohn MR, Morales *et al* (2012) A membrane fusion protein α SNAP is a novel regulator of epithelial Apical Junctions, *PLoS one* **7**(4) e34320

Nawshad A, LaGamba D, Olsen BR, Hay ED, (2004) Laser Capture Microdissection (LCM) for Analysis of Gene Expression in Specific Tissues During Embryonic Epithelial-Mesenchymal Transformation, *Developmental Dynamics*, **230**:529-534

Needham M, Stockley RA, (2004), α 1-Antitrypsin deficiency .3:Clinical manifestations and natural history, *THORAX*, 59:441-445

NHS, (2010) Chronic Obstructive Pulmonary Disease, [<http://www.nhs.uk/Conditions/>

Chronic-obstructive-pulmonary-disease/Pages/Introduction.aspx], Updated on 11.11.2010. [Accessed 7.12.2010]

Nightingale J, Patel S, Suzuki N, Buxton R, Takagi T *et al* (2004) Oncostatin M, a Cytokine Released by Activated Mononuclear Cells, Induces Epithelial Cell-Myofibroblast Transdifferentiation via Jak/Stat Pathway Activation, *Journal of The American Society of Nephrology*, **15**:2-32

Ning QM, Wang XR, (2007), Response of Alveolar Type II Epithelial Cells to Mechanical Stretch and Lipopolysaccharide, *Basic Science Investigations*, **74**:579-585

NordiQC, (2005), Nordic immunohistochemical quality control; epitope retrieval, [Accessed on June 2015] available from [http://www.nordiqc.org/Techniques/Epitope_retrieval.htm]

Nowark TJ, Handford AG, (2004), *Pathophysiology: Concepts and applications for healthcare professionals*, 3rd Edition, McGraw-Hill, pgs. 321-340

Ochoa CD, Baker H, Hasak S, Matyal R, Salam A, Hales CA, (2008) Cyclic stretch affects cell control of pulmonary smooth muscle cell growth, *Respiratory Cell and Molecular Biology* **39**:105-112

Ohbayashi M, Kubota S, Kawase A, Kohyama, Kobayashi Y and Yamamoto T (2014) Involvement of epithelial-mesenchymal transition in methotrexate-induced pulmonary fibrosis, *The Journal of Toxicological Sciences*, **39**(2):319-330

Overbeek SA, Braber S, Koelink PJ, Henriicks PAJ, Mortaz E *et al* (2013) Cigarette smoke-induced collagen destruction; key to chronic Neutrophilic airway inflammation?, *PLOS ONE*, **8**(1):e55612

Paavilainen L, Edvinsson Å, Asplund A, Hober S, Kampf C *et al* (2010) The Impact of Tissue Fixatives on Morphology and Antibody-based Protein Profiling in Tissues and Cells, *Journal of Histochemistry & Cytochemistry*, **58**(3):237-246

Palena C, Hamilton DH, Fernando RI, (2012) Influence of IL-8 on the epithelial-mesenchymal transition and tumour microenvironment, *Future Oncology*, **8**(6):713-722

Pardo A, Selman M, (2012) Role of Matrix Metaloproteases in Idiopathic Pulmonary Fibrosis, *Fibrogenesis and Tissue Repair*, **5**(1):59

Park JW, Ryter SW, Kyung SY, Lee SP, Jeong SH, (2013), The phosphodiesterase 4 inhibitor rolipram protects against cigarette smoke extract-induced apoptosis in human lung fibroblasts, *European Journal of Pharmacology*, **706**:76-83

Pass HI, Mitchell JB, Johnson DH, Turrisi AT, (1996) Lung Cancer: Principles and Practice, *Lippincott-Raven Publishers* Pgs. 232, 294-298, 706°

Perez RE, Navarro A, REzaiekhalth MH, Marby SM, Ekekezie II, (2011), TRIP-1 regulates TGF- β 1-induced epithelial-mesenchymal transition of human lung epithelial cell line A549, *American Journal of Physiology - Lung Cellular and Molecular Physiology*, **300**: L799-L807

Percoco G, Bénard M, Ramdani Y, Lati E, Lefeuvre L, (2012) Isolation of Human epidermal layers by laser capture microdissection: application to the analysis of gene expression by quantitative real-time PCR, *Experimental Dermatology*, **21**:531-534

Pilling D, Fan T, Huang D, Kaul B, Gomer RH, (2009) Identification of markers that distinguish Monocyte-Derived Fibrocytes from Monocytes, Macrophages and Fibroblasts, *PLoS ONE*, **4**(10):e7475

Pirozzi G, Tirino V, Camerlingo R, Franco R, La Rocca A, *et al* (2011). Epithelial to mesenchymal transition by TGF- β ₁ induction increases stemness characteristics in primary non small cell lung cancer line, *PLoS One*, **6**(6)e21548

Puente-Maestu L, Stringer WW (2006) Hyperinflation and its management in COPD, *International Journal of COPD*, **1**(4):381-400

Rangasamy T, Misra V, Zhen L, Tankersley CG, Tudor RM, Biswal, (2009), Cigarette smoke-induced emphysema in A/J mice is associated with pulmonary oxidative stress, apoptosis of lung cells, and global alterations in gene expression, *American Journal of Physiology, Lung Cellular and Molecular Physiology*, **296**:888-900

Rock JR, Barkauskas CE, Cronic MJ, Xue Y, Harris JR *et al* (2011). Multiple stromal populations contribute to pulmonary fibrosis without evidence for epithelial to mesenchymal transition, *Proceedings of the National Academy of Sciences*, **108**(52): E1475-1483

Rogel MR, Soni AN, Troken JR, Sitikov A, Trejo HE, Peidge KM, (2011), Vimentin is sufficient and required for wound repair and remodelling in alveolar epithelial cells, *FASEB J* **25**

Ruifrok AC, Johnston DA, (2001) Quantification of histological staining by color deconvolution, *Analytical & Quantitative Cytology & Histology*, **23**:291-299

Sarir H, Henricks PAJ, Van Houwelingen, Nijkamp FP, Folkerts G, (2008), Cells, Mediators and Toll-Like Receptors in COPD, *European Journal of Pharmacology*, **585**:346-353

Satio F, Tasaka S, Inoue K, Miyamoto K, Nakano Y, Ogawa Y, *et al*, (2008) Role of Interleukin-6 in bleomycin - induced lung inflammation in mice, *American Journal of Respiratory cell and molecular biology* **38** : 566-571

Sawada K, Mitra AK, Radjabi AR, Bhaskar V, Kistener EO *et al* (2008) Loss of E-cadherin promotes ovarian cancer metastasis via $\alpha 5$ -integrin, which is a Therapeutic target, *Cancer Res* **68**(7):2329-2339

Schneider M, Hansen JL, Sheikh SP. (2008) S100A4: a common mediator of epithelial-mesenchymal transition, fibrosis and regeneration in diseases? *J Mol Med (Berl)*; **86**(5):507-22.

Scullion NJ, (2008), Patient-focused outcomes in chronic obstructive pulmonary disease, *Nursing standard* **21**: (21) 50-56

Sezgin M, Sankur B, (2004), Survey over image thresholding techniques and quantitative performance evaluation, *Journal of Electronic Imaging*, **13**(1): 146-165

Simpson JE, Ince PG, Shaw PJ, Heath PR, Raman R *et al* (2011), MicroArray analysis of the astrocyte transcriptome in the aging brain: relationship to Alzheimer's pathology and APOE genotype, *Neurobiology of Aging*, **32**: 1795-1807

Smyth LJC, Starkey C, Vestbo J and Singh D. (2007) CD4 regulatory cells in COPD patients. *Chest*; **132**:156-63

Sohal S, Reid D, Soltani A, Ward C, Weston S *et al* (2010), Reticular basement membrane fragmentation and potential epithelial mesenchymal transition is

exaggerated in the airways of smokers with chronic obstructive pulmonary disease, *Respirology*, **15**(6):930-938

Sohal S, Reid D, Soltani A, Ward C, Weston S *et al* (2011) Evaluation of epithelial mesenchymal transition in patients with chronic obstructive pulmonary disease, *Respiratory Research*, **12**:130

Sohal S, Walters, (2013) Epithelial mesenchymal transition (EMT) in small airways of COPD patients, *THORAX*, **68**:783-784

Stearns SC and Koella JC, (2008), *Evolution in Health and Disease*, Second Edition, Oxford University Press Pgs. 52-55

Stolk J, Seersholm N, Kalsheker N, (2006), Alpha₁ - antitrypsin deficiency: current perspective on research, diagnosis, and management. *Int J Chron Obstruct Pulmon Dis*. 2006 June; **1**(2): 151–160

Strandberg K, Palmberg L, Larsson K, (2007) Effect of formoterol and salmeterol on IL-6 and IL-8 release in airway epithelial cells, *Respiratory medicine*, **101**: 1132-1139

Strieter RM, (2008) What Differentiates Normal Lung Repair and Fibrosis? *American Thoracic Society* **5**:305-310

Sutherland ER, Martin RJ, (2003) Airway Inflammation in Chronic Obstructive Pulmonary Disease: Comparisons with asthma, *Journal of Allergy and Clinical Immunology*, **112**:819-827

Tanjore H, Xu XC, Polosukhin VV, Degryse AL, Li B *et al* (2009) Contribution of epithelial derived fibroblasts to bleomycin-induced lung fibrosis, *American Journal of Respiratory and Critical Care Medicine*, **180**:657-665

Todd NW, Luzina IG, Atamas SP, (2012) Molecular and cellular mechanisms of pulmonary fibrosis, *Fibrogenesis and Tissue Repair*, **5**:11

Togo S, Holz O, Liu X, Sugiura H, Kamio K, Wang X *et al* (2008) Lung Fibroblast repair functions in Patients with Chronic Obstructive Pulmonary Disease are Altered by Multiple Mechanisms, *American Journal of Critical Care Medicine*, **178**:248-260

Tomcik M., Palumbo-Zerr K., Zerr P., Avouac J., Dees C., Sumova B., Distler A., Beyer C., Cerezo L.A., Becvar R., Distler O., Grigorian M., Schett G., Senolt L., Distler J.H.W. (2014) S100A4 amplifies TGF β -induced fibroblast activation in systemic sclerosis. *Annals of the Rheumatic Diseases* **7**:2013-2045.

Tortora GJ, Derrickson BH, (2009), *Principles of Anatomy and Physiology: Maintenance and Continuity of the Human Body*, 12 Edition Volume 2, John Wiley & sons (Asia) Pte Ltd

Tyurina YY, Shevedova AA, Kawai K, Tyurin VA, Komminreni C *et al* (2000) Phospholipid signalling in apoptosis peroxidation and externalisation of phosphatidylserine, *Toxicology*, **148**: 93-101

Van der Strate BWA, Postma DS, Brandsma CA, Melgert BN, Luinge MA, Geerlings M *et al* (2006), Cigarette Smoke-Induced Emphysema: A Role for the B Cell?, *American Journal Respiratory Critical Care Medicine*, **173**:751-758

Vehviläinen P, Hyytiäinen M, Keski-oja J, (2009) Matrix association of latent TGF-beta binding protein 2 (LTBP-2) is dependent on fibrillin-1, *Cellular Physiology*, **221**:586-593

Wang M, Hada M, Huff J, Pluth JM, Anderson J *et al.* (2012). Heavy ions can enhance TGF β mediated Epithelial to Mesenchymal Transition, *Journal of Radiation Research*, **53**: 51-57

Warford A, Akbar H and Riberio D, (2014), Antigen retrieval, blockig, detection and visualisation systems in immunohistochemistry: A review and practical evaluation of tyramide and rolling circle amplification systems, *Elsevier Methods*, **70**:28-33

Willis BC, duBois RM and Borok Z, (2006) Epithelial Origin of Myofibroblasts during Fibrosis in the Lung, *Proceedings of the American Thoracic Society*, **3**: 377-382

Willis BC and Borok Z, (2007) TGF- β -induced EMT: Mechanisms and implications for fibrotic lung disease, *American Journal of Physiology Lung Cellular Molecular Physiology*, **293**:L525-L534

Windoffer R, Beil M, Magin TM, Leube RE (2011), Cytoskeleton in Motion: the dynamics of Keratin Intermediate Filaments in epithelia, *The Journal of Cell Biology*, **194**(5) 669-678

Wynn TA, (2008), Cellular and molecular mechanisms of fibrosis, *Journal of Pathology*, **214**(2):199-210

Yamauchi Y, Kohyama T, Takizawa H. (2010) Tumor necrosis factor- α enhances both epithelial-mesenchymal transition and cell contraction induced in A549 human alveolar epithelial cells by transforming growth factor. *Exp. Lung Res.*; **36**:12-24

Yao X, Ireland SK, Pham T, Temple B, Chen R *et al* (2014) TEL1 promotes EMT in A549 lung cancer cells through suppression of E-cadherin, *Biochemical & Biophysical Research communications* **455**(3-4):277-284

Zhaodong L, Dranoff JA, Chan EP, Uemura M, SévignyJ, Wells RG, (2007), Transforming Growth Factor- β and Substrate stiffness Regulate portal Fibroblast Activation in Culture, *Heptology*, **46**(4):1246-1256

Zhong H, Belardinelli L, Maa T, Zeng D, (2005), Synergy between A2B adenosine receptors and hypoxia in activating human lung fibroblasts, *American Journal of Respiratory Cell Molecular Biology*, **32**(1):2-8

Zong-Xian J, Qi-Lin A, Mi X, (2006), Cigarette smoke extract inhibits the proliferation of alveolar epithelial cells and induces apoptosis, *Acta Physiologica Sinica*, **58**(3): 244-254

Appendix A

**Study Ethical
Approval
Salford University
Research Ethics
Committee
+
Material Transfer
Agreement**

Academic Audit and Governance Committee

**Research Ethics Panel
(REP)**



To Dr Lucy Smyth
cc: Ms Denise Rennie
From Tim Clements, Contracts Administrator
Date 7th June 2010


MEMORANDUM

Subject: Approval of your Project by REP
Project Title: Investigation of lymphocyte and fibroblast roles in lung pathogenesis in COPD.
RGEC Reference: REP10/077

Following your responses to the Panel's queries, based on the information you provided, I can confirm that they have no objections on ethical grounds to your project.

If there are any changes to the project and/or its methodology, please inform the Panel as soon as possible.

Regards,


pp
Tim Clements
Contracts Administrator
TC/JH

For enquiries please contact
Tim Clements
Contracts Administrator
Contracts Office
Enterprise Division
Faraday House
Telephone 0161 295 6907 Facsimile 0161 295 5494
E-mail: t.w.clements@salford.ac.uk

Shipment of Samples from the University Hospital of South Manchester to Salford University for Research Purposes

Please sign form and fax back to us on 0161 291 5806 to confirm that you have received the samples listed below and that you are happy to take responsibility for these samples with regards to the Human Tissue Act 2004. If you have any queries regarding the samples please contact us by email on tsouthworth@meu.org.uk or call 0161 291 5920.

Date of Shipment: ____/____/2015____

Destination of Shipment: **School of Environment and Life Science, University of Salford, Lab 206/207 Cockcroft Building, Salford M5 4WT. Tel 0161 295 5723**

Sample Collection Protocol: _UN3373_

Description of Transferred Sample:	Check	Patient Number/s:
<5g Clinical lung sample/s for laboratory research purposes only		
<50ml Clinical blood sample/s for laboratory research purposes only.		

Transferred samples will be used for the following agreed research purposes under the direction of Dr Lucy Smyth, ELS, University of Salford. Data generated from this research will be shared between UHSM APG and ELS FIR group, Salford.

- Fibroblast research (role in COPD): Primary fibroblasts will be grown from tissue resections and fibrotic reversal strategies will be investigated.
- Small lung resections will be formalin fixed and wax embedded for immunohistochemical investigation of inflammatory and fibrotic markers expressed in subject groups.
- Small lung resections will be snap frozen for PCR investigation of inflammatory gene expression and to identify common respiratory infections.

Sample Disposal Date: As itemised in HTA file at recipients address

Shipper Name: **Airway Pharmacology Group:**_____

Shippers Signature: _____

Date: ____/____/2015

Recipients Name: **University of Salford Fibrosis Inflammation + Repair Group: Dr Lucy Smyth**

Recipients Signature: _____

Appendix B

Standard Operating Procedures (SOPs)

written for this research

Leica TP1020

Automatic tissue processor for the histology laboratory



The Leica TP1020 is a modular automated tissue processor designed for the following applications:

- Fixation
- Dehydration
- Paraffin wax infiltration of histological tissue specimens



Warnings for operating the instrument

- The carousel may not be rotated manually.
- Caution when lowering the carousel and keep fingers out of the space between the container lid and the upper rim of the container.
- Caution in the case of power failure, the carousel automatically descends into a station.
- Instruments equipped with vacuum function may only be operated with the aluminium containers supplied.
- While operating the instrument, no liquid may enter in contact with any of the electrical connections or the interior of the instrument.
- Make sure you observe the level indicators on the reagent and paraffin stations.
- Caution when handling solvents as it may be an explosion hazard.
- Always wear adequate protective clothing.
- The heated wax baths may only be used with paraffin.

Some General Key functions

Programming button 'PROG':

To call and quit the programming mode, in which programmes are set up, edited and altered, and to display a programme which is currently activated.

Lock button 'KEY SYMBOL':

To lock all control panel functions as protection against accidental changes of programmed parameters.

- To activate and quit the lock function, press 'KEY' for 5 seconds.

Time button 'CLOCK SYMBOL':

To set the time and to indicate the total duration, start time and expected end time of automatic tissue processing programmes.

'THREE ARROWS SYMBOL':

Used to start/stop carousel during an up/down movement.

'START' button:

To immediately start processing

'PAUSE/CONT' button:

To pause and resume

'STOP' button:

To immediately stop the up/down movement. To abort a processing cycle press twice.

'ARROW UP/DOWN SYMBOL' buttons:

For vertical carousel movement

'V' button:

To connect or disconnect vacuum function in the manual processing mode.

'ARROW LEFT/RIGHT SYMBOL' buttons:

The cursor jumps to the next data entry position in the direction of the arrow.

'PLUS/MINUS' buttons:

To increase or decrease numerical values.

To set a preprogrammed setting going

1. Lift the carousel cover (up arrow) and fill all stations with the corresponding reagents as shown below:

Beaker number	Solution	Duration (mins)	Temperature (°C)
1	50% Alcohol	60 mins	Room temperature
2	90% Alcohol	60 mins	Room temperature
3	100% Alcohol	60 mins	Room temperature
4	100% Alcohol	60 mins	Room temperature
5	Histoclear	60 mins	Room temperature
6	Histoclear	60 mins	Room temperature
7	Empty	0 mins	Room temperature
8	Empty	0 mins	Room temperature
9	Empty	0 mins	Room temperature
10	Empty	0 mins	Room temperature
11	Wax	90 mins	60 °C
12	Wax	90 mins	60 °C

Note that 1L is an adequate amount of reagent to fill the stations to the required level. The different concentrations of alcohol (manufactured and supplied by fisher) the following formulas may be applied:

1L of 50% alcohol

500ml water
500ml alcohol

1L of 90% alcohol –

100ml water
900ml alcohol

Histoclear used in the TP1020 was manufactured and supplied by national diagnostics.

2. Label cassettes suitably to identify your clinical tissue – in pencil.
3. Assemble the cassette with the tissue and a metal lid. (lids can be reused).
4. Load the cassettes + tissue into the basket of the automated processor.
5. Slot the basket into the carousel of the automated processor
6. **Ensure the basket is in position 1** (use the circle arrow to position the basket)
7. Lower the basket into starting container 1 (50% alcohol) using the down arrow.
8. Press 'START' button and select programme 1 using the plus or minus buttons. If an error message appears – check the wax is fully melted in the heated pots. If happy with this:
9. Press 'START' + the key icon a second time to override the error message and the programme will begin.
10. Once an automatic processing cycle has been completed, 'DONE' and the position (station number) of the basket will be displayed. Press any key to confirm the message and turn off the sound signal.
 - a. Samples can sit in the molten wax overnight – but not recommended for longer.
11. Raise the lid with the up arrow to lift the specimens from the wax.
12. Unhook the basket and replace it back into the wax **quickly** before the wax starts to set.
13. Remove the cassettes with forceps one by one – proceed with the wax mounting procedure.
14. **ESSENTIAL AND SIMPLE MAINTANANCE STEPS FOR EACH USE**
 - a. **Once all the cassettes are removed, take out the basket and place it in the hot oven (near the technicians prep room) to melt off excess wax before re-using (place blue roll underneath so not to damage the oven with excess wax). It is the user's responsibility to do this – NOT the next person that needs to use it.**
 - b. **Check the filling level and quality of the liquid in each station (reagent and paraffin stations) and refill if necessary.**
 - c. **Lower the lid with the down arrow to prevent evaporation.**

To Programme the TP1020 for paraffin wax infiltration of histological tissue specimens

Programmes are **created** step by step in the programming mode. Programming parameters have to be entered for each station individually. The TP1020 has a memory capacity of 9 programmes.

1. To select a programme mode press the 'PROG' key. For paraffin wax specimens select programme 1.
2. Follow the directions on the laminated card to set up a new programme.
3. Check through the list of programmes so you do not overwrite another setting.
4. Press the key symbol button to lock the panel which will protect programme settings against accidental alterations/misuse.

Error Warning Codes

Note: To override the warning codes and start processing, press the key symbol button and start simultaneously.

Code	Possible root cause	Troubleshooting
W:01, W:02, W:03 in manual processing mode	Paraffin in stationd 10/11/12 still solid	-To quit the warning code press any key -Check if the paraffin is really molten -If you find that the paraffin is molten, pause the automatic processing cycle, or in the manual processing mode press key and the corresponding arrow button to lower or lift the basket.
W:04, W:05, W:06 when starting an automatic process cycle	Total duration of programme from start until the basket reaches the first paraffin station is less than 8 hours. Paraffin stations 10/11/12 possibly still solid upon arrival of tissue basket	-Check there is sufficient time for paraffin to liquefy -If this is not ensured, fill the station with liquid paraffin

Code	Possible root cause	Troubleshooting
E:01	Cache memory defective	-Call technical services
E:03, E:04, E:05	Drive malfunction	-Switch off main switch and next switch it on, try again -Call technical services
	Clock component defective	-Connect paraffin station
E:07 E:08 paraffin station 1 E:09 Paraffin station 2 E:10 Paraffin station 3	Paraffin station not connected, paraffin station connected to the wrong socket, excess temperature switch-off mechanism has responded	-Paraffin station is connected to wrong socket - Disconnect and allow to cool down, reconnect paraffin station, if yellow pilot lamp lights, use of

		paraffin bath may be continued. -Exchange paraffin station -Call technical services
E:11	Loss of processing data (current process)	-Press any key to confirm error message 'abort' will be displayed -Restart processing cycle -Call technical services
E:12	Loss of programme settings	-As above (E:11)
E:13	Erroneous data entry for delayed start function (eg: desired start time would be earlier than current time)	-Correct erroneous data entry

Preparing formalin fixed paraffin embedded cell suspension

Preparation of mould

- Remove the bottom of a 1mL syringe (internal diameter 4mm) using a scalpel or Stanley knife. Make sure the cut edge is a flat surface without any burr to prevent snags in the cell agar mixture.
- Each syringe can hold up to a final volume of 0.6mL utilising up to 30-50x10⁶ cells. This can be cut into 5-6mm cylinders to make multiple blocks.

Preparation of cell suspensions

- Grow cells to normal protocol and harvest via trypsinisation method
- Wash cells in PBS and centrifuge at 400g for 10 minutes to create a pellet
- Resuspend pelleted cells in 4-10% formalin at room temperature. 2x10⁶ cells/mL of formalin is optimum
- Leave standing for 2 hours (without mixing) to allow cell sedimentation
- Once the cells have collected in a 1-1.5mL volume, remove the bulk of formalin with a pastette and discard
- Transfer the remaining 1.5mL formalin cell suspension into a microcentrifuge tube for further sedimentation. This will take around 20-30 minutes
- Remove formalin. This should leave you with a pellet of ~10-50µl volume.

NB cells that refuse to sediment in the allotted time, centrifuge for a maximum of 2 minutes at 300g

Agar/Agarose gel

This can be made whilst the cells are undergoing sedimentation

- Make 4% agar (or agarose) made in deionised water
 - 1% agarose gel is 1g of agarose to 100mL dH₂O
- Add agarose to dH₂O and swirl
- Place the gel solution into the microwave oven and boil and swirl the solution until all of the small translucent Agarose particles are dissolved. Stopping the microwave oven and swirling the flask every 30 seconds helps dissolve the Agarose faster.
 - **Caution:** Always wear protective gloves, goggles, and a lab coat while preparing and casting Agarose gels. The vessels containing hot Agarose can cause severe burns if allowed to contact skin. Additionally, molten Agarose can boil over when swirled
- Place agarose gel in water bath at 60°C

Adding cells to agarose/agar

- Place tube containing cells into the 60°C water bath for 2-3 minutes
- Warm a plastic pipette (with tip diameter of 2mL) on a hotplate set at 45°C
- Transfer a small quantity of agar/agarose to the microcentrifuge tube containing the cells
 - i.e. 40µL of agar to a volume of cells estimated to be 40µL. As a rule the combined volume of cells and agar should result in a final agar concentration of 2%
- Hold the tube containing the cells just below the surface of water bath and gently mix the cell suspension taking it up and extruding it 2 times, using the pre-warmed pipette.
- Then quickly transfer the mixture to the mould
 - Extrude very carefully
 - Avoid air bubbles
 - "if the agar will cells sets prior to transfer to the mould then the tube or pipette containing the mix can be reheated in a steam bath and the transfer can be repeated." This should have no effect on the cell ultra structure
- Allow the mix to set at room temperature for 5 minutes
- Place at 4°C for 2-3 minutes

Extruding Mixture from the Mould

- Push syringe plunger slowly to extrude the cell-agar mixture from the syringe
- Cut to required plug size using a scalpel. The smooth edge formed when you cut the end of the syringe acts as a good cutting guide
- Place the cell-agar plugs into 10% formalin for 2 hours at room temperature with occasional shaking

Processing into a paraffin block

- Remove the agar plugs with a spatula
- Dehydrate in ethanol using a graded series from 10 -100% in steps of 10% in which it is given two 30 minute washes at each step
 - The plugs can be left in one of the higher ethanol concentrations e.g. 70% overnight
- Place the plugs in xylene for 2 hours with several changes
- Place the plugs into molten paraffin for 2 hours with several changes
- Mount plugs into paraffin blocks and store until needed for positive IHC control

Alternatively

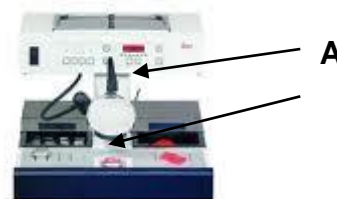
- Place the agar plugs into individual cassettes and put through the automatic tissue processor on programme 2
 - NB this has less ethanol stages!
- Mount plugs into paraffin blocks and store until needed for positive IHC control

If you find you are having any trouble refer to the below journal as it has a trouble shoot guide.

Reference

Morgan JM, (2001), A Protocol for preparing cell suspensions with formalin fixation and paraffin embedding which minimises the formation of cell aggregates, *Journal of Cellular Pathology*, 5.171-180

Leica EG1150
Paraffin embedding station



Warnings for operating the instrument

- Paraffin is flammable and should therefore be handled with due care. Do not use sharp tools to remove solidified paraffin from the work areas, as they may destroy the coating on the surface. Use the plastic spatula supplied with the instrument.
- During operation the paraffin reservoir, mold warmer, cassette warmer, work area as well as the forceps holder are hot.
- Do not store flammable substances near the instrument.

How To Operate the EG1150

- Activate the stand by switch. The green LED in the on/off button indicates that the instrument is ready to operate.
- Fill the paraffin reservoir with paraffin wax flakes + allow to thoroughly melt overnight.
- Press against the dispenser handle (A) with the mold to manually operate paraffin flow.
- To orientate the samples, the mold should be filled approximately one third with paraffin.
- Place on the refrigeration spot (B) so that the paraffin becomes semi-liquid, and orientate the sample as required.
- Fill up the remaining area of the mold with paraffin.
- Place mold onto the Leica EG1150 C cold plate for approximately 30 minutes until completely set.



Warnings for operating the instrument

- Be very careful when handling microtome knives or blades.
- Always remove the knife/blade before detaching the knife holder from the instrument. Knives not in use should always be stored in a knife case.
- Never place a knife anywhere with the cutting edge facing upwards
- Always clamp the specimen block before clamping the knife
- Lock the handwheel and cover the knife edge with the knife guard prior to any manipulation of knife or specimen, prior to changing specimen block and prior to all work breaks.
- Always wear safety goggles.
- No liquid must enter the interior of the instrument

How To Operate the RM2125

Clamping the specimen:

- Rotate handwheel clamp until specimen clamp is in uppermost position
- lock the handle of the handwheel in the 12 o'clock position
- Insert a specimen block into the specimen clamp

Inserting the knife/disposable blade:

- Carefully insert knife or disposable blade into the knife holder and clamp

Trimming the specimen:

15. Select a thickness section appropriate for trimming.
16. Turn the handwheel to trim the specimen down to the desired level.

Sectioning the specimen:

1. For sectioning use a different part of the blade edge than for trimming.
2. Start sectioning by rotating the handwheel evenly in a clockwise direction.
3. Pick up the sections and mount them on microscope slides.

Changing the specimen:

1. Bring specimen to uppermost position (via handwheel) and lock the handwheel in 12 o'clock position.
2. Cover the blade edge with the knife guard.
3. Remove the specimen from the specimen clamp and insert a new specimen block.

4. Use the coarse feed wheel to move the specimen backwards far enough to be able to start trimming the new specimen block.

Auto slide stainer

Leica CP023

Coloured tags denote the protocol as follows:

Yellow	Giemsa (Blood stain for WBC nuclei)
Red	Haematoxylin + Eosin (cytoplasm – red, nuclei – blue)
White	Collagen (indicator of fibrosis).

H+E stain

- Turn the tap on at the back (handle rotates in line with the copper piping)
- Switch on machine at the front
- Machine goes through a setup procedure – moving arm tests + parks
- On the screen, select the red H+E icon, open the protocol
- Carefully go through the protocol and remove all the relevant lids from the solution pots. **Double/triple check the stations listed correspond to the lids removed.** This is separate to the protocol *steps*. Do not confuse the two!
- Ensure there is an **empty basket** in the loading draw and also one in the **exit** station (25). **Failure to do this will result in the rack of slides being dropped + broken** at the end of the staining procedure.

NB failure to remove ALL the correct lids prior to initiating staining will BREAK the machine and cost 100's or 1000's pounds to repair.

- Top up solutions as required – located in cupboard beneath the machine. Ethanol in fume cupboard with Alyson Forshaw. Use solutions neat unless directed otherwise. Dilute ETOH with distilled water in the tubs by the sinks.
- Select the Red tag and assemble on the rack – check orientation is correct: tag arm should point forward along the rack 'nose'
- Load slides into the rack – ideally label- up so it is not submerged in the stain. But take care to assess the actual tissue sample will be fully submerged in each solution.

NB: label all slides in pencil – any ink pen will leach into the solutions + spoil them.

- Check again solution lids are correctly removed!
- Load rack + tag + slides into loading draw – tag pointing towards you.
- Close the draw
- Protocol will start.
- At the end – allow sufficient time for slides to dry
- Clean slides with a tissue – mount with DPX onto coverslip then lower sample slide over it (best way to avoid air bubbles).
- **TURN OFF TAP – (has leak issues) and the autostainer.**

Collagen Stain

Set up water bath - do first prior to setting up autostainer:

- Set water bath at 56°C – ensure it is about ½ full then place in the fume hood.
 - Pour Bouin's solution into a glass coplin jar and place in the water bath.
 - Solutions are stored in the cupboard beneath the autostainer.
 - Place thermometer into water bath + allow to reach temperature.
- Meantime:

Set up the autostainer

- Turn the tap on at the back (handle rotates in line with the copper piping)
- Switch on machine at the front
- Machine goes through a setup procedure – moving arm tests + parks
- Select menu / programmes
- On the screen, select the white Masson's Trichrome **stain A** icon,
- Press details to open the protocol
- Carefully go through the protocol and remove all the relevant lids from the solution pots. **Double/triple check the stations listed correspond to the lids removed.** This is separate to the protocol *steps*. Do not confuse the two!
- Ensure there is an **empty basket** in the loading draw.
- Place a basket containing distilled water in the **exit** station (25).
 - **Failure to do this will result in the rack of slides being dropped + broken** at the end of the staining procedure.

NB failure to remove ALL the correct lids prior to initiating staining will BREAK the machine and cost 100's or 1000's pounds to repair.

- Top up solutions as required – located in cupboard beneath the machine. Ethanol in fume cupboard with Alyson Forshaw. Use solutions neat unless directed otherwise. Dilute ETOH with distilled water in the tubs by the sinks.
- Take the mini-rack + place on the white tag (Tag arm aligned to rack 'nose').
- Load slides into the rack – ideally label- up so it is not submerged in the stain. But take care to assess the actual tissue sample will be fully submerged in each solution.

NB: label all slides in pencil – any ink pen will leach into the solutions + spoil them.

- Check again solution lids are correctly removed!
- Load rack + tag + slides into loading draw – tag pointing towards you.
- Close the draw. Programme should automatically start, however:
- Screen MAY request supervisor code = slide
- Select the white label, assign it to location 35 or 36 (depending where your start basket is)
- Press confirm
- On the list of programmes scroll down to Masson's A, press start.
- Once slides are in the exit draw, remove them + place into the warmed Bouin's solution in the water bath for **1hour**.
- Take slides from the Bouin's and reload in the rack with white tag.
- On the autostainer, check through Masson's Trichrome stain protocol C + remove the relevant lids.
- When fully checked, load the rack in the draw to initiate protocol part (C).
- Clean slides with a tissue – mount with DPX onto coverslip then lower sample slide over it (best way to avoid air bubbles).
- **TURN OFF TAP – (has leak issues) and the autostainer.**

Operation of the Lazer capture microscope (Leica),
Wythenshawe Hospital NWLC

Background

This microscope is designed both for normal light microscope techniques and is equipped with florescence channels. Uniquely it can be used to isolate selected areas of cells or tissue using a lazer to section out the area of interest. The selected section drops into an eppendorf and can be used for downstream analysis such as gene or protein identification by PCR or western blots (respectively).

Switch On + setup procedure


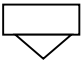



Switch on the following devices:

- PC main switch / Leica software icon to initiate software
- Leica box (bottom of stack) using the key, AND a switch to the rear of the box. (Lazer needs some warmup time)

The top box is for florescence and is not needed unless a florescent antibody stain has been used.

- Special lazer capture slides must be used for this technique that allows the lazer to section through the tissue and the slide at the same time.
- **Important:** Prior to sectioning the tissue, the slides must be prepared by 30mins under a UV lamp – in a tissue culture flow cabinet UV is fine. This is done to prevent static issues when micro-dissecting the tissue later.
- Cryostat sections in OCT made directly onto the UV treated slide. This must be kept cold during IHC procedures and transport to preserve the RNA integrity.
- A revised IHC protocol is recommended that has incubations reduced to a minimum, aiming to complete staining within 60mins; again to preserve RNA.

Lazer Calibration procedure

- **Check the protective guard is in place in front of the lazer!**
- When the software is open select 'options' / 'microscope control' to enable operation of the microscope from the PC.
- Setup the collection tubes: Unload the tube collection port with an icon similar 
- The tube holder is ejected and 0.5ml eppendorfs can be loaded into the holes, the lid must be clipped backwards securely as this is used to catch the sample.
- Return the tube holder back into the microscope the smooth bit first.
- Using an icon in lower left of the screen, select which positions the tubes are in: eg select position B if tube has been inserted in the 2nd position.
- Setup the stage: Unload the slide stage with an icon like this: 
- Position the slide on the stage and slot back onto the scope – ensuring the slide handle is nearest to you (there is a notch on the right hand side which serves as a clip).
- Once both slide and tubes are in place, test the microscope can locate which tube is which: Select 'collector' / move to reference point. This should move a tube into position and it's cap be in focus at x200 magnification.
- To calibrate the lazer: Move the slide to an area of slide without tissue.
- Select 'lazer calibrate' / ok, 'options', and use settings similar to the following: power = 30, speed = 10-15 (quite slow).
- It then sections out a shape like this: 
- Click in the centre of it and it creates another one opposite. 
- Do this twice more to create a square of cutout shapes. 
- NB: ensure 'no cap' is selected so the bits of slide are not collected! To do this switch between 'collector' and 'specimen'.
- Once this is done the microscope is calibrated to that slide, so when you use the software to indicate which section to dissect out, it's co-ordinates are accurate.

Sectioning of tissue of interest.

- Having calibrated the lazer, practise with a test cut either on an unwanted section of tissue or separate area of slide.
- Use the icons to select, circle, square, freehand tool to identify an area of interest.
- On the screen allow about 1cm distance away from the object – this allows for the width of the lazer ‘burn’ and avoids the area of interest from being damaged.
- Do all the above with ‘no cap’.
- Once setup with the lazering technique focus on the structure of interest and highlight this using the above mentioned icons.
- Ensure collector (A/B/C etc) is selected to catch the tissue!
- Initiate sectioning ‘start’
- The lazer moves around the highlighted area. If successful the tissue will fall into the lid which can be checked by viewing the collector under the microscope.
- Often small areas are not completely burned through, which can be corrected with the ‘move and cut’ option that allows you to manually direct the lazer with the PC mouse.
- Good practise also, is to measure the area being sectioned using the ruler function which puts an area scale to the section.
- Images should be taken throughout the process ‘capture’ to document the tissue being collected.
- Work as quickly as possible and place lazer captured material on ice or -20/-80 until ready for the PCR steps.

Shutdown procedure.

- Unload all sample tubes and sample slides
- Turn off PC by normal shutdown procedures
- Turn of microscope box and lazer box
- **Leave area tidy!**

Using ImageJ for image analysis

ImageJ is a FREE programme that can easily be downloaded from the website below.

<http://rsbweb.nih.gov/ij/download.html>

Once downloaded make sure you install it on your computer or it will not work.

Note: you cannot download and install any programme on university computers

There are hundreds of various extra tools called Plugins that you can download (mainly from the ImageJ website) and add to the basic ImageJ programme. These are only required for specific types of image analysis and you are most likely not to need these.

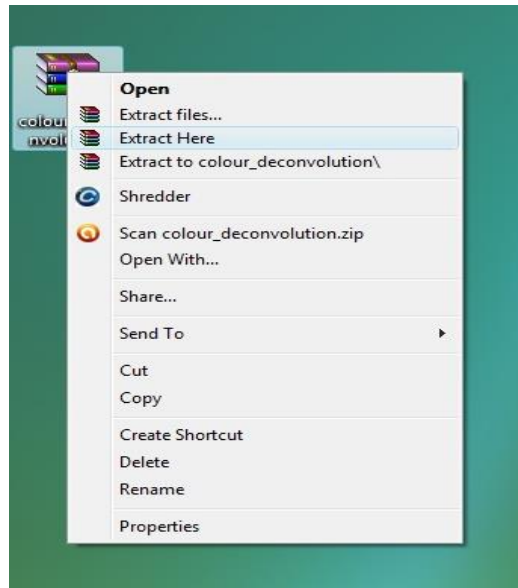
Plugin download and installation

One Plugin you may need is colour deconvolution therefore this is used for showing a step by step installation for this.

Download the Plugin from:

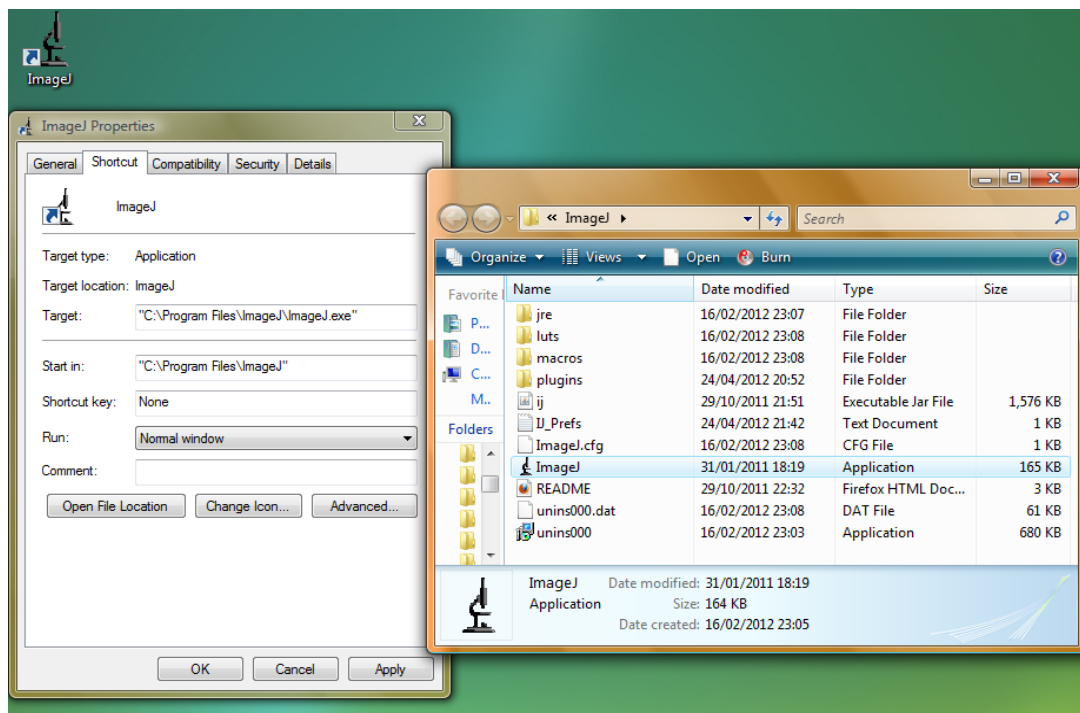
<http://www.dentistry.bham.ac.uk/landinig/software/cdeconv/cdeconv.html>

To install this Plugin you will need to extract the file from the WinRaR.zip file. This is achieved by right clicking on the zipped file



Place the java and class files into one file.

Right click on ImageJ, select properties and then open file location

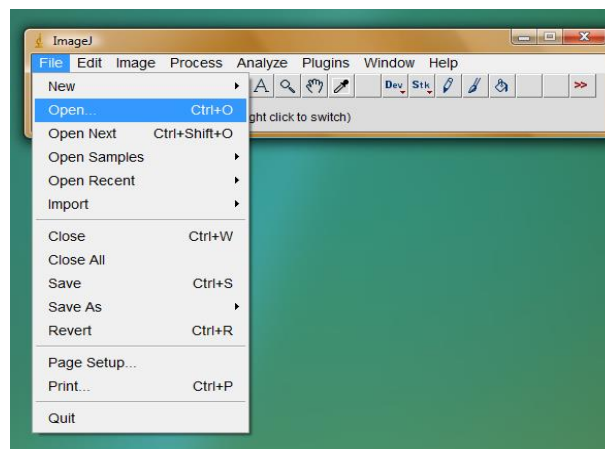


Open the Plugin file then cut and paste the colour deconvolution file into this.

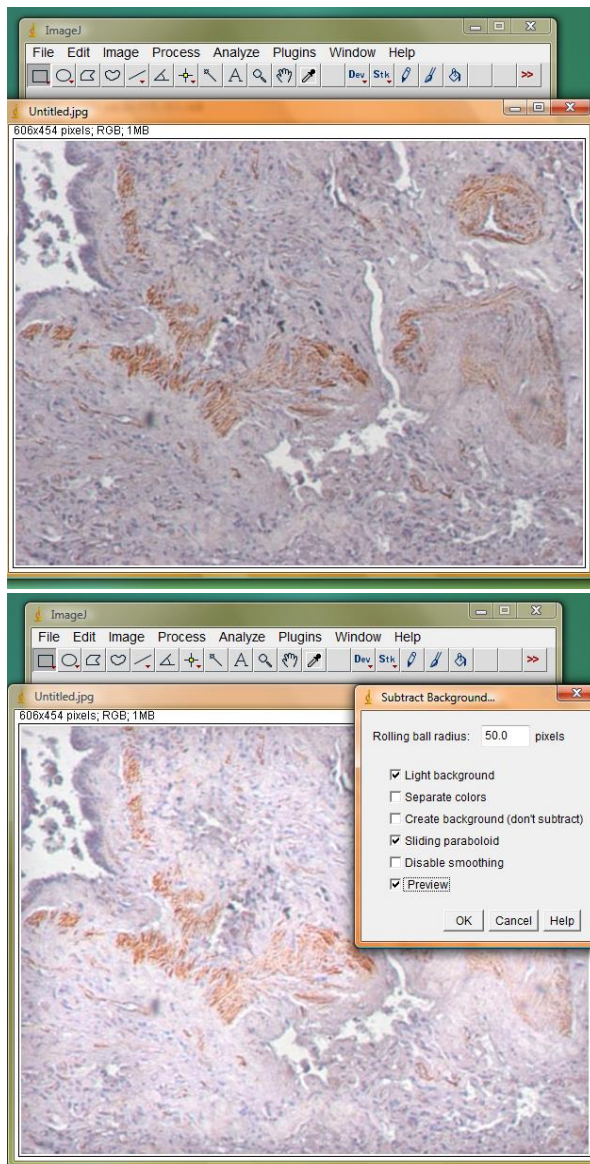
Image analysis

Subtract background is good to use on all images, to correct and shadowing or colour effects in your images.

Open the ImageJ programme



Then select Process - Subtract background.

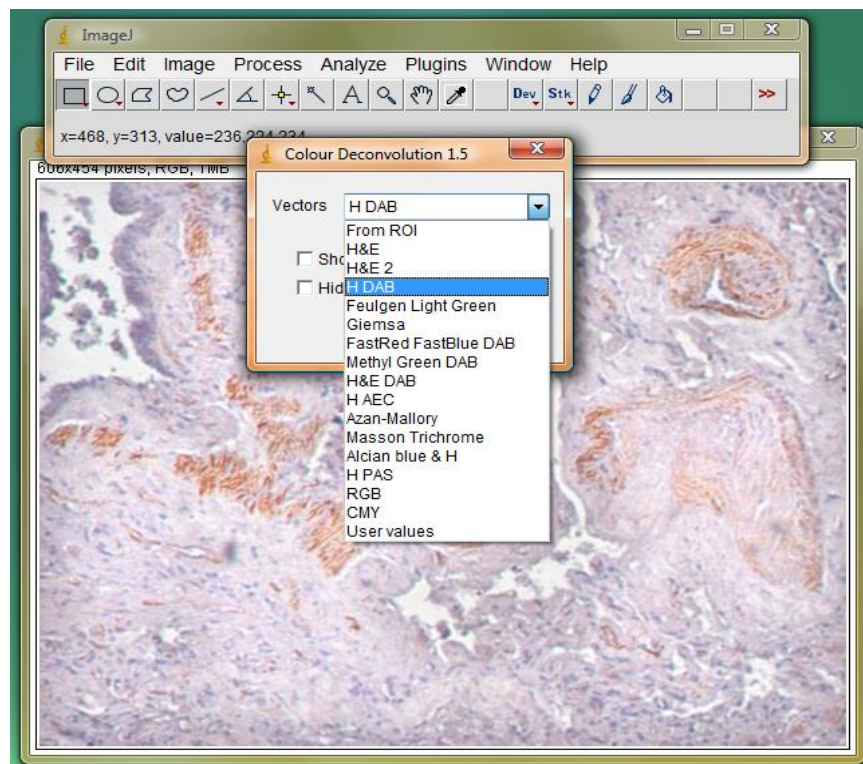


The next step is put the image through Colour Deconvolution.

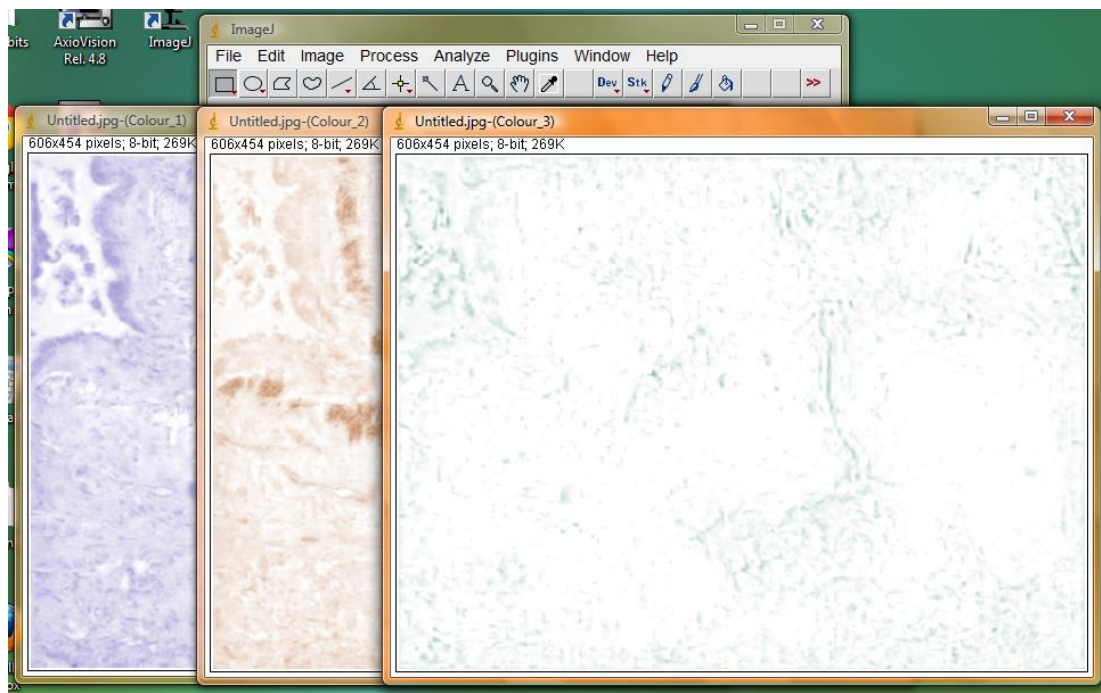
Colour Deconvolution

This plugin allows you to segment standard histological stain combinations such as Haematoxylin & Eosin (H & E), and DAB with counter stains such as Haematoxylin or Methyl Green.

Go to Plugins-colour deconvolution and select the stain of interest e.g. H DAB. Then click ok.



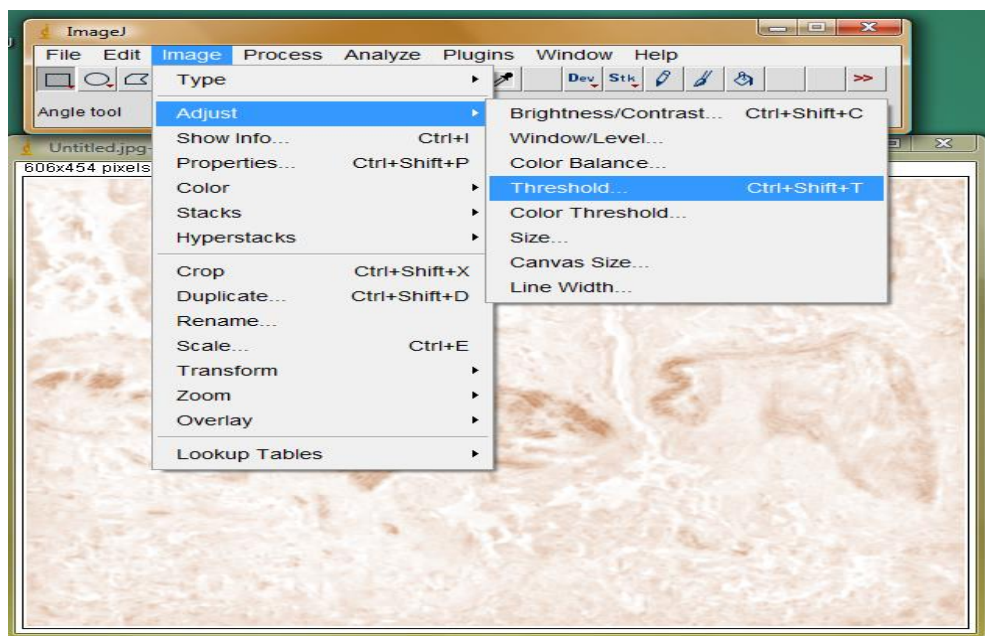
The image will then be split into 3 components. If you have a 2 colour stain, one image should be white as below.



Following deconvolution, thresholding can be used to select the area of interest for measuring the area stained or alternatively the image can be converted straight to a binary image.

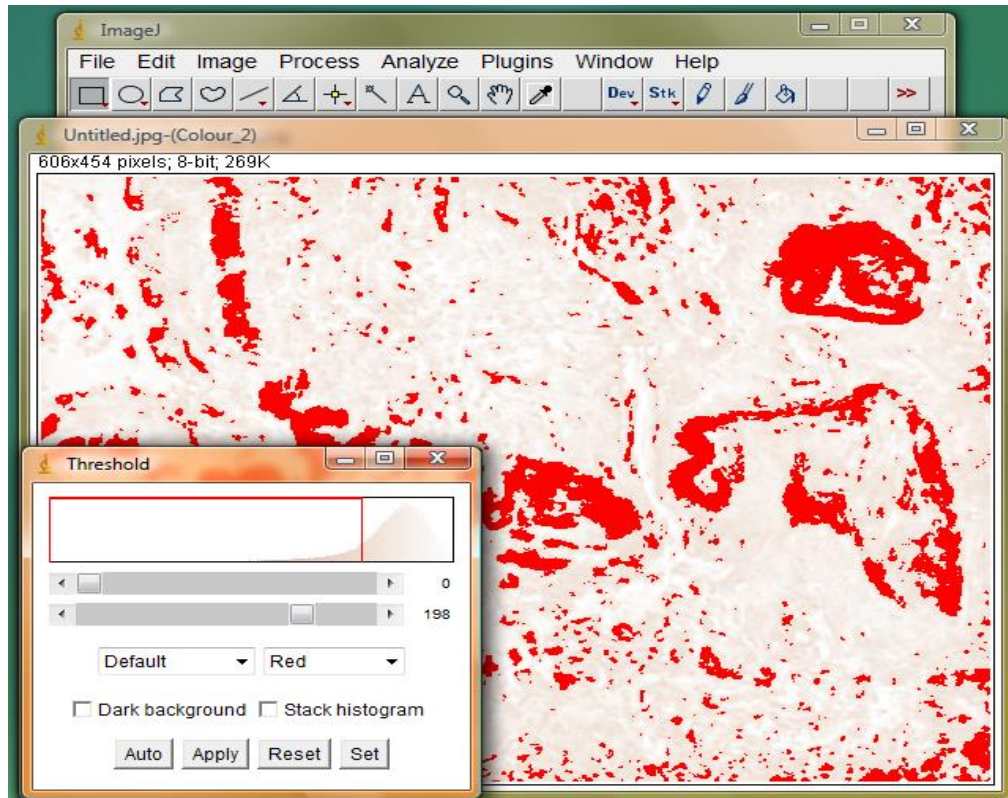
Thresholding

Select the image in which you wish to measure the area of staining. Then go to Image-Adjust-Threshold.



You can either select the auto setting or alternatively move the sliders until you have selected all of the stained areas.

Note: If you have a florescent or confocal image you should also check the dark background.

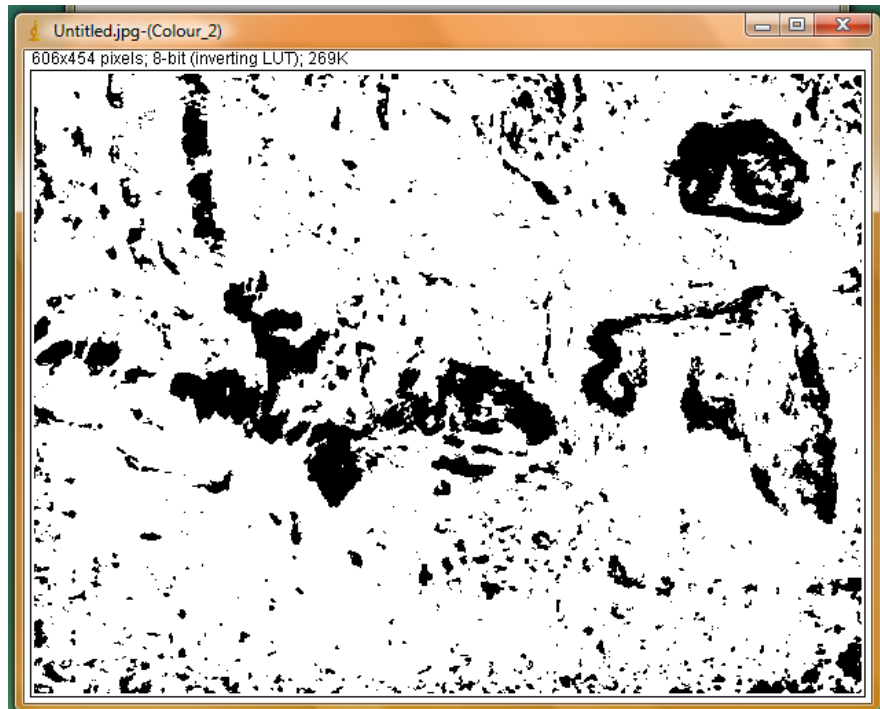


If the auto setting works well, you can proceed to Process-Binary-Make Binary and click apply.

This is used if you are not interested in intensity values.

Note: Antigen-antibody reactions are not always [stoichiometric](#). It has been suggested that stoichiometry depends on the size of the antigen involved (Oda and Azuma 2000); so the darkness of the stain is in a direct linear relationship with the amount of reaction products. In particular [DAB](#) does not follow Beer-Lambert law. For more information see

Van der Loos CM, 2008, Multiple Immunoenzyme Staining: Methods and Visualizations for the Observation with Spectral Imaging, *Journal of Histochemistry & Cytochemistry*, 56(4):313-328

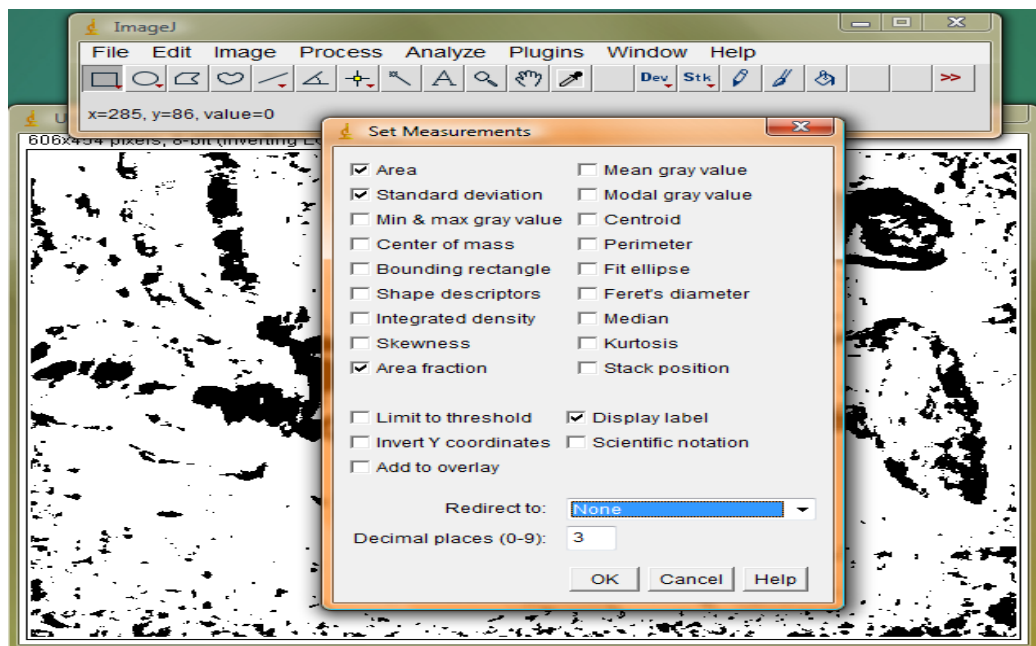


The stained areas that you want to measure will be black; ImageJ regards the black areas as the object of interest. Do not change the defaults unless you want measure the unstained areas.

The image is now ready for analysis.

Analysis

Go to Analysis - Set measurements. Choose the parameters you want to measure and make sure you select Display label.



If you are interested in the percentage of area stained make sure you select Area Fraction in addition to Area.

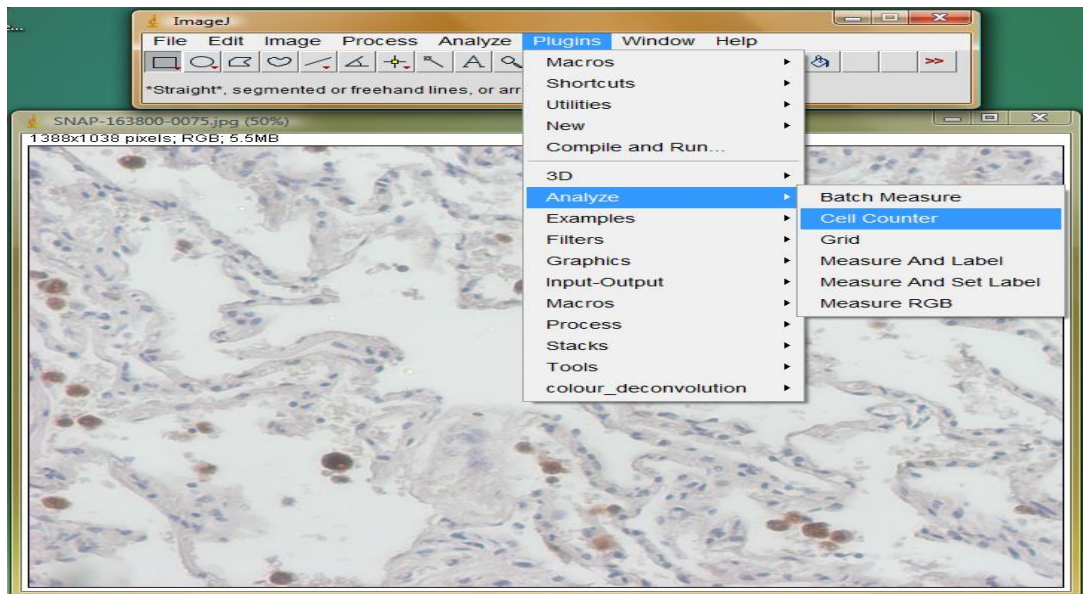
Finally go to Analyse -Measure. The results table will come up which you can save or annotate the results in a excel spreadsheet.

	Label	Area	StdDev	%Area
1	Untitled.jpg-(Colour_2)	275124	91.798	15.300

Cell Counting

This tool is perfect for counting singular stained cells such as macrophages.

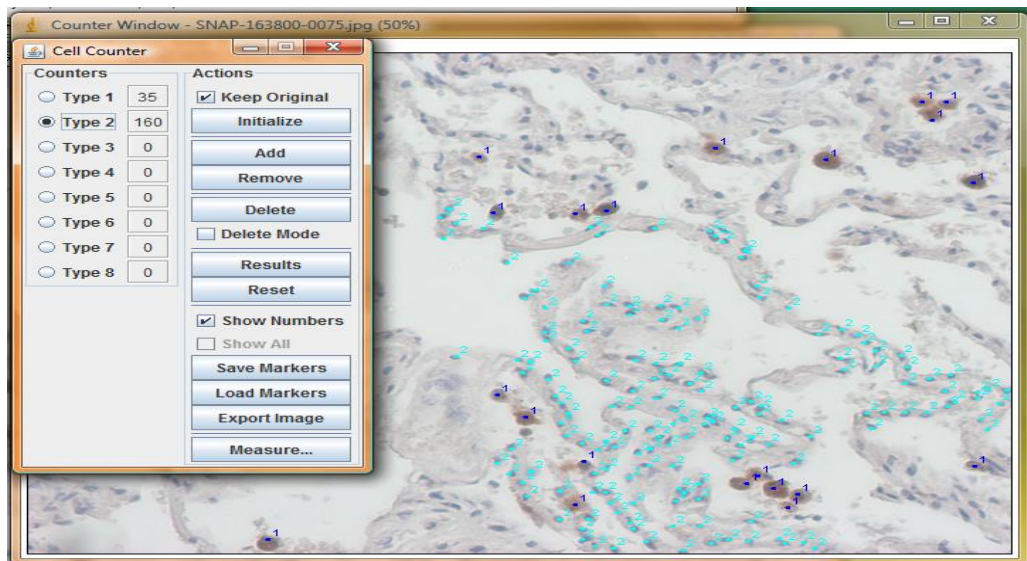
Open the image then go to Plugins-Analyse-Cell counter



Then select keep original (this produces a duplicate of the selected image) and initialize.

Select the counter you want to use i.e. Type 1 then start counting by clicking on each cell that has been stained.

You can alternate between the counters if you have multiple stains or if you would like to count cells stained i.e. DAB and nuclei stained by haematoxylin.



If the image proves difficult to do multiple counts on you could split the images using colour deconvolution first and then do separate counts on the separate DAB and Haematoxylin images.

References

Oda M, Azuma T, 2000, Reevaluation of stoichiometry and affinity/avidity in interactions between anti-hapten antibodies and mono- or multi-valent antigens, *Molecular Immunology*, 37(18): 1111-1122

Ross J, 2009, ImageJ Seminar: Introduction to image analysis, Biomedical Imaging research unit,
http://www.fmhs.auckland.ac.nz/sms/biru/_docs/Image_Analysis_Basics.pdf
 [Accessed on 23rd April 2012]

Van der Loos CM, 2008, Multiple Immunoenzyme Staining: Methods and Visualizations for the Observation with Spectral Imaging, *Journal of Histochemistry & Cytochemistry*, 56(4):313-328

Multiscan FC (Plate reader in teaching lab)

- Turn on Multiscan FC (switch at back)
- Turn on computer Username: Ascentuser
Password: els204
- Select Skanit for Multiscan FC 2.5.1 program and click on Log in button (no password)
- Create a New session
- Layout - Select wells by clicking and dragging with left mouse button
 - select desired action with right mouse buttone.g. Sample = Unknowns , Horizontal with replicates, OK
Standard = Calibrators, vertical with replicates, Concentrations - series
- initial value :600
- OP: /
- Step by 2
- Unit pg/mL
- Top of the screen select Protocol. Make the desired protocol by right clicking in Protocol Steps and select specific steps needed.
 - e.g. -Plate In
 - Photometric 1; Parameters Normal & Filter Abs 450
 - Photometric 2; Parameters Normal & Filter Abs 570
 - Plate Out
- Press start Button; give your session a name e.g. Patient number and date of experiment
- Top of screen select Results; in the left column select Photometric 1, right click and choose blank subtraction (average). Repeat for subsequent photometrics.
- Select Predefined Calculation - Difference 1-2
 - 1. Blanksubtraction1
 - 2. Blanksubtraction2
- Select curve fit (quantitive curve fit) and then Four parameter Logistic. Across the page you can now select graph which will give you your standard curve. The Coeff. Of Determ. R2: should equal 1 (or very close to this value)
- Table; Gives you your raw data in plate map format which can then be opened in excel to save and put into graphs etc or you can select List; which opens results in a list format which also can be opened in excel.